Direct Electrochemistry of Redox Enzymes as a Tool for Mechanistic Studies

Christophe Léger, Patrick Bertrand

Direct Electrochemistry of Redox Enzymes as a Tool for Mechanistic Studies

Christophe Léger* and Patrick Bertrand

Laboratoire de Bioénergétique et Ingénierie des Protéines, CNRS UPR 9036, IBSM, and Université de Provence, 31 chemin Joseph Aiguier, 13402 Marseille Cedex 20, France

Received August 1, 2007

Contents

* E-mail: christophe.leger@ibsm.cnrs-mrs.fr.

1. Introduction

This review regards the use of dynamic electrochemistry to study the mechanism of redox enzymes, with exclusive emphasis on the configuration where the protein is adsorbed onto an electrode and electron tranfer is direct. We still often come across the statement these days that redox enzymes are too large and too fragile to interact directly with a metallic electrode without being at least partly denatured. It is still held that since the active site of these enzymes is deeply buried in the protective protein matrix, direct electron exchange with an electrode can only occur under exceptional conditions. Yet 20 years have passed since it was shown that direct electron transfer (ET) can occur between an electrode and a large, catalytically active enzyme,[1–13] and about one hundred examples have already been reported. The oxidoreductases that are most auspicious for achieving direct "wiring" interact with their soluble redox partner (cytochrome, ferredoxin, quinone, or redox dye) by an outer sphere ET which occurs at (or close to) the surface of the enzyme, where the electrode can also interact. Having redox enzymes directly connected to electrodes made it possible to exploit the naturally high efficiency of these biological systems for developing selective third-generation biosensors,[14–16] environmentally sound biofuel cells,[17−19] heterogeneous catalysts,[20] and even biomolecular electronic components.[21] By combining dynamic electrochemistry and scanning probe microscopic techniques, it has now become possible to characterize the protein−electrode interface and electron exchange processes in great detail.[22–25] Closer to our concerns, this configuration has recently proved useful for learning about the kinetic and molecular aspects of the catalytic mechanism of redox enzymes—this is the topic of the present review.

Redox enzymes intervene in a number of biological processes, the most important of which may be the bioenergetic metabolism.[26] In living organisms, many essential reactions are thermodynamically allowed only because they are coupled to the very exergonic hydrolysis of ATP. The nonredox enzyme called ATP-synthase is responsible for maintaining the ATP/ADP ratio far from equilibrium by catalyzing the endergonic phosphorylation of ADP; as a source of free energy, this enzyme uses a gradient of electrochemical potential of the proton, which is built by the redox enzymes in the respiratory and photosynthetic chains, hence the importance of electron-transfer reactions

10.1021/cr0680742 CCC: $71.00
Published on Web 07/11/2008

Christophe Léger obtained his Ph.D. in physical chemistry at the University of Bordeaux I, France, where he studied dendritic patterning in electrodeposition under the supervision of Françoise Argoul. In 1999, he joined Fraser Armstrong at the University of Oxford, U.K., to study redox enzymes by electrochemistry, and he has been fascinated by this topic ever since. In 2002, he was hired by the French National Center for Scientific Research (CNRS) in Marseilles. He is interested in bioinorganic chemistry, in enzyme kinetics, and in studying the mechanism of multicenter redox enzymes.

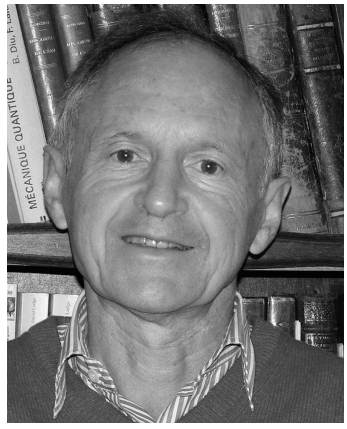

Patrick Bertrand received his undergraduate education at the *Ecole Centrale de Paris*. After having worked for three years as scientific attaché at the French Embassy in Bucharest, he joined the Laboratory of Condensed Matter Electronics at the University of Provence, in Marseilles, where he started to study the magnetic properties of iron−sulfur clusters under the supervision of Jean-Pierre Gayda. He received his Ph.D. in physics in 1977 and his *doctorat es sciences* in 1981. Since 1989, he has been a Professor at the Université de Provence. In 1993, he participated with his group in the creation of the Laboratory of Bioenergetics and Engineering of Proteins of the CNRS, headed by Mireille Bruschi. Although he enjoyed using EPR spectroscopy to identify and characterize the metal centers of numerous proteins, he is now convinced that great advances in the catalytic mechanism of redox enzymes can be made by using electrochemical techniques.

in sustaining life. Other vital processes catalyzed by redox enzymes include crucial steps in the global element cycles[27] and the regulation of metabolic processes. In some cases, redox enzymes are merely used for detecting a given molecule and for triggering a cascade of reactions, including the synthesis of other enzymes; hence, their turnover frequency need not be high. In contrast, when their physiological function is to transform a substrate, they may do so thousands of times per second in a very selective manner. This diversity of functions and efficiencies translates into an extraordinary variety of structures. Redox enzymes may be very small and consist of a single chain of a hundred amino acids or less and no prosthetic (nonproteic) cofactor, but catalytic performance may also be very costly for the cell: mitochondrial Complex I (NADH-Ubiquinone oxidoreductase) is a transmembrane complex assembled from 45 different proteins with a total molecular weight approaching 1 MDa; it houses a flavin at the site of NADH oxidation and nine iron−sulfur (FeS) clusters.[28–30] Most interestingly, an enzyme does much more than catalyzing a reaction: it does so at the right rate, considering its substrate is often the product of another enzyme and *vice versa*; it resists inactivation by potent inhibitors and stressful chemicals present in the cell; it fastens partly-transformed catalytic intermediates that may be harmful, *etc.* Hence, the enzymes' structures and mechanisms are complex because their catalytic properties are manifold.

A significant difference between the chemist's synthetic inorganic catalysts and the large multicenter enzymes we study is that the mechanism of the latter involves a number of steps of various nature, which occur in a concerted manner on distinct sites of the protein that may be very far apart from one another. We illustrate this by considering the mechanism of NiFe hydrogenase,[31] whose structure is shown in Figure 1. This enzyme catalyzes the reversible transformation between molecular hydrogen and protons according to $H_2 \rightleftarrows 2H^+ + 2e^-$. It is a complex of two proteins and consists of about 10000 atoms, including one Ni and 12 Fe ions. The active site chemistry *per se*, involving the heterolytic splitting of dihydrogen, occurs at a NiFe cluster which is buried inside the protein matrix. The electrons produced or consumed at the active site are sequentially transferred to the redox partner (a cytochrome) via a chain of FeS clusters. The active site is also connected to the solvent by gas channels and by a yet unidentified proton-transfer machinery, involving protonable amino acid side chains and ordered water molecules. Some of the steps in the mechanism, e.g. proton and electron transfers and diffusion along the channels, remain difficult to study using conventional techniques, and very little is known about how the interplay between all these events gives the enzyme its global properties in terms of selectivity, catalytic directionality, and resistance to chemical stress.

Over the last 15 years, the elucidation of the three-dimensional structures of many redox enzymes (and particularly metalloenzymes) has inspired research on their mechanism by providing a molecular framework for interpreting their biochemical and spectroscopic properties, and an instrumental road map for studies based on genetic engineering. A major contemporary challenge is to decipher this structural information in relation to the mechanism to understand how subtle differences in structure among enzymes within a given family can greatly diversify their catalytic properties. Theoretical modeling and spectroscopic studies, combined with potentiometric titrations, have taken mechanistic investigations down to the atomic scale by giving detailed pictures of the electronic structure of redox cofactors; this approach requires that the reactive intermediates along the catalytic pathway be stable enough to be isolated and characterized. Time-resolved techniques, e.g. rapid freeze-quench or stopped-flow, allow short-lived intermediates to be trapped and examined, but they are very demanding in terms of quantity of biological material, which may be in scarce supply. Studying how enzymes *work* has always meant examining the *rates* of the catalyzed processes, and enzyme kinetics as an academic subject has just celebrated its centennial. However, as far as the molecular mechanism is concerned, a main limitation of steady state kinetics is that the nature of the rate-limiting step in the global catalytic

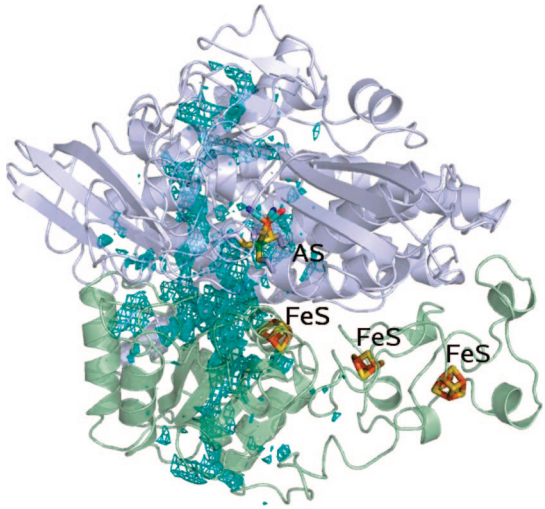

Figure 1. Model of the structure of *D. fructosovorans* NiFe hydrogenase,[32,33] showing the two proteins assembled in the heterodimer (light blue and green), the buried active site (AS), the three lined-up iron−sulfur (FeS) clusters used for transferring electrons, and the putative gas channels (turquoise grid) which connect the active site to solvent. Apart from an active site glutamate,[34] the residues involved in proton transfer are not established with certainty and therefore are not represented. This figure was made by C. Cavazza.

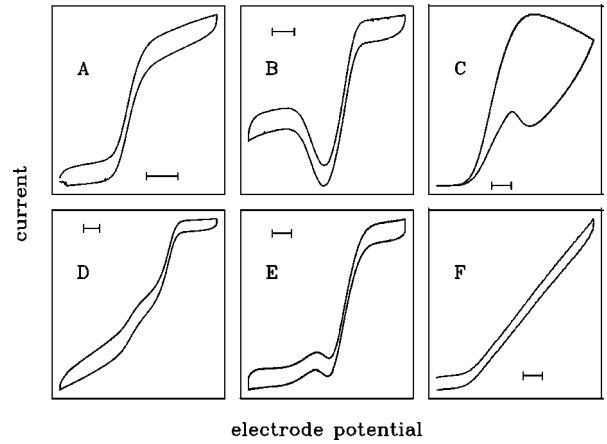

Figure 2. A collection of rather exotic catalytic voltammograms obtained with adsorbed enzymes in the absence of mass transport control. The enzymes are *Escherichia coli* fumarate reductase (panels A and D),[12,36,37,38] *E. coli* DMSO reductase (panel B),[39,40] *E. coli* nitrate reductase (panel E),[41,42] and *Allochromatiun vinosum* NiFe hydrogenase (panels C and F) (under conditions of slow and fast scan rate, respectively).[43,44] In all cases, the horizontal segment is for $i = 0$ and has a length of 100 mV. Panel C is drawn using data provided by A. K. Jones.[45] Adapted with permission from refs 36, 38, 40, and 42–44. Copyright 2001−2005 American Chemical Society.

process cannot always be established with certainty, so that it is not always clear which step the overall rate relates to. Direct electrochemistry now adds to the ensemble of techniques that are available in enzymology. In these 60 pages, we hope to convince the reader that it provides information that may be highly relevant to the mechanism, original, and complementary to that obtained from other techniques. Of even greater value is the fact that thought-provoking electrochemical experiments have forced us to explore new concepts and to question ideas that may otherwise have been taken as settled.

The principle of direct electrochemistry is easily explained by comparing this technique to the more traditional solution assays of enzyme activity. In *homogeneous enzyme kinetics*, the enzyme may be mixed in a cuvette with its substrate and a redox partner (otherwise called a mediator or cosubstrate), which provides a source or a sink of electrons for the redox transformation of the substrate and whose absorbance depends on its redox state (note that we call the *substrate* the molecule that the enzyme transforms into a product, and not a solid material, as in the language of surface science). In the steady state, the rates of substrate and cosubstrate transformations are equal to the turnover rate of the enzyme and can therefore be determined by following the absorbance change of the solution. In *mediated electrochemistry*, the consumption of the redox partner is detected as a current wave resulting from its electrochemical recycling on the electrode (see chapters 4 and 5 in ref 35); only the mediator interacts with the electrode, and the homogeneous catalytic process which occurs in the bulk of the electrochemical cell is fundamentally the same as that in solution assays. Here we shall be interested in a third configuration originally called "protein film voltammetry" (PFV), where the enzyme is adsorbed onto the electrode and electron transfer is direct. When the electrode potential is appropriate, electrons flow between the substrate and the electrode, via the active site of the enzyme, and the magnitude of the current is simply proportional to the turnover rate. Ideally, interfacial ET may be fast and the electrode may be rotated at high speed to avoid mass transport control, so that the current response directly reports on the intrinsic properties of the enzyme.

There are two fundamental reasons PFV is potentially much more informative than the other methods for assaying the enzyme. First, the potential of the electrode can be continuously swept to provide whichever driving force is required to elicit catalysis, and each data point along the voltammogram can be thought of as an "initial rate"[46] in a solution assay that would be carried out under precise control of the redox conditions. Thus, PFV adds the potential dimension to enzyme kinetics. Figure 2 collects catalytic voltammograms observed for various enzymes and shows that these signals may have very odd shapes. Extracting mechanistic information from this data depends on our ability to model the signals. In Figure 2A, the electrode potential where the activity kicks on (defined as the inflection point of the sigmoidal transition toward the plateau) is an important characteristic of the steady state current response because this relates to the minimal driving force that must be provided by the physiological redox partner of the enzyme to sustain catalysis.[41] This catalytic, or "operating" potential is somehow related to (but need not equate) the reduction potential of the active site of the enzyme, since substrate transformation can proceed only when the active site converts into a certain redox state. The catalytic potential need not agree with values for the active site reduction potentials obtained by potentiometry, since we now know that it may be affected by, and report on, the thermodynamics and kinetics of all sorts of steps in the catalytic cycle, most obviously substrate binding and protonations but also intramolecular electron transfer when this process happens to limit turnover. All of these effects are potentially important in making the redox properties match catalytic function. At high overpotential, the catalytic wave often shows one or two other sigmoidal features. For example, the activity may be "boosted" when a certain electrode potential is reached (panel D and E). Instead, or in another range of electrode potential, it may be

attenuated or even "switched off" as the driving force is increased (panels B, C, and E). This demonstrates that the turnover rate of a redox enzyme may not merely increase in a monotonic fashion upon increasing the driving force, an observation that has both mechanistic and physiological[41] consequences, as discussed herein, but which is most likely to escape detection in traditional experiments.

Second, the superiority of PFV comes from the fact that a change in catalytic turnover rate *instantly* translates into a variation of current. It is essential in this respect that the current response is not convoluted and obscured by cosubstrate diffusion and intermolecular electron transfers (as is the case for mediated electrochemistry). Together with the precise redox control afforded by the electrode potential, this excellent temporal resolution of the activity assay makes it possible to characterize precisely how activity quickly evolves with time following an instant change in experimental conditions; this has proved particularly useful for studying the kinetics of inhibition, activation, or inactivation of several enzymes, as these processes involve redox and redox-coupled transformations that occur on short time scales and thus cannot be resolved in normal activity assays.

From an operational perspective, PFV also has a number of other advantages, not the least being that, in comparison with other popular techniques, it requires very small amounts of often priceless biological material. Indeed, the electroactive coverage of enzyme on the electrode is usually in the pmol/cm^2 range, and data have been obtained with about one zepto mol of enzymes (50000 molecules) adsorbed at an electrode.[47] In the most favorable cases, many experiments can be carried out with the same enzyme film which can be transferred between different solutions, in a process that is like instant dialysis, and used again and again to determine how temperature, pH, substrate and inhibitor concentrations, isotope substitutions, *etc.* affect the catalytic response.

Of course, drawbacks exist. Not all enzymes can be directly wired to an electrode. Those that have been successful so far often contain an active site that is either relatively exposed at the surface of the protein (e.g. cytochrome *c* peroxidase) or buried in the protein matrix but connected to the surface by a chain of redox cofactors (e.g. hydrogenase in Figure 1). Sometimes membrane bound enzymes can be cleaved, either chemically or by genetic engineering, and it is possible to study an active subcomplex that has a surface exposed redox site which connects the electrode to the active site. A second inconvenience is that a parameter that is so easily measured in solution assays, the value of k_{cat}, cannot always be determined in PFV because the exact amount of adsorbed enzyme is either not accurately determined or even unknown. Last, the chemical identity and structure of the postulated catalytic intermediates will sometimes remain elusive, and complementary techniques must be called for. However, electrochemistry is an invaluable technique because it yields information about kinetics and energetics that often cannot be obtained with conventional methods. This will be illustrated hereinafter.

This review is organized as follows. In section 2, we comprehensively list the models that have been developed to interpret the voltammetry of adsorbed redox proteins (section 2.1) and enzymes, first in the case where mass transport can be ignored (section 2.2) and then when the catalytic response of the enzyme is convoluted with substrate mass transport to a rotating or stationary electrode (section 2.3). Section 2.4 is devoted to the modeling of chronoamperometric catalytic data. Having done so will allow us to highlight major results in the subsequent sections by skipping over algebra, only referring to the content of section 2. In section 3, we have organized case studies according to the type of information on the mechanism that was gained, rather than arranging the results by family of enzyme or by type of reaction. We have selected results which illustrate that PFV could be used to learn about all aspects of the mechanism: inter- and intramolecular electron transfer, active site redox chemistry, including chemical reactions that are coupled to electron transfer to the active site during turnover, catalytic bias, inhibition, redox activation and inactivation, and diffusion along substrate channels. In each case, our goal was to explain how this information could be acquired and what makes it original and valuable rather than detailing results which can be found in the original literature.

Recent reviews with a slightly different and/or narrower focus include refs 24, 40, 41, and 48–54.

2. Modeling the Voltammetry of Adsorbed Redox Enzymes

2.1. Noncatalytic Voltammetry

We first consider the situation where the current−potential response reveals the direct electron transfer (ET) between the electrode and the redox centers of a strongly adsorbed molecule, under conditions where there is no catalysis: the voltammetric signal consists of one or several pairs of current peaks which reveal the oxidation and reduction of each redox site as the electrode potential is swept upward or downward across its reduction potential (at least in the simplest cases, see below). The noncatalytic situation refers most obviously to proteins but also to redox enzymes if the substrate is absent or if catalysis is either blocked by an inhibitor[55] or outrun by using a high enough scan rate that the catalytic cycle cannot be completed over the time scale of the voltammetric experiment.[56] Usually, the electroactive coverage is relatively small and so is the current; however, the fact that the faradaic current drops to zero at high enough overpotential (after the entire sample has been fully reduced or oxidized) makes base line subtraction and data analysis relatively straightforward.

The advantages of noncatalytic PFV with respect to redox potentiometry have been discussed in recent reviews.[48,51–53,57] Most importantly, the information that can be gained extends well beyond the measurement of reduction potentials because, in noncatalytic voltammetry, the scan rate is a crucial experimental parameter which can be varied to learn about the kinetics of various processes (electron transfer and chemical reactions) that may occur on very different time scales; unstable species can also be kinetically trapped and examined simply by using a scan rate that is high enough that it does not transform during the time it takes to record the voltammogram. Hereafter, we only consider the theory and applications of noncatalytic voltammetry inasmuch as it is useful for discussing the voltammetry of adsorbed enzymes.

2.1.1. The Case of Pure Electron Transfer (ET)

2.1.1.1. The Nernstian Regime for Isolated One- or Two-Electron Centers. The simplest case of electrochemical response relates to a one-electron redox center, when the scan rate is low enough that the ratio of oxidized over reduced species remains equal to that predicted by the Nernst equation. The

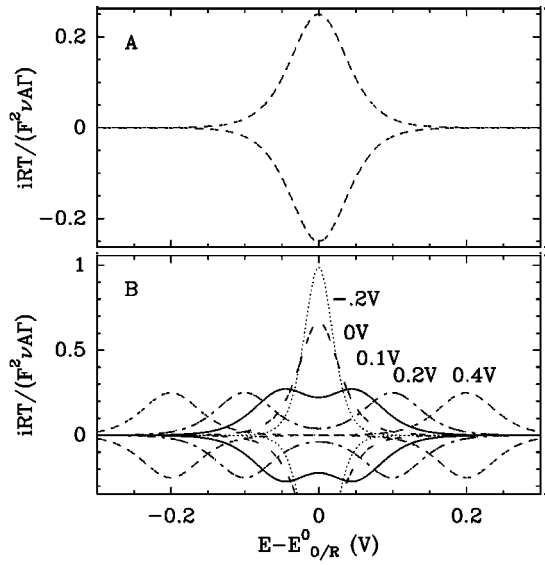

Figure 3. Normalized current−potential response for a $n = 1$ (panel A and eq 1) or $n = 2$ (panel B and eq 3) redox center immobilized on an electrode. In panel B, the different curves are calculated for $E^0_{O/I} - E^0_{I/R}$ between 0.4 and −0.2 V, as indicated.

current equation is therefore simply obtained by differentiating the Nernst equation;[58,35] for the anodic peaks, this leads to

$$i^{n=1}_{Lav}(E^0) = \frac{F^2 \nu A \Gamma}{RT} \frac{\exp[f(E-E^0)]}{(1+\exp[f(E-E^0)])^2} \quad (1)$$

We use the convention according to which oxidation produces a positive current. We denote by A, the electrode surface; Γ, the electroactive coverage; $\nu = dE/dt$, the scan rate; F, R, and T have their usual meanings and $f = F/RT$.

Equation 1 (dashed line in Figure 3A) describes a peak whose height $i_p = F^2\nu A\Gamma/4RT$ is proportional to scan rate, as opposed to $\sqrt{\nu}$ when the current response is convoluted by diffusion of the redox species toward the electrode. There is no separation between the anodic and cathodic peaks; the peak potential is simply the reduction potential of the redox couple and the full width at half height is $2\ln(3+2\sqrt{2})/f$ (89 mV at 20 °C). The electroactive coverage can be estimated from the total peak area, which equates $FA\Gamma\nu$.

Nonideal behaviors in the reversible limit have been observed and reviewed in refs 57 and 59. They include residual peak separation and peak widths larger than those predicted by the Nernst equation. Excess peak widths are accounted for by assuming a distribution of reduction potentials,[60−62] or empirically by substituting $\exp[n_{app}f(E-E^0)]$ for $\exp[f(E-E^0)]$ in eq 1, with $n_{app} < 1$.[63]

$$i^{n=1}_{Lav}(E^0) = \frac{F^2 \nu A \Gamma}{RT} \frac{\exp[n_{app} f(E-E^0)]}{(1+\exp[n_{app} f(E-E^0)])^2} \quad (2)$$

Armstrong and co-workers and Elliott and co-workers have also identified cases where the peak width significantly increases as the temperature is lowered, instead of being proportional to T.[57,64]

Enzyme active sites are often two-electron centers, for which we define three redox states termed O (oxidized), I (intermediate, or half-reduced), and R (reduced) throughout this paper. We note $E^0_{O/I}$ and $E^0_{I/R}$ the corresponding reduction potentials and $E^0_{O/R} = (E^0_{O/I} + E^0_{I/R})/2$. The corresponding current equation was derived in ref 65 (equivalently in ref 35, eq 1.57):

Scheme 1. Definition of the Four Reduction Potentials in a Molecule Containing Two Redox Sites A and B

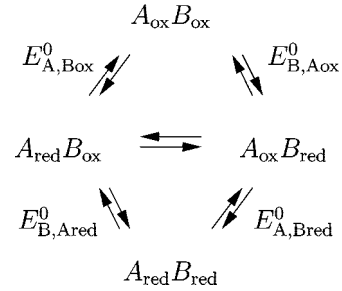

There are only three independent parameters in this scheme, since the four reduction potentials are related to each other by eq 6.

$$i^{n=2}_{Lav}(E^0_{O/I},E^0_{I/R}) = \frac{F^2 \nu A \Gamma}{RT} \delta^{-1/2} \frac{\xi^{1/2} + 4\delta^{1/2} + \xi^{-1/2}}{(\xi^{1/2} + \delta^{-1/2} + \xi^{-1/2})^2} \quad (3a)$$

$$\delta = \exp[f(E^0_{I/R} - E^0_{O/R})] \quad (3b)$$

$$\xi = \exp[2f(E - E^0_{O/R})] \quad (3c)$$

(δ is noted K^{-1} in ref 65). Curves calculated from eq 3a are plotted in Figure 3B. If $E^0_{I/R} \ll E^0_{O/I}$, two $n = 1$ peaks centered at $E = E^0_{O/I}$ and $E^0_{I/R}$ are observed, whereas if δ is large, a single peak occurs, whose features differ significantly from those of a one-electron peak: the height can be up to four times larger and the width twice as small. Working curves have been derived that relate the peak width[66] or height[35] to δ (the latter may be underestimated as a consequence of nonideal peak broadening). Peak narrowing can also arise for a single one-electron reaction if the ET is followed by a first-order, irreversible reaction ("EC" mechanism); in this case, the forward and backward peaks are no longer symmetrical.[67] Thus, to interpret the narrowness of a peak in terms of δ being large, it is important that both the forward and backward peaks should be narrow. Regarding two-electron reactions, it has been noted[35] that a peak twice that given by eq 1 is not obtained for $E^0_{O/I} = E^0_{I/R}$ but rather when $E^0_{O/I} - E^0_{I/R} = (RT/F)\ln 4$.

When δ is large, that is when the half-reduced active site disproportionates, eq 3 can be replaced with

$$i^{n=2}_{Lav}(E^0_{O/R}) \approx \frac{4F^2 \nu A \Gamma}{RT} \frac{\exp[2f(E-E^0_{O/R})]}{(1+\exp[2f(E-E^0_{O/R})])^2} \quad (4)$$

and this has prompted[66] the use of a very popular equation

$$i^{n_s,n_{app}}_{Lav}(E^0_{O/R}) \equiv \frac{n_s n_{app} F^2 \nu A \Gamma}{RT} \frac{\exp[n_{app} f(E-E^0_{O/R})]}{(1+\exp[n_{app} f(E-E^0_{O/R})])^2} \quad (5)$$

where a given center contributes to the signal according to its stoichiometric number of electrons ($n_s = 1$ or 2) and ideal peak widths are obtained with $n_{app} = n_s$ while broadening results in lower n_{app} values. Some confusion may arise by using eq 5 with $n_s < n_{app}$, although this was proposed as a way of accounting for "repulsive interactions" between the adsorbed redox sites.[63] Except for fitting nonideal data, there is no obvious advantage in using eq 5 rather than eq 3, since the number of parameters is the same. Moreover, the behavior predicted by eq 3 when δ is small cannot be fit to eq 5.

2.1.1.2. The Nernstian Regime for Multicenter Proteins. Redox enzymes often house several redox centers which can be addressed using voltammetry, provided either each center can communicate directly with the electrode or at least one can, and intramolecular electron transfer is possible on the time scale of the experiment. If these processes are rapid, the Nernst equation can be used for each redox center, but the question as to how redox interactions affect the voltammetry sometimes received incorrect and misleading answers. This prompted us to clarify this point by examining the simple case of a protein containing two redox sites in the Nernstian limit.

Scheme 1 shows the four possible redox states of a molecule containing two reducible sites. They are often called "microstates", which is actually a fanciful term to use in the context of classical thermodynamics. To characterize the thermodynamics of this system, *four* (rather than two) reduction potentials need be considered, because the reduction potential of each center may depend on the redox state of the other center. Hence, we call $E^0_{A,Box}$ and $E^0_{A,Bred}$ the reduction potential of center A when center B is oxidized or reduced, respectively, and similarly for center B. Since free energies and reduction potentials add up to zero when one goes around the thermodynamic cycle in Scheme 1, these four "microscopic" reduction potentials are not independent:

$$E^0_{A,Box} - E^0_{A,Bred} = E^0_{B,Aox} - E^0_{B,Ared} = \Delta E \qquad (6)$$

The so called "redox interaction" ΔE is either positive or negative, resulting in anticooperative or cooperative behavior, respectively. Anticooperative behavior is expected from simple electrostatic considerations:[68] the reduction of one center decreases its charge, making more difficult the reduction of the other center. However, electrostatics alone cannot predict the magnitude or even the sign of this interaction, which may be affected by charge compensations resulting from coupled protonations[69] and/or subtle conformational changes. Regarding tetraheme cytochromes, where this aspect has been studied in great detail, ΔE values have been found in the range −50 to +100 mV (see ref 70 for a review).

We define n(Aox) as the number of oxidized centers Aox, n(Aox) = n(Aox, Box) + n(Aox, Bred), and similarly n(Box), n(Ared), *etc.* The total number of molecules is n_{tot} = n(Aox) + n(Ared). Although both n(Aox) and n(Box) can be expressed as a function of three independent reduction potentials, it is important to note that the total number of centers that are oxidized at a given potential, n^{ox} = n(Aox) + n(Box), which equates to

$$\frac{n^{ox}}{n_{tot}} = \frac{1 + e^{f(E^0_{B,Aox} - E^0_{A,Box})} + 2e^{f(E - E^0_{A,Box})}}{1 + e^{f(E^0_{B,Aox} - E^0_{A,Box})} + e^{f(E - E^0_{A,Box})} + e^{-f(E - E^0_{B,Ared})}} \qquad (7)$$

can be written as a function of only *two* independent parameters, E_1 and E_2:

$$\frac{n^{ox}}{n_{tot}} = \frac{1 + 2e^{f(E - E_1)}}{1 + e^{f(E - E_1)} + e^{-f(E - E_2)}} \qquad (8a)$$

$$e^{fE_1} = e^{fE^0_{A,Box}} + e^{fE^0_{B,Aox}} \qquad (8b)$$

$$e^{-fE_2} = e^{-fE^0_{A,Bred}} + e^{-fE^0_{B,Ared}} \qquad (8c)$$

The immediate consequence is that, by using electrochemistry or any other technique which is sensitive to n^{ox} (or to its variation with E) but which cannot discriminate between n(Aox) and n(Box), a maximum of two independent parameters can be measured, and full characterization of Scheme 1 is not possible (that is not to say that redox interactions can never be detected, see below). In contrast, techniques such as NMR[71] or EPR[72] can be used to gain more information, provided the centers have distinctive spectroscopic signatures. In practice, however, the accuracy of the potentiometric titrations followed by EPR or NMR is often not sufficient to unambiguously determine all the parameters that characterize a molecule containing several redox sites, and simplifying assumptions must be made.

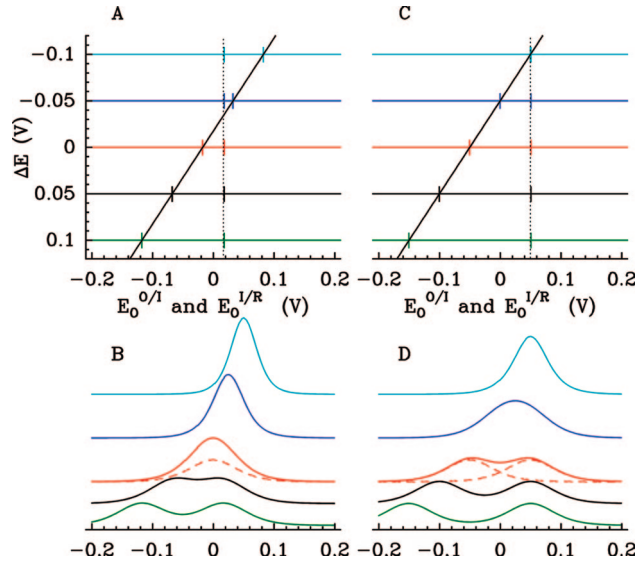

Figure 4. The noncatalytic signal for an adsorbed molecule containing two redox sites depends on their redox interaction. According to the notations in Scheme 1, the signals have been calculated with $E^0_{A,Box} = E^0_{B,Aox} = 0$ in panels A and B, and $E^0_{A,Box}$ = +50 mV and $E^0_{B,Aox}$ = −50 mV in panels C and D. The colors correspond to various values of the redox interaction ΔE. The top panels show how this affects the macroscopic reduction potentials (solid and dotted black lines); the bottom panels show the corresponding voltammograms.

The physical meaning of E_1 and E_2 in eq 8 appears when one considers a "macroscopic" description of the system, with three "overall" redox states O, I, and R (oxidized, one-electron reduced, and fully reduced). Equation 8a is exactly that expected for the sum $2n_O + n_I$ if one identifies E_1 and E_2 with the reduction potentials $E^0_{O/I}$ and $E^0_{I/R}$ corresponding to the consecutive one-electron reductions of the fully oxidized molecule. Thus, these potentials characterize the whole molecule, as opposed to the individual centers, and are termed "macroscopic"[70,73,74] or sometimes "formal."[75] Equations 8b/c give the relations between these two macroscopic potentials and the "microscopic" parameters. The noncatalytic current for such system is simply deduced by differentiating eq 8 with respect to E. This current equation takes exactly the form obtained for a single center that can accept two electrons ($i^{n=2}_{Lav}$ in eq 3) with $E^0_{O/I} \equiv E_1$ and $E^0_{I/R} \equiv E_2$.

How redox interactions affect the voltammetry of a protein that contains two centers is illustrated in Figure 4 for two simple situations. In the left panels, we first consider a system characterized by $E^0_{A,Box} = E^0_{B,Aox} = 0$ V and various values of the interaction ΔE (Y-axis). Panel A shows how the values of $E^0_{O/I}$ (dotted line) and $E^0_{I/R}$ (solid lines) depend on ΔE. For $\Delta E = 0$ (red curves), the two macroscopic potentials are separated by (RT/F) ln 4 = 36 mV (at T = 298 K), and the

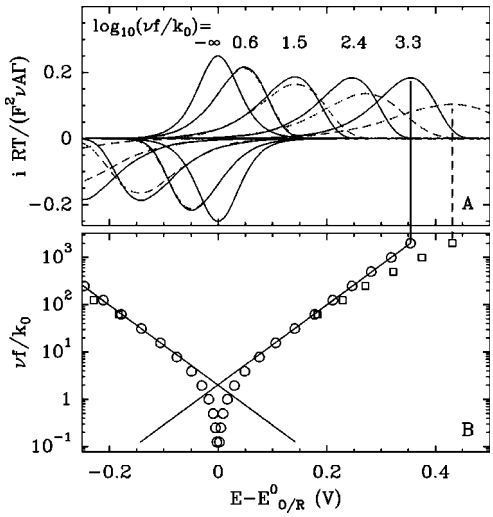

Figure 5. The solid lines in panel A correspond to cyclic voltammograms calculated using the BV equations (eqs 9 with $\alpha = {}^1/_2$). The circles in panel B show how the peak positions depend on scan rate. The solid lines in panel B are given by eq 10. The dashed lines in panel A and the squares in panel B are calculated using the Marcus theory of interfacial ET with $\lambda = 0.7$ eV (eq 13). The plot of peak positions against log(scan rate) is usually represented rotated clockwise; see e.g. Figure 8.

voltammetric signal in panel B is simply twice a one-electron peak located at $E = 0$ V. Note that the more general case of a molecule containing N identical and *noninteracting* centers was treated by Flanagan and co-workers:[75] the noncatalytic signal is N times the same peak given by eq 1 ($i_{Lav}^{n=1}$), centered on the unique *microscopic* reduction potential (eq 8 in ref 75), and no statistical correction applies. When the interaction is anticooperative ($\Delta E > 0$, black and green lines in Figure 4A and B) the two peaks tend to separate, and the signal can still be fit to the sum of two $n = 1$ peaks, but their positions are not simply related to the reduction potential of the centers and the peak separation tends to $\Delta E + 36$ mV as ΔE increases. If the redox interaction is negative, a single peak sharper than $n = 1$ is observed, which can be fit to eq 3; there is no reason to deconvolve the data to either one or the sum of two $n = 1$ peaks (eq 2) with $n_{app} > 1$.

In the right panels, we consider the other limiting case where $E^0_{A,Box} \gg E^0_{B,Aox}$ and we start with $\Delta E = 0$ (red). If ΔE is small or positive, the signal can be fit to a sum of two $n = 1$ peaks to determine $E^0_{A,Box}$ and $E^0_{B,Ared} = E^0_{B,Aox} - \Delta E$. This can be understood as follows: with A being the most oxidizing center, it is reduced when B is still oxidized (hence the peak at $E^0_{A,Box}$), whereas electron transfer to B occurs only after the reduction of A (hence the peak at $E^0_{B,Ared}$). Again, the two peaks merge if ΔE is negative.

From these considerations, it is clear that the three independent parameters in Scheme 1 cannot be deduced from the voltammetric signals. When the data can be simulated as a sum of $n = 1$ peaks, the sign or magnitude of the redox interaction cannot be determined unless additional information from independent sources is available. However, observing a sharp peak ($n_{app} > 1$) for a protein containing one-electron redox sites proves that a cooperative redox interaction exists ($\Delta E < 0$), as illustrated in a recent study of the tetraheme cytochrome *c*554.[76] Regarding multicenter enzymes and proteins, the important (although somehow trivial) conclusion is that the reduction potentials of the *individual* centers can be determined by deconvoluting the Nernstian noncatalytic signal using a sum of Laviron peaks (eqs 1 and 3) only if the redox centers do not interact. Although redox interactions may have a great influence on the shape of the noncatalytic voltammogram and may make it difficult to interpret, they do not change its magnitude (the area under the peaks), which can be used to determine electroactive coverage.

2.1.1.3. Beyond Equilibrium. Considering voltammetric experiments carried out at relatively fast scan rates, deviations from the Nernstian peak shapes are expected to occur when the rate of electron transfer is not fast enough to maintain equilibrium between the redox site and the restless electrode potential. This results in peak broadening and in the oxidative and reductive peaks being shifted to higher driving forces. Although of practical interest,[36,56,77,78] no rigorous theoretical treatment has been given for multicenter molecules under nonequilibrium conditions (fast scan rates). In the following, we briefly discuss the various models that have been proposed to describe the nonequilibrium regime in the case of a single redox center.

2.1.1.3.1. Using Butler−Volmer (BV) Equations. Modeling requires that the way in which the interfacial ET rates depend on electrode potential be specified. The empirical Butler−Volmer equations predict that ET rates increase exponentially with the driving force. For a one-electron couple, the first-order rate constants of oxidation and reduction resulting from electron transfer to/from the electrode read

$$k_{ox} = k_0 \exp[(1-\alpha) f(E - E^0_{O/R})] \quad (9a)$$

$$k_{red} = k_0 \exp[-\alpha f(E - E^0_{O/R})] \quad (9b)$$

Here, k_0 is the common value of the rate at zero driving force and α is a transfer (or symmetry) coefficient, which we shall take equal to ${}^1/_2$.

Using these equations, Laviron calculated in ref 79 the voltammetric peak shapes expected for an adsorbed one-electron center as a function of scan rate, as illustrated by the solid lines in Figure 5 (see refs 80 and 81 for the case $n = 2$). The Nernstian limit is recovered when the scan rate is smaller than k_0/f; at a higher scan rate, the peak shape tends to the irreversible limit given by eqs 18 and 19 in ref 79: the peak area (in units of AV) remains proportional to the charge passed and to the scan rate, the width at half height (129 mV at 20 °C) is independent of scan rate, and the peak position is proportional to the logarithm of the scan rate. The straight lines in Figure 5B are the peak positions predicted in this irreversible limit:

$$E_p = E^0_{O/R} \pm f^{-1} \ln(f\nu/2k_0) \quad (10)$$

Thus, the value of k_0 can be deduced from voltammograms recorded at different scan rates. The analysis of peak positions against scan rate (Figure 5B) is often adopted in preference to peak shape analysis because it is less sensitive to the choice of the baseline. Similarly, the accurate determination of peak areas may not be very easy at fast scan rates. Equation 10 shows that the peak position is only sensitive to the logarithm of k_0/ν; therefore, only the order of magnitude of k_0 can be determined. Because of nonidealities, this measurement cannot always be accurate.

2.1.1.3.2. Predictions using the Marcus Theory of Interfacial Electron Transfer (ET). Although BV equations are both extremely simple and well-tried, they have no physical basis. In the 1960s, Marcus developed a model based on a molecular description of ET between small molecules in solution.[82,83] He showed that this process requires the

formation of a transient complex, in which the kinetics of the ET step can be described by an equation of the form

$$k = C \exp\left(-\frac{(\Delta G^0 + \lambda)^2}{4\lambda RT}\right) \quad (11)$$

ΔG^0 is the standard free energy of the reaction, which is related to the standard reduction potentials of the donor D and the acceptor A according to $\Delta G^0 = F(E^0_D - E^0_A)$. The parameter λ, called the "reorganization energy", is all the greater that large molecular rearrangements accompany the transfer (both the geometries of the molecules that are oxidized or reduced and the polarization of the surrounding solvent should be considered). The expression of the pre-exponential factor C depends on the strength of the electronic coupling between the acceptor and the donor. If it is strong enough (adiabatic transfer), C simply equates kT/h, as given by the classical transition state theory. When it is weak (this is so for long distance, "nonadiabatic" ET), C is proportional to the square of a matrix element of the interaction between the initial and final states: it depends on the overlap of the molecular wave functions of D and A, and therefore on the nature of the redox centers, on their distance, and on the intervening medium. An exponential decrease of C with distance is expected. In the literature, nonadiabatic transfers are often referred to as electron tunneling processes. We note that eq 11 is only valid provided the temperature is high enough that all modes which contribute to changing the geometry of the molecules when the electron is transferred can be treated classically. This should be so at room temperature.

To deduce from eq 11 the equation describing the interfacial ET between a molecule whose reduction potential is E^0 and a metallic electrode whose potential is E, the starting equation is

$$k_{red/ox} = C' \exp\left(-\frac{[\pm F(E - E^0) + \lambda]^2}{4\lambda RT}\right) \quad (12)$$

and this rate is integrated across the density function of electronic states in the electrode, with the contribution of each state being weighted according to Fermi−Dirac statistics. Making the reasonable assumptions that both the value of C' and the density of states are the same for all the states (irrespective of their energy), an analytical expression is obtained,[84,85] which has the good taste to depend only on E, E^0, and λ:

$$k_{red/ox} = \frac{k_{max}}{\sqrt{4\pi\lambda/RT}} \int_{-\infty}^{\infty} \frac{\exp\left(-\frac{1}{4\lambda RT}[\lambda \pm F(E - E^0) - RTx]^2\right)}{1 + \exp(x)}\, dx \quad (13)$$

where k_{max} is the asymptotic value of the rate constant at large overpotential. Equation 13 is the expression which is referred to as Marcus theory applied to interfacial ET kinetics. The rates can be numerically evaluated from eq 13 using standard routines.[86] Alternatively, a simple and accurate numerical method was described in the appendix of ref 37. We used it to calculate the plots of k_{ox}/k_0 against $E - E^0$ in Figure 6, where k_0 denotes the value of the ET rate when $E = E^0$. At low overpotential, Marcus theory predicts that the ET rate increases exponentially: BV equations with $\alpha = {}^1/_2$ are given justification. At a higher driving force, the rate asymptotically approaches a plateau value k_{max}, passing through $k_{max}/2$ when the overpotential equates λ. This plateau is the electrochemical counterpart of the inverted region for intermolecular and intramolecular ET.

Turning back to the voltammetry of adsorbed species as a function of scan rate, the Butler−Volmer formalism predicts that, at scan rates well above k_0/f, the peaks should be asymmetric, with a steeper slope on the high-overpotential side (see the solid lines in Figure 5A). Using Marcus theory rather than Butler−Volmer equations, the fact that the ET rate levels off at high overvoltage makes the voltammetric peak more symmetrical at moderate scan rates and much broader when the scan rate is so fast that the peak separation approaches the reorganization energy (dashed lines in Figure 5A). Figure 5B demonstrates that only when the peak separation is greater than λ (in eV) does it becomes sensitive to λ. Bowden and co-workers have derived an analytical expression of the current−potential response in the irreversible limit.[87]

2.1.1.3.3. Confrontation with Experimental Results. Armstrong and co-workers have thoroughly discussed the application of the BV and Marcus models to the voltammetry of adsorbed proteins.[57,88] The nonidealities have been reviewed.[57,89] Distribution of reduction potentials,[60–62] spatial distribution of potentials within the electrode double layer,[90–96] and distribution of ET rate constants exhibited by redox centers in the layer[61,62,96–107] have all been suggested to account for nonideal peak widths or separations. In addition to linear scan voltammetry, stair case voltammetry,[108] square wave voltammetry[109] and Fourier transform voltammetric techniques[110–114] have also be used to evaluate interfacial electron transfer kinetics of adsorbed proteins. The latter are highly sensitive to nonidealities (including kinetic and thermodynamic dispersion).

For adsorbed redox proteins, reported values of k_0 vary greatly, from a few inverse seconds to 15000 s^{-1}, in which case the peaks remain visible at scan rates as high as 3000 V/s.[88,115] Needless to say, the situation of fast ET is more desirable if the focus is on studying biologically relevant processes rather than interfacial electrochemistry.

Since the reorganization energy is a parameter of great mechanistic significance, many strategies have been developed to estimate its value from the shape of the voltammetric response or from the dependence of the ET rate on E; this obviously requires examining transient currents obtained at an overvoltage that is high enough that the predictions of the Butler−Volmer and Marcus models differ significantly. However, a complication arises from the fact that the interfacial ET rate may be limited ("gated") by a process that is distinct from ET. In that case, the leveling off of the apparent ET rate may be incorrectly interpreted as the ET rate reaching the maximal value predicted by Marcus theory, and the reorganization energy may be greatly underestimated.[109,116–118] Related to this point is the dependence of k_0 on the distance between the redox site and the electrode. This has been often investigated by using cytochrome c adsorbed on self-assembled monolayers (SAMs) of carboxyl alkanethiol ($HS(CH_2)_nCOOH$). In most cases, the ET rate was found to decrease exponentially with the chain length for long chains ($n > 8$), whereas it plateaus at short lengths, suggesting a change in the rate limiting step.[116,118–127] Various interpretations have been proposed (see refs 24 and 127−129 for reviews). They often refer to protein dynamics, and of course, this is reminiscent of the gating processes evidenced in the case of intermolecular ET.[109,130–132]

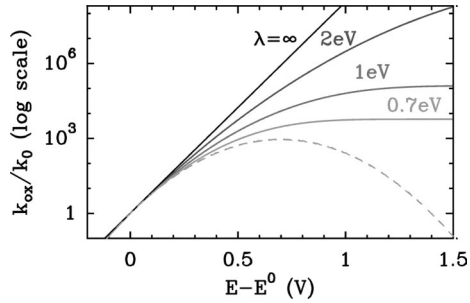

Figure 6. Dependence of the rate of interfacial, oxidative ET on the electrode potential according to the BV (black) or Marcus theory of interfacial ET for different values of the reorganization energy λ (solid gray lines). The dashed line is the traditional Marcus paraboloid with $\lambda = 0.7$ eV, showing the inverted region at high driving force. For interfacial ET, the rate levels off at a high driving force instead of decreasing.

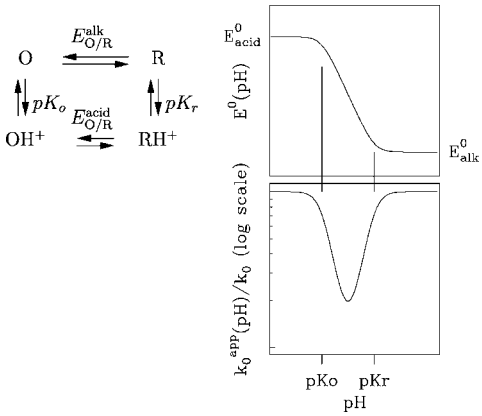

Figure 7. Square scheme depicting the protonation of species O and R with pK_a values as indicated. The right panels show how the apparent reduction potential (top panel and eq 14) and the apparent interfacial ET rate constant (bottom panel and eq 15) depend on pH when protonation and deprotonation are fast with respect to *vf*.

2.1.2. Chemical Processes Coupled to ET

By "coupling" we refer to a nonredox process which either is driven by or makes thermodynamically more favorable the electron transfer event. The most obvious example is protonation (since reduction will increase the pK_a of the redox site), but the coupled process may also be the binding or release of any ligand, including the substrate, product, or inhibitor of the enzyme, or even a conformational change. Fast coupled processes will influence the thermodynamics of the reaction by displacing the redox equilibrium, whereas slow steps may limit ("gate") the overall rate of the reaction. Of course, the important issue is not the chemistry being fast or slow in absolute terms, but rather fast or slow relative to the time scale of the voltammetric experiment[67] or, most importantly, of catalytic turnover (this will be discussed in section 2.2.4.2).

Coupled systems are discussed in terms of square schemes in which each oxidation state of a redox site exists in two chemically distinct forms. Hereafter, we consider the case of a protonation using the notations in Figure 7.

2.1.2.1. Fast Coupled Chemical Processes.

2.1.2.1.1. The Nernstian Regime. If interfacial ET and proton uptake and release are all fast with respect to *vf*, the *n*-electron O/R couple behaves like an uncomplicated electron transfer reaction with an apparent pH-dependent reduction potential given by

$$E^{app}_{O/R}(pH) = \underbrace{E^{alk}_{O/R} + \frac{1}{nf}\ln\frac{K_o}{K_r}}_{E^{acid}_{O/R}} + \frac{1}{2f}\ln\frac{[H^+]+K_r}{[H^+]+K_o} \quad (14)$$

The reduction potential tends to the limit $E^{acid}_{O/R}$ when the pH is below pK_o and pK_r, and it tends to $E^{alk}_{O/R}$ under alkaline conditions. In the intermediate pH range, the *n*-electron reduction of O is coupled to a protonation and the reduction potential decreases (at most) 2.3/*nf* per pH unit (Figure 7). This upper limit of the slope is reached only when the difference between pK_r and pK_o is large.

Of course, eq 14 can be used to interpret how a reduction potential depends on the concentration of a ligand other than the proton. Heering and co-workers used it to determine by protein film voltammetry the dissociation constants K_o and K_r from the oxaloacetate-concentration-dependent potential of the active site flavin in fumarate reductase.[66] This equation was also used for studying substrate binding to the redox center of an otherwise nonredox enzyme, e.g. the dinuclear Fe_2 site of porcine purple acid phosphatase[133] or the $[4Fe4S]^{3+/2+}$ of a DNA-repair enzyme called MUTY.[134]

2.1.2.1.2. Fast Coupled Processes and Slow Interfacial ET. In a series of papers starting with ref 135, Laviron has reported the theoretical study of surface electrochemical reactions coupled to protonations (this also applies to any ligand binding process) when the chemical steps are at equilibrium. The conclusion that will also be relevant to the interpretation of catalytic voltammograms hereafter is that the model described above for pure electron transfer still applies in that case, apart from the following differences: (1) the overvoltage is now defined with reference to the apparent reduction potential given by eq 14, and (2) from the peak splitting at fast scan rate and eq 10, an *apparent* k_0 can be defined, whose value is pH-dependent and smaller than the actual value in the pH-range where protonation is coupled to reduction; that is, pK_o < pH < pK_r (Figure 7, bottom):

$$\frac{k_0^{app}(pH)}{k_0} = \frac{1+\sqrt{\frac{K_o K_r}{[H^+]^2}}}{\sqrt{\left(1+\frac{K_o}{[H^+]}\right)\left(1+\frac{K_r}{[H^+]}\right)}} \quad (15)$$

(See eq 42 or 42a in ref 135, noting that in eq 42, the last two 1/2 exponents should read −1/2.) For a one-electron process, the minimum value of k_0^{app}/k_0 is reached when pH = (pK_o + pK_r)/2. The corresponding equations in the case of *two* coupled reactions (e.g. two protonations) are given in the appendix of ref 44 and in Laviron's papers. He has also examined a number of other cases, including the most complex two-electron/two-proton bicubic scheme (see ref 136 and references therein).

Direct experimental evidence for this effect comes from fast-scan PFV studies of ferredoxins. Figure 8 shows the so-called "trumpet plot" of peak positions against scan rate relative to the $[3Fe4S]^{+/0}$ couple of *Azotobacter vinelandii* ferredoxin I (AvfdI). At low scan rates, the peak positions can be used to measure the reduction potential of the couple, whose dependence on pH can be fit to eq 14 to demonstrate

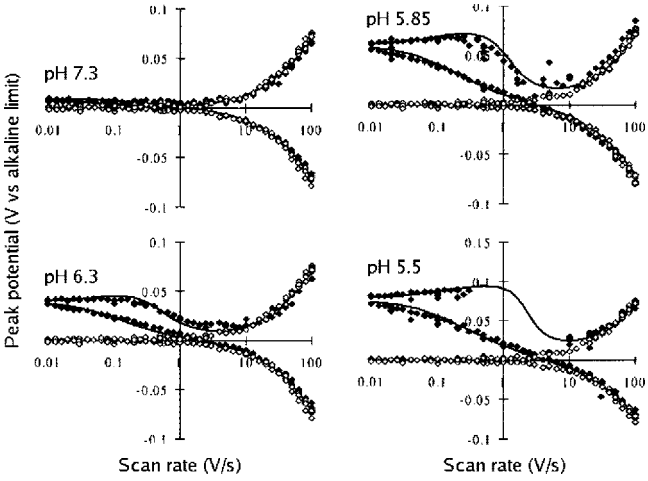

Figure 8. Positions of the oxidation and reduction peaks of the [3Fe4S] cluster of the D15N mutant of *Azotobacter vinelandii* ferredoxin I as a function of scan rate (log scale) for a range of different pH values (solid symbols). The peak positions are quoted in reference to the alkaline limit (data points at pH 8.35 shown as open symbols). Reprinted with permission from ref 137. Copyright 1998 American Chemical Society.

that reduction is coupled to protonation at pH below $pK_r = 6.9$. Figure 8 shows that, at moderate scan rates (e.g. $\log(\nu) < 0.1$), the peak separation is all the greater that the pH is low: the coupled protonation, even though it is fast on the voltammetric time scale, makes the apparent k_0 smaller, in agreement with eq 15 and Figure 7 (bottom).

2.1.2.2. Slow Chemical Processes. Figure 8 shows that, under acidic conditions and at high scan rates ($\log(\nu) > 0.1$), the trumpet plot of the $[3Fe4S]^{+/0}$ couple of AvFdI is highly distorted. This is because the protonation and deprotonation steps, which easily occur when the cluster is reduced and reoxidized at moderate scan rate, become slow on the voltammetric time scale when the scan rate is increased. At $pH < pK_r$, protonation is faster than deprotonation, and in the intermediate range of scan rates, protonation does proceed during the reductive scan, but the reoxidation is hindered ("gated") on the reverse scan by the deprotonation: the oxidative peak disappears. If the scan rate is so high that even the protonation is outrun during the reductive scan, uncoupling occurs: the voltammetric signature becomes identical to that obtained under alkaline conditions. This suggests that, by examining how the voltammetry depends on pH and scan rate, it is possible to measure the rate of (de)protonation of the center that gives rise to the peak, and indeed this strategy was extensively used for determining the rates and the mechanism of proton transfer to and from the buried $[3Fe4S]^{+/0}$ cluster in AvFdI.[137–139] This work was summarized in recent reviews (see e.g. refs 52 and 53). References 57, 109, and 140 include other examples of the use of noncatalytic fast scan voltammetry for scrutinizing redox-coupled reactions relevant to biological function. Regarding the theoretical modeling of the fast scan data, the case of $n = 1$ and $n = 2$ reversible surface electrochemical reactions followed by irreversible chemical reactions was addressed by Laviron in refs 65 and 67, but the data is usually fit using the numerical solution of the appropriate differential equations.[57,109,137–140]

Thus, in noncatalytic experiments, it is possible to explore continuously the limiting situations where ligand binding and release is effectively fast (at equilibrium) or too slow to occur (uncoupling) simply by changing the scan rate. For the catalytic case we shall discuss in section 2.2.4.2, coupled reactions affect the *steady state* voltammetric response, but whether they are effectively fast or slow depends on the time scale that is set by the intrinsic turnover rate of the enzyme.

2.2. Catalytic Voltammetry in the Absence of Mass Transport Control

For an adsorbed enzyme in the presence of its substrate, the redox state of the active site changes upon transforming the substrate into the product, and in a certain range of electrode potential, the electrode can substitute for the soluble redox cosubstrate (redox partner) by being able to regenerate the oxidation state of the enzyme. This results in an electron flow between the electrode and the substrate, *via* the active site and the chain of redox relays if there is one. This is measured as a current which is simply proportional to the product of the electroactive coverage and the turnover rate. The latter can be as high as thousands per second, resulting in a great amplification of the current, which can therefore be measured even when the electroactive coverage is too low to detect noncatalytic signals.

2.2.1. Transition from Noncatalytic to Pure Catalytic Regimes

Limoges and Savéant[141] have recently described the continuous transition from noncatalytic to catalytic voltammetry on the basis of a very simple scheme where a one-electron active site can be heterogeneously oxidized or reduced upon exchanging electrons with the electrode, and oxidizes the substrate with pseudo-first-order rate constant k_2. In this model, both interfacial electron transfer kinetics and mass transport are assumed to be fast (substrate depletion can be avoided by using hydrodynamic methods).

The theoretical treatment shows that the current is the sum of two contributions.[141] The first is the Nernstian noncatalytic signal whose magnitude is proportional to $\nu\Gamma$ (eq 1), while the second contribution arises from steady state catalysis, has a sigmoidal shape, and has a magnitude proportional to $k_2\Gamma$. The relative weight of the two contributions is given by the dimensionless parameter $\lambda = k_2/f\nu$, showing that an increase of turnover rate or a decrease of the scan rate has the same effect on the current potential response. Figure 9 shows that, starting from the reversible Nernstian behavior at low values of λ, reversibility is lost progressively as λ increases while the curve tends towards an S-shape. There is no trace of cathodic current above $\lambda = 1$, and the hysteresis resulting from the residual noncatalytic contribution vanishes for $\lambda > 10$.

The fact that the catalytic and noncatalytic contributions are additive suggested to the authors a convenient strategy for the treatment of experimental data, which consists of extracting the catalytic contribution from the total current by subtracting the noncatalytic response measured in the absence of substrate. Although the noncatalytic contribution is usually very small with respect to the catalytic current, the subtraction procedure is useful also because it removes the charging current. The author's second suggestion that the noncatalytic contribution be determined at fast scan rates (when $\lambda \rightarrow 0$), after appropriate normalization, may not be practical because the hypothesis of reversibility of ET is likely to fail when the scan rate is high enough to outrun catalysis (in other words, fast scan rates distort the noncatalytic data, Figure 5).

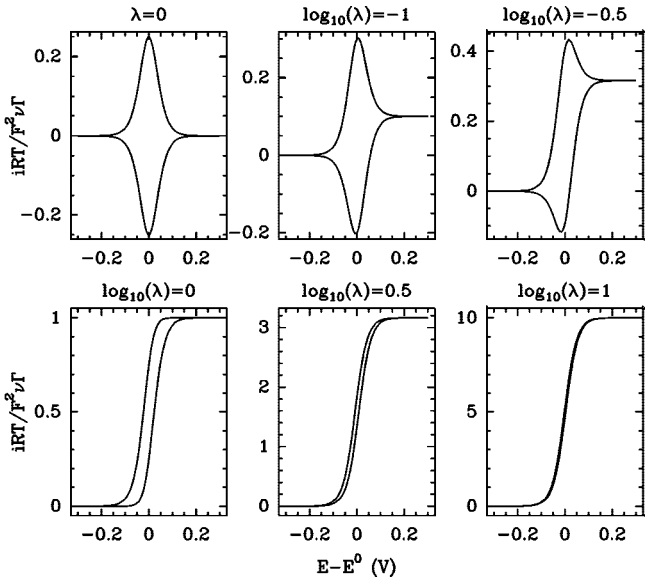

Figure 9. Dimensionless current−potential responses for increasing values of the kinetic parameter $\lambda = k_2/fv$, k_2 is the turnover rate of the enzyme under the most oxidizing conditions, and v is the scan rate. The charging current is omitted. Reprinted and adapted from Figure 4 in ref 141, Copyright 2004, with permission from Elsevier.

2.2.2. From Phenomenological Equations to Kinetic Models

Independently of the use of a model based on a reaction scheme, it is often useful to describe the catalytic signal by using phenomenological parameters which characterize the potential location and the steepness of the experimental signal. When the wave is approximately sigmoidal (S-shaped), it can be fit to

$$i = \frac{i_{\lim}}{1 + \exp[\pm n_{cat} f(E_{cat} - E)]} \quad (16)$$

or equivalently to a straight line of slope $\pm n_{cat}f/2.3$ in a Heyrovsky−Ilkovich plot of $\log_{10}((i_{\lim} - i)/i)$ against E.[47] (This plot is usually used in a different context, to analyze sigmoidal polarographic waves recorded under steady state *diffusion-limited* conditions:[142] for an n-electron electrochemical reaction that is reversible, i.e. the Nernst equation is obeyed at all times, the plot is linear with a slope $-nf/2.3$.) Alternatively to the use of the semilog transform, the catalytic voltammograms for an adsorbed enzyme can be differentiated; then E_{cat} is identified with the potential of the maximal derivative while the half-width of the derivative is equated to 89 mV/n_{cat}.[143] $i_{\lim}$ is the limiting value of the current that is reached on the plateau, at high driving force.

E_{cat} is called "enzyme potential" or "catalytic potential"[158] or "operating potential."[144,145] Typical "n-values" are in the range 1−2; the greater n_{cat}, the steeper the sigmoid. When the wave shape is not sigmoidal (as often occurs, see e.g. Figure 2), the results may be analyzed with current equations designed *ad hoc* by combining sigmoidal functions,[39,146–150] in which case the features of the voltammograms are characterized with potentials and n-values. For example, a voltammogram like that in Figure 2B may be characterized by the values of E_{cat} and E_{sw} (the potentials of the main wave and of the "switch"); the values of n_{cat} and n_{sw}, which define the steepness of the voltammetric features; and the ratio $i_{peak}/i_{\lim}$, which defines the decrease of activity observed at low potential.

In this approach, the relation between E_{cat} and n_{cat} and the properties of the enzyme remains unclear. The n-value is sometimes said to correspond to the number of electrons in the rate-determining step[147,151] and the pH dependence of E_{cat} is interpreted to deduce the electron/proton stoichiometry of this redox step. Over the last ten years, a number of theoretical models have been developed to give justification to eq 16 and physical meaning to the phenomenological parameters. Wave shapes much more complex than sigmoids have also been predicted by analyzing various kinetic schemes. These models will now be reviewed.

The turnover rate of a redox enzyme and its dependence on the various experimental parameters (including the electrode potential) are determined by a number of steps which may be explicitly included in a kinetic scheme:

1. *Interfacial Electron Transfer.* This occurs between the metallic electrode (including graphite; the case of a semiconducting material will not be treated here) and either the enzyme active site or the redox site that is the closest to the electrode. The rate of interfacial ET depends on the efficiency of the electronic coupling between the electrode and this redox site (section 2.1.1.3.2). This is the only step whose rate depends on the electrode potential, and this dependence is strong (exponential at low driving force), in contrast with the no-more-than-linear relation between rate and species concentration in homogeneous kinetics (the rate of oxidation or reduction of the enzyme by its soluble redox partner changes from first to zeroth-order kinetics as the concentration of cosubstrate increases).[46] This difference is one of the fundamental reasons more information can be gained from PFV studies than in homogeneous kinetics.

2. *Intramolecular Electron Transfer.* In the case of multicenter enzymes, electrons are transferred from the exposed redox center to the active site along an often linear chain of redox relays. This occurs in a succession of steps whose first-order rates depend on the reduction potentials of the relays, their electronic coupling, and the reorganization energy of the redox processes.[82,83] This is usually claimed to be fast[152,153] (but see below, sections 2.2.6 and 3.3).

3. *Redox Transformations of the Active Site.* This is the catalytic redox chemistry *per se*. The active site alternates between oxidized and reduced redox states as a consequence of the antagonist ET to/from the substrate and the electrode.

4. *Coupled Chemical Steps.* Electron transfer to the active site is often coupled to chemical steps, including (de)protonation(s) and binding and release of substrate and product. These steps are likely to affect the reduction potential of the active site; they may also be slow.

5. *Mass Transport.* An effect that is not relevant to homogeneous kinetics is the transport of substrate from the bulk of the electrochemical cell to the electrode surface where the enzyme is immobilized, and the diffusion of product away from the electrode. If mass transport is rate limiting, it can mask or distort important features of the signal.

It has been supposed that the above processes give additive contributions in an equation analogous to the expression of the conductance of resistors connected in series:[12]

$$\frac{1}{i} \approx \frac{1}{i_{ET}} + \frac{1}{i_{cat}} + \frac{1}{i_{Lev}} + \ldots \quad (17)$$

This equation shows that, in order to learn about the mechanism, a key issue is to arrange that the current−potential response reflects the inherent properties of the enzyme by avoiding rate limitations by mass transport and interfacial electron transfer.

Unfortunately, not all kinetic models support eq 17: only in limiting situations are the contributions of the factors we listed additive; they often interfere to give a particular shape to the current−potential response. Including all the effects we have enumerated in a single model and current equation would not be practical because the number of adjustable parameters would become too large for an unambiguous determination of all. Instead, we shall start by describing the catalytic response in the case of a minimal catalytic scheme and we elaborate step by step by including successively (and simultaneously whenever possible) the contributions of interfacial ET, intramolecular ET, substrate binding, *etc.* We shall first consider that mass transport is fast enough that the substrate concentration at the electrode surface always equals that in the bulk. This makes it possible to derive exact and meaningful closed-form expressions of the steady state current−potential responses even for relatively complex schemes and to factorize the numerous parameters (rate constants and reduction potentials) into a smaller number of apparent parameters; from an operational point of view, this decreases greatly the number of parameters that need to be adjusted to fit the data. In contrast, when mass transport must be accounted for, numerical analysis is often required and this somehow blurs the physical meaning of the rate equations; we discuss the effect of rate determining mass transport in section 2.3.

Theoretical models relevant to adsorbed electrocatalysts were first proposed in the early 1980s for polymer coated electrodes with attached redox systems (section 2.3.2) and only in the mid 1990s[37,154] for adsorbed enzymes. The important difference is that only in the latter case is it considered that a catalyst−substrate complex must form before the transformation of the substrate occurs with first-order kinetics. In contrast, former models of "catalytic electrodes" assumed bimolecular reaction between catalyst and substrate and will be relevant to enzyme electrochemistry only for $s < K_m$ (s is the concentration of substrate). Another difference is that, in the case of redox polymer electrodes, "electron diffusion" within the multilayer of catalyst may limit the current;[155] this has no counterpart when redox enzymes are directly connected to electrodes. The odd wave shapes seen in Figure 2 have not been observed for adsorbed synthetic catalysts, and this called for examining more complex kinetic schemes.

Our most important conclusion will be that since the catalytic current is proportional to the concentration of the active-site state that is competent to transform the substrate, in many cases the voltammogram can be thought of as a titration curve of this species. Therefore, in the steady state, whether the concentrations of redox species are close to equilibrium (if turnover is very slow) or not, modeling the voltammograms returns reduction potentials of the enzyme at the temperature of the experiment, for given pH and substrate concentrations. However, it will appear that these reduction potentials are only *apparent* values which can depart from the true equilibrium reduction potentials of the active site for a number of reasons, which we shall examine below.

2.2.3. The Basic Model

From now on and until section 2.4, we shall focus on steady state oxidative catalysis. We concentrate on two-electron reactions, since this is the general case, although important counterexamples exist, including the four-electron conversion between oxygen and water by cytochrome *c* oxidase and photosystem II.[26] We split the catalytic cycle into two halves. In an oxidative half-cycle, two successive one-electron transfers from the active site to the cosubstrate (the electrode in our case) oxidize the active site to a state that is competent to perform the two-electron oxidation of the substrate. This occurs in flavoenzymes for example, where the flavin exists in the redox states quinone (oxidized), semiquinone (intermediate or half reduced), and quinol (reduced) or in mononuclear molybdoenzymes where the Mo active site cycles between redox states VI, V, and IV. In NiFe hydrogenases in contrast, the dinuclear active site cluster is believed to consist of Fe^{2+} throughout the catalytic cycle while the Ni ion alternates between redox states 3+ and 2+; hence, the active site cannot accumulate the two "holes" (positive charges) required to oxidize di-hydrogen; in that case, it is meaningful to consider the entire enzyme−substrate complex, which can indeed accumulate two electrons, from the most reduced $Ni^{2+}Fe^{2+}H_2$ to the two-electron oxidized $Ni^{2+}Fe^{2+}2H^+$, *via* the half-reduced form, formally $Ni^{3+}Fe^{2+}H^+H^-$.

Scheme 2. Schemes Used for Modeling Oxidative Catalysis

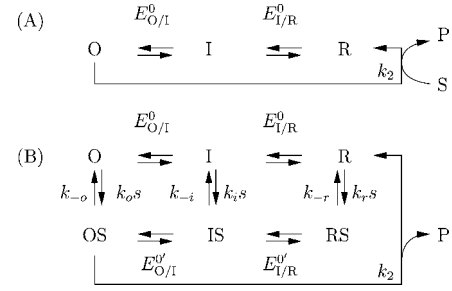

O, I, and R are the three redox states of the active site, which can bind substrate S and transform it into product P.

Therefore, the minimal catalytic cycle includes the three redox states of the active site, as shown in Scheme 2A. We depict as horizontal arrows the redox transformations between the three redox states (O, I, and R). The oxidized active site is transformed into R with a first-order rate constant k_2, which incorporates substrate binding and transformation and product release. For now, we will keep quiet about substrate diffusion from the bulk of the electrochemical cell to the electrode surface.

If the chemical steps described by k_2 are much slower than electron transfers, the redox equilibria are not displaced by the turnover; thus, the concentration of oxidized active site is simply related to the electrode potential and to the values of $E^0_{O/I}$ and $E^0_{O/R}$ by the Nernst equation. The activity is proportional to the concentration of O and increases from naught at low electrode potential to a limiting value i_{lim} at high driving force according to[36]

$$i = \frac{i_{lim}}{1 + \exp[f(E^0_{O/I} - E)] + \exp[2f(E^0_{O/R} - E)]} \quad (18a)$$

$$i_{lim} = 2FA\Gamma k_2 \quad (18b)$$

The divisor of eq 18a is a Nernstian contribution whose meaning is straightforward: a catalytic current appears when the electrode potential is high enough that the oxidized form of the active site is formed. The catalytic signal given by eq 18 is plotted in Figure 10A for different values of $E^0_{O/I} - E^0_{I/R}$. If $E^0_{O/I} \ll E^0_{I/R}$; that is, if the half reduced state of the active site disproportionates, the catalytic wave is steep ($n_{cat} \approx 2$ in eq 16) and centered on $E_{cat} = E^0_{O/R}$ (dotted line). If the half reduced state is

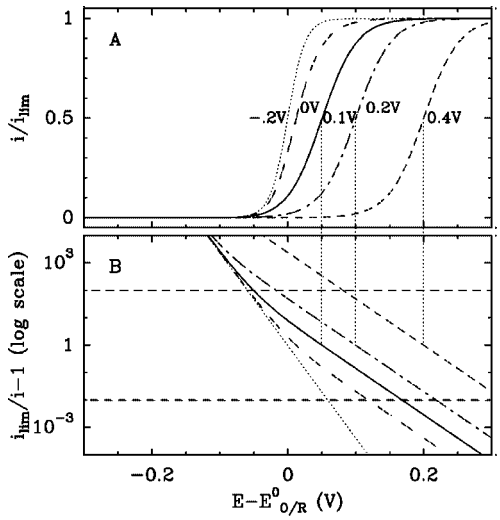

Figure 10. Effect of the thermodynamic stability of the half-reduced state of the active site on the shape and potential location of the catalytic wave according to Scheme 2A and eq 18a. In the Heyrovsky−Ilkovich plot (panel B), horizontal dashed lines indicate the range that is experimentally accessible. The values of $E^0_{O/I} - E^0_{I/R}$ are the same as those in Figure 3B.

thermodynamically stable ($E^0_{O/I} > E^0_{O/R}$), since no catalysis occurs until the electrode potential is high enough that state I can be oxidized into O, the wave is centered on $E^0_{O/I}$ and has an $n_{cat} = 1$ shape. For intermediate situations ($E^0_{O/I} \approx E^0_{I/R}$), eq 18 cannot be identified to eq 16, with the wave being steeper at the onset of catalysis (low driving force) than when closer to the plateau. Forcing the fit to a pure sigmoid returns *n*-values between one and two, whereas using eq 18 requires adjusting just as many parameters and returns the two reduction potentials of the active site.

These very simple considerations somehow restrain the validity of the statement according to which the *n*-value of the wave reveals the number of electrons transfered in the rate-limiting step. Here, n_{cat} reflects the redox thermodynamics at the active site, but it is not related to the reaction that sets the rate constant k_2 and the limiting current. See, however, section 2.2.6.

For this type of signal, a useful representation is the Heyrovsky−Ilkovich plot of $\log_{10}((i_{lim} - i)/i)$ against E (Figure 10B, and for a reductive process Figure 4 in ref 37). According to eq 18, the semilogarithmic transform of the catalytic wave reveals a crossover between two limiting behaviors

$$\log_{10}\left(\frac{i_{lim}}{i} - 1\right) \approx \begin{cases} \dfrac{f}{2.3}(E^0_{O/I} - E) & \text{at high potential,} \\ \dfrac{2f}{2.3}(E^0_{O/R} - E) & \text{at low potential,} \end{cases} \tag{19}$$

From a practical point of view, the data is mostly affected by the baseline subtraction process when *i* is close to either naught or i_{lim}, making the semilog transform highly unreliable for $|\log_{10}[(i_{lim}/i) - 1]| \gtrsim 2$. Hence, the transition between $n = 1$ and $n = 2$ can be detected in experiments only if $E^0_{O/I}$ is close enough to $E^0_{O/R}$. For an example, see Figure 3B in ref 36.

2.2.4. Substrate Binding and Release

We now start expanding the catalytic scheme by considering substrate binding with the dissociation constants K_o, K_i, and K_r (vertical arrows in Scheme 2B). The substrate-bound,

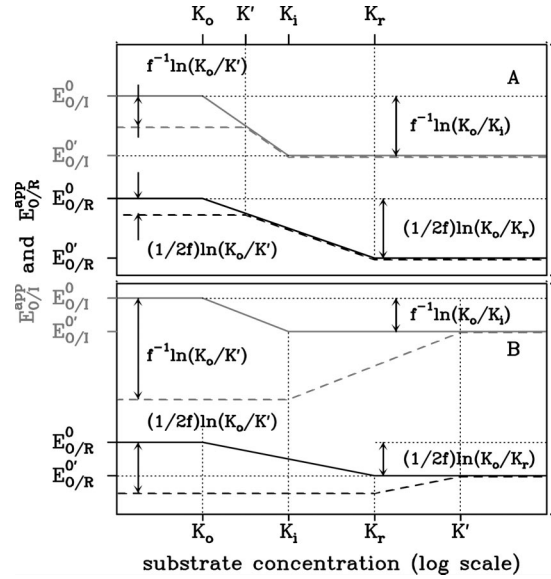

Figure 11. Pourbaix-like diagrams showing the concentration dependences of $E^{app}_{O/I}$ (gray) and $E^{app}_{O/R}$ (black) in the case $K_o < K_i < K_r$; *s* increases from left to right on a logarithmic scale. This is for oxidative catalysis; the corresponding diagram for a reduction can be found in ref 156. The solid lines illustrate the expected behavior when substrate binding/release is at equilibrium (eq 21). The dashed lines show the behaviors predicted by eq 23. Panel A illustrates the case where k_2 is small enough that K' is only slightly greater than K_o. Panel B illustrates the case $K_o \ll K'$. We chose $\alpha_i = \alpha_r = 1$ (so that the distinction in eq 23 is irrelevant and $K_m = K'$). Adapted with permission from ref 156. Copyright 2007 American Chemical Society.

oxidized active site OS is transformed into R with a first-order rate constant k_2, which incorporates substrate transformation and product release. The reduction potential of the substrate-bound OS/IS couple is given by $E^{0'}_{O/I} = E^0_{O/I} + f^{-1} \ln(K_o/K_i)$. A similar relation holds for $E^{0'}_{I/R}$.

2.2.4.1. Substrate Binding/Release at Equilibrium in the Steady state. We will first consider the situation in which the binding and release steps are fast relative to reactions within the enzyme−substrate complex (k_2) so that despite the fact that the system is driven out of equilibrium, the ratios of populations of substrate-bound and substrate-free species simply obey the mass action law (e.g. $\Gamma_{OS}/\Gamma_O = s/K_o$, where *s* is the substrate concentration).

In this case, the current equation takes the same form as eq 18, but eq 18b is replaced with

$$i_{lim} = \frac{2FA\Gamma k_2}{1 + K_o/s} \tag{20}$$

that is, the limiting current follows Michaelis−Menten kinetics with $K_m = K_o$, and the reduction potentials of the active site in the divisor of eq 18a take apparent substrate concentration dependent values according to

$$E^{app}_{O/I} = \underbrace{E^0{}_{O/I} + \frac{1}{f}\ln\frac{K_o}{K_i}}_{E^{0'}_{O/I}} + \frac{1}{f}\ln\frac{s + K_i}{s + K_o} \tag{21a}$$

$$E^{app}_{O/R} = \underbrace{E^0{}_{O/R} + \frac{1}{2f}\ln\frac{K_o}{K_r}}_{E^{0'}_{O/R}} + \frac{1}{2f}\ln\frac{s + K_r}{s + K_o} \tag{21b}$$

(solid lines in Figure 11).

This model suggests that eq 18a can still be used to analyze the voltammograms; for each set of experimental conditions, only three adjustable parameters need to be adjusted to fit the wave: i_{lim}, $E^{app}_{O/I}$, and $E^{app}_{O/R}$. The substrate concentration dependence of these parameters allows the dissociation constants to be measured using eqs 21, and the value of the dissociation constant from the oxidized active site can be independently determined from the concentration dependence of the limiting current (eq 20). See ref 36 for an illustration of this strategy.

Therefore, provided the above equilibrium hypotheses apply, the position of the catalytic wave and its dependence on substrate concentration and pH can be interpreted as simply as the position of a noncatalytic signal (eq 14) to learn about the thermodynamics of the chemical processes (substrate binding and protonations) that are coupled to the redox transformations of the active site.

2.2.4.2. Departure from Equilibrium. To allow for slow coupled chemistry in Scheme 2B, we explicitly introduce substrate binding steps with pseudo-first-order rate constants $k_o s$, $k_i s$, and $k_r s$ and substrate release with first-order rate constants k_{-o}, k_{-i}, and k_{-r}. These rates relate to dissociation constants in a straightforward manner, $K_o = k_{-o}/k_o$, etc., but equilibrium is no longer assumed.

As demonstrated in ref 156, the activity increases from naught at low electrode potential to a limiting value i_{lim} at high driving force according to

$$i_{lim} = \frac{2FA\Gamma k_2}{1 + K_m/s} \tag{22a}$$

$$K_m = \frac{k_2 + k_{-o}}{k_o} = K_o\left(1 + \frac{k_2}{k_{-o}}\right) \tag{22b}$$

$$\frac{i}{i_{lim}} = g\left(E, s, A\Gamma, E^0_{O/I}, E^0_{I/R}, k_2, k_o, K_o, k_i, K_i, k_r, K_r\right) \tag{22c}$$

The function g gives the dependence of i on the experimental parameters s, E, and $A\Gamma$ and on the nine independent parameters in Scheme 2B; it is given in the Supporting Information of ref 156 (eq S3), where we use the notation $\alpha_i = k_i/k_o$ and $\alpha_r = k_r/k_o$.

Figure 12 illustrates the variety of wave shapes that can be calculated from eq 22, all of which have already been observed in various contexts (Figure 2). At low driving force, the current increases in a sigmoidal manner toward a first plateau or peak (dashed lines). Depending on the values of the parameters, additional features can occur at higher driving force; panel B shows a "switch," panel C shows a "boost," and the voltammogram in panel D exhibits both. Each feature may be fit to a sigmoidal function with an apparent number of electrons ranging from one to two, although each part of theses waves need not be exactly sigmoidal.

At high driving force and under saturating conditions, the activity tends to a value i_{lim} that is proportional to k_2 (this is because binding steps no longer limit the turnover rate when $s \rightarrow \infty$), and the Michaelis constant takes a very usual form (eq 22b).[46] From eqs 22a and b, it is clear that the magnitude of the limiting current may be used to determine K_m and k_2 (provided the electroactive coverage $A\Gamma$ is known) but that it contains little information about the catalytic cycle. In contrast, the shape and the position of the catalytic signal are very sensitive to the entire sequence of events which defines the catalytic reductive half-cycle in Scheme 2B and to the thermodynamic properties (reduction potentials and dissociation constants) of some of the intermediates.

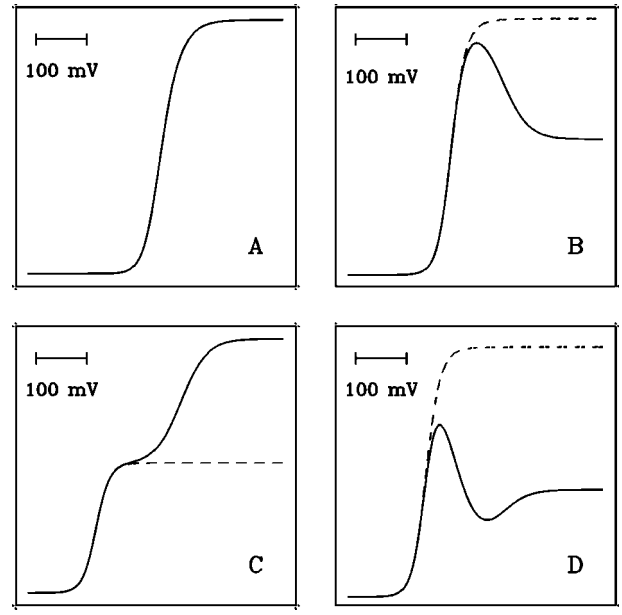

Figure 12. Examples of steady state catalytic voltammograms calculated from eq 22 (solid lines). The dashed lines correspond to the approximation given by eq 23. Adapted with permission from ref 156. Copyright 2007 American Chemical Society.

We have shown[156] that an approximate equation obtained from eq 22 by taking the low-driving-force limit often describes accurately the *entire* wave shape when the latter is sigmoidal (i.e. when the wave has no "switch" nor "boost"; see for example Figure 12A). This current equation, which we plot using dashed lines in Figure 12, is given by

$$i = \frac{i'}{1 + \exp[f(E^{app}_{O/I} - E)] + \exp[2f(E^{app}_{O/R} - E)]} \tag{23a}$$

$$i' = \frac{2FA\Gamma k_2}{1 + K'/s} \tag{23b}$$

$$E^{app}_{O/I} = E^0_{O/I} + \frac{1}{f}\ln\frac{K_o}{K_i} + \frac{1}{f}\ln\frac{s + K_i}{s + K'} \tag{23c}$$

$$E^{app}_{O/R} = E^0_{O/R} + \frac{1}{2f}\ln\frac{K_o}{K_r} + \frac{1}{2f}\ln\frac{s + K_r}{s + K'} \tag{23d}$$

$$K' = \frac{K_m + (\alpha - 1)K_o}{\alpha} = K_o\left(1 + \frac{k_2}{\alpha k_{-o}}\right) \tag{23e}$$

$$\delta = \exp[f(E^0_{I/R} - E^0_{O/I})] \tag{23f}$$

$$\alpha = \begin{cases} \alpha_i = k_i/k_o & \text{if } \delta \ll 1 \\ \alpha_r = k_r/k_o & \text{if } \delta \gg 1 \end{cases} \tag{23g}$$

(The equation which applies in the case of reductive catalysis can be found in ref 156.) Note that a small (respectively large) value of δ corresponds to the situation where the half-reduced state of the active site is thermodynamically stable (respectively unstable). As a guideline, the n-value of the wave is more likely to approach 1 when δ is small (*cf.* the discussion of eq 18a), in which case the apparent value of $E_{O/I}$ is a

function of α_i (not α_r), whereas if δ is large, K' in eq 23 depends on α_r.

When substrate transformation is slow with respect to substrate dissociation (strictly, when $k_2 \ll k_{-o}$ and $k_2 \ll \alpha k_{-o}$), both K_m and K' tend to K_o (*cf.* eqs 22b and 23e). In this limit where substrate binding is at equilibrium in the steady state, indicated by solid lines in Figure 11, eqs 20 and 21 apply and the model in section 2.2.4.1 is recovered.

In the general case, eq 23c shows that $E_{O/I}^{app}$ tends to $E_{O/I}^{0'}$ (the reduction potential of the O/I couple when the active site is bound to substrate, defined in eq 21a) when *s* is larger than both K' and K_i. Remarkably, at low substrate concentration, the position of the one-electron wave tends to a limit which departs from the reduction potential of the substrate-free active site (dashed lines in Figure 11). Even when *s* is smaller than both K' and K_i, $E_{O/I}^{app}$ remains shifted from $E_{O/I}^{0}$ by an amount $f^{-1}\ln[K_o/K'] = -f^{-1}\ln[1 + k_2/(\alpha k_{-o})]$, which tends to zero only if substrate release is very fast. The reasoning is similar for the position of the two-electron wave.

This has an important consequence regarding the qualitative interpretation of the position of a catalytic wave for an adsorbed enzyme: even at the lowest substrate concentrations, the value of E_{cat} cannot always be interpreted as the reduction potential of the substrate-free active site. This is in contrast with the prediction of eq 21, which is based on the assumption of fast substrate binding and release.

Equations 23c and d only differ from eqs 21a and b in that K' substitutes for K_o, and this implies that, by examining the substrate concentration dependence of the apparent reduction potentials determined from fitting the data to eq 18a, one may mistake K' for the dissociation constant K_o. This will remind enzymologists of a familiar situation, whereby the Michaelien dependence of activity on concentration can be used to determine a K_m value which, strictly speaking, cannot be identified with K_o (eq 22b). Equations similar to eqs 21 are used to interpret the pH dependences of the position of the wave,[36,157] and our remarks above also apply: the apparent acidity constants determined under turnover conditions will equate the equilibrium values only if (de)protonation steps are fast on the time scale of turnover.

2.2.4.3. Nonsigmoidal Wave Shapes Resulting from the Rates of Substrate Binding Being Dependent on the Redox State of the Active Site. The fact that Scheme 2B may predict wave shapes that are far from being sigmoidal (Figure 12) was first anticipated in a study of *E. coli* DMSO reductase,[39] and this explanation has been generalized and applied to several other enzymes.[41,42,158–160] The parallel between Figures 2 and 12 is intentional, although we do not claim that the model we have just described could explain both the wave shapes in Figure 2B, D, and E and how they depend on substrate concentration.

In ref 156, there was no attempt to delimit the various behaviors predicted by eq 22c in the parameter space. However, it is clear that the wave shape can only be "simple", as in Figure 12A, if the binding rates obey $k_i = k_r = k_o$ or $k_i = k_r = 0$. We could also derive a simple necessary (but not sufficient) condition for the wave to exhibit at high driving force a sigmoidal attenuation of activity with $n_{switch} = 1$:

$$\underbrace{k_i/k_o}_{\alpha_i} > \underbrace{1 + \frac{K_o}{K_i}\frac{s + K_i}{K_m - K_o}}_{\alpha_i^{min}} \qquad (24)$$

(An equation similar to eq 24 can be derived for a hypothetical two-electron switch.)[156] From eq 24, we conclude that there can be no one-electron switch unless $\alpha_i > 1$. Equation 24 also predicts that, for a given value of α_i, the switch should disappear when *s* exceeds a certain value. This is a consequence in our model of the rates of binding being proportional to *s* and increasing as *s* is raised until k_2 fully limits turnover. However, we note that the substrate concentration that makes α_i^{min} greater than α_i is not simply related to K_m and can be high if substrate binding is slow on the time scale of turnover (this increases the difference between K_m and K_o; see eq 22b).

Of course, it may not be practical to fit voltammetric data by adjusting the *ten* parameters in eq 22. Reference 156 illustrates how, in a particular case, the rate equation could be greatly simplified by examining the substrate concentration dependence of the features of the wave, leading to an unambiguous determination of a subset of parameters (Figure 46 below).

2.2.5. Slow Interfacial ET Kinetics

So far we have implicitly assumed that all ET steps are very fast, so that the electron exchange between the active site and the electrode is Nernstian. We shall now explore situations where this assumption fails as a consequence of either interfacial or intramolecular ET being slow (sections 2.2.5 and 2.2.6, respectively).

2.2.5.1. Effect of Slow Interfacial ET Kinetics in the Absence of Coupled Processes. To examine the effect of interfacial ET kinetics on the wave shape, we first return to the simple catalytic cycle in Scheme 2A, which disregards substrate binding, and we no longer assume Nernstian equilibrium. We note k_{OI} and k_{IO} the rate constants that relate to electrochemical oxidation of I and reduction of O, respectively ($k_{OI}/k_{IO} = \exp(f(E_{O/I}^0 - E))$), and similarly for the I/R transformation. The catalytic current equates $2FA\Gamma k_2$ times the steady state concentration of species O and reads[37]

$$\frac{i_{lim}}{i} = 1 + \frac{k_{OI}}{k_{IO}}\left(1 + \frac{k_{IR}}{k_{RI}}\right) + k_2\left(\frac{1}{k_{RI}} + \frac{1}{k_{IO}}\left[1 + \frac{k_{IR}}{k_{RI}}\right]\right) \qquad (25)$$

If the rate constants depend on *E* as predicted by the Butler−Volmer (BV) formalism (eqs 9), the current equation becomes[157]

$$\frac{i_{lim}}{i} = a + b \qquad (26a)$$

$$a = 1 + \exp[f(E_{O/I}^0 - E)] + \exp[2f(E_{O/R}^0 - E)] \qquad (26b)$$

$$b = \frac{k_2}{k_0^{O/I}}\exp\left[\frac{f}{2}(E_{O/I}^0 - E)\right](1 + \exp[f(E_{I/R}^0 - E)]) + \frac{k_2}{k_0^{I/R}}\exp\left[\frac{f}{2}(E_{I/R}^0 - E)\right] \qquad (26c)$$

$$i_{lim} = 2FA\Gamma k_2 \qquad (26d)$$

This is a function of the following five independent parameters: $E_{O/I}^0$, $E_{O/R}^0$, $k_2/k_0^{O/I}$, $k_2/k_0^{I/R}$, and the limiting current.

In the Nernstian limit $k_2/k_0 \to 0$, the term *b* approaches zero (eq 26c) and eq 18 is recovered. Otherwise, the four

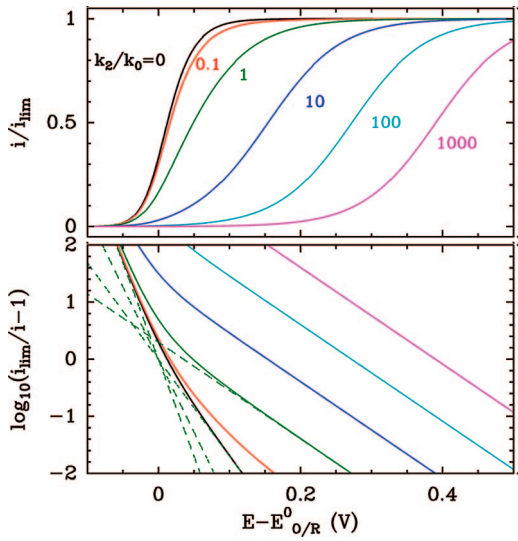

Figure 13. Plot of i/i_{lim} given by eq 26, for increasing values of k_2/k_0: 0 (black); 0.1 (red); 1 (green); 10 (dark blue); 100 (turquoise); 1000 (magenta). We chose $E^0_{O/I} = E^0_{I/R}$ and $k_0^{O/I} = k_0^{I/R}$. For the green curve ($k_2/k_0 = 1$), dashed lines indicate the four contributions in eqs 26b and c.

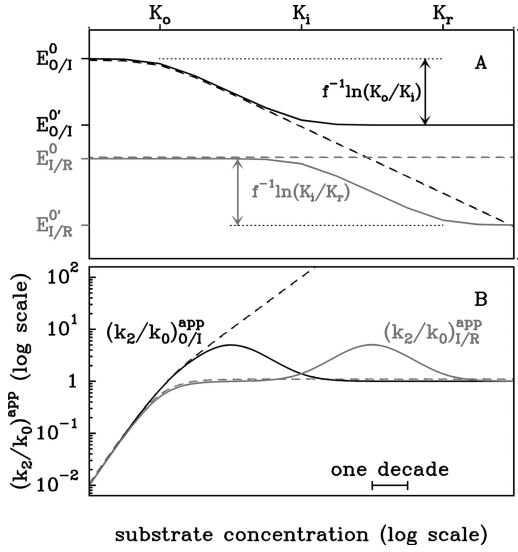

Figure 14. Apparent values of E^0 and $(k_2/k_0)^{app}$ given by eqs 21 and 28, respectively, for the O/I and I/R couples of the active site (black and gray lines, respectively), illustrating the effect of allowing substrate binding to all three redox states of the active site (solid lines) or only to the oxidized form (dashed lines). In the former case, the three dissociation constants are indicated along the top X axis; in the latter, K_o is the same but K_i and K_r were set to ∞.

terms in eq 26b and c will contribute with slopes of 1, 2, 1.5, and 0.5f/2.3, respectively, in the Heyrovsky−Ilkovich plot of the wave (Figure 13). The terms with lower n values contribute increasingly when the driving force increases, so that the i against E curve is a sigmoidal wave which broadens at high electrode potential (see e.g. the green line in Figure 13A). The terms $n = {}^3/_2$ and $n = {}^1/_2$ reveal the deviation from Nernstian equilibrium which results from the steady state competition between the reduction of the active site, with rate k_2, and its reoxidation following interfacial ET, with a rate that is proportional to k_0; hence, the greater k_2/k_0, the more the steady state concentrations of species depart from their equilibrium values, and the broader the wave.

The irreversible limit at large k_2/k_0 was discussed in ref 37 (see Figure 5 therein). The dominant term in eq 26 is of the form $k_2/k_0 \exp[(f/2)(E_1 - E)]$, where E_1 is the greater of $E^0_{O/I}$ and $E^0_{I/R}$, and the $n_{cat} = {}^1/_2$ wave is centered on

$$E_{cat} = E_1 + (2/f)\ln(k_2/k_0) \qquad (27)$$

When this limit is reached, increasing k_2/k_0 further produces no further broadening, with the irreversible wave being only shifted to higher driving force by the ET limitation (Figure 13). This is reminiscent of the prediction related to noncatalytic voltammetry in the irreversible limit at fast scan rate, where the peak width becomes independent of scan rate and the peak potential is proportional to $\ln(fv/k_0)$ (eq 10 in section 2.1.1.3).

As a rule, in order for the electrochemical data to depend on the properties of interfacial ET, the system must be driven away from equilibrium; this is usually achieved by using transient techniques, such as fast-scan cyclic voltammetry or chronoamperometry. Here we show that *steady state* data can reveal the properties of interfacial ET because the catalytic reaction competes continuously with the redox transformation of the active site following electron transfer. How distributed interfacial ET kinetics affects the wave shape will be described in section 2.2.5.4.

2.2.5.2. Conjunction of Fast Coupled Processes and Slow Interfacial ET Kinetics. Now consider again Scheme 2B, in which the species O, I, and R can bind substrate with dissociation constants K_o, K_i, and K_r, respectively. The reasoning is the same for protonation instead of substrate binding. Assuming that all binding steps are rapid so that equilibrium is maintained and that the ET kinetics is described by BV equations, it is shown in the appendix of ref 157 that the current equation takes the same form as eq 26 but with the following differences:

(i) the limiting current follows Michaelis−Menten kinetics with $K_m = K_o$ (eq 20),

(ii) the reduction potentials of the active site $E^0_{O/I}$ and $E^0_{I/R}$ are replaced with the apparent potentials $E^{app}_{O/I}$ and $E^{app}_{I/R}$ already defined in eqs 21 (solid lines in Figure 14A), and

(iii) less expectedly, the terms k_2/k_0 are replaced with $(k_2/k_0)^{app}$:

$$\left(\frac{k_2}{k_0^{I/R}}\right)^{app} = \frac{k_2\left/\left(1+\frac{K_o}{s}\right)\right.}{k_0^{I/R}} \times \frac{\sqrt{\left(1+\frac{K_i}{s}\right)\left(1+\frac{K_r}{s}\right)}}{1+\sqrt{\frac{K_r K_i}{s^2}}} \qquad (28a)$$

$$\left(\frac{k_2}{k_0^{O/I}}\right)^{app} = \frac{k_2\left/\left(1+\frac{K_o}{s}\right)\right.}{k_0^{O/I}} \times \frac{\sqrt{\left(1+\frac{K_o}{s}\right)\left(1+\frac{K_i}{s}\right)}}{1+\sqrt{\frac{K_o K_i}{s^2}}} \qquad (28b)$$

(solid lines in Figure 14B). Equations 28 show that two factors cause $(k_2/k_0)^{app}$ to depend on s:

(i) As in the simplest case of Scheme 2A, interfacial ET influences the shape of the wave when k_0 is small with respect to turnover number, but now, the turnover number depends on s, and k_0 must be compared with $k_2/[1 + (K_o/s)]$. As s decreases, the values of $(k_2/k_0)^{app}$ tend to zero and the Nernstian limit is recovered.

(ii) Another cause of substrate concentration dependence for $(k_2/k_0)^{app}$ comes from the second factors on the right-hand sides of eqs 28. This effect is the same as that predicted by Laviron[135] in the noncatalytic case where ligand binding at equilibrium decreases the apparent value of k_0 (eq 15 and Figure 7, bottom). In the case of the O/I couple for example, it increases the apparent value of $k_2/k_0^{O/I}$ when s is between K_o and K_i, that is when substrate binding is coupled to ET.

The important conclusion is that eq 26 can still be used to fit the voltammograms irrespective of whether substrate binds to one or several redox states of the active site, as long as substrate binding and release are fast enough that equilibrium is maintained; there are still five adjustable parameters [i_{lim}, two reduction potentials, and two $(k_2/k_0)^{app}$], but the concentration dependences of these parameters depend on (and inform of) the binding pattern.

2.2.5.3. The Peculiar Case of Substrate Binding to a Single Redox State of the Active Site. In contrast to Scheme 2B, it is most often assumed in the literature that substrate binding occurs only when the active site is in the redox state that is competent to transform the substrate (i.e. state O or R according to whether oxidative or reductive catalysis is considered).[37,158,161−163] Here we evaluate the consequences of this hypothesis on the predicted wave shape without prejudging whether this assumption applies.

In the framework of Scheme 2B, exclusive binding to state O is achieved by letting $k_i = k_r = 0$; hence, $K_r = K_i = \infty$. According to the discussion of eq 24, the shape is sigmoidal (monotonic) for all values of k_2. Using eqs 20, 21, 26, and 28, the following current equation is obtained:

$$\frac{i}{2FA\Gamma} = \frac{k_2}{1 + \frac{K_o}{s}a + \frac{k_2}{k_0}b} \tag{29a}$$

$$a = 1 + \exp[f(E^0_{O/I} - E)] + \exp[2f(E^0_{O/R} - E)] \tag{29b}$$

$$b = \exp\left[\frac{f}{2}(E^0_{I/R} - E)\right] + \exp\left[\frac{f}{2}(E^0_{O/I} - E)\right](1 + \exp[f(E^0_{I/R} - E)]) \tag{29c}$$

In this equation, k_2/k_0 and the reduction potentials are those at $s = 0$, and the only dependence on s is in the denominator of eq 29a. Equation 29 is equivalent to eq 4a in ref 37 (in the limit of fast mass transport, $L \to \infty$ and $Q = 1$ according to Heering's notations), eq 6b in ref 161, or eq 11 in ref 163.

If substrate binds only to the oxidized state of the active site, eqs 21 and 29 predict that the apparent reduction potentials of the active site should decrease for $s > K_o$, as indicated in Figure 14A. Unless k_2/k_0 can be neglected, the Nernstian contribution (the term a) is weighted by $1/s$ and vanishes at high s (resulting in eq 16 in ref 161): the wave becomes dominated by the $n = {}^1/_2$ and $n = {}^3/_2$ contributions and takes an irreversible shape. These two predictions are qualitatively different from the behavior predicted by the model which accounts for binding to more than one redox state of the active site.

In conclusion, although the hypothesis that substrate binds to a single redox state of the active site will sometimes apply, the analysis above shows that this assumption greatly restricts the substrate concentration dependence of the potential location and shape of the wave. Conversely, this assumption can be easily assessed by examining the manner in which the active site reduction potentials shift and the wave transforms upon varying substrate concentration. We are not aware of a case where this assumption was proved valid.

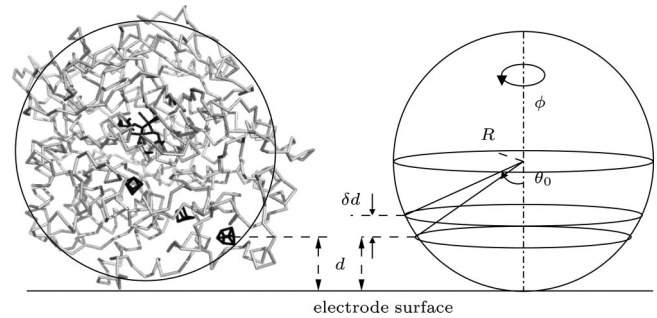

Figure 15. Geometric model used to calculate the probability density function of the distance between the surface-exposed redox relay and the electrode.

2.2.5.4. Distribution of Enzyme Orientations and of k_0 Values. All models above predict that a limiting current should be reached at moderate driving force. This is because Butler−Volmer equations make the rate of interfacial ET increase exponentially with the driving force; hence, the ET rate should eventually exceed the rate k_2 of substrate conversion by the enzyme−substrate complex. In the case of Marcus theory, the rate of interfacial ET starts to level off when the overpotential exceeds the reorganization energy of the reaction (Figure 6). Therefore, whatever the ET model, the catalytic current is expected to increase with overpotential at moderate driving force, until it reaches a limiting value. In contrast, a slope is often observed at high driving force (see e.g. Figures 2D and F).

Signals showing no strict limiting current have long been observed for redox processes involving an adsorbed catalyst at a rotating disk electrode (see ref 164 and references therein). To explain these observations, Jiang and Anson proposed a model based on a wide, Gaussian distribution of reduction potentials of the catalyst−substrate complex.[164] However, since the buried active site of an enzyme is located in a well-defined chemical environment, it should not be perturbed by the distant electrode and a wide distribution of active site reduction potentials is unlikely. Instead, the linear current−potential behavior at high driving force could be accounted for by considering the effect of disorder in the orientation of enzyme molecules adsorbed on the electrode: this introduces a distribution of tunneling distances d between the electrode and the surface-exposed relay, and hence a distribution of interfacial ET rate constants.[44]

In ref 44 the distribution of orientations was assumed to be such that, within a certain range of width d_0, all of the possible distances between the electrode surface and the exposed relay, which is the entry point for electrons in the enzyme, occur with a constant probability density:

$$p(d) = 1/d_0 \quad \text{for} \quad d \in [d_{min},\ d_{min} + d_0] \tag{30}$$

Although this is indeed the only probability density function that makes it possible to predict a linear relationship between i and E if Butler−Volmer kinetics is assumed (see below), eq 30 has not been given other justification than fruitfulness and simplicity. However, this kind of distribution can be inferred from geometrical considerations that are too simple to be concealed. Let us think of the globular enzyme as a sphere laying on a plane (the electrode surface) in a random orientation (Figure 15). On the surface of the sphere, a dot marks the

position of the surface-exposed cluster and its distance d to the electrode sets the electron tunneling rate. The probability that d will belong to the interval $[d, d + \delta d]$ is proportional to the area of the sphere included between these two altitudes. Using spherical coordinates, this area can be defined by $\varphi \in [0, 2\pi]$ and $\theta \in [\theta_0, \theta_0 + \delta\theta]$; θ_0 is the angle with the z axis ($\theta \in [0, \pi]$) defined by $R(1 - \cos\theta_0) = d$. The area is given by

$$A = 2\pi R^2 \sin\theta_0 \, \delta\theta \tag{31}$$

Using $R \sin\theta_0 \, \delta\theta = \delta d$, it turns out that the probability density function of d is actually *independent* of d:

$$p(d) = \frac{1}{2R} \tag{32}$$

This justifies eq 30. It is certainly not safe to assume that all the orientations of the enzymes have the same probability, but the conclusion is identical if the allowed orientations are restricted to a cone, for example, provided all these orientations are equally likely. This explains the observation[161] that the value of d_0 obtained from fitting the electrochemical data (see below) may be smaller than $2R$, the greatest characteristic length of the enzyme.

The distribution of k_0 values is obtained by combining the probability density function of d (eq 30) and the expected exponential dependence of k_0 on d

$$k_0(d) = k_0^{\max} \exp(-\beta d) \tag{33}$$

where $k_0^{\max} = k_0(d_{\min})$ and β is a decay constant the value of which is typically of the order of 1 Å^{-1}. This gives

$$p(k_0) = \begin{cases} (\beta d_0)^{-1} k_0^{-1} & \text{for } k_0 \in [k_0^{\min}, k_0^{\max}] \\ 0 & \text{for any other value} \end{cases} \tag{34}$$

with $k_0^{\min} = k_0^{\max} \exp(-\beta d_0)$. According to eq 34, the fact that the tunneling distances are equally likely results in the smallest k_0 values having the greatest likelihood, which is obviously very unfortunate.

The linear change in catalytic current at high driving force results from the contribution of enzyme molecules having low k_0 values with respect to the turnover rate k_2, which contribute only at high driving force (eq 27). Using the generic equation eq 26 with a single value of k_2/k_0 and apparent values of E^0, the current is easily integrated across all possible values of k_0 in the range $[k_0^{\min}, k_0^{\max}]$ (eq 34) to obtain the corrected current i^*, represented by[44]

$$i^* = \frac{i_{\lim}}{a}\left(1 + \frac{1}{\beta d_0} \ln \frac{a + (k_2/k_0^{\max})b}{a + (k_2/k_0^{\max})b \exp(\beta d_0)}\right) \tag{35}$$

In Figure 16A, the solid lines are plots of eq 35 in the case $E_{O/I}^{app} = E_{O/R}^{app} = E^0$. Panel A corresponds to $k_2/k_0^{\max} = 10$ and increasing values of βd_0 (from left to right). A large value of βd_0 corresponds to a distribution of tunneling distances that is wide with respect to β^{-1}. As βd_0 increases, the number of enzyme molecules having a small value of k_0 increases, and this results in a transition from a sigmoidal wave to a linear current response. If βd_0 is small, $k_0^{\min}$ is very close to $k_0^{\max}$, and the distribution of tunneling distances has no effect: the limiting case given by eq 26 is recovered. The distortion of the wave when $k_2/k_0^{\max}$ increases for a given value of βd_0 is illustrated in Figure 16B.

If the limiting current is not reached in the experimental range of electrode potential, eq 35 reduces to

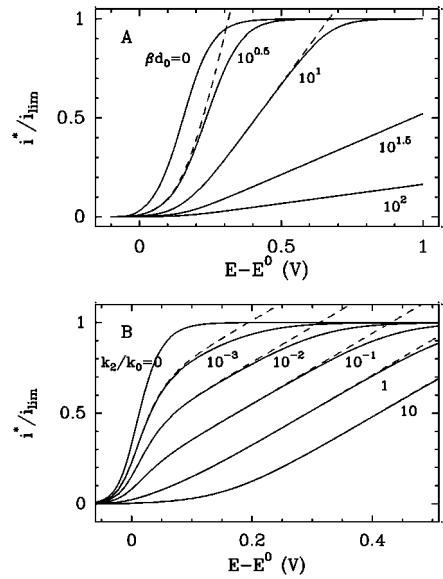

Figure 16. Steady state voltammograms calculated from eq 35 with $E_{O/I}^{app} = E_{O/R}^{app} = E^0$ (solid lines), and approximations given by eq 36 (dashed lines) for $E_{O/I}^0 = E_{I/R}^0 = E^0$. Panel A: $k_2/k_0^{\max} = 10^1$ and βd_0 increasing from left to right as indicated. Panel B: $\beta d_0 = 10$ and $k_2/k_0^{\max}$ increasing from from left to right, starting from the limiting case $k_2/k_0 = 0$. Adapted with permission from ref 44. Copyright 2002 American Chemical Society.

$$i^* \approx \frac{i_{\lim}}{\beta d_0 a} \ln \frac{a + b}{b} \tag{36}$$

(dashed lines in Figure 16). Remarkably, this current equation, which can be used to fit the entire wave shape, does not contain more adjustable parameters than when the enzyme is adsorbed in a single orientation (compare with eq 26). The slope of the linear part of the voltammogram is

$$\partial i^* / \partial E = \frac{i_{\lim}}{\beta d_0} \frac{F}{2RT} \tag{37}$$

This shows that the high driving force slope of the voltammogram is proportional to the limiting current. But whereas the limiting current cannot always be measured from the data, the slope can, and the change in slope against pH or substrate concentration can be fit to determine acidity and Michaelis constants, for example. See the studies of catalytic proton reduction and hydrogen oxidation,[157] arsenite oxidation,[165] or nitrate reduction.[166]

This model is simple enough that the distribution of interfacial ET rates can be simply included in any rate equation that is based on BV equations. See for example the work in ref 167, where a one-electron reaction is considered and the signal is assumed to reflect the contributions from three different subpopulations of enzymes, with each being characterized by a distribution of k_0 values. In refs 158 and 161, mass transport is also considered in addition to the above distribution of ET rates.

Whatever current equation is chosen to fit the data (eqs 18, 26, 35, and 36), it only matters that the signal is not too blurred by slow interfacial ET kinetics, so that the apparent reduction potential of the active site may be measured, since only these parameters are relevant to the mechanism, as illustrated above and further in section 2.2.6.

2.2.5.5. Marcus Theory Applied to Catalysis. The situation where direct ET between the electrode and the active

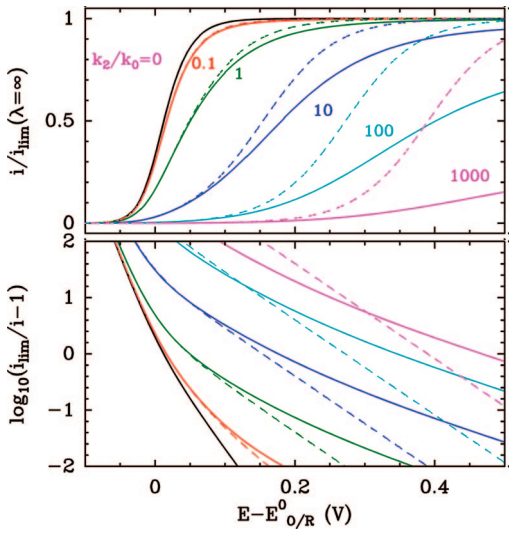

Figure 17. Plot of i/i_{lim} calculated using Marcus theory with $\lambda = 0.5$ eV (solid lines) or Butler−Volmer equations (dashed line, valid for $\lambda \rightarrow \infty$) for the same values of k_2/k_0 as in Figure 13. In the top panel, the current is normalized by $i_{lim}(\lambda=\infty) = 2FA\Gamma k_2$, whereas the true limiting current is used for calculating the semilog transforms in the bottom panel.

site is described by Marcus theory (section 2.1.1.3.2) was discussed by Heering and co-workers in ref 37. To predict the wave shape, they used eqs 13 and 25 to calculate the electrochemical rate constants from $E - E^0$, k_0, and λ. Figure 17 shows voltammograms calculated for the same k_2/k_0 values as in Figure 13, but using the Marcus equation with $\lambda = 0.5$ eV (see also Figure 6 in ref 37). As expected, the wave shape departs from that predicted using Butler−Volmer equations only in the potential range where the irreversible contribution ($n = {}^1/_2$) dominates.

Whereas noncatalytic studies have been confined to conditions (peak separation lower than reorganization energy) under which the models based on either BV or Marcus theory do not differ significantly, the catalytic wave shapes are often examined over a very large range of electrode potential. It would be interesting to examine how substituting Marcus for BV affects the wave shapes when the distribution of k_{max} values is accounted for.

2.2.6. Intramolecular ET Kinetics

When interfacial electron transfer kinetics was considered above, the overpotential was defined with respect to the reduction potential of the active site, implicitly assuming that electron transfer between the electrode and the active site was direct. This is not so in the case of multicenter enzymes, where the active site is connected to the electrode by a chain of redox relays (hemes, copper centers, or iron−sulfur clusters). We will now examine how intramolecular ET kinetics may transform the wave shape in the simplest case of an enzyme housing a single relay: first in the case where $k_0 \rightarrow \infty$ (section 2.2.6.1) and then permitting slow interfacial ET (section 2.2.6.2).

In order to explicitly consider intramolecular ET steps, the catalytic scheme must include all the redox states of the enzyme (the "microstates" defined in section 2.1.1.2) and the transitions between them. For example, enzymes such as chicken liver sulfite oxidase and flavocytochrome b_2 house a two-electron active site (Mo center or flavin, respectively) which is connected to a single one-electron relay (a heme in

Scheme 3. Catalytic Scheme Which Accounts for Intramolecular ET between a Two-Electron Active Site "A" and a Relay "R"[a]

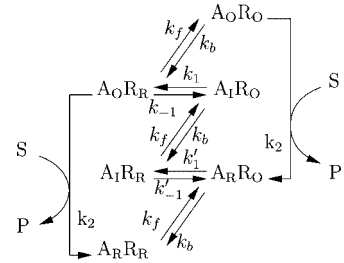

[a] Adapted with permission from ref 145. Copyright 2006 American Chemical Society.

both cases); these enzymes can exist in $3 \times 2 = 6$ redox states, as illustrated in Scheme 3, where again we omit substrate binding. The intramolecular electron exchange between the active site and the relay (the reduction potential of which we note as E^0_R) is described by the rate constants k_1, k_{-1}, k'_1, and k'_{-1}. Their ratios are set by thermodynamics:

$$K_1 = k_1/k_{-1} = \exp[f(E^0_R - E^0_{O/I})] \quad (38a)$$

$$K'_1 = k'_1/k'_{-1} = \exp[f(E^0_R - E^0_{I/R})] \quad (38b)$$

Here we consider a single value of E^0_R because we assume that there are no redox interactions between the active site and the relay. We also neglect the effect of substrate binding on the reduction potential of the active site.

2.2.6.1. Reversible Limit. In the case $k_0 \rightarrow \infty$, the resolution of the system of equations is rather simple, because Scheme 3 can be transformed into a simpler version that considers only three independent species which interconvert with potential-dependent rate constants. (Hence, the treatment in ref 37, which we criticized in footnote 52 of ref 145, was actually correct.) In this reversible limit, it is remarkable that the current equation for Scheme 3 is again exactly given by eq 18 but with two important differences:[145]

(i) i_{lim} equates $2FA\Gamma k_{cat}$ with

$$1/k_{cat} = 1/k_2 + \underbrace{1/k_1 + 1/k'_1}_{1/k_i} \quad (39)$$

(ii) the true reduction potentials of the active site are replaced with apparent reduction potentials which depend on the kinetics of intramolecular ET, and this dependence is surprisingly simple: it is merely governed by the ratio k_{cat}/k_i, where k_i is the slower of the two forward rate constants for intramolecular ET between the active site and the relay ($1/k_i = 1/k_1 + 1/k_1'$).

$$E^{app}_{O/I} = E^0_{O/I} + f^{-1} \ln\left(1 + \left[\exp\left(f\Delta E^{lim}_1\right) - 1\right]k_{cat}/k_i\right) \quad (40a)$$

$$\exp\left(f\Delta E^{lim}_1\right) = K_1\{1 + k'_1/[K'_1(k_1 + k'_1)]\} \quad (40b)$$

$$E^{app}_{O/R} = E^0_{O/R} + (2f)^{-1} \ln\left(1 + \left[\exp\left(2f\Delta E^{lim}_2\right) - 1\right]k_{cat}/k_i\right) \quad (40c)$$

$$\exp\left(2f\Delta E^{lim}_2\right) = K_1k_1'/(k_1 + k_1') \quad (40d)$$

The apparent reduction potentials of the active site are shifted by the amounts ΔE_1 and ΔE_2, which are at most equal to ΔE^{lim}_1 and ΔE^{lim}_2; the limiting situation corresponds to iET being fully rate limiting ($k_{cat} = k_i$). If intramolecular ET is

very fast, $k_{cat}/k_i \approx 0$; hence, $E^{app}_{O/I} = E^0_{O/I}$ and $E^{app}_{O/R} = E^0_{O/R}$: the redox chain merely mediates the driving force provided by the electrode and has no effect on the apparent reduction potentials of the active site. In contrast, when intramolecular ET is slow, the enzyme behaves as if the active site had apparent redox properties which depend on the reduction potentials of the relay.

The presence of the relay always increases the difference $E^{app}_{O/I} - E^{app}_{O/R}$ and thus tends to make the catalytic signal more closely resemble a one-electron wave.[145] When intramolecular ET is fully rate limiting, $n_{cat} = 1$, which is the number of electrons in the rate limiting step (and E_{cat} reveals the reduction potential of the "slow" relay). The converse is not true: observing $n_{cat} = 1$ does not imply that intramolecular ET is rate limiting.

For example, we will consider a simple situation where K_1' is large ($E^0_R > E^0_{I/R}$) and $E^0_{O/I} > E^0_{I/R}$; hence, $\exp(f\Delta E_1^{lim}) = K_1$. The position of the $n = 1$ wave is simply related to $E^0_{O/I}$, E^0_R, and k_{cat}/k_i according to

$$E^{app}_{O/I} = E^0_{O/I} + f^{-1} \ln\left(1 + \left[\exp\left(f\left(E^0_R - E^0_{O/I}\right)\right) - 1\right] \frac{k_{cat}}{k_i}\right) \quad (41)$$

Equation 41 is plotted against k_{cat}/k_i in Figure 18. When intramolecular ET is very fast ($k_{cat}/k_i \approx 0$), the wave is centered on the reduction potential of the active site ($E^{app}_{O/I} = E^0_{O/I}$), whereas, if intramolecular ET limits turnover ($k_{cat}/k_i \approx 1$), $E^0_{O/I}$ matches the reduction potential E^0_R of the relay. Ideally, in intermediate situations, the ratio k_{cat}/k_i may be deduced from the position of the catalytic wave.

The influence of intramolecular ET kinetics on E_{cat} described above is of a kinetic nature. Independently, redox interactions may exist between the relays in the enzyme (section 2.1.1.2), but this has neither been detected nor taken into account in an electrochemical model (see ref 168 for a treatment of how this affects light-driven intramolecular ET in the tetraheme subunit of the *R. viridis* reaction center).

Last, we note that an enzyme such as NiFe hydrogenase (Figure 1), which houses 3 relays, has $3 \times 2^3 = 24$ redox states, and has a rate equation much more complex than that above (unpublished results of ours). Complex I, with 9 relays, can exist in 1536 redox states! This makes clear that, regarding multicenter respiratory enzymes, calculating or measuring the individual rate constants for intramolecular ET from one center to the next is one thing, but combining these individual rate constants to determine the overall rate of turnover is quite another. The linear arrangement of the cofactors may suggest that the turnover rate can be obtained by summing reciprocal rate constants, whereas the complete kinetic scheme that incorporates all the redox states is highly interconnected and characterized by rate equations that are difficult to write down, not to mention factorize.

2.2.6.2. Effect of Slow Interfacial Electron Transfer Kinetics. Scheme 3, which takes into account intramolecular ET, was solved in ref 145 using the Butler−Volmer equations to describe the kinetics of interfacial ET between the electrode *and the relay*. Introducing slow interfacial kinetics can greatly disfigure the wave for some extreme values of the parameters (see Figure A1 in the appendix of ref 145); however, we believe that these extreme cases have not yet been observed in experiments. Our analysis suggested that, in *most* cases, the effect of slow interfacial ET kinetics is to broaden the wave in a way that is similar to introducing $n = {}^1/_2$ and $n = {}^3/_2$ contributions (eq 26). Once more, apparent values of k_2/k_0 can be defined; they are proportional to the true value of k_{cat}/k_0^R (k_0^R is the rate of ET between the electrode and the relay when $E = E^0_R$), but they also depend on the properties of the ET chain in a manner which is too complex to be usefully discussed here. We will simply conclude that for multicenter enzymes, although apparent values of k_2/k_0 will often need to be adjusted to fit the data, their physical meaning may not always be straightforward.

Most importantly, in both cases (fast or slow interfacial ET) it is as if the ET between the active site and the electrode were direct but the reduction potentials of the active site take apparent values that are modified by the presence of the redox chain if intramolecular ET limits turnover (eq 40).

2.2.7. Redox Activation and Inactivation

The catalytic signals sometimes exhibit very complex shapes (Figure 2). In Figure 12, we showed that this may result from the rates of substrate binding being dependent on the redox state of the active site, but other reasons have been put forward. For example, Heering and co-workers discussed the case of a hypothetical enzyme where two redox relays provide two parallel ET pathways to the active site; they show that the catalytic wave may consist of a main signal and a boost, each centered on the reduction potential of one of the relays.[37]

When the position of a boost or a switch happens to be close to the reduction potential of one of the redox sites in a multicenter enzyme, the voltammograms are sometimes modeled by assuming that the enzyme exists in two forms, characterized by distinct Michaelis parameters, for example, and whose reversible interconversion depends upon the redox state of a particular redox center. The current equation is obtained by combining the rate equations for each form of the enzyme, weighting each contribution by a Nernstian term

$$1/(1 + \exp(n_{sw} f(E - E_{sw}))) \quad (42)$$

where the switch potential is equated to the reduction potential of a certain center. This was done in studies of succinate dehydrogenase,[146–148] DMSO reductase,[39] nitrate reductase,[159] and the Fp subcomplex of Complex I.[158] The two rate equations that were combined came from either a kinetic[158] or a phenomenological [39,146–148,159] model (the latter being defined by an equation such as eq 16).

In addition to these examples where the voltammogram has a complex shape but remains in a steady state, there are cases where it exhibits a spectacular hysteresis. In the case of NiFe hydrogenase (Figure 19A/B), this results from the fact that the active site transforms into an inactive state during the potential sweep (see section 3.6 below). Departure from steady state can occur, provided inactivation is fast enough to proceed on the time scale of the experiment while reactivation is sufficiently slow. In ref 141, Limoges and Savéant have examined how reversible or irreversible inactivation affects the electrochemical response for the three distinct mechanisms depicted in Scheme 4. In all cases, they considered a one-electron active site (with reduction potential $E^0_{O/R}$), interfacial electron transfer in the Nernstian limit, and efficient mass transport of substrate. Their goal was to identify a mechanism that can reproduce the voltammograms in Figure 19A and B, which exhibit a decrease in activity on the scan to high potential and a recovery of activity on the reverse sweep, with a large hysteresis at high driving force.

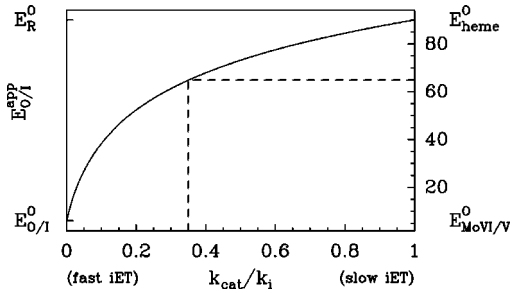

Figure 18. How the apparent reduction potential of the active site (and thus the position of the catalytic wave) depends on the kinetics of intramolecular ET (iET) in the case of an enzyme that houses a single relay,[145] whose reduction potential is E^0_R. This is a plot of eq 41 which is valid if $E^0_R > E^0_{I/R}$ and $E^0_{O/I} > E^0_{I/R}$. k_{cat} and k_i are defined in Scheme 3 and eq 39. The right labels illustrate the case of sulfite oxidase discussed in section 3.3.

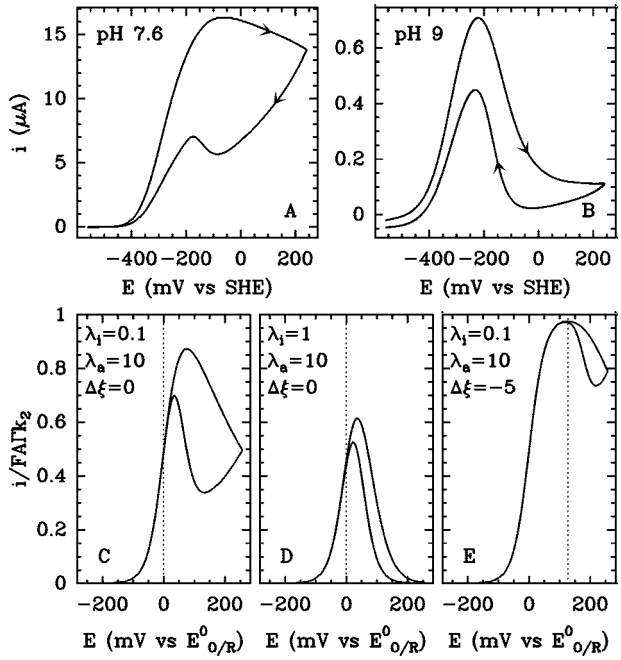

Figure 19. The top panels show hydrogen oxidation by *A. vinosum* NiFe hydrogenase at low scan rate and for two different values of the pH, as indicated.[43] The data were provided by Anne K. Jones.[45] The bottom panels illustrate the predictions of Scheme 4C, calculated from eqs 52−53 in ref 141. We denote by k_i and k_a the first-order rate constants of inactivation and reactivation, respectively, and $\lambda_{subscript} = k_{subscript}/f\nu$. The reactivation is preceded by a reduction step at E^0_a. $\Delta\xi = f(E^0_{O/R} - E^0_a)$. The dotted line indicates the value of E^0_a. Adapted with permission from ref 43, copyright 2003 American Chemical Society, and ref 141, copyright 2004 Elsevier.

Assuming that the oxidized form of the active site irreversibly inactivates in a first-order process with rate k_i (Scheme 4A), the voltammetry is found to be S-shaped and close to steady state when the scan rate is too fast for inactivation to occur ($k_i/f\nu \lesssim 10^{-2}$), whereas, at smaller scan rates, it shows a peak on the scan to high potential followed by a typical irreversible decrease on the reverse sweep (Figure 5 in ref 141).

If reversibility of the inactivation is allowed for (inactivation rate constant k_i, reactivation rate constant k_a, equilibrium constant $K = k_i/k_a$, Scheme 4B), the predicted wave shapes are similar, but steady state voltammetry is now observed when the activation and reactivation processes are both either slow or fast on the voltammetric time scale. In the former situation, inactivation is too slow to proceed. In the latter,

Scheme 4. Catalytic Schemes Accounting for the Transformation of the Active Site into an Inactive State[a]

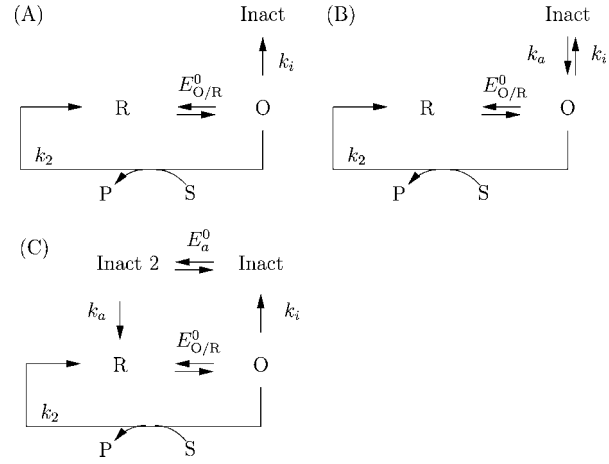

[a] According to Limoges and Savéant in Ref 141.

the inactivation/reactivation process is so fast that it merely acts as a coupled chemical equilibrium which pulls the oxidation of the active site and shifts the position of the wave to lower driving force by an amount $-f^{-1}\ln(1 + K)$ and decreases the limiting current by a factor of $(1 + K)$ (Figure 6, lower panels, in ref 141).

Last, the authors examined a model called "chemical inactivation/redox reactivation", where the active site, after it is oxidized at $E = E^0_{O/R}$, irreversibly transforms into an inactive state with a first-order rate constant k_i; the inactive state can be reduced at $E = E^0_a$ and then gives back the reduced form of the active site with a rate constant k_a (Scheme 4C). Only this model could predict voltammograms showing a decrease in oxidative activity at high driving force, followed by reactivation during the reverse sweep (Figure 19C−E). This appears for selected values of the different parameters that govern the equations, showing that this behavior is a consequence of a subtle interplay between thermodynamics and kinetics.

In studies of the (in)activation chemistry of hydrogenases (section 3.6), signals such as those in Figures 19A and B are interpreted by equating the reduction potential of the reactivation process and the position of the inflection point on the scan to low potentials.[43,169−174] However, the signals in Figures 19C and D have been calculated for $E^0_{O/R} = E^0_a$ and clearly the location of the inflection point on the reverse scan is shifted from E^0_a; the location of the *peak* on the reverse scan seems to be a better indicator.[141] For both NiFe and FeFe hydrogenases, the reactivation potential is well above the catalytic potential, which in terms of the parameters in Scheme 4C translates into $\Delta\xi = f(E^0_{O/R} - E^0_a) < 0$, whereas only situations where $\Delta\xi \geq 0$ were examined in ref 141. Panel E shows a voltammogram calculated with $\Delta\xi = -5$. The shape is less similar to those experimentally observed, but this may be a mere consequence of interfacial ET kinetics and film loss being neglected in the model. Again, the inflection point is located above the value of E^0_a, which is indicated by a vertical dotted line. It will be important to understand why this model does not seem to support the way in which the experimental data is usually interpreted.

2.3. Effect of Mass Transport

The above analyses do not consider the substrate depletion near the electrode surface that results from its consumption

by the catalytic process. Unless mass transport is very efficient, the enzyme may experience a substrate concentration s_0 that is lower than that in the bulk, s_b, and the complexity arises from the fact that s_0 changes during the sweep. Two situations must be considered according to whether the electrode is stationary and mass transport occurs by diffusion only, or substrate supply to the electrode is hydrodynamically controlled, for example by rotating the electrode. The latter case is examined first because the voltammetry can remain in a steady state and it is therefore more easily described.

2.3.1. Rotating Disk Electrode

In a classical and popular configuration, the enzyme is adsorbed onto a rotating disk electrode whose spinning precludes the diffusion layer from indefinitely spreading. If the scan rate is low enough, the concentration profile in the depletion layer relaxes to a steady state at every electrode potential. That is not to say that spinning the electrode always removes the mass transport limitation: only at infinite electrode rotation rate or in the potential region where there is no activity does the enzyme experience a substrate concentration that is strictly equal to the bulk concentration.

To address the case of steady state mass transport being partly limiting, the usual treatment[37,53,161,158,163] uses the Levich equation[58]

$$i_{\mathrm{Lev}} = nFAm_0(s_b - s_0) \tag{43}$$

to relate the current corresponding to the flux of substrate toward the electrode to the substrate concentrations in the bulk (s_b) and on the electrode (s_0), and to the mass transport coefficient $m_0 = 0.62D^{2/3}\omega^{1/2}\nu^{-1/6}$; D is the substrate diffusion coefficient, ω the electrode rotation rate, and ν the kinematic viscosity. In the steady state, this current equates the rate of enzyme turnover, which is a function of E, s_0, and other parameters which characterize the catalytic mechanism.

$$i = f(E,\ s_0,\ \ldots) \tag{44}$$

One equates this current to the Levich equation to determine s_0, the value of which is substituted back in eq 44 to give the current as a function of the experimental parameter s_b.

This strategy assumes that steady state conditions apply. This assumption is easily assessed in experiments by checking that the catalytic signal is independent of scan rate (at slow enough scan rate) and/or scan direction.

2.3.1.1. Effect of Mass Transport on the Wave Shape in a Simple Case. Mass transport may affect not only the magnitude of the catalytic signal (i_{lim}) but also its *shape*, and although this was discussed in the literature in the context of kinetic schemes more complex than Scheme 2A,[37,53,158,161,162] we shall examine first a case where $E^{\mathrm{app}}_{\mathrm{O/R}}$ and $E^{\mathrm{app}}_{\mathrm{O/I}}$ do not depend on s_0, for example, the current equation for Scheme 2B (eqs 23) with $K_i = K_r = K'$ and k_2 small, so that the substrate concentration only appears in the Michaelian dependence of i_{lim} on s_0:

$$i_{\mathrm{lim}} = \frac{2FA\Gamma k_{\mathrm{cat}}}{1 + K_{\mathrm{m}}/s_0} \tag{45}$$

Straightforward manipulations give

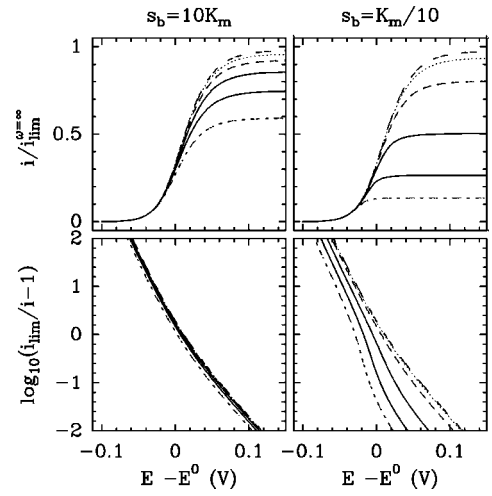

Figure 20. $i/i_{\mathrm{lim}}^{\omega=\infty}$ (top panels) and log transforms (bottom) obtained from eq 46 in two situations: $s_b = 10K_m$ (left) or $K_m/10$ (right), for different values of the parameter $m'_0 = m_0 s_b/\Gamma k_{\mathrm{cat}}$ that is proportional to $\sqrt{\omega}$ ($m'_0 = {}^1/_8$, ${}^1/_4$, ${}^1/_2$, 1, 2, and 4 in the direction of increasing current; this simulates a 1000-fold increase in ω). In both cases, we chose $E^{\mathrm{app}}_{\mathrm{O/I}} = E^{\mathrm{app}}_{\mathrm{O/R}}$.

$$\frac{i}{2FA\Gamma} = \frac{k_{\mathrm{cat}}/(1 + K_{\mathrm{m}}/s_0)}{a} \tag{46a}$$

$$a = 1 + \exp\left[f\left(E^0_{\mathrm{O/I}} - E\right)\right] + \exp\left[2f\left(E^0_{\mathrm{O/R}} - E\right)\right] \tag{46b}$$

$$s_0 = \frac{s_b}{2}\left[c + \sqrt{c^2 + 4K_{\mathrm{m}}/s_b}\right] \tag{46c}$$

$$c = 1 - \frac{K_{\mathrm{m}}}{s_b} - \frac{\Gamma k_{\mathrm{cat}}}{m_0 s_b}\frac{1}{a} \tag{46d}$$

The complexity arises from the dependence of c (hence s_0) on E *via* the term $1/a$ in eq 46d. Note that s_0 tends to s_b at high a (when there is no activity); what occurs on the plateau is discussed in section 2.3.1.3. Equation 46 is plotted in Figure 20 for s_b greater or lower than K_m (left and right panels, respectively) and for different values of a parameter that is proportional to $\omega^{1/2}s_b/\Gamma k_{\mathrm{cat}}$, using linear (top) and semilogarithmic (bottom) representations. As expected, the effect of slowing down the rotation rate is greater when the catalytic current is high (large Γk_{cat}) and the substrate concentration is small. When s_b is high with respect to K_m, the mere effect of decreasing ω is to decrease the limiting current but the wave shape is hardly modified. At low s_b, changing the rotation rate is more effective and modifies the wave shape: the signal is planed off in a way that sharpens strongly the wave in the high potential region (see the log transform in the lower right panel). See also the discussion of Figure 2 in ref 37.

2.3.1.2. More Realistic Models. The above approach can be applied to examine the effect of substrate depletion in the case of any rate equation giving the steady state current as a function of s_b. For example, Heering and co-workers treated a model where substrate binds only to the reduced form of the active site, and direct ET to the active site is modeled using Butler−Volmer equations.[37] Reda and Hirst recently extended this model to include a distribution of k_0 values. Their expression of the current reads[161]

$$\frac{i^*}{2FA\Gamma k_2} = \frac{1}{\beta d_0\left(1+\frac{K_m}{s_0}a\right)} \times \ln\left[\frac{\left(1+\frac{K_m}{s_0}a\right)k_0^{max}+k_2 b}{\left(1+\frac{K_m}{s_0}\right)k_0^{max}\exp(-\beta d_0)+k_2 b}\right] \quad (47)$$

This is equated to $2FAm_0(s_b - s_0)$ to solve for s_0, but since no analytical solution exists, it is necessary to obtain a numerical solution for each set of parameters being tested in the fitting procedure.

In ref 158, Hirst and co-workers derived two operational rate equations for reductive catalysis. The first one considers substrate binding to a single redox state of the active site (reduced, R) and Nernstian interconversion between two forms of the enzyme depending on the redox state of a redox center close to the active site. The second model assumes substrate binding to two different states of the active site (I and R). In both cases, BV equations are used to describe interfacial ET (no distribution is considered), steady state mass transport is accounted for, and the decrease in signal magnitude over time due to film denaturation or desorption is modeled as an exponential decay of Γ.

2.3.1.3. Effect of Mass Transport on the Plateau. The Koutecky−Levich analysis uses plots of reciprocal limiting current against $\omega^{-1/2}$ for a range of s_b, to linearly extrapolate the value of i_{lim} corresponding to s_b at infinite rotation rate. The data is then treated to determine K_m and Γk_{cat} either by nonlinear regression or by using the linear graphs that are familiar to enzymologists.[46] This strategy was applied to laccase,[1] fumarate reductase,[12] cytochrome-*c* peroxidase,[175] nitrite reductase,[149] and hydrogenase,[55,176] to cite but a few enzymes.

The Koutecky−Levich analysis is based on the following approximate expression:[12]

$$\frac{1}{i_{lim}(\omega)} = \underbrace{\frac{1+\frac{K_m}{s_b}}{nFA\Gamma k_{cat}}}_{1/i_{lim}^{\omega=\infty}} + \frac{1}{nFAm_0 s_b} \quad (48)$$

The validity of this equation can be assessed using eq 46 with $a = 1$ (high driving force limit), as discussed in refs 37 (particularly in footnote 14) and 161. This has broad interest because at high driving force the current becomes independent of E and E_{cat} and the dependence of the latter on s need not be explicit; hence, the only remaining hypothesis is that of Michaelien kinetics (eq 45). The equation for i_{lim} reads

$$i_{lim}(\omega) = 2FA\Gamma k_{cat}/(1 + K_m/s_0) \quad (49a)$$

$$s_0 = \frac{s_b}{2}\left[c + \sqrt{c^2 + \frac{4K_m}{s_b}}\right] \quad (49b)$$

$$c = 1 - \frac{K_m}{s_b} - \frac{\Gamma k_{cat}}{m_0 s_b} \quad (49c)$$

(this is equivalent to eqs 12 in ref 161).

The solid lines in Figure 21 show how $1/i_{lim}$ depends on $\Gamma k_{cat}/m_0 s_b$ (this is proportional to $1/(s_b\omega^{1/2})$ for several values of the ratio K_m/s_b. A clear deviation is observed from the predictions of eq 48 (dashed lines). The conclusion is that, by analyzing the data with the Koutecky−Levich model, one may overestimate n and D (particularly at high K_m/s_b and high ω) and the value of i_{lim} at infinite ω (particularly at low K_m/s_b and low ω). Thus, the plot of the extrapolated $i_{lim}^{\omega=\infty}$ against s_b may lead to overestimating K_m and k_{cat}.[37] However, from a practical point of view, one would expect the slow desorption of the enzyme over the course of the experiment to be the main obstacle to obtaining reliable values of the Michaelis parameters.

When mass transport cannot keep up with substrate depletion, that is in the limit where Γk_{cat} is greater than $m_0 s_b$, the last term in eq 49c dominates and the limiting current tends to $2FAm_0 s_b$: it becomes proportional to $s_b\omega^{1/2}$ and independent of Γk_{cat}. This extreme situation has been found in the case of NiFe hydrogenase, which exhibits extremely high activity when it is adsorbed at a graphite electrode (Figure 2 in ref 177).

Finally, we note that the electrode rotation rate may also influence the turnover rate if there is inhibition by the product, whose dispersal from the electrode surface is more efficient when the electrode is spun at higher rates. In that case, the slope of the Koutecky-Levich plot may exhibit a weak dependence on s_b, in contrast to eq 48. This was observed in the case of proton reduction by NiFe hydrogenase (see the discussion of Figure 3 in ref 157).

2.3.2. Stationary Electrode

When the electrode is not rotated, there is no theoretical limit to the spatial extension of the depletion layer, and this usually results in peak-shaped voltammograms showing a continuous decrease in current at high driving force. The current response is convoluted by the diffusion process which is not at steady state. This makes more difficult the analytical derivation of the current responses; hence, the kinetic schemes that have been examined are much simpler than those discussed above. From an operational point of view, the important conclusion below will be that, using a stationary electrode, the Michaelis constant can be only roughly estimated from the change in peak current against substrate concentration.

Most models were developed assuming one-electron catalysis and linear (as opposed to radial) diffusion of substrate (see, however, ref 178 for the case of radial diffusion to sparse clusters of enzyme molecules on the electrode surface). We have transposed the equations to the case of oxidative catalysis.

Andrieux and Savéant[179] assumed reversible (Nernstian) interfacial ET to/from the catalyst ($E^0_{O/R}$) and irreversible, *bimolecular* reaction with substrate (second-order rate constant k_2); the model was generalized to the case of reversible transformation (second-order backward rate constant k_{-2}) by Aoki and co-workers.[180] The current is shown to be the sum of two contributions, a substrate-concentration independent noncatalytic current given by $i_{Lav}^{n=1}$ (eq 18 in section 2.1) and a catalytic wave, the relative magnitude of which is governed by the kinetic parameter $\lambda = k_2\Gamma(Df\nu)^{-1/2}$. For small values of λ, when the reaction is so slow that no depletion occurs, the current is a steady state sigmoid centered on $E^0_{O/R}$ and tends to $i_{lim} = k_2 FA\Gamma s_b$ at high driving force. For large values of λ, the current is peak-shaped on the forward scan, with a typical diffusive trail at high driving force, and the peak current equates $i_p = 0.496FAs_b(Df\nu)^{1/2}$. The usual value of 0.446 (instead of 0.496) is obtained if reversibility is allowed

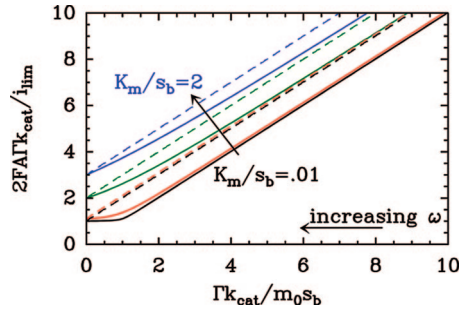

Figure 21. Plot of $2FA\Gamma k_{cat}/i_{lim}$ against $\Gamma k_{cat}/m_0 s_b$, according to eqs 49 (solid lines) and 48 (dashed lines), for different values of the parameter K_m/s_b: 0.01 (black), 0.1 (red), 1 (green), 2 (blue).

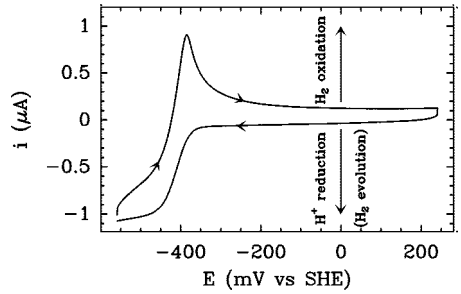

Figure 22. Proton reduction and hydrogen reoxidation by *A. vinosum* hydrogenase adsorbed at a stationary electrode under a nitrogen atmosphere. Reprinted with permission from ref 157. Copyright 2002 American Chemical Society.

($k_{-2} \neq 0$).[180] For $k_{-2} = 0$, the oxidative peak potential is $E_p = E^0_{O/R} + (0.78 - \ln \lambda)/f$.[179] The dependence on λ is weaker if reversibility is allowed, particularly for large values of λ (Figure 3 in ref 180).

The change from S- to peaked-shaped voltammetry upon increasing $\lambda = k_2\Gamma(Df\nu)^{-1/2}$ explains the weird shape of the signal in Figure 22, which comes from *A. vinosum* NiFe hydrogenase adsorbed at a stationary electrode and immersed into a solution initially *free* of hydrogen.[55,157] The negative current corresponds to proton reduction by the adsorbed enzyme; the hydrogen that is produced accumulates near the electrode surface and its catalytic reoxidation on the return scan results in the oxidative peak. The reductive signal is sigmoidal whereas hydrogen reoxidation is peak-shaped because the value of λ is much smaller for reductive than oxidative catalysis: this results from (i) the enzyme being about ten times less active for hydrogen production than hydrogen oxidation[157] and (ii) the diffusion coefficient of protons being about an order of magnitude greater than that of molecular hydrogen.

Xie and Anson have discussed the case where nonideal behavior is supposed to result in an apparent n value ($n_{app} > 1$) in the Nernst equation (see section 2.1.1.1; n_{app} is called g in Anson's paper).[63] They also considered the situation where ET is described by Butler−Volmer equations. The two main differences with the above Nernstian model are that (i) E_p now depends on s_b and the peak current increases with s_b more slowly than being proportional to s_b (unless irreversibility is reached) and (ii) it is no longer possible to obtain the catalytic current by subtracting the current measured with the catalyst in the absence of substrate from the total current measured in the presence of substrate.

In ref 154, Xie and Anson explicitly mention metalloenzymes and assume Michaelien kinetics: the competent form of the catalyst must bind substrate (second-order rate constant for binding k_o, first-order release k_{-o}, dissociation constant K_o) before transforming it in an irreversible step with first-order rate constant k_2 (the original notations are k_2, k_{-2}, $1/K_2$, and k_3, respectively). They show that for small values of s_b/K_o (effectively resulting in bimolecular kinetics) the behavior is the same as above except that k_2/K_o now substitutes for the former bimolecular rate constant k_2. For larger values of s_b/K_o and large values of the kinetic parameter $\lambda = (k_2/K_o)\Gamma(Df\nu)^{-1/2}$, the current remains proportional to s_b whereas, for moderate values of λ, the current levels off at higher s_b/K_o, revealing saturation of the catalyst−substrate complex. It was emphasized that whether binding is at equilibrium has little influence on the shape of the voltammetry (note that the complex wave shapes in Figure 12 are only expected if substrate binding is not at equilibrium *and* substrate binds to several redox states of the active site). No strategy was proposed to extract a Michaelis constant from the data.

Honeychurch and Bernhardt recently treated the similar situation where the enzyme is adsorbed on a stationary electrode using a fully numerical approach, assuming one-electron redox chemistry, BV kinetics, linear diffusion of substrate, and Michaelien behavior for the enzyme−substrate reaction.[181] Consistent with earlier work, they found that the mass-transport limitation results in a voltammogram that is peak-shaped on the forward scan at low concentration of substrate (when enzyme kinetics is bimolecular) and S-shaped on both the forward and reverse scan under saturating conditions (when the turnover rate is independent of substrate concentration); see Figure 2 in ref 181. They also emphasize that fitting the peak current as a function of bulk substrate concentration to the Michaelis−Menten equation overestimates the Michaelis constant, by a factor of two in their numerical example.[181] This is a simple consequence of the current being limited by mass transport only at $s_b < K_m$. Yet this strategy was sometimes used to get an estimate of K_m when the electrode cannot be rotated (Figures 4 in ref 182, 5 in 183, or 3 in 184).

2.4. Chronoamperometry at the Rotating Disk Electrode

A major advantage of PFV with respect to solution assays is that the activity can easily be sampled every fraction of a second, whereas in homogeneous kinetics the time scale of the measurement is of the order of several minutes. Hence, rapid changes in turnover rates can be resolved, complementing time-resolved spectroscopy experiments which can be used to trap intermediates on the millisecond time scale. This has two distinct applications.

(1) Time and potential dependent activation and inactivation processes can be probed in potential-step experiments where the activity is not at steady state. This yields information on the kinetics and energetics of the reactions involved. The analysis of these data is often straightforward and will be exemplified in section 3.6.

(2) A change in activity may also be induced by rapidly changing a concentration of substrate or inhibitor. The time-dependent catalytic response may be either very close to steady state if the enzyme quickly adapts to the new conditions or delayed by slow reactions whose rates can then be measured. The concentrations may be changed stepwise simply by adding in the electrochemical cell aliquots of concentrated solutions of substrate or inhibitor, or they may

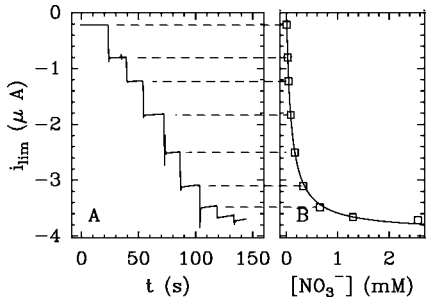

Figure 23. Chronoamperometric determination of the Michaelis constant for nitrate reduction by *R. sphaeroides* NapAB. The electrode was poised at −450 mV *vs* SHE, rotated at 2 krpm, and nitrate was added from stock solutions while the activity was continuously recorded as a current. In panel B, the change in current is fit to the Michaelis−Menten equation to determine K_m. Reprinted with permission from ref 156. Copyright 2007 American Chemical Society.

be progressively varied, in the case of gaseous substrates or inhibitors, by equilibrating the cell solution with different gas phases.

2.4.1. Stepwise Changes in Reactants Concentration

Figure 23 illustrates the simple chronoamperometric determination of a Michaelis constant from an experiment where the concentration of substrate was stepwise increased. The potential was chosen so that the current is measured on the plateau at high driving force, the electrode was spun at a high rate, and the change in i_{lim} against s_b was simply fit to the Michaelis−Menten equation in panel B; of course, the same approach can also be used in the case of non-Michaelien kinetics.[185] Importantly, the entire relation between activity and concentration is obtained in a couple of minutes; hence, the complications due to film desorption discussed in section 3.1.4 are minimized. This experiment may be repeated at different electrode potentials to determine the dependence of K_m on E (refs 42 and 186).

2.4.2. Continuous Changes in Reactants Concentration

A particular kind of experiment can be carried out with gaseous substrates or inhibitors, as the activity can then be monitored in a single chronoamperometric run where a slow and continuous change of substrate or inhibitor concentration against time results from the buffer composition spontaneously re-equilibrating with the atmosphere above the electrochemical cell.[187] This may occur after an aliquot of solution saturated with a certain gas has been injected in the cell or when a cell initially equilibrated with a certain atmosphere is progressively degassed.

The important point is that the modeling of these experiments is rather easy because the change in concentration against time happens to be exactly exponential (see the discussion of Figure 2 in ref 187). This is a straightforward and fortunate consequence of the equilibration process resulting from mass transport across the liquid/gas interface and the concentration in the gas phase above the cell being constant: the application of Fick's first law predicts that the change in concentration in the cell follows first-order kinetics.

For example, if the substrate gas, e.g. H_2, initially dissolved in concentration $s(0)$ is flushed away by bubbling argon in the cell at $t \geq t_0$, the time-dependent substrate concentration is $s(t) = s(0) \exp[-(t - t_0)/\tau]$ (Figure 24A). If Michaelis−Menten kinetics is obeyed, the activity evolves with time according to

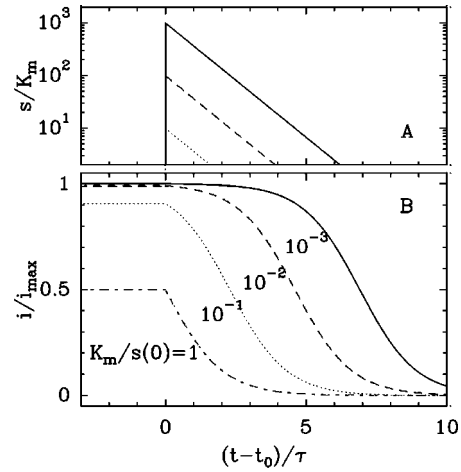

Figure 24. Plot of equation 50 for various values of $s(0)/K_m$.[187] An exponential decay of substrate concentration (panel A) results in a sigmoidal change in current (panel B).

$$i(t) = \frac{i^{max}}{1 + \frac{K_m}{s(0)} \exp\frac{t - t_0}{\tau}} \quad (50)$$

where i^{max} is the current extrapolated to infinite concentration of substrate. If $K_m/s(0) \gg 1$, the current decreases exponentially with time constant τ and not much information can be gained from it. If $K_m/s(0)$ is small, the substrate concentration may remain saturating long enough that i remains close to i^{max} for a little while, despite the fact that s is decreasing; in that case, the change in activity against time is a portion of a sigmoid (Figure 24B) and the value of $K_m/s(0)$ can be determined by fitting the data to eq 50. If $K_m/s(0) \ll 1$, $i(0)$ is close to i^{max} and $\log(K_m/s(0))$ can be determined from the intercept at $t = t_0$ of the semilog plot of $\log(i/i^{max} - 1)$ against t (Figure 3 in ref 187 or Figure S3 in ref 188). The value of t_0 must be precisely known, since an error Δt_0 makes the value of K_m wrong by a factor of $\exp(\Delta t_0/\tau)$. In contrast, the value of τ is adjusted in the fitting procedure and need not be known *a priori*.

In another kind of experiment, the substrate concentration may be kept constant, and an aliquot of solution saturated with a gaseous inhibitor may be injected in the cell at $t = t_0$. Hence, the concentration of inhibitor "I" decays according to $I(t) = I(0) \exp((t_0 - t)/\tau)$. In the following, we let $t_0 = 0$. Assuming bimolecular inhibition kinetics, the differential equation that describes the evolution of the concentration of enzyme in its active (inhibitor-free) form reads

$$\frac{d\Gamma_a(t)}{dt} = -k_i^{app} I(0) e^{-t/\tau} \Gamma_a(t) + k_a[1 - \Gamma_a(t)] \quad (51)$$

where k_i^{app} is the substrate concentration dependent (hence "apparent") second order rate constant of inhibition and k_a is the first-order rate constant for inhibitor release.

If inhibitor binding and release are fast, strictly if $k_i^{app} I(0)$ and k_a are both greater than $1/\tau$, the fraction of enzyme in the inhibited state continuously equilibrates with the inhibitor in solution, and the current changes with time according to

$$i(t) = \frac{i(0)}{1 + \frac{I(0)}{K_I^{app}} \exp\left(-\frac{t}{\tau}\right)} \quad (52)$$

and only the apparent inhibition constant $K_I^{app} = k_a/k_i^{app}$ can be measured. If inhibition is competitive, K_I^{app} is greater than the true inhibitor dissociation constant K_I:[187]

$$K_I^{app} = K_I(1 + s/K_m) \quad (53)$$

Hence, the competitive character of the inhibition process can be demonstrated by examining how K_I^{app} depends on s. This was exemplified by our study of CO inhibition of wild type NiFe hydrogenase,[187] further described in section 3.7.

In contrast, if $K_i^{app}I(0)$ and k_a are small, as occurs for inhibition by CO of both cytochrome *c* nitrite reductase[189] and certain mutants of NiFe hydrogenase (Figure 55 in section 3.7), the change in activity against time runs behind the change in inhibitor concentration; this delay embeds the information on the rate constants for inhibitor binding and release which can be determined by fitting the chrono-amperometric data to the general solution of eq 51, valid for all values of k_i and k_a:

$$\frac{i(t)}{i(0)} = e^{k_i^{app}I(0)\tau e^{-\frac{t}{\tau}} - k_a t}\left(e^{-k_i^{app}I(0)\tau} + \int_0^t k_a e^{-k_i^{app}I(0)\tau e^{-\frac{u}{\tau}} + k_a u}\, du\right) \quad (54)$$

If the inhibition is competitive, k_a should be independent of s while

$$k_i^{app} = \frac{k_i}{1 + s/K_m} \quad (55)$$

that is, a high concentration of substrate slows inhibitor binding (Figure 2C in ref 189).

The case of irreversible inhibition is simpler than when the inhibitor can be released, because eq 51 is replaced with

$$\frac{d\Gamma_a(t)}{dt} = -k_{inhib}(t)\,\Gamma_a(t) \quad (56)$$

In this equation, the pseudo-first-order rate of inhibition k_{inhib} may be time-dependent. Since the current is proportional to the instant value of $\Gamma_a(t)$, the data can be analyzed without making any assumption about $k_{inhib}(t)$ by transforming eq 56 into

$$k_{inhib}(t) = -\frac{d \log i(t)}{dt} \quad (57)$$

to obtain the instant rate of inhibition. For example, one may expect this rate of inhibition to decrease exponentially with time if the concentration of inhibitor does so and if the inhibition process is bimolecular. This will be illustrated in Figure 52, section 3.6 below. Again, the dependence of k_{inhib} on s may be used to determine whether inhibition is competitive.

3. Case Studies

3.1. Prelims

Redox enzymes are such complex systems that a combination of techniques must always be used to elucidate their mechanism. However, from crystallography to spectroscopy, none of the commonly implemented techniques is expected to be useful for *every* enzyme; PFV also has restrictive requirements. In a sense, it is quite similar to trying to understand the mechanism from a crystal structure: the first prerequisite is that the enzyme consents to adsorb or crystallize; the second is that the adsorbed or irradiated protein retains the native properties one is trying to study, so that the electrochemical or diffraction data actually tells us something about how the enzyme catalyzes its reaction under physiological conditions. Just as it is now recognized that intense X-ray irradiation can modify the protein structure or the redox states of the cofactors,[190,191] it is regrettable yet doubtless that not all published electrochemical data obtained with enzymes directly exchanging electrons with the electrode embed mechanistically relevant information. This somehow trivial warning is inappropriate if the goal is to *use* the wired-enzyme in some kind of electroanalytical device, for example as a biosensor[14] or as an electrode of a fuel cell,[17] in which case efficiency will be the only concern. Yet if the focus of the study is on mechanistic issues, care should be taken and ideally some proof should be given that, for each electrode material used, the enzyme mechanism is not altered by the immobilization. This will sometimes be laborious because PFV can provide information that is difficult to confirm with conventional techniques and, unfortunately, there is no single, simple criterion that can be used to unambiguously discriminate between trustworthy and suspect data. Yet it will often be possible to find and put forward some indications of the well-being (or otherwise) of the adsorbed enzyme before proceeding to interpret the results. This is illustrated below with the goal of providing both experimentalists and non-electrochemist readers with ways of assessing the relevance of the data. Later on, in sections 3.2–3.7, we shall discuss a number of examples taken from the literature, whose variety will demonstrate that direct electrochemistry of enzymes can be used for studying every aspect of the catalytic mechanism, including inter- and intramolecular electron transfers, active site chemistry and reactions with inhibitors, complex redox-linked modulations of activity, and even substrate channeling.

3.1.1. Attaching the Enzyme

Several methods have been proposed to attach enzymes to electrodes in a configuration that allows direct electron transfer and retention of activity (see refs 192−194 for recent reviews). Former studies carried out with smaller redox proteins obviously served as a great source of inspiration. The procedures were sometimes optimized to increase the film stability and/or to control the orientation of the enzyme, realizing that random binding may result in a larger number of enzyme molecules being either electrically disconnected or adsorbed in a conformation that blocks substrate access to the active site or does not favor fast interfacial electron transfer, with the resulting complications (signal broadening and shift to higher driving force) discussed in section 2.2.5.

3.1.1.1. Graphite Electrodes and Other Forms of Carbon. The simplest but also one of the most useful strategies, initially proposed and extensively used over the years in Armstrong's group, consists in adsorbing the enzyme onto a freshly polished pyrolytic graphite edge (PGE) electrode[195,196] either by repeatedly cycling the electrode in a dilute (≈1 μM) solution of enzyme or by painting the electrode with a very small amount (≈1 μL) of a more concentrated protein sample. The adsorption of negatively charged proteins may be favored by the inclusion of polyamines such as polymixin or neomycin, which promote the electrostatic electrode/

protein interaction. (We have observed that, under certain conditions, neomycin on graphite gives peaks that look like noncatalytic signals; control experiments with no protein should always be performed.) This simple strategy proved successful even for enzymes as large as *E. coli* membrane-bound DMSO[39] and nitrate[42] reductases, which consist of three subunits and which house seven redox centers in addition to a buried Mo active site; it is remarkable that, in either case, there was no evidence of broadening resulting from slow interfacial ET, suggesting that electron exchange is very fast on the time scale of turnover (Figures 44 and 45 below). The stability of the enzyme films varies greatly, from days in the best situations (see below an example with laccase) down to minutes in the case of DMSO reductase[39] or Complex II,[146] but PFV experiments can be quick enough that some mechanistic information is gained before the film falls off. From a very pragmatic point of view, there is no doubt that this somewhat blind strategy that consists in direct adsorption onto graphite has a very good track record.

When basal plane[197,114] or highly oriented[198] pyrolytic graphite (HOPG) is polished with emery paper and/or alumina, the structure of the interface should be rough and similar to that obtained with edge plane graphite. In the work of Taniguchi and co-workers, the HOPG surface was peeled off with adhesive tape to adsorb fructose dehydrogenase on a fresh basal-plane.[199] The rate of ET for the ferro/ferricyanide redox couple is much faster at edge-plane graphite than at basal-plane graphite;[200] this can be used to test the nature of the electrode surface and the presence of edge-plane defects.[114]

Glassy carbon was also used, although less frequently.[144,201,202] Gorton and co-workers tested the adsorption of various laccases on spectrographic graphite and HOPG.[203] Karyakin and co-workers have used electrodes based on carbon filament material and treated with sulfuric acid to adsorb hydrogenases.[204–206] Some recent reports concern the adsorption of arsenite oxidase[207] and xanthine oxidase[208] on carbon nanotube modified glassy carbon electrodes; other examples of direct electron transfer between enzymes and carbon nanotubes are cited in ref 209. Compton and co-workers have recommended that all electrochemical experiments where carbon-nanotube-modified electrodes are employed should be compared with PGE electrodes to rule out the possibility that electrocatalysis arises from the presence of metal impurities in the nanotubes.[210]

Laccases seem to form unstable films on pyrolytic graphite,[1,211] but Armstrong and co-workers recently investigated the adsorption of the enzyme from *Pycnoporus cinnabarinus* on a graphite surface modified by the covalent attachment of anthracene based units.[211] In laccase, the electrons provided by a phenolic substrate are transferred *via* a surface-exposed type-1 copper site to the trinuclear copper active site where reduction of oxygen occurs. The design of the electrode was aimed at orienting the enzyme for promoting fast electron transfer, by providing a surface which mimics the phenolic substrate. Their result was spectacular: the film retained high activity for weeks.

3.1.1.2. Bare Gold. Site-directed mutagenesis has been used to introduce cysteine residues on the surface of blue copper proteins (azurin and plastocyanin), thus facilitating protein chemisorption on unmodified gold.[212–215] When this strategy was used to promote direct ET to a surface cysteine mutant of *Alcaligenes faecalis* **copper-containing nitrite reductase**, only poor catalytic activity could be detected (although some noncatalytic signals were observed);[216] pyrolytic graphite edge eventually proved to be a better choice for studying this enzyme.[167,185] In contrast, **cytochrome c nitrite reductase** (ccNiR) retains activity when it is immobilized onto an *unmodified* Au(111) surface.[217] Heering and coworkers used the reactivity of two thiols present at the surface of a ferredoxin from *Pyroccocus furiosus* to directly immobilize the protein on a bare gold electrode, with an orientation such that the cluster is exposed to solution, providing an electrode surface with docking sites for the potential attachment of redox enzymes[218] (see section 3.1.1.7 below). Gorton and co-workers adsorbed tabacco **peroxidase**[219] and **laccase**[220] on gold electrodes previously polished chemically and/or electrochemically.

3.1.1.3. Modified Gold. Adsorption onto gold electrodes covered with self-assembled monolayers (SAMs) of alkanethiols is a strategy that was time-tested for small proteins: peptides, alkanethiols and MPA were used for promoting the adsorption on gold of azurin,[78,118,221–223] various cytochromes,[224,225] (see ref 226 for a review) and, somewhat less frequently, ferredoxins.[227] Similar strategies proved efficient for redox enzymes. Moura and co-workers adsorbed the **di-heme peroxidase** from *P. denitrificans* onto gold covered with dithiopyridine.[228] The **copper-containing nitrite reductase** (CuNiR) from *Achromobacter xylosoxidans* was immobilized by Ulstrup and co-workers onto a single-crystal Au(111) electrode surface modified with a self assembled monolayer of cysteamine[182] or methylbenzenethiol.[127] Recently, Heering and co-workers obtained reliable catalytic signals for NiFe **hydrogenase** adsorbed at a gold electrode covered with polymyxin.[230] Gorton and co-workers have systematically studied the adsorption of **sulfite oxidase** on various SAMs.[229]

Gold and modified-gold electrodes, unlike graphite, have the favorable optical and topographic properties that make it possible to use spectroscopic methods to inspect the adsorbed protein or enzyme. Fluorescence resonance energy transfer[223] and surface-enhanced resonance Raman and infrared absorption (see refs 24 and 231 for reviews) are very promising approaches in this respect.

3.1.1.4. Covalent Binding. Butt and co-workers covalently attached *Shewanella frigidimarina* Ifc3 **fumarate reductase** to a gold electrode by labelling the enzyme with 2-pyridyl disulfide.[232] Martin and co-workers obtained films of *Rhus vernicifera* **laccase** stable for up to 8 h when carbodiimide coupling was used to bind the enzyme to a gold electrode covered with a monolayer of mercapto propionic acid (MPA)[77] (see also ref 233 for the attachment of cytochrome *c* to alkanethiol monolayer electrodes). Judging by the shape of the voltammetric response for attached laccase (Figure 25),[77] interfacial ET appeared to be rather fast despite the fact that this enzyme is heavily glycosylated. (Glycosylation is an enzyme-catalyzed post-translational modification step which adds saccharides to a protein in order to increase its stability or to assist folding). One would expect that the presence of this insulating layer would make ET between the electrode and the enzyme slow, as observed for example for horseradish peroxidase in refs 163 and 234, but that it is not so demonstrates our lack of comprehension of the electrode/enzyme electronic interaction in some cases. Astier and co-workers reported that carbodiimide coupling of *Alcaligenes faecalis* **copper nitrite reductase** (CuNiR) to a carboxylate-terminated SAM electrode did not result in any catalytic response, whereas a noncatalytic peak sensitive to

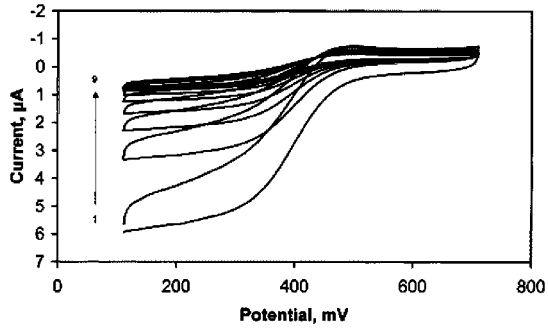

Figure 25. Dioxygen reduction by *Rhus vernicifera* laccase covalently bound to a modified gold electrode. The different voltammograms illustrate inhibition by fluoride in the range 0−53 mM (labeled 1−9). Reprinted with permission from ref 77. Copyright 2003 American Chemical Society.

scan rate ($k_0 \approx 10\ s^{-1}$) was observed.[216] De Lacey and co-workers achieved direct ET to immobilized *Desulfovibrio gigas* NiFe **hydrogenase** by forming an amide bond between the glutamic residues surrounding the surface-exposed [4Fe4S] cluster of this enzyme (Figure 1) and either carbon electrodes[198] or carbon nanotubes[235] functionalized with amine groups. This immobilization was carried out at low pH and low ionic strength to take advantage of the enzyme's dipole moment and to encourage the adsorption of the enzyme in the orientation appropriate for fast electron transfer, i.e. with the surface exposed FeS cluster facing the electrode.

3.1.1.5. Reconstitution. Willner and co-workers have demonstrated that catalytic electron transfer to FAD or $NAP(P)^+$ dependent enzymes attached to gold electrodes or single-walled carbon nanotubes can be achieved by reconstitution of the apo-enzyme using an attached tether consisting of a redox relay unit and a FAD or NADP group. The latter may "plug" into the enzyme in the reconstitution step and substitute for the missing active site.[236–238] This is a brilliant strategy for designing biosensors[239] and biofuel-cells, but in some of the tested configurations, the shape of the voltammetric signal for glucose oxidation by reconstituted and wired **glucose oxidase** shows a typical exponential increase with electrode potential (Figure 6A in ref 240, Figures 2 and 3 in ref 241, or Figure 6 in ref 237), which may indicate that interfacial ET is slow with respect to turnover (Figure 16). Whatever the origin of this effect might be, it has precluded so far the use of this strategy in the context of mechanistic studies.

3.1.1.6. Affinity Binding. Provided the protein/enzyme can be genetically engineered, it may be modified at the N- or C *-terminus* with a poly-histidine motif or "his-tag", whose micromolar affinity for nickel or cobalt can be used for binding the enzyme to a column (in the purification process) or to an electrode. An obvious limitation of this general strategy is that the protein *termini* may not be optimally located. Nitrilo-triacetic acid (NTA) was used as a metal-chelating agent for attaching a ferredoxin:$NADP^+$ reductase[242] and cytochrome *c* oxidase;[243–245] considering the advantages of this approach in terms of orientational control, it is unfortunate that in this configuration direct ET is either quite slow ($0.002\ s^{-1}$ in ref 245) or does not occur. NTA can be grafted to aryl diazonium for the subsequent modification of graphite[246] or to pyrrole for electrogeneration of a poly(pyrrole)-NTA film,[247] but again with no evidence yet that this can promote direct ET to a bound, his-tagged protein. Martin and co-workers achieved direct ET to his-tagged thioredoxin, plastocyanin, and cytochrome **P450**c17 by using an Acbstacn (1-aceto-4-benzyl-triazacyclononane) ligand covalently attached to a gold surface covered with MPA by carbodiimide coupling.[248,249] In the case of thioredoxin, comparison with the film of protein randomly immobilized at a SAM-modified electrode by using the method that was successful for laccase[77] showed that tethering increased the film stability and homogeneity and the ET rate (k_0 increased from $0.1\ s^{-1}$ to $8\ s^{-1}$). However, only at graphite electrodes has it been possible to observe the biologically-significant cooperative two-electron chemistry of thioredoxins.[64] With respect to P450 BM3 in DDAB films,[251] a three-fold increase of k_0 was also observed when the enzyme was covalently bound to a basal plane graphite electrode using the thiol specific reagent *N*-(1-pyrene)iodoacetamide.[252]

3.1.1.7. Redox Assemblies. It was demonstrated that catalytic electron transfer can occur with sub-monolayer assemblies of an enzyme connected to the electrode *via* another redox protein, in a way that may or may not mimic the natural ET pathway. Dutton and co-workers managed to adsorb on a SAM-modified gold electrode a preformed cytochrome *c*/**cytochrome c oxidase** complex (Figure 33 below) which retains an oxygen−reduction activity that is reversibly inhibited by CO, showing that this arises from cytochrome *c* oxidase catalysis.[253] Likewise, cytochrome *c* adsorbed onto bare gold by Heering and co-workers could serve as a redox dock for several enzymes, namely yeast cytochrome *c* peroxidase and *Paraccoccus denitrificans* cytochrome cd_1 nitrite reductase and nitric oxide reductase[47] (see also section 3.3). In a subsequent paper, the authors describe the attachment of cytochrome *c* to single-walled carbon nanotubes in an orientation that will certainly prove appropriate for relaying electrons to redox enzymes.[254] Conductive wiring of an immobilized photosynthetic reaction center[255] or sulfite oxidase[256] to an electrode by horse-heart cytochrome *c* was also reported. In ref 257, Demaille and co-workers describe a reconstituted photosynthetic electron transfer chain where the proteins were solubilized (rather than adsorbed); they could examine in detail the inter-protein interactions (ferredoxin/PSI and ferredoxin/FNR) and could determine binding and dissociation rates and a shift of the reduction potential of ferredoxin when complexed with FNR. We shall not describe this work further because the signals result from homogeneous catalysis, which is out of the scope of this paper.

3.1.1.8. Surfactant and "Layer-by-Layer" Films. Enzymes can be embedded into layers of surfactants[258] (often DDAB or DMPC), cast onto an electrode (often basal plane graphite), or adsorbed using the so called layer-by-layer strategy whereby the enzyme is inserted into alternated layers of charged polymers, often PSS and PDDA. This was used for both soluble and membrane-bound enzymes (references will be given in the following section), although catalytic ET was not evidenced in every case. Transmembrane enzymes (pyruvate oxidase,[259] Complex II,[260] cytochrome bo_3[261]) have been incorporated in electrode-supported lipid bilayers; in these cases, the physiological activity was clearly retained but ET was mediated by the natural cosubstrate, a quinone located in the membrane, rather than direct. Cytochrome *c* oxidases from various organisms were also immobilized in supported bilayers aimed at providing a native-like environment;[243–245,262,263] in these studies, the emphasis was on spectroscopic rather than kinetic properties.

3.1.1.9. Porous and Nanostructured Materials. The research in the fields of biosensors, biofuel cells, and bioelectronics has motivated the studies of biocompatible electrode surfaces having pores or nanostructures whose sizes are similar to those of enzymes. This includes nanoparticles (graphite,[20] silica,[264,265] gold,[266–268] Pt, etc.) and nanotubes,[235,269] quantum dots, and mesoporous materials (electrodeposited oxides,[278,271] ITO, carbon, etc). The reader will find many examples in recent reviews.[193,194,209,272–274] These studies do not focus on the catalytic mechanism and will not be described hereafter, yet they represent important new avenues for protein electrochemistry.

3.1.2. Observing Reasonable Noncatalytic Signals

The effect of the immobilization on the properties of redox *proteins* has been discussed, often with emphasis on cytochromes adsorbed onto modified gold electrodes[275–277] (see ref 226 for a review). For multicenter redox enzymes, the redox sites that are buried within the protein matrix should not be perturbed by the distant interface unless troublesome unfolding has occurred.

Electroactive coverage is usually significantly lower for large enzymes than for small redox proteins, and consequently, noncatalytic signals have been reported in only very few (but varied) cases: for enzymes adsorbed onto graphite electrodes,[196] this includes a soluble fragment of the otherwise membrane-bound *E. coli* fumarate reductase,[36,38,66,278] *Shewanella frigidimarina* flavocytochrome c_3,[56,279,280] a subcomplex of complex I,[158] chicken liver sulfite oxidase,[229,281] arsenite oxidase,[165] xanthine oxidase,[208] a single NiFe hydrogenase,[55] multi-heme nitrite reductase,[189,282] nitric-oxide reductase,[283] phtalate dioxygenase,[284] cytochrome *c* peroxidase,[175,285] and *Paracoccus denitrificans* amine dehydrogenase.[202] Noncatalytic data was also reported for a laccase covalently attached to a monolayer of thiol self-assembled on a gold electrode,[77] for Photosystem-I solubilized in detergent and adsorbed on modified gold,[286] and for a number of enzymes embedded into alternate layers of charged polymers or layers of surfactants.[258] This occurred for a bacterial reaction center,[287] photosystems I[288] and II,[289] bovine milk xanthine oxidase,[290] *Rhodobacter capsulatus* xanthine dehydrogenase[183] and DMSO reductase,[291–293] bacterial sulfite dehydrogenase,[184,294] nitric oxide synthase,[295,296] aldehyde oxidoreductase[297], and various P450 heme-enzymes (refs 114, 249, 251, 252, 265, and 298– 311) (refs 251, 298, and 305 include surveys of P450 electrochemistry).

For adsorbed enzymes, a preliminary diagnosis of health can come from noncatalytic electrochemical studies themselves, since the conformity of the peaks to ideal predictions (section 2.1) reports on the homogeneity of reduction potentials, and the values of the measured reduction potentials can be compared to those measured under potentiometric, equilibrium titrations. Ideally, both values should agree within a few millivolts, noting that the accuracy of redox titrations is rarely better than ±10 mV. In some favorable cases, the electrochemical surface may actually mimic the charged membranes where many biological processes occur; in this case, observing a discrepancy between the two techniques does not necessarily mean that the reduction potential measured in the potentiometric titration is more relevant.[52]

Flavocytochrome c_3 (fcc3) is a soluble **fumarate reductase** that houses a flavin active site and four *c*-type hemes in a single subunit (63.8kDa, pdb 1QJD).[312,313] The UV−vis spectrum of the FAD is masked by the intense bands from the four hemes; with the enzyme adsorbed at a PGE electrode, the FAD noncatalytic signal is easily distinguished as a sharp peak (small δ in eq 3 or $n_{app} > 1$ in eq 5) above the four broader $n = 1$ signals which span 300 mV. The entire envelope could be fit to a sum of independent contributions (Figure 26A) to determine the five reduction potentials and their dependences on pH. The concordance with the result of redox potentiometry was very good, within 30 mV for all centers. *E. coli* fumarate reductase (FrdAB, pdb 1FUM) shares a similar active site and mechanism, but the electron transfer chain consists of three aligned FeS clusters.[314] The reduction potentials of the four centers were also determined using PFV (Figure 26B) and found to match independent measurements.[36,38,66,278] The assumption that the centers are redox-independent was explicitly made and questioned,[36] but it should be recognized that the relatively low intensity of the peak currents observed for large multicenter enzymes often precludes the use of noncatalytic PFV to investigate the possible redox cooperativity between the different redox centers (section 2.1.1.2). Should redox interactions be suspected or detected[76] (as in multiheme cytochromes for example), it is important to think of the nontrivial relation that exists between the "macroscopic" reduction potentials measured in PFV (or UV−vis if the centers are indistinguishable for example) and their "microscopic" counterparts, which can sometimes be determined from titrations followed by NMR or EPR.

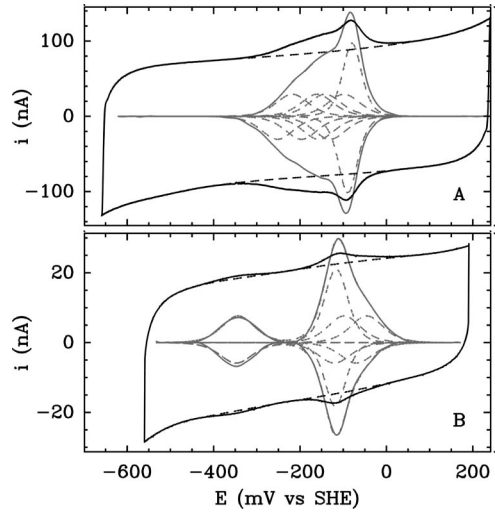

Figure 26. Noncatalytic voltammograms for *Shewanella frigidimarina* flavocytochrome c_3 (panel A)[40,56] and *E. coli* fumarate reductase (FrdAB, panel B).[36,40] The black traces are not to scale; they show the raw voltammograms (plain line) and the baseline (dashed line). The gray lines are the baseline subtracted signal (continuous line) and the individual contributions (eqs 1 and 5). Reprinted with permission from ref 40. Copyright 2000, 2001 American Chemical Society.

In a number of cases, the situation is less favorable in that not all individual signatures can be distinguished, even at the lowest scan rate. Although this is unexpected because the different redox sites in an enzyme are usually connected, plausible explanations have been offered. For example, with two-electron signals being sharper than $n = 1$ peaks, the former may appear just above background when the latter is too small to be detected. This was suspected for *A. faecalis* **arsenite oxidase**[165], where the [3Fe4S] and Rieske-type [2Fe2S] signals were not detected whereas a sharp peak, shifting −60 mV per unit of pH, was attributed to the two-

electron:two-proton $Mo^{VI/IV}$ transition of the active site; consistently, the fact that the Mo^{V} center cannot be detected in EPR experiments suggests that it disproportionates. Thus, PFV provides again a unique handle on the active site. **Sulfite oxidase**[315] illustrates a situation where the Mo active site escapes detection whereas the single electron relay in this enzyme, a heme, is detected as an $n = 1$ peak.[281] In this enzyme, the active site and heme domains are separated by a flexible hinge and a possible conformation of the protein is such that the two domains are so far apart from one another that intramolecular ET cannot take place. Armstrong and co-workers explained the absence of a stoichiometric Mo signal in PFV by the fact that the adsorbed enzyme exists mainly in a frozen conformation that is not efficient for intramolecular ET but in which the hemes do communicate with the electrode to give the observed prominent $n = 1$ peak.[281] The fact that a large fraction of the adsorbed enzyme does not engage in catalysis explains that the activity calculated from the magnitude of the catalytic current and the heme coverage is more than one order of magnitude lower than expected if all these hemes could receive electrons from the Mo active site at a rate similar to that observed in solution assays (see also section 3.3).

For **P450** enzymes, it was emphasized[298] that the reduction potentials of the heme $Fe^{III/II}$ couple measured by direct electrochemistry when the enzyme is cast into a DDAB film are consistently 100−300 mV more positive than those measured in solution titrations. Martin and co-workers[77,298] underlined another discrepancy with solution studies: apart from an early work with P450cam adsorbed on graphite,[316] electrochemical investigations with many P450 enzymes cast into DDAB films did not detect the positive shift in reduction potential upon binding of substrate that is the basis of the regulation mechanism proposed by Gunsalus and co-workers[317–320] and explains why selective substrate oxidation occurs in preference to O_2 reduction. It has been proposed that this inconsistency may result from DDAB molecules blocking access to the substrate-binding cavity[302] or from partial unfolding induced by the immobilization and electric field effects, as occurs on various Ag/SAM electrodes.[321]

In some cases, the active site or a redox relay dissociates from the enzyme over the course of the electrochemical experiment. This is undesirable but easily detected, provided this released center spontaneously adsorbs and gives a noncatalytic signal. Partial release of the active site is the lesser evil if its signature appears in a region where there is no catalytic activity or, in case it overlaps the catalytic signal, if its signature can be eliminated by subtraction (we assume that the apo-enzyme is fully inactive and does not contribute to the catalytic signal). Published noncatalytic data bringing unambiguous evidence of partial loss of redox centers under certain conditions include flavoenzymes[158,322] and laccase.[77]

3.1.3. The Right Reactions, at a Reasonable Potential and Overpotential

The integrity of an enzyme adsorbed to an electrode surface is much more easily assessed than that of a redox protein because, to put it simply, treating the enzyme roughly usually makes it stop working. Common sense suggests that the adsorbed enzyme should catalyze the same process as in solution assays, and at a comparable rate. Again, observed discrepancies can sometimes be given other justification than the interaction with the electrode denaturing the enzyme, with the best case being when the adsorbed enzyme exhibits *greater* activity than in solution assays.

Hence, one will collect evidence for the enzyme specifically catalyzing the transformation of the right substrate, knowing that many enzymes, and certainly most respiratory enzymes, are specific with respect to the reaction they catalyze. However, there are some exceptions: for example membrane-bound nitrate reductases also catalyze chlorate reduction at a significant rate and some P450 enzymes have broad substrate specificity. *Nonphysiological* electrocatalytic activity may also indicate denaturation (this is defined as significant and/or irreversible unfolding of the protein or loss of redox cofactors, which makes the enzyme loose its ability to catalyze the physiological reaction). There is abundant literature on the stable and direct electrochemistry of myoglobin, hemoglogin, and **P450** films grown either layer by layer or from using gels or surfactants. Although this is not physiological, these films are active regarding O_2 and NO reduction, but Koper and co-workers have recently pointed out that this activity may result from the heme that is released in the film rather than from (or in addition to that from) the intact protein. Their claim is based on the observation that myoglobin-DDAB and heme-DDAB films give the same electrochemical response,[323] and they reached the same conclusion about layer-by-layer assemblies of myoglobin or heme and polystyrenesulfonate.[326] Hence, they stressed the importance of control experiments, including the comparison of experiments carried out with either a heme or a heme-containing protein.[325] Their conclusions were challenged by Rusling and co-workers;[324] the debate was published in refs 323–326. With a highly reactive substrate such as NO, great care must be taken that the detected current does not come from contaminant nitrite formed upon reaction with traces of oxygen,[327–329] since nitrite reduction by adsorbed hemoglobin and myoglobin was also demonstrated. For **P450** (monooxygenase) enzymes, there are fewer reports of activity with physiological substrates[265,300–302,310,311] than evidences for noncatalytic direct ET. These enzymes catalyze the insertion of one atom of oxygen into an organic substrate (this is usually an insertion into a C−H bond) while the other oxygen atom is reduced to water, with the concomitant oxidation of NAD(P)H; the electrode may substitute for the electron donor NAD(P)H. As previously noted,[298] the P450-catalyzed oxidation of the substrate is usually detected as an additional oxygen-reduction current and the two processes are difficult to uncouple. Chromatography−mass spectrometry detection of the product will be useful to establish catalysis unambiguously.

It may indeed be possible to check that the enzyme not only catalyzes the transformation of the physiological substrate but also makes the right product. This has been achieved for example by determining the electron-stoichiometry of the catalytic process: Anson and co-workers, in an earlier report on oxygen reduction by *Polyporous versicolor* **laccase** adsorbed onto a rotating electrode, used the value of the slope of the Koutecky−Levich plot, which depends on the number of electrons in the overall redox reaction (eq 48), to confirm that the enzyme catalyzed the reduction of oxygen to water and not to hydrogen peroxide. Gorton and co-workers studied the reduction of oxygen by laccase adsorbed onto bare or thiol-modified gold electrodes; they found that hydrogen peroxide is produced in the former case.[220] In the case of hydrogenase, mass spectrometry has

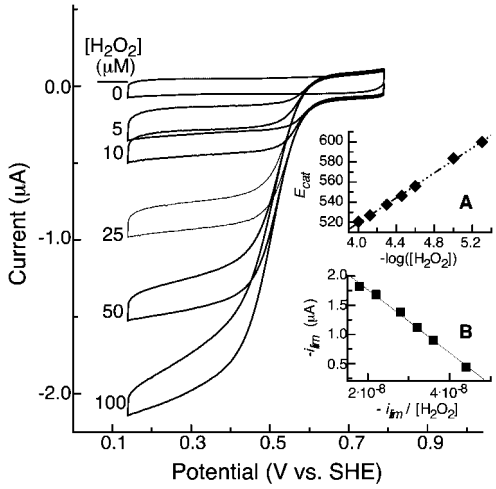

Figure 27. H_2O_2 reduction by the di-heme peroxidase from *N. europaea* adsorbed at a graphite electrode rotated at 2 krpm. The insets show E_{cat} against $-\log(s)$ and a Eadie−Hofstee plot of $-i_{lim}$ against $-i_{lim}/s$. Reprinted with permission from ref 330. Copyright 2004 American Society for Biochemistry and Molecular Biology.

been used to check that the cathodic current resulted from hydrogen production.[205]

The examination of the electrode potential where activity occurs can also be very insightful. For example H_2O_2 reduction was reported for a number of **cytochrome c peroxidases** (ccp) adsorbed onto various electrode materials.[331,332] As noted by Andreu and co-workers,[163] in most of these studies, catalysis occurs at an electrode potential (typically <0.1 V *vs* SHE at pH 7) close to the reduction potential of the $Fe^{III/II}$ couple of the active site; but this redox couple is not part of the normal catalytic cycle which involves the *high-potential* two-electron transformation between a ferryl iron close to a radical cation (the so-called "Compound I") and a ferric state. In contrast, catalytic reduction of H_2O_2 was observed at potentials more consistent with the involvement of Compound I for ccp,[175,285,333,334] a bacterial (di-heme) ccp (Figure 27),[250,330] and horseradish peroxidase.[163] Similarly for **laccases**, oxygen reduction is expected to occur at very high electrode potential (Figure 25);[77,203,211,335] otherwise, the electrochemical signal may not divulge much about the physiological catalytic process. One may also keep in mind that, as far as biological electron transfers are concerned, if one excludes certain intramolecular processes that take place right after photoexcitation in reaction centers,[26] the physiological range of reduction potentials at pH 7 only extends down to about −500 mV *vs* SHE (this extreme limit is exemplified by the ferredoxin interacting with the reaction center in green sulfur bacteria).

Once specific activity is evidenced, an additional way of testing the soundness of the adsorbed enzyme is to probe a specific inhibition process which can also be compared to known properties as determined in traditional solution assays. For example, Butt and co-workers described the inhibition by CO and air of hydrogen/proton conversion by *M. elsdenii* iron-**hydrogenase** adsorbed onto glassy carbon.[144] The inhibition of laccase activity by fluoride was also reported by Martin and co-workers (Figure 25).[77]

Last, since interfacial electron transfer is of little interest to the biochemist, it is undesirable that the catalytic signal is broadened and shifted to higher driving force by sluggish electron exchange between the enzyme and the electrode (section 2.2.5), and it is a prerequisite for PFV studies that the immobilization procedure is optimized in this respect.

3.1.4. The Right Michaelis Parameters and Their Dependences on pH

A straightforward characterization of the kinetic properties of an enzyme involves the measurement of its Michaelis parameters (k_{cat} and K_m). In PFV, this involves measuring the dependence of the limiting current on substrate concentration under conditions where there is no mass transport limitation (eq 22). This can be fit to the Michaelis−Menten equation to determine $nFA\Gamma k_{cat}$ from the limiting current extrapolated to infinite concentration, and K_m, the concentration such that the limiting current is half its maximal value. Measuring k_{cat} requires that the electroactive coverage $A\Gamma$ be determined from the magnitude of the noncatalytic signal. If the coverage is too low for noncatalytic studies, a lower value of the turnover number can be estimated by using as an *upper* value the electrode coverage that would have resulted in detectable noncatalytic signals. The Michaelis constant can be determined even when the noncatalytic signal is below the detection limit from the relative change in limiting current against substrate concentration, provided the unknown coverage remains constant.[149,165]

Conceptually, all this is very simple. In practice, when the electroactive coverage can be estimated from the area beneath the noncatalytic peaks, this is usually not performed with an accuracy better than 25%,[12] and film desorption can be a real problem for determining the value of K_m. Complete Koutecky−Levich analysis (section 2.3.1.3) has been reported,[12] but it may not be practical in all cases: this involves the extrapolation of the catalytic current to infinite rotation rate for every substrate concentration (and for the same protein film, unless normalization by the electroactive coverage is possible); this takes quite some time, during which the electroactive coverage may decrease. An alternative, time-saving strategy involves the chronoamperometric measurement of the increase in current measured at a fixed potential (on the plateau) and at a high electrode rotation rate (to minimize mass transport control), upon stepwise addition of aliquots of substrate (Figure 23); under these conditions, moderate film loss over the course of the experiment leads to underestimating the value of K_m. For the least stable films, it is possible to evaluate the Michaelis constant from the instantaneous percentage increase in current upon stepwise additions of substrate.[158] When the current keeps increasing linearly at high driving force instead of reaching a well defined limiting value (Figure 2F), the model in section 2.2.5.4 and ref 44 suggests that the slope at high driving force is proportional to the unknown limiting current; thus, the change in slope against substrate concentration can be used to measure the Michaelis constant but not the absolute turnover number, and this does not solve the problem of film desorption (see ref 165 for an application to *Alcaligenes faecalis* **arsenite oxidase**). When the electrode cannot be rotated, the procedure that consists in analyzing the change in *peak* current measured at a stationary electrode[182−184] leads to overestimating the value of K_m (see section 2.3.2 and ref 181; this is without counting film desorption). Thus, in most cases, the values of k_{cat} and K_m cannot be determined with very high accuracy, and clearly there would be no advantage in using PFV only to measure

these parameters; needless to say, we have written this review because we think that PFV proved much more useful than that.

Yet, related to establishing the integrity of the adsorbed enzyme, the question arises as to whether the Michaelis parameters measured with the enzyme connected to an electrode should match those measured in more traditional solution assays with soluble partners/cosubstrates. In the context of biosensors, the aim is to design an enzyme-electrode whose K_m value is as high as possible to increase the linearity of the response (physiological values are usually low, in the range 10−100 μM). In contrast, for mechanistic studies, it is certainly common sense that an approximate agreement between the Michaelis parameters measured in solution assays and with the enzyme immobilized is a good sign; this was actually observed in many cases. However, for some enzymes, the electrochemical value of k_{cat} and/or its dependence on pH differed significantly from those observed in solution assays.

A now classical example is *A. vinosum* NiFe **hydrogenase**, whose turnover rate for H_2 oxidation lies in the range 1500−9000 s^{-1} when it is adsorbed at a graphite electrode (that is significantly higher than that observed using methyl viologen or methylene blue as the electron acceptor);[55] moreover, it is hardly dependent on pH,[157,187] whereas a bell-shaped change in activity against pH is observed in solution assays. These observations were rationalized by considering that, in traditional experiments, intermolecular electron transfer is rate-determining. This is supported by the observation that the turnover rate in solution assays shows no isotope effect[176] and is strongly dependent on which electron acceptor is used.[336,337] By using the electrode as a more efficient electron partner, the kinetics is no longer dependent on the slow interaction with the soluble redox dye and the *intrinsic* turnover rate of the enzyme can be measured. Martin and co-workers[77] also reported that the pH dependence of O_2 reduction activity by *R. vernicifera* **laccase** covalently bound to a modified gold electrode was weaker than in solution assays, although no comparison was made regarding absolute turnover rates.

In some cases, the calculated electrochemical turnover rate was found to be smaller than expected from solution assays. This may sometimes reveal that the immobilization process is detrimental to catalysis, and this is unfortunate. If not, it may be that the coverage of enzyme that actually engages in catalysis has been overestimated. Related to this is our discussion above of the voltammetry of **sulfite oxidase** on graphite.[281] Another example is given by the recent study by Ulstrup and co-workers[217] of **cytochrome c nitrite reductase** adsorbed on Au(111): no noncatalytic electrochemical signal could be detected, but the electroactive coverage was estimated by imaging the gold surface using in situ scanning tunneling microscopy. Combining this information with the value of the catalytic current measured in the presence of substrate and the turnover rate in solution assays, it was concluded that about 4% of the imaged structures are catalytically active, and the remaining enzymes do not contribute to the catalytic current.[217] The situation was more favorable for *Achromobacter xylosoxidans* **copper nitrite reductase** adsorbed on Au(111),[127,182] although, in that case, the comparison between turnover rates is made difficult by the great dispersion of the values obtained in solution assays.

It is also textbook knowledge that, strictly speaking, the values of K_m and k_{cat} do not merely characterize the steps for substrate binding and transformation *at the active site*: just as the maximal turnover rate is influenced by the rate of electron transfer to/from the redox cosubstrate if this process is slow, the Michaelis constant, unlike an equilibrium dissociation constant, is a parameter that may depend on all rates in the catalytic cycle, including intermolecular electron exchange.[46] (See ref 338 for an example of concomitant changes in k_{cat} and K_m upon modification of an enzyme in the region involved in electron exchange with the cosubstrate.) This is a fundamental reason moderate differences may be observed between Michaelis parameters measured with the enzyme either adsorbed or in solution.

Lastly, we have assumed above that the Michaelis constant can be estimated from the change in *limiting* current against substrate concentration. Complications may arise if the wave shape is so complex that the choice of electrode potential where the current is measured becomes equivocal. For example, electrochemical Michaelis parameters and inhibition constants were shown to strongly depend on electrode potential in the case of adsorbed *E. coli* nitrate reductase[42] (Figure 2E), and it is not clear what exactly should be compared to the values measured in solution assays which are carried out without accurate control of the driving force.

3.1.5. Catalytic Signal Being Independent of Protein/Electrode Interactions

Early PFV experiments led to the major discovery that the activity of a redox enzyme may not vary in a monotonic fashion upon increasing the driving force (Figure 2).[11,41,156] Initially this came as quite of a surprise, and much effort has been devoted to making sure that the complex dependence of activity on electrode potential revealed an intrinsic property of the enzyme, rather than an artifact resulting for example from potential-dependent enzyme reorientation, as this would be physiologically irrelevant.

A non-monotonic change in activity against driving force was first observed by Armstrong and co-workers for a soluble subcomplex of mitochondrial (beef heart) **Complex II** (succinate dehydrogenase, or SDH, pdb 1NEN)[340] reducing fumarate (Figure 50).[11,146,147,341] The authors were able to independently confirm their electrochemical observation by showing the result of a spectrophotometric solution assay in the presence of reduced methyl viologen as electron donor: the reductase activity of the enzyme *increases* over the course of the assay as the concentration of electron donor decreases and so does the driving force for the reaction: this mirrors the change in activity that is detected in electrochemical experiments when the electrode potential is made less negative.[341] It was also noted that the voltammetry is independent of the nature of the electrode surface (graphite or bare gold)[341] and that the enzymes from *E. coli* and beef heart have exactly the same electrochemical behavior despite the fact that they share only ca. 50% homology (the identity is located in regions of the protein that are shielded from the solvent).[148] Hence, there is no doubt that the voltammetry reveals intrinsic and interesting properties of the enzyme that are conserved between the two enzymes.

The signature in Figure 2B is similar for most enzymes from the **DMSO reductase** family for which PFV data is available[39,42,159,160,342] with the exception of arsenite oxidases.[143,165] These enzymes share a common catalytic subunit, but they have very little overall homology, suggest-

ing that these electrochemical data do relate to the active site chemistry. In their study of periplasmic nitrate reductase, Butt and co-workers have also correlated the acceleration of the turnover rate observed over the course of solution assays and the non-monotonic electrocatalytic response, which is similar to that in Figure 46 (see the inset of Figure 5 in ref 343).

The "unusual" voltammetric signature of D-gluconate dehydrogenase was observed on electrode surfaces as diverse as carbon paste, glassy carbon, basal plane graphite, and gold-plated platinum.[344] The shape of the voltammogram for fumarate reduction by *Shewanella frigidimarina* **fumarate reductase** (Ifc3) did not depend on whether the enzyme is adsorbed on pyrolytic graphite or covalently bound to gold.[232,345] Similarly, the anaerobic oxidative inactivation of NiFe **hydrogenase** (section 3.6) is observed irrespective of whether the enzyme is adsorbed on graphite[43] or on gold covered with polymyxin.[230] **Cytochrome c nitrite reductases** also exhibit a shutdown of activity at low electrode potential,[149,150,189,346] and again, this was observed with enzymes from different organisms and using electrode surfaces as different as graphite and single-crystal gold.[217]

3.2. Interfacial and Intermolecular Electron Transfer

To relieve the frustration of the biologists and bioinorganic chemists who have followed the discussion up to this point, we shall now start describing the use of PFV to learn about the various steps which contribute to the catalytic cycle of redox enzymes. Interfacial ET relates to electron tunneling between the electrode and the enzyme, a step that substitutes for intermolecular ET in homogeneous kinetics. *In vivo*, redox enzymes may interact with other proteins which are either anchored to or included in charged membranes, and it has sometimes been suggested that the interaction between the protein and certain electrode surfaces may mimic some physiological situations.[124] This can be illustrated by the very peculiar case of the periplasmic **cytochrome** c^m_{555} of *A. aeolicus*. This electron-transfer protein contains a flexible, cysteine-terminated 62-residue extension by which it is tethered to the membrane. Imitating the physiological configuration, Armstrong and co-workers used this natural lead to attach the protein to a modified gold electrode;[115] the observed value of k_0 was extremely high (15000 s^{-1}), and most importantly, it was 500 times greater than that measured with the protein c^s_{555}, which only differs from c^m_{555} in that it lacks the proteic extension and was therefore directly adsorbed on the electrode. Hence, in this case, electrode−protein electron transfer appears to be faster when the protein is able to explore a wide range of orientations, so that conformations having a better electronic coupling are accessed very frequently. Together with the observation that the greatest ET rates are observed under conditions of high ionic strength, this suggested to the authors that fast ET can be associated with loose interactions. This conclusion may hold *in vivo* and suggests that electron transport in real biological systems may be faster in situations where the components of a transient complex are not connected together in a single, well defined manner.[347–356]

Hildebrandt and co-workers have also emphasized the similarity between self-assembled monolayers and biological membranes.[357]

In the case of bare metal electrodes, the protein−electrode interaction is not expected to mimic the physiological

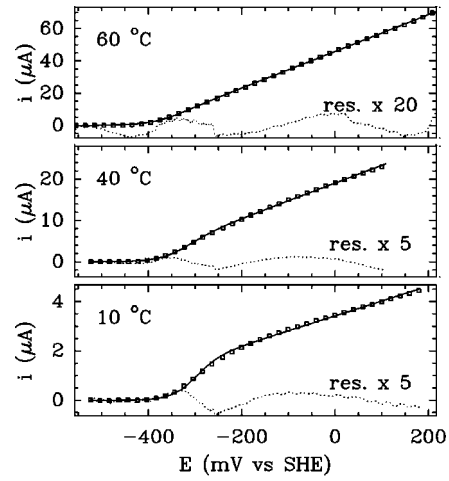

Figure 28. Hydrogen oxidation by *A. vinosum* NiFe hydrogenase adsorbed at a graphite electrode, under 1 bar of H_2, pH 7, at three different temperatures. Note the fact that the sigmoidal contribution to the wave shape is only seen at the lowest temperature, and the absence of limiting current at high potential. This is interpreted in terms of a distribution of orientations of the enzyme molecules adsorbed onto the electrode surface. Only one experimental point in every 10 collected has been plotted. The signals are fit to eq 36. Reprinted and adapted with permission from ref 44. Copyright 2002 American Chemical Society.

situation. Yet there are several reasons this process needs to be studied and characterized, not the least being that, in many cases, interfacial ET is not fast enough to maintain the adsorbed enzyme in Nernstian equilibrium. Therefore, interfacial ET kinetics must be explicitly considered to derive the rate equation that will be used to fit the data and to extract the mechanistically-relevant information.

We have described in section 2.2.5 how interfacial ET is included in theoretical models of catalysis. Generally, slow interfacial ET is expected to broaden the catalytic signal: the value of n_{cat} in eq 16 may be as small as $^1/_2$ if Butler−Volmer (BV) kinetics is obeyed or even smaller if ET is so slow and the reorganization energy is so small that Marcus theory is more appropriate than BV kinetics (Figure 17). This should significantly influence the *shape* of the steady state catalytic data if $k_0 < k_{cat}$, which is not to say that the limiting current should be compared to k_0.[253] Indeed, if BV kinetics is assumed, the interfacial ET rate increases with the driving force until it is no longer rate-determining, while, according to Marcus theory, the maximal rate of ET is much greater than k_0 (Figure 6). In the former case, it is expected that the current should tend to a limiting value which relates to the maximal turnover of the enzyme (k_{cat}) whereas, in the latter, the limiting current may relate to the maximal rate of interfacial ET predicted by Marcus theory.

The above simple considerations often fail: in many cases, instead of reaching a limiting value at high driving force, the current keeps increasing in a linear fashion with the electrode potential, as shown in Figure 28 for hydrogen oxidation by *A. vinosum* **hydrogenase**. The fact that the slope correlates with high turnover rate is obvious in Figure 28: upon increasing the temperature of the same enzyme film, the magnitude of the current increases greatly while the sigmoidal contribution to the wave at ≈ -300 mV becomes less and less defined. In this case, the turnover rate of the enzyme is particularly high (it exceeds several thousands per second),[55] and thus, interfacial ET needs to be very fast to keep up with the catalytic process, but similar linear changes in current against E at high driving force have been observed

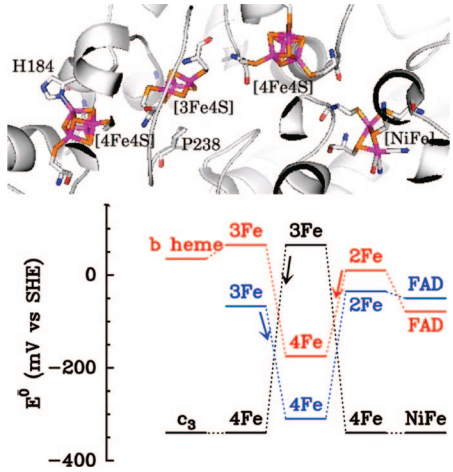

Figure 29. The ET chain in *D. fructosovorans* NiFe hydrogenase (98 kDa, pdb 1YQW, Figure 1). Consisting of three FeS clusters, it connects the NiFe active site to the distal FeS cluster that is exposed at the surface of the protein (on the left) and interacts with the redox partner; under physiological conditions, the latter is a low-potential c_3-type cytochrome. The bottom diagram depicts the thermodynamics of the ET chain in NiFe hydrogenase (black), and two flavoenzymes discussed in the text, *E. coli* succinate dehydrogenase[340] (red) and fumarate reductase[314] (blue). The arrows show the most penalized ET step in the direction of physiological electron flow (H_2 oxidation, succinate oxidation, fumarate reduction). The top panel is reprinted with permission from ref 360. Copyright 2006 American Chemical Society.

for all sorts of enzymes: **copper enzymes** (nitrite reductase[167] and laccase[211]), **flavoenzymes** (complex I,[158,151,161] flavocytochromes b_2,[145] and *E. coli* fumarate reductase[12,38]), **molybdoenzymes** (arsenite oxidase,[165] nitrate reductase,[160] sulfite oxidase[229]), and **heme enzymes** (nitrite reductase, Figure 3 in ref 149, and cytochrome *c* peroxidase[37,163]). The correlation between high activity and the absence of limiting current is backed up by other observations: for *Paracoccus pantotrophus* **nitrate reductase**, the greater activity for chlorate reduction than for nitrate reduction correlates with a greater slope in the voltammogram when chlorate is the substrate;[358] for *E. coli* **fumarate reductase**, which reduces fumarate about 40 times faster than it oxidizes succinate,[36] the slope is observed only for the reductive (fast) reaction (Figures 30, 35, and 40). The effect is also more evident at higher substrate concentrations; it may be masked at low substrate concentration because turnover is slow and also because the mass transport limitation should be more stringent (this artificially flattens the signal; see Figure 20). It is also remarkable that similar enzymes may or may not exhibit this behavior: for example, strict plateaus are observed in the case of the periplasmic **nitrate reductase** NapAB in refs 156 and 343, whereas inclined limiting currents occur for the assimilatory nitrate reductase NarB in ref 160.

This linear change in current against driving force was long surprising until we realized that not all enzyme molecules on the electrode surface may be orientated in exactly the same configuration and that this distribution of orientation should result in a spread of interfacial ET rate constants: the enzyme molecules that have large k_0 already contribute to the catalytic signal at low driving forces, whereas the enzymes that are misorientated and have poor electronic coupling with the electrode only contribute to the catalytic signal above a certain driving force that is all the greater that the electronic coupling is weak (Figure 13). The simple (and rather ingenuous) model in section 2.2.5.4 and

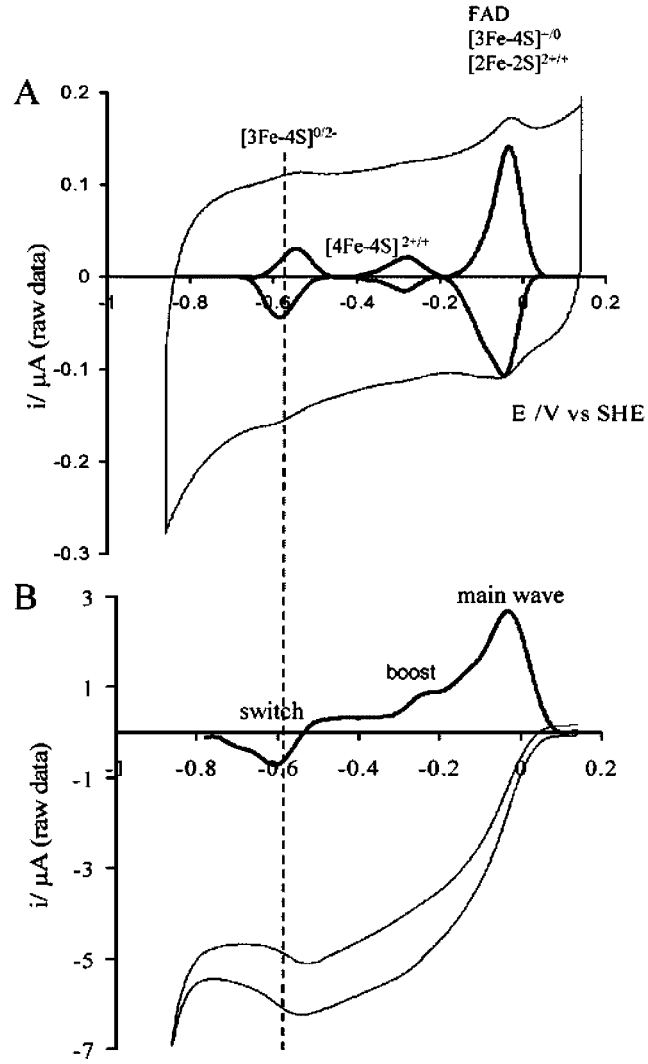

Figure 30. (A) Noncatalytic signal for *E. coli* FrdAB showing the hyper-reduction of the [3Fe4S] cluster at ≈ −600 mV, pH 5, 25 °C. (B) The signal for fumarate reduction under the same conditions reveals an attenuation of activity at an electrode potential which closely matches the reduction potential of the $[3Fe4S]^{0/2-}$ couple. The derivative of the catalytic signal is also shown in panel B. Reprinted with permission from ref 38. Copyright 2005 American Chemical Society.

ref 44 leads to a distribution of k_0 values that can be used to average the rate equation and results in an exactly linear change in current against E at high driving force. Conversely, we interpret this linearity in the framework of the above model as the *signature* of a continuous distribution of orientations that distributes the rates of interfacial ET. This may be reminiscent of a common situation for inter-protein electron transfer. Indeed, it is now admitted that distributions of orientations and electron transfer rates also exist in protein−protein electron transfers, as evidenced in NMR experiments,[347–354] soft-docking,[355] and molecular dynamics simulations,[356] but the heterogeneity of intermolecular ET rate constants is likely to escape detection in traditional kinetic measurements. In contrast, the distribution of interfacial ET rate constants is evident from the *shape* of the PFV data, and this illustrates an advantage of measuring the complete dependence of rate on driving force rather than a single value of the rate as in homogeneous kinetics.

Copper-Containing Nitrite Reductase (CuNiR, 37 kDa, pdb 2AFN)[359] houses a type-1 Cu ET relay and a buried

type-2 Cu active site, and the CuNiR from *A. faecalis* assembles as a homotrimer. The wave shapes obtained with this enzyme adsorbed at a graphite electrode could be fit assuming that the trimeric structure is reflected in a distribution of the k_0 rates around three main values corresponding to different distances between the type-1 sites and the electrode.[167] The values of E_{cat} and $i_{lim}/\beta d_0$ were assumed to be identical for all three subpopulations, which only differed by the values of k_2/k_0^{max} in eq 36.

The voltammograms for H_2O_2 reduction by adsorbed **cytochrome c peroxidase** reported by Andreu and co-workers also show an exactly linear change in current against E under conditions of high substrate concentration (Figure 2 in ref 163), but the authors claimed that no satisfactory fits of the data could be obtained with eq 36. Instead, they considered a model that describes interfacial ET using Marcus theory (Figure 17) and diffusoconvective mass transport towards the RDE (section 2.3.1). The assumption was also made that k_{cat}/K_m is the same as that determined in solution experiments, and the analysis was focused on the high-driving force part of the data (low potential) to estimate the reorganization energy of the reduction of Compound II.

Certain large redox enzymes seem to have many entry points (e.g. multiple hemes close to the protein surface) and in vivo have a broad range of electron donor/acceptor partners. Others may house a buried active site that is connected to the redox partner by a linear chain of redox cofactors. This is so for NiFe **hydrogenases**, where the chain consists of a [4Fe4S] cluster that is proximal to the active site, a medial [3Fe4S] cluster, and a distal [4Fe4S] cluster that is exposed at the surface of the protein (Figures 1 and 29). Similarly in *E. coli* **fumarate reductase** (FrdAB), the soluble subcomplex of the membrane bound fumarate reductase FrdABCD,[314] the chain consists of a [2Fe2S] cluster that is proximal to the active site flavin, a medial [4Fe4S] cluster, and a distal [3Fe4S] cluster. The question arises as to whether all three clusters are actually used for transferring electrons and whether the distal cluster is the only entry/exit point for electrons in the enzyme. Indeed, it may be argued that the medial cluster could also exchange electrons directly with the electrode or the soluble redox partner, bypassing the most-exposed cluster. Such a short circuit, which may be considered as unlikely based on the exponential decrease in ET rates with distance (eq 33), can be discarded on the basis of several recent PFV investigations.

In the case of *E. coli* **fumarate reductase**, whose redox chain is terminated by a surface exposed [3Fe4S] cluster (Figure 29B), Figure 30 shows that the catalytic rate drops at very high driving force, when the electrode potential is taken below the reduction potential of the $[3Fe4S]^{0/2-}$ couple (−600 mV *vs* SHE at pH 5, as determined from the noncatalytic data in panel A). Even if this reduction potential is too low for the hyper-reduced state of the cluster to be involved under physiological conditions (normal operation relies on the $[3Fe4S]^{+/0}$ couple), this observation implies that at least some of the electrons enter the adsorbed enzyme *via* the surface exposed [3Fe4S].[38]

In the case of NiFe **hydrogenase**, the putative end of the relay system is the [4Fe4S] cluster that is coordinated by an unusual histidine ligand (H184 in Figure 29). Using site-directed mutagenesis, H184 could be substituted for a cysteine.[360] Control experiments show that this mutation does not impair protein folding, cluster assembly or active site chemistry, but the mutant exhibits extremely slow rates of interfacial ET, judging by the shape of the catalytic signals (Figure 8B in ref 360). That this does not result from the orientation of the mutant being different from that of the wild type enzyme is proven by the following observation. A second mutant was purified, in which H184 is substituted by the noncoordinating amino acid glycine, with the structural consequence that the distal [4Fe4S] cluster has an open coordination site on the solvent exposed Fe. With the H184G variant adsorbed at an electrode, the interfacial ET slows down dramatically when an exogenous alkanethiol binds to the exposed Fe: this mirrors the observations made with the cysteine mutant. This demonstrates that the distal cluster cannot be bypassed and also that all-sulfur coordination of the distal cluster in NiFe hydrogenase is detrimental to interfacial ET.[360]

3.3. Intramolecular Electron Transfer (iET)

The presence of a high potential [3Fe4S] cluster right in the middle of the ET chain in NiFe **hydrogenase** (Figures 1 and 29) came as a surprise when the structure was solved in 1995,[32] and it was unclear how fast electron transfer could occur in the presence of a very "uphill" (endergonic) step. For *E. coli* **fumarate reductase**, the redox chain is also arranged as an electron "roller coaster" (the term is borrowed from Alric and co-workers[168]), with the reduction potential of the medial [4Fe4S] cluster being much lower than those of the adjacent [2Fe2S] and [3Fe4S] clusters (Figure 29). This cluster had even been proposed to be "off-pathway",[361] or involved in a secondary pathway[66] before the X-ray structure demonstrated in 1999 that the centers are arranged in the sequence flavin-[2Fe2S]-[4Fe4S]-[3Fe4S]. Linear chains of FeS clusters occur in many respiratory enzymes, including mitochondrial Complex I, where no fewer than seven lined up [4Fe4S] clusters connect the active site flavin to the site of quinone reduction.[29] However, there have been very few measurements of electron transfer rates between FeS clusters in respiratory enzymes.[362] This is a consequence of two main limitations: FeS clusters lack the well-resolved UV−vis features that are required for time-resolved spectroscopic studies and iET can be difficult to trigger in non-light-driven enzymes.[145] Hence, the techniques that proved successful for studying photosynthetic iET have no utility in these systems. Nevertheless, it is generally believed that iET is fast with respect to the active site chemistry in respiratory enzymes, so that it does not limit turnover,[363] and NiFe hydrogenases are actually cited as a paradigm in this respect.[152]

By using site directed mutagenesis and direct electrochemistry, it was recently possible to demonstrate that the uphill ET transfer from the medial [3Fe4S] to the distal [4Fe4S] is rate limiting in a mutant of NiFe **hydrogenase**.[360] The method was based on the fact that the *shape* of the catalytic signal given by eq 26 or 36 depends on the ratio of k_0^{max} over k_2, where k_0^{max} describes interfacial ET while k_2 incorporates all intramolecular steps whose rates are independent of E. The way the shape of the signal depends on k_2 and k_0^{max} is illustrated in the top panels of Figure 31, where the two pairs of solid lines show twice the same catalytic signals for hydrogen oxidation and formation by wild-type *D. fructosovorans* NiFe hydrogenase.[187] The signals were fit to eq 36, and the dashed lines have been recalculated assuming that either k_0^{max} or k_2 was smaller (panel A and B, respectively), with the second parameter being kept constant. The *magnitude* of the signal decreases in both cases, but

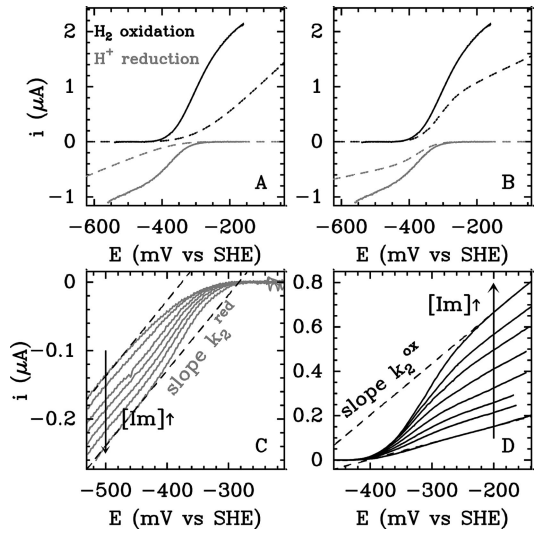

Figure 31. Panels A and B show as solid lines a pair of baseline subtracted voltammograms for hydrogen oxidation under 1 bar of H_2 (black trace) or proton reduction under 1 bar of Ar (gray trace), by *Desulfovibrio fructosovorans* NiFe hydrogenase adsorbed on graphite, pH 7, 2 krpm, 40 °C. The dashed lines show voltammograms recalculated from eq 36 by assuming slower k_0 (panel A) or k_2 (Panel B). The bottom panels shows how the voltammetry of the H184G mutant of *D. fructosovorans* NiFe hydrogenase is affected by increasing concentrations of imidazole. Adapted with permission from ref 360. Copyright 2006 American Chemical Society.

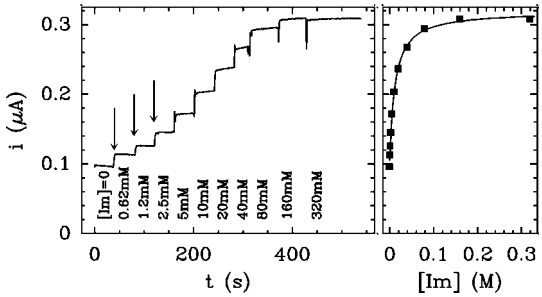

Figure 32. The current for hydrogen oxidation by the H184G mutant of *D. fructosovorans* NiFe hydrogenase adsorbed at a graphite electrode increases upon stepwise addition of exogenous imidazole; this chronoamperometric experiment, which mirrors the chemical rescue demonstrated in solution assays (see Figure 3 in ref 360) and leads to the same conclusions, illustrates the relative ease of aquiring kinetic data in PFV. 40 °C, pH 7, 3000 rpm, $E = -150$ mV. Unpublished results.

importantly, the recalculated wave *shapes* are different. The signal merely becomes more irreversible if k_0^{max} is decreased (panel A), whereas slowing k_2 at constant k_0^{max} increases the sigmoidal character of the wave (panel B). Hence, by examining how the wave distorts, it is possible to determine whether the change in turnover rate results from a change in the kinetics of interfacial or intramolecular ET. We used this approach to characterize the chemical rescue by exogenous imidazole of the H184G mutant of *D. fructosovorans* NiFe hydrogenase, where the histidine that ligates the distal cluster is changed into a glycine (Figure 29). The activity of this mutant increases about 10-fold upon binding of exogenous imidazole to the free coordination site of the distal cluster (ref 360 and Figure 32), but neither solution assays nor the chronoamperometric experiment shown in Figure 32 can distinguish whether this is caused by an acceleration of iET (from medial [3Fe4S] to distal [4Fe4S]) or intermolecular ET (from distal [4Fe4S] to the soluble electron acceptor or the electrode). The bottom panels in Figure 31 show how increasing the concentration of imidazole affects the voltammograms for proton reduction and hydrogen oxidation by the glycine mutant. For proton reduction (panel C), the slope of the voltammogram at high driving force (dashed lines) is independent of imidazole concentration, showing that the intrinsic activity of the enzyme is unaffected (eq 37), but the way the shape changes reveals acceleration of interfacial ET upon imidazole binding (compare panels 31A and C). For hydrogen oxidation (panel D), the signal is also better defined at higher imidazole concentration, since interfacial ET is faster, but the increase in the value of the slope at high driving force and the change in shape also reveal the acceleration of an intramolecular process, and this can only be ET from medial [3Fe4S] to distal [4Fe4S] where imidazole binds. Hence, this step, which is very endergonic in the wild type enzyme, must be slower than the active site chemistry in the mutant. Whether it is also slow in the *wild type* enzyme is still unknown.

In the P238C mutant of *D. fructosovorans* NiFe hydrogenase, the medial [3Fe4S] cluster is replaced with a [4Fe4S] cluster (Figure 29), and this makes the redox chain nearly iso-potential.[364] This mutant is nearly as active as the wild type (WT) enzyme in solution assays of H_2 oxidation, suggesting that uphill ET does not limit the turnover rate in the WT. However, this only reflects the fact that *intermolecular* ET limits the turnover rate in solution assays;[55] hence, speeding up iET does not increase the overall activity. Concluding about the rate of iET in WT and P238C NiFe hydrogenase will require performing other experiments with a faster electron acceptor: the electrode should be ideal in this respect.

Another and more general strategy for using PFV to learn about the kinetics of iET consists in interpreting the value of the catalytic potential, which is affected by the kinetics of iET when this process partly limits the turnover rate (section 2.2.6 and Figure 18). The concept of "control center" has been introduced in ref 40 by Armstrong and co-workers to encompass earlier assumptions that the catalytic potential may relate to a relay center, rather than to the active site, depending on the nature of the rate limiting step in turnover.[144,253,281] The "control center" is defined as the center along an ET chain up to which electron exchange with the electrode is fast, so that the rate-determining step in catalysis occurs right after it,[167] suggesting that the location of the main wave is a simple readout of the rate limiting step in turnover. The model described in section 2.2.6 gives this concept theoretical justification, at least in the case of enzymes consisting of only one active site and one relay, and extends this approach beyond the "all or nothing" description whereby iET is either fast or rate limiting. It is predicted that slow iET makes the wave more closely resemble $n_{cat} = 1$ (in the absence of limitations by interfacial ET) and that the catalytic potential continuously drifts from the potential of the relay to that of the active site upon increasing the rate of iET (eq 41 and Figure 18).[145] Hence, provided the reduction potentials of the relay and of the active site are known (from noncatalytic voltammetry or potentiometric titrations), the rate of intramolecular ET can be estimated from the position of the catalytic signal, as illustrated below.

The usefulness of this concept may go beyond the interpretation of the catalytic potential to evaluate the rate of iET. A potentially physiological implication is that,

provided iET is at least partly rate limiting, the value of E_{cat}, that is the minimal driving force that must be provided by the soluble redox partner for catalysis to proceed, departs from the reduction potential of the active site. If iET is so fast that it does not limit turnover, there is no reason to think that the various factors that influence tunneling rates along the redox chain have been optimized by natural evolution; Dutton and co-workers have even proposed that the only engineering principle of ET chains in enzymes is that the intercenter distance is small enough that iET is fast and reduction potentials do not matter.[152,363] This simply explains that, in some cases, the reduction potentials of the centers along a chain are clearly not optimized for speed (Figure 29). But this also suggests that these unimportant redox properties should vary through evolutionary changes, whereas they do appear to be conserved within each family of enzyme. Our alternative proposal is that since fast iET is not a requirement in redox enzymes, an ET chain that *slows* iET may actually confer advantage because in that case the *apparent* redox properties of the active site can be modulated by those of the ET chain.[145]

The drawing in Figure 33 depicts the supramolecular assembly of cytochrome *c*/**cytochrome c oxidase** at a modified gold electrode, as conceived and achieved by Dutton and co-workers.[253] The authors showed that cytochrome *c* monolayers alone display a reversible noncatalytic signal at +240 mV, pH 8 (Figure 33A), in agreement with the value determined in potentiometric titrations, and that interfacial ET obeys BV kinetics with $k_0 \approx 20\ s^{-1}$. When a preformed complex of cytochrome *c* and cytochrome *c* oxidase is adsorbed on the gold electrode, catalytic reduction of oxygen is observed, and the value of E_{cat} at +225 mV is consistent with the mandatory requirement for cytochrome *c* to mediate electrons from the electrode to cytochrome *c* oxidase, as occurs under physiological conditions. Considering the wave shape and the above discussion, the heme of cytochrome *c* appears to be the control center for oxygen reduction: the fact that the catalytic process is limited by inter-protein ET is apparent from the position of the catalytic wave, which is centered on the reduction potential of the cytochrome. However, some ambiguity remains, since this is also close to the reduction potential of the CuA center, at +250 mV.

Using a somehow similar configuration, Heering and co-workers[47] have shown that yeast cytochrome *c* (YCC) chemisorbed on bare gold in a configuration where fast ET is achieved ($k_0 \approx 2000\ s^{-1}$) can serve as a docking site for mediating electron transfer to various enzymes, namely **cytochrome c peroxidase** (ccp), **nitric oxide reductase** (NOR), and **cytochrome cd$_1$ nitrite reductase** (cd_1 NiR). For the latter, the remarkable conclusion was drawn that the current revealing nitrite reduction resulted from the turnover of as few as ≈50000 enzyme molecules coadsorbed on cytochrome *c*. In all three cases, the position of the wave was discussed in terms of ET kinetics. For catalytic H_2O_2 reduction by the adsorbed YCC−cytochrome *c* peroxidase complex, the wave is centered on the YCC reduction potential, in stark contrast to ccp directly adsorbed on graphite,[175] for which the wave is close to the reduction potential of Compound I at much higher potential. This and the fact that the wave shape is close to $n_{cat} = 1$ suggest that inter-protein (rather than interfacial) ET from ccp to YCC limits turnover. For catalysis by cd_1 NiR docked onto YCC, n_{cat} is greater than one; this is unexpected considering that this enzyme catalyzes a one-electron reaction at an active site heme. The authors suggest that this reveals the positive redox cooperativity between the heme groups either within or between NiR subunits; redox interactions of either sign have been evidenced using potentiometric titrations in cd_1 nitrite reductases from various organisms.[365–367] Last for nitric oxide oxidation by the YCC/NOR complex, the catalytic potential at +108 mV is significantly lower than the reduction potential of YCC and more closely matches that of the active site heme b_3 (in the range 20−60 mV), suggesting that inter-protein ET is not rate-determining in that case either.

Coming back to intramolecular electron transfer in multicenter enzymes, recent PFV experiments with **copper nitrite reductase**[167] adsorbed at a graphite electrode are also consistent with the finding[185] that ET from the surface exposed type-1 copper site to the active site type-2 copper is rate determining under high nitrite concentrations, where substrate binding is fast and occurs before iET. The catalytic wave is complicated by a superposition of signals, but at high substrate concentration and over a large range of pH, the value of E_{cat} exactly matches the reduction potential of the type-1 copper site (Figure 7 in ref 167). Upon decreasing the concentration of substrate, E_{cat} increases with a slope of about 60 mV per decade until it becomes close to the reduction potential of the type-2 copper active site (Figure 6 in ref 167).

In ref 145, using the model in section 2.2.6, we estimated iET rates from the exact location of the catalytic signals for **flavocytochrome** b_2 and **sulfite oxidase**. In chicken liver sulfite oxidase,[315] the molybdenum active site passes on electrons to cytochrome *c* via a small heme domain that is tethered to the Mo domain by a flexible loop. The values of $E^0_{O/I}$ and $E^0_{I/R}$ (for $Mo^{VI/V}$ and $Mo^{V/IV}$, respectively) interpolated at pH 8 from the data in ref 368 are +6 mV and −184 mV (hence, the half-reduced state of the active site is stable). When the enzyme is adsorbed onto an electrode,[281] a one-electron noncatalytic peak at +90 mV reveals the reduction potential of the heme relay; under saturating concentrations of substrate, a one-electron catalytic wave is observed, whose position (E_{cat} = +65 mV at pH 8, 20 °C) shows little dependence on pH, and this contrasts with what is observed for the reduction potentials of the molybdenum couples.[368] From the values of the reduction potentials above and eq 41, the ratio or k_i/k_{cat} was found to lie in the range 2.7−4.8 depending on the exact value of $E^0_{O/I}$ (the labels on the right *Y*-axis of Figure 18 are for sulfite oxidase). This is in reasonable agreement with the iET rates determined at pH 8 using flash photolysis on the same enzyme.[369] This shows that intramolecular ET is neither very fast nor fully rate-limiting: the rates of ET from Mo to heme and of chemical transformation at the active site must be of the same order of magnitude.[145]

To conclude on the above approach that consists in estimating whether or not iET is fast by comparing the position of the wave and the reduction potentials of the different centers, we may warn against data overinterpretation. There are very few cases where the E^0 of the centers and the value of E_{cat} can both be determined in PFV (under identical conditions but for the presence of substrate), and one will often have to rely on the independent results of potentiometric titrations. Moreover, the shift in E_{cat} that may result from substrate binding (section 2.2.4) or product retention (as suggested in ref 158) could be mistakenly

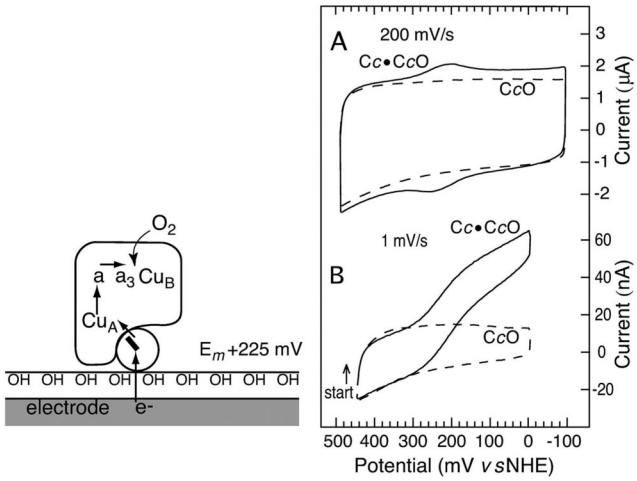

Figure 33. The drawing on the left shows the design of a cytochrome *c*−cytochrome *c* oxidase complex adsorbed at a modified gold electrode. Right: voltammetry of the complex at a relatively fast (panel A) or slow (panel B) scan rate. Catalytic oxygen reduction in panel B is specifically inhibited by carbon monoxide (see Figure 10B in the original paper). Note that the orientations of both the potential and current scales are the reverse of all others in this paper. Reprinted with permission from ref 253. Copyright 2001 American Chemical Society.

interpreted in relation to the kinetics of iET or *vice versa*. Of course, a single value of E_{cat} is a rather crude characteristic of the kinetics of a multicenter enzyme, considering that this potential may be affected by all steps in the catalytic mechanism. Unambiguous interpretation of the data may rely on a systematic and quantitative investigation of how this potential depends on various experimental parameters.

Noncatalytic experiments were used by Martin and coworkers to evidence slow iET from the surface-exposed type-1 copper site to the buried trinuclear copper active site in *R. vernicifera* **laccase** attached to a modified gold electrode (*cf.* section 3.1.1.4).[77] At low scan rate, the noncatalytic signal consists of a single peak whose area is independent of scan direction, which reveals the complete four-electron oxidation and reduction of all four copper ions in the enzyme. In contrast, at faster scan rates, complete oxidation is observed only during the first scan, and the signal is substoichiometric on all subsequent scans (Figure 34A). This suggests that complete oxidation can proceed on the voltammetric time scale at all scan rates, whereas iET is slow enough that complete reduction cannot be achieved over the course of a fast sweep to low potential. After the sweep is reversed, only the fraction of enzyme that has been reduced in the previous scan can be (quickly) reoxidized, and the same peak is obtained as from the second scan. Consistently, Figure 34B shows that the ratio of the anodic over cathodic charges passed during the first and second sweeps increases from one to four upon increasing the scan rate. Although no theoretical description of noncatalytic voltammetry is available yet for multicenter enzymes, it would be interesting to further pursue the analysis of this data to deduce the rate of iET from the change in current ratios and peak shapes against scan rate; this could be compared to the turnover frequency determined under the same conditions to establish whether iET to the active site limits the rate of oxygen reduction in this system.

In the above discussion of the catalytic wave shapes, we have only commented on the position of the main wave, at the onset of activity. At higher overpotential, the catalytic signals

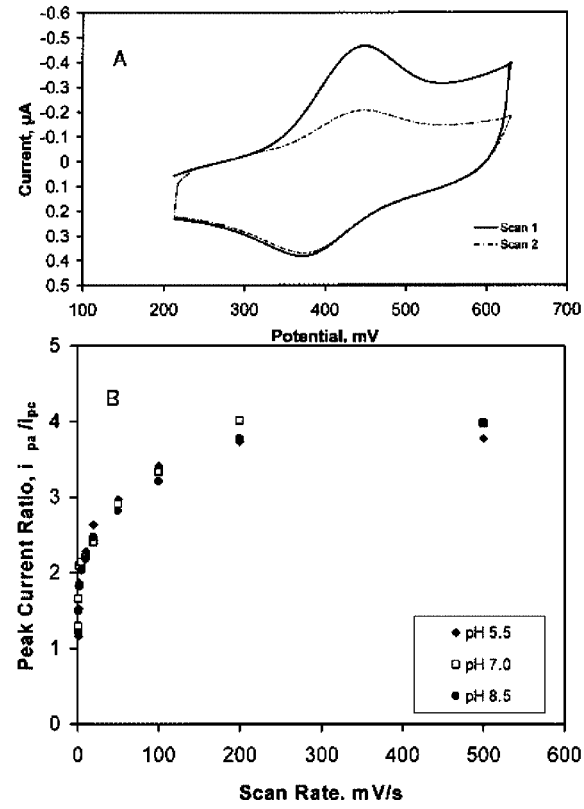

Figure 34. Noncatalytic voltammetry of *Rhus vernicifera* laccase immobilized on modified gold. Panel A: successive scans at 50 mV/s after a reductive poise at 200 mV, showing that the peak area is greater on the first oxidative sweep than on all subsequent sweeps. The ratio of anodic over cathodic peak areas is plotted against scan rate in panel B. Reprinted with permission from ref 77. Copyright 2003 American Chemical Society.

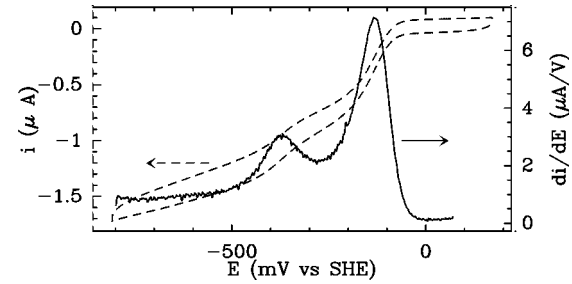

Figure 35. Dashed black line: catalytic reduction of 250 μM fumarate by *E. coli* FrdAB adsorbed at a graphite electrode at pH 8, $\omega = 6000$ rpm; for comparison with Figure 26A. The plain line shows the derivative of the reductive scan. Adapted with permission from ref 38. Copyright 2005 American Chemical Society.

sometimes show one or two other sigmoidal features (Figure 2).[40,41,48] For example, the activity may be "boosted" and rise again when a certain electrode potential is reached (as occurs for **fumarate reductases**),[12,38,66,232] or instead it may be attenuated or even "switched off" as the driving force is increased while catalytic activity is recovered on the reverse sweep: a peak of activity on the sweeps to both more positive and more negative potentials was observed with very diverse enzymes, namely the soluble "SdhAB" subcomplex of both bacterial and mitochondrial **Complex II** (succinate dehydrogenases),[11,146–148] the "Fp" flavoprotein subunit of mitochondrial **Complex I**[158] (but not the "1λ" subcomplex[151]), D-gluconate dehydrogenase,[344] all Mo enzymes from the **DMSO reductase** family for which PFV data are available[39,159,156,160,186] (except arsenite oxidases[143,165]),

cytochrome c nitrite reductases,[149,150,189,346] and all NiFe and FeFe **hydrogenases** studied so far.[43,141,169,370] The origin of the effect is not always clear, and obviously the cause need not be the same in every case; hereafter, we focus on two examples where a boost or a switch is interpreted as revealing a variation of iET kinetics.

As discussed above, iET in *E. coli* **fumarate reductase** (FrdAB) involves a low potential [4Fe4S] cluster that is located in the middle of the chain (Figure 29). The potential of this cluster is easily measured in noncatalytic experiments, as illustrated in Figure 26B,[38,40,66] where the outer trace is a voltammogram recorded at pH 8 in the absence of substrate. The faradaic current, obtained after subtracting the charging current, is shown in the same panel (not to scale). The peak at ≈ -100 mV on the noncatalytic signal results from the redox transitions of the active site flavin, the proximal [2Fe2S] cluster, and the distal [3Fe4S] cluster, while the weaker signal occurring at ≈ -350 mV is unambiguously assigned to the low potential [4Fe4S] cluster.[66] The catalytic signal recorded under conditions of high concentration of fumarate is shown in Figure 35. The value of E_{cat} is close to that of the active site flavin determined from the noncatalytic data in Figure 26B. Most surprisingly, as first noted in 1993,[12] a further sigmoidal increase in current occurs at lower potential. This "boost" is all the more prominent that substrate concentration is high, and it is also more clearly seen at high pH,[66] where the fumarate reduction activity is lower (for example, it is barely visible in Figure 30, where conditions of low pH where chosen to facilitate the hyper-reduction of the [3Fe4S] cluster). It cannot be missed that the location of the boost is very close to the reduction potential of the $[4Fe4S]^{2+/+}$ couple.[66] An additional demonstration of this correlation has recently been given by studying a series of mutants for which both the reduction potentials of the [4Fe4S] cluster and the locations of the boost span a range of 100 mV (Figure 8 in ref 38).

Additional insights regarding the origin of the boost in Figure 35 came from studies in which the rate of release of the competitive inhibitor oxaloacetate (OAA) from the active site flavin in FrdAB was measured as a function of the electrode potential.[38,66] The reduction potential of the active site flavin was determined in noncatalytic experiments, and its dependence on OAA concentration was interpreted using an equation similar to eq 14 to show that this inhibitor binds more tightly to oxidized rather than reduced flavin (Figure 6 in ref 66). Catalytic experiments were then carried out in the presence of both fumarate and OAA, using a concentration of inhibitor which was low enough that it could bind only to oxidized flavin (K_o < [OAA] < K_r). When the electrode potential is stepped to take the enzyme from conditions where it is oxidized and bound to OAA, to reducing conditions where it becomes able to release OAA and reduce fumarate, the recovery of activity is slow and limited by the rate of OAA release (Figure 36A).[12] Reactivation is faster when the applied potential is lower, and the quite unexpected (but very robust[38,66]) observation is that the first-order rate constant of OAA release exhibits a Nernstian (sigmoidal) dependence on potential with $n_{cat} = 1$ and a midpoint potential that correlates well with the reduction potential of the medial [4Fe4S] cluster, both in WT enzyme[66] (Figure 36B) and in mutants.[38] The magnitude of the variation reveals a 2- to 5-fold increase in the rate of OAA release, depending on temperature, amino-acid sequence, and buffer composition.

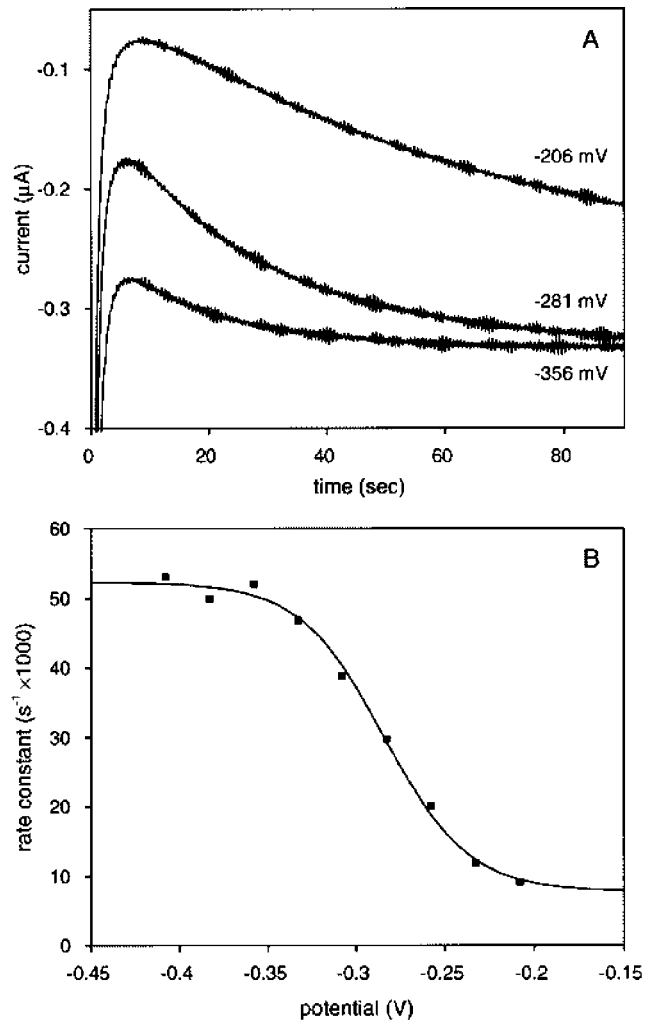

Figure 36. (A) Catalytic current showing the recovery of fumarate reductase activity when the release from the active site of the inhibitor oxaloacetate is triggered by applying a reducing potential (the chronoamperometric trace includes the interfacial charging current which decays during the first 10 s after the step). In panel B, the first-order rate constant for reductive activation is fit to a Nernstian sigmoid, which appears to be centered on the reduction potential of the medial [4Fe4S] cluster. Reprinted with permission from ref 66. Copyright 1997 American Chemical Society.

Taken together, these results strongly suggest that both the rate of fumarate reduction and the rate of OAA release from the active site flavin are faster when the medial cluster is reduced under turnover conditions, a conclusion that could never have been reached without the precise potential control that PFV provides. Although it is unlikely that the quinol pool that supplies electrons to fumarate reductase will ever be reducing enough so as to maintain the medial [4Fe4S] reduced under turnover conditions,[38] these results provide original information on the kinetics of electron transport in a multicenter enzyme. The acceleration observed at low potential reveals an acceleration of the rate-determining step in catalysis, which can be either flavin reduction (resulting from iET to the active site) or flavin reoxidation (upon hydride transfer from reduced flavin to fumarate and succinate release). The latter possibility was considered as unlikely because this would invoke an interaction between the medial cluster and the active site which is difficult to explain considering they are 20 Å apart.[38] Hence, the effect must reveal the interesting but complex possibility that, in this enzyme, iET to the active site is rate limiting and faster when

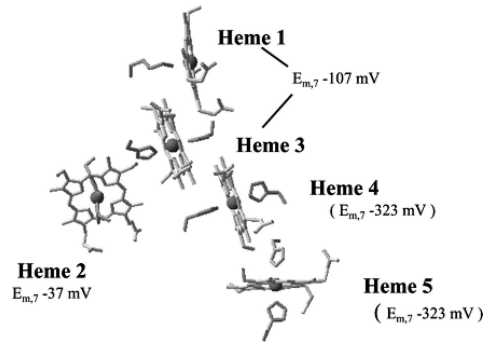

Figure 37. Assignment of the reduction potentials of the five hemes in the cytochrome *c* nitrite reductase from *E. coli* according to ref 149. The catalytic heme, which binds nitrite during turnover, is labeled "1". Reprinted with permission from ref 149. Copyright 2002 American Society for Biochemistry and Molecular Biology. Moura and collaborators[371] concluded from their titrations of the *D. desulfuricans* enzyme that hemes 1 to 5 have the following reduction potentials: −80, −50, −480, −400, +150 mV.

the medial cluster is reduced. This is in accordance with the boost being more visible at higher substrate concentration when turnover is faster and at higher pH when the reduction of the flavin is thermodynamically less favorable and possibly slower.[66]

This emphasizes an important difference between electron transfer in respiratory versus photosynthetic enzymes: in studies of photosynthetic iET, charge separation is triggered by a flash of light, but this does not change the overall electron "load";[168] in contrast, the number of electrons in a respiratory enzyme during a solution assay depends on antagonist electron transfers to and from the substrate and the redox partner, and under steady state turnover conditions, neither the overall charge of the enzyme nor the redox state of the individual centers can be determined using traditional techniques. Yet, the study of FrdAB demonstrates that the electron load may sometimes modulate the catalytic rate. It is interesting that a similar conclusion was drawn regarding a distinct fumarate reductase where electron transfers are mediated by hemes rather than by FeS clusters,[232] whereas in NiFe **hydrogenases**, no modulation of the rate of hydrogen oxidation occurs when the electrode potential is swept across the reduction potential of the very oxidizing cluster which is located in the middle of the ET chain (Figure 29).[55] In quinone oxidoreductases that house an odd number of one-electron redox relays and use obligatory two-electron substrates, it may also occur that not all redox states can be sampled during turnover under physiological conditions; in contrast, artificial one-electron dyes and the electrode are less restrictive redox partners.

Cytochrome *c* nitrite reductases (pdb 1FS7),[372] unlike the copper and cd_1 nitrite reductases mentioned in this section, catalyzes the *six-electron* reduction of nitrite to ammonium without releasing any intermediate, although NO and hydroxylamine are alternative substrates.[373] The enzyme from *E. coli* contains five hemes, four of which are arranged as in c_3 cytochromes while the fifth has a single axial ligand and binds nitrite during turnover (Figure 37).[373] The cytochrome *c* nitrite reductases from *Desulfovibrio* species are copurified with their physiological electron donor, the tetraheme NrfH, as a 2:1 complex ($NrfA_2NrfH$) which contains 14 hemes.[371] The structure of the complex from *D. vulgaris* Hildenborough suggests a physiological $NrfA_4NrfH_2$ organization (pdb 2J7A).[374] In multi-heme nitrite reductases, the characterization of each center by traditional spectroscopic methods proved very difficult: the UV−vis absorption bands are indistinguishable, and the information embedded in the EPR spectra is blurred by strong intercenter spin−spin interactions. For the *E. coli* enzyme, the current assignment of the reduction potentials to the five hemes is summarized in Figure 37; this is based on the results of potentiometric titrations monitored by EPR and on magnetostructural correlations between the *g*-values and the angle between the imidazoles planes of the heme axial histidine ligands.[375] The reduction potentials determined by Moura and co-workers in the case of the *D. desulfuricans* enzyme are indicated in the caption of Figure 37.

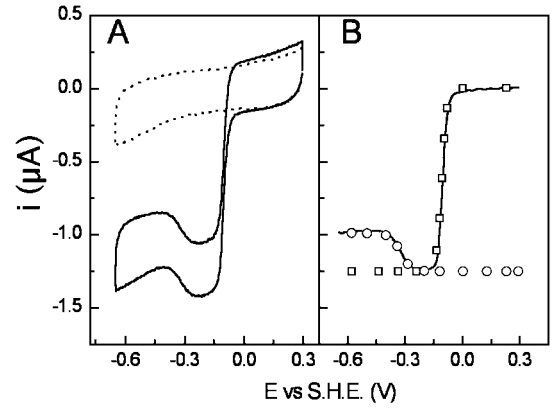

Figure 38. Typical voltammogram for nitrite reduction by ccNiR under conditions of low substrate concentration. Butt and co-workers model the signal as a $n_{cat} = 2$ main wave (squares) followed by a $n = 1$ switch at higher driving force. Reprinted with permission from ref 50. Copyright 2006 Research SignPost.

Figure 38 shows a typical voltammogram for nitrite reduction by *E. coli* cytochrome *c* nitrite reductase at low substrate concentration and at pH 7.[50,150] The signal is indistinguishable from that obtained with the *D. desulfuricans* enzyme,[189] suggesting a common mechanism and redox thermodynamics. It is characterized by a sharp ($n_{cat} \approx 2$) main wave at about ≈ -100 mV, followed by a $n_{sw} \approx 1$ attenuation at a potential that is close to that attributed to hemes 4 and 5 in Figure 37.[149,150] Hence, this decrease in activity at low potential was attributed to the reduction of this (or these) center(s).[149,150] Recent experiments by Butt and co-workers showed that, under low nitrite concentrations, the potential of the switch decreases upon increasing the pH until it levels off at high pH ($pK_a \approx 7$) whereas the magnitude of the switch is greater under alkaline conditions.[150] The authors' conclusion is that the switch results from an accumulation of uncompensated negative charge in the area of the enzyme around heme 4 or 5. To explain that this effect is damped at high concentration of nitrite, they propose that the reduction of the relay triggers a conformational change which slows down turnover, but only when turnover is slow does the electron reside on the relay for sufficient time to permit the change in conformation[150] (see the further discussion of ccNiR at the end of the following section).

3.4. Active Site Chemistry

The redox properties of the active site of an enzyme are usually thought of as being major determinants of activity. Just as protonations may have a strong effect on reduction potentials (section 2.1.2), substrate binding also affects the reduction potential of the active site if the dissociation constant is redox state dependent (eq 21). This is believed to have great physiological relevance. For example, in

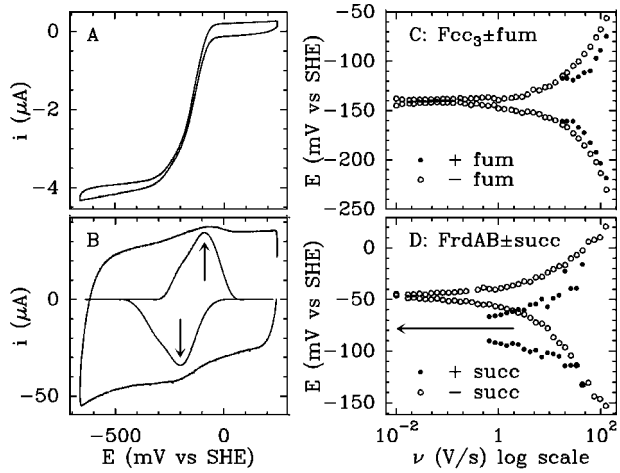

Figure 39. Voltammetry of adsorbed flavocytochrome c_3 (fcc3) in the presence of fumarate at a slow scan rate, where catalysis is at steady state, and a fast scan rate, where catalysis is outrun (panels A and B, respectively). Panel C is a trumpet plot showing the FAD noncatalytic peak position against scan rate for fcc3 without substrate (empty circles) or in the presence of 0.42 mM fumarate (filled circles). Panel D shows the same experiment but with *E. coli* fumarate reductase in the absence of substrate (empty circles) or with 50 mM succinate (filled circles). Reprinted with permission from refs 36 and 56. Copyright 2000, 2001 American Chemical Society.

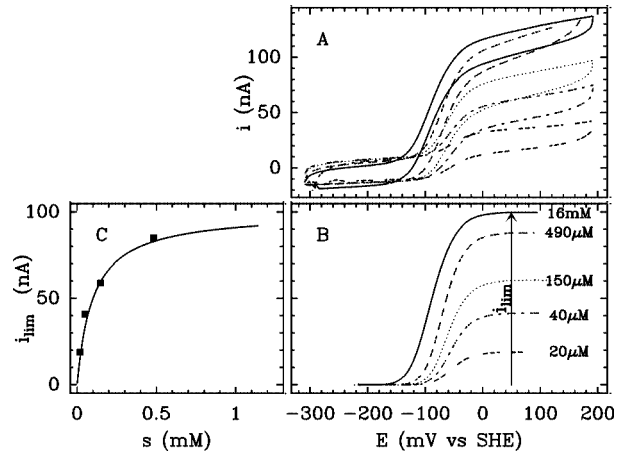

Figure 40. Raw (panel A) and baseline subtracted (panel B) voltammograms for succinate oxidation by *E. coli* fumarate reductase for various concentrations of succinate (as indicated) at pH 7.5, $\nu = 1$ mV/s, 20 °C, $\omega = 3$ krpm. In panel C, the limiting current is plotted against succinate concentration and fit to the Michaelis−Menten equation. Adapted from ref 36. Copyright 2001 American Chemical Society.

discussing the properties of flavin active sites, Stankovich emphasized that "redox properties generally match catalytic function, and when they do not, substrate binding often regulates the redox properties."[376] However, the effect of substrate binding is difficult to probe in conventional experiments because it is not possible to carry out the titration of the active site in the presence of substrate without the enzyme transforming it. Since equilibrium cannot be achieved, it is difficult to ensure that the measured reduction potentials correspond to thermodynamic properties. This is especially critical for hydrogenase (proton reduction) and photosystem II (water oxidation), since their substrate is inseparable from the solvent.[157,378]

Figure 39 illustrates the first method that can be used with PFV to access this invaluable information on the redox properties of the active site in the presence of substrate.[56] It is based on the examination of noncatalytic data recorded in the presence of substrate at fast scan rate; the second method below will deal with the interpretation of catalytic data. Panel A shows a steady state catalytic voltammogram for fumarate reduction by *S. frigidimarina* **flavocytochrome** c_3 (fcc3). Upon increasing the scan rate, the transformation predicted in Figure 9 is observed: starting from being S-shaped at steady state, an hysteresis is observed at moderate scan rates (not shown), and the signal starts resembling that obtained in the absence of substrate when the scan rate becomes so fast that the enzyme is taken to low potential only for a time that is too short for catalysis to proceed (Figure 39B); yet, during this very brief excursion to low potential, the entire enzyme is reduced and reoxidized. The transient current response is broadened by interfacial ET, but after baseline subtraction, it still clearly shows peaks on either scan, which reveal the prominent (δ is large) contributions of the active site flavin. The fact that the signals at high scan rates have the same size irrespective of the presence of fumarate showed that no stoichiometric reduction of the substrate occurs; hence, the flavin remains bound to *fumarate* (not succinate), a very reactive species that cannot be isolated, much less titrated. In this particular case, it is clear that no shift occurs with respect to the value measured in the absence of substrate (empty symbols in Figure 39C); only the peak separation is smaller when fumarate is bound, suggesting slightly faster ET.[56] The same experiment was carried out with *E. coli* **fumarate reductase** in the presence of succinate, as illustrated in panel D.[36] This time, the noncatalytic signal in the presence of substrate was detected at relatively small scan rates because with succinate oxidation by this enzyme being slow, the scan rate need not be very high to outrun catalysis. The FrdAB flavin signal is clearly shifted to low potential in the presence of succinate, suggesting that its binds more strongly to oxidized than reduced flavin (eq 14).

The interpretation of catalytic signals is the second strategy for accessing the effect of substrate binding on the active site reduction potential. This is simply because, provided intramolecular ET is fast, the catalytic wave reports directly on the redox transformations that occur at the active site while the enzyme is turning over. The simplest illustration comes from the study of succinate oxidation by the enzyme we have just discussed in relation to Figure 39D, *E. coli* **fumarate reductase**.[36] This enzyme is biased to function as a fumarate reductase *in vivo*, hence the low current for succinate oxidation in Figure 40A. With the maximal turnover rate being much slower than when the enzyme reduces fumarate, it is reasonably safe to assume that, in this process, all steps other than hydride transfer from succinate to flavin (*i.e.* iET, substrate and product binding and release, including deprotonation) should be fast enough on the time scale of turnover that the enzyme turns over in the regime where ET is Nernstian and substrate binding/release is at equilibrium (section 2.2.4.1). The increase in current at high potential reveals the formation of the oxidized and substrate-bound form of the active site, and the voltammogram can be simply interpreted as a titration curve of this species. Hence, the dissociation constant between succinate and oxidized flavin (K_o) can be deduced from the change in limiting current against substrate concentration (Figure 40C and eq 20), and most importantly, the waves in Figure 40B can be fit to eq 18 to determine the reduction potentials of the active site flavin under given conditions of

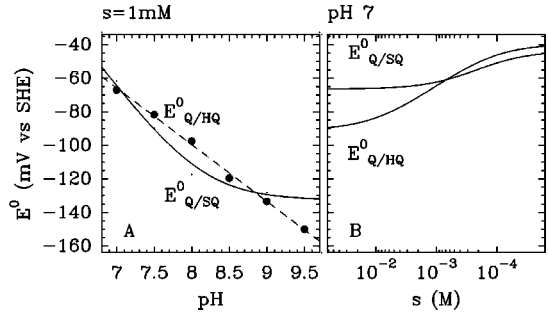

Figure 41. Apparent reduction potentials of the active site flavin of *E. coli* fumarate reductase measured under turnover conditions by fitting to eq 18 voltammograms such as those in Figure 40B. The results are shown in Pourbaix diagrams of E^0 against pH at constant s (panel A) or E^0 against $-\log(s)$ at constant pH (panel B) and fit to eq 21 to determine acidity and dissociation constants. Here, the notations O/I/R apply to the flavin in its redox states quinone (Q), semiquinone (SQ), and hydroquinone (HQ), respectively. Adapted with permission from ref 36. Copyright 2001 American Chemical Society.

pH and substrate concentration. In a second step, the dependence of these parameters on substrate concentration and pH can be plotted in Pourbaix diagrams showing E^0 against pH or $\log(s)$ and interpreted to determine the values of the pK_a and substrate dissociation constants of the active site in each of its redox states. At 1 mM succinate, the pH dependence of the reduction potentials of the flavin quinone/semiquinone and quinone/hydroquinone couples in Figure 41A confirms the overall 2-electron:1-proton stoichiometry observed in the absence of substrate and returns the pK_a of the flavin semiquinone. In panel B, the dependence on succinate concentration at pH 7 is fit to eqs 21 to determine K_o, K_i, and K_r; the ≈50 mV negative shift of $E^0_{Q/HQ}$ upon saturation with succinate is fully consistent with the data in Figure 39D.

This strategy makes it possible to model catalytic data by *allowing* substrate (proton or succinate) binding to any redox state of the active site without using a model that explicitly includes all binding steps; this would add unnecessary parameters that cannot be unambiguously deduced from the fits. Which state(s) substrate and protons bind to can be deduced *a posteriori* from the values of the acidity and dissociation constants measured from the pH− and substrate− concentration dependences of the reduction potentials of the active site (Figure 41).

A similar method was applied in a study of proton reduction by *A. vinosum* NiFe **hydrogenase**.[157] The reaction was studied at low temperature (5 °C) to decrease the turnover rate and, consequently, to minimize the broadening due to slow interfacial ET. The data in Figure 42 shows that, in spite of this, the wave shape is slightly distorted due to the existence of a distribution of interfacial ET rate constants (section 2.2.5.4). Hence, the reductive counterpart of eq 36 was used to fit the data (lines in Figure 42) to measure the reduction potentials of the active site and the limiting current (strictly, only a parameter that is proportional to i_{lim}). In a second step, the detailed pH-dependence of these parameters (Figure 43) was used to measure the acidity constants of the different redox states of the active site, namely the states "SI" (oxidized), "C" (half-reduced), and "R" (reduced).[31,379] In light of the considerations in section 2.2.4.2, we now understand that these acidity constants have apparent values which may depart from the true dissociation constants unless proton uptake and release are both very fast on the time scale

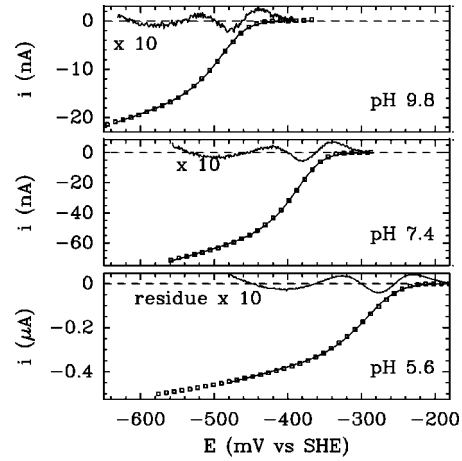

Figure 42. Proton reduction by *A. vinosum* NiFe hydrogenase at 5 °C, $\nu = 6$ mV/s, $\omega = 6$ krpm, and pH values as indicated. The squares show the baseline subtracted voltammograms (only one experimental point in every 10 collected has been plotted). The lines are fits to the reductive counterpart of eq 36, from which the reduction potentials of the active site can be determined. Adapted with permission from ref 157. Copyright 2002 American Chemical Society.

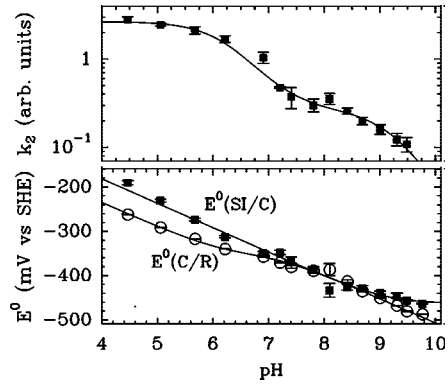

Figure 43. Proton reduction by *A. vinosum* NiFe hydrogenase at 5 °C. Normalized values of $i_{lim}/\beta d_0$ and active site reduction potentials obtained from the fits in Figure 42. The fit of this data allows the acidity constants of the active site to be determined. The error bars show the differences between the parameters determined for scanning in the oxidative and the reductive directions. Adapted with permission from ref 157. Copyright 2002 American Chemical Society.

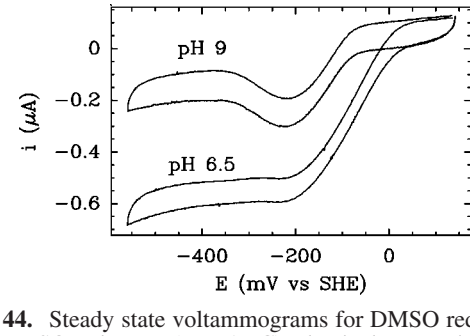

Figure 44. Steady state voltammograms for DMSO reduction by *E. coli* DMSO reductase (DmsABC) adsorbed on graphite, 25 °C, 5 mV/s, $s = 20$ mM (this is well above K_m), and pH as indicated.[39,40] Reprinted with permission from ref 40. Copyright 2003 American Chemical Society.

of turnover. A mechanistically important conclusion was that the uptake of a "third", labile proton in the active site, with acidity constant p$K_a \approx 7$, enhances the activity about 10-fold.[157] This finding is fully consistent with the pH-dependence of the FTIR data,[380] although, obviously, only

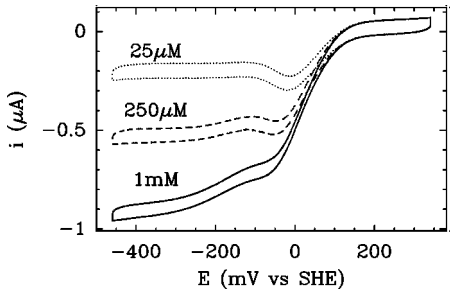

Figure 45. Steady state voltammograms for nitrate reduction by *E. coli* nitrate reductase (NarGHI) adsorbed on graphite, at pH 7, 30 °C, 10 mV/s, *s* as indicated. Reprinted with permission from ref 42. Copyright 2004 American Chemical Society.

PFV was able to resolve how this third proton affects the turnover rate.

It has been suggested that the mechanism deduced from these experiments may not reveal the physiological situation because, in PFV, the driving force greatly exceeds that provided by natural redox partners.[381] We acknowledge that, just as most enzymes function *in vivo* at substrate concentrations lower than K_m, they are unlikely to be subjected to extreme driving forces, determined by the reduction potential and the concentrations of the physiological, membrane-associated electron donor or acceptor: the activities that are measured on the limiting plateaus in PFV may never be reached *in vivo*. Clearly, the physiologically most important region of potential is certainly the low driving force region (around the main wave) that PFV is able to investigate precisely and from which information about the thermodynamic properties of the active site is actually gained.

Recently, the study of NADH oxidation by the flavoprotein subcomplex of mitochondrial **Complex I**[158] showed that a difference of 45−70 mV (depending on pH) exists between the catalytic potential measured under turnover conditions at high concentration of substrate and the reduction potential of the free active site, determined in noncatalytic voltammetry or equivalently in redox titrations followed by EPR.[158] Hirst and co-workers suggested that this could arise either from slow iET (sections 2.2.6 and 3.3) or from the *product* NAD^+ being retained during active site reoxidation.

Arsenite oxidases (100 kDa, pdb 1G8K)[382] belong to the DMSO reductase family of enzymes,[383−386] which collects bacterial enzymes of diverse functions despite housing similar mononuclear Mo active sites. These enzymes contain a conserved catalytic subunit where the active site Mo is bound to two pterin molecules, resulting in a minimal coordination of the metal by four thiolates. They are remarkably diverse in terms of oligomeric architecture and cofactor content. Accessory modules may be connected to the catalytic subunit to provide the ET chain and, in some cases, the site of interaction with the quinone pool.[387−391] An FeS cluster proximal to the Mo cofactor (Moco) is always present in the catalytic subunit of multicenter enzymes in this family; this cluster is a [4Fe4S] cluster in all cases but arsenite oxidases, where electrons are transferred from the active site to a high potential [3Fe4S] cluster and farther to a Rieske-type [2Fe2S] cluster. Also unique to arsenite oxidases is the fact that the Moco is not covalently attached to the protein: the Mo-binding residue, which is a serine, (seleno)cysteine, or aspartate in other members of this family, is an alanine in arsenite oxidase. Regarding the enzyme from *A. faecalis*, the EPR signatures of the $[3Fe4S]^+$ and $[2Fe2S]^+$ clusters can be detected, but the Mo ion remains silent in the course of potentiometric titrations,[391] suggesting that the Mo^V state tends to disproportionate ($E^0_{VI/V} \ll E^0_{V/IV}$). Since the Mo^V state is the usual spectroscopic handle to molybdenum, the active site in arsenite oxidase does not seem inclined to disclose any information . . . unless it is connected to an electrode.[165] In noncatalytic, electrochemical investigations, the broad ($n = 1$) signatures of the clusters were too faint to be detected but a sharp ($n > 1$) peak could be assigned to the active site $Mo^{VI/IV}$ couple, giving access to its reduction potential (≈290 mV at pH 6, 0 °C). Considering the linear dependence of the latter on pH (−59 mV per pH unit over 6 pH units compared to the theoretical −54 mV/pH), this two-electron reduction appears to be coupled to the uptake of two protons. Upon addition of arsenite, a wave centered on approximately the same potential as the noncatalytic peak demonstrates substrate oxidation and the Michaelis constant agrees with the value obtained in solution assays. Taken together, these results suggested that the oxidized active site can be described as Mo^{VI} bis-oxo (rather than protonated MoOOH) and that the presence of a "spectator" oxo ligand makes the reduction potential of the Moco high enough that it can oxidize arsenite.[165]

The PFV study of a very similar enzyme, although from a different organism (NT26), was also reported by Bernhardt and co-workers in ref 143. The wave is broad (close to $n_{cat} = 1$), and its position is less dependent on pH than that for the *A. faecalis* enzyme (−33 mV/pH in ref 143 *versus* ≈ −60 mV/pH, Figure 6 in ref 165). Based on the *n*-value of the wave, the authors suggest that an iET step limits the rate of arsenite oxidation.

Whereas arsenite oxidases exhibit relatively "simple" wave shapes,[143,165] showing a sigmoidal increase in activity as the electrode potential is swept across the reduction potential of the active site, all other enzymes in the **DMSO reductase** family share a common, complex dependence of activity on driving force. This was first described in the case of the membrane bound DMSO reductase from *E. coli* (DmsABC, 90 kDa)[39] and then with several related enzymes, namely periplasmic[156,160,186,343] and membrane bound[42,159] nitrate reductases. Since these enzymes share a common catalytic subunit but have very little overall homology, it is likely that the electrochemical data relate to the mechanism at the active site. Figure 44 shows steady state voltammograms for DMSO reduction by DmsABC.[39] The voltammogram recorded at high pH illustrates a typical electrochemical signature for this family of enzymes.[41] When the electrode potential is taken down, the reductive activity first increases to a maximum (*i* decreases to a minimum), before it drops and eventually plateaus off at high driving force; since this occurs at steady state, the same profile of activity is observed on the return scan. This clearly shows that the reductase activity of the enzyme is not the greatest under the most reducing conditions; instead, it appears to be optimized in a certain potential window. This was once considered as an unusual observation,[11,344] simply because this could not have been detected in traditional assays where the driving force is not a control parameter that can be easily adjusted. Such complex dependence of activity on potential has now been evidenced in PFV for many different enzymes, and understanding what this means in terms of mechanism is a challenge that must be tackled. The analogy between the activity of a redox enzyme being optimized over a certain potential range and the usual bell-shaped curves of activity against pH was noted:[39,41] just as maximal activity commonly

requires that the pH not be extreme, important (or faster) steps in the catalytic cycle of a redox enzyme may occur when the active site is in an intermediate redox state. In the case of *E. coli* DmsABC,[39] experimental limitations precluded the substrate concentration dependence to be studied, but the fact that the shape of the signal is strongly dependent on pH (Figure 44) suggested a catalytic mechanism involving a crucial protonation step when the Mo is in its intermediate redox state (Mo^V); at low potential, the Mo is quickly reduced to Mo^{IV} before the protonation can proceed, forcing the mechanism into a less-active route (hence the decrease in activity).[39] This mechanism explains that the low potential attenuation of activity is no longer seen under acidic conditions, when the rate of proton uptake may be high enough that taking the high or low potential reaction pathway makes no difference. In short, according to this model, the fact that the sequence of events in the catalytic cycle depends on the driving force is the reason the turnover rate need not vary in a monotonic fashion with the electrode potential.

A similar electrochemical signature was observed for the soluble NarGH fragment of the membrane bound **nitrate reductase** from *P. pantotrophus* by Butt and co-workers in ref 159. This enzyme is homologous to DmsABC and has a similar active site, but an aspartate in NarG, rather than a cysteine in DmsA, coordinates the Mo ion. (See refs 393 and 394 for comparative studies of the prokaryotic complex iron−sulfur molybdoenzymes.) In the case of *P. pantotrophus* NarGH, the fact that the attenuation of activity disappears at high concentration of substrate (rather than at low pH in the case of DmsABC) suggested to the authors a mechanism similar to that described above except that *nitrate* binding (rather than protonation) can occur either before or after Mo^V is further reduced to Mo^{IV} (the species that is competent to reduce nitrate), with binding to fully reduced Mo resulting in slower turnover. The authors derived a current equation for the corresponding scheme, and qualitative agreement with the data was demonstrated (Scheme 2 and Figure 9A in ref 159). They also proposed an alternative mechanism according to which the reduction of a redox center remote from the active site (e.g. one of the FeS clusters that belong to NarH) switches the enzyme into a less active form, e.g. by affecting its Michaelis parameters (Scheme 3 and Figure 9B in ref 159).

The data in Figure 45 are replotted from ref 42 and show nitrate reduction by *E. coli* **nitrate reductase** (NarGHI, 224 kDa, pdb 1Y4Z).[388] This large membrane-bound enzyme consists of three subunits and houses two *b*-type hemes (in NarI) and five FeS clusters (one in NarG,[395,396] four in NarH) in addition to a Moco (in NarG). At low concentration of nitrate, the activity reaches a maximum at about −25 mV, pH 7 and drops at higher driving force (dotted line in Figure 45). As the nitrate concentration is raised, a "boost" develops at ≈ -150 mV and takes over the low potential part of the wave at millimolar concentrations. A similar behavior was observed with the NarGH subcomplex, showing that the wave shape is independent of the presence of the di-heme cytochrome NarI.[42] Considering how complex it looks, no quantitative description of the wave shape has been attempted yet, but the resemblance to the predictions of Scheme 2B shown in Figure 12 cannot be missed. The work in ref 42 focused on chronoamperometric determinations of Michaelis and inhibition constants and how these depend on potential. The finding that the apparent affinity for substrate (K_m) may depend on the driving force is certainly a major aspect of this study. Regarding the measurement of inhibition constants, the authors showed that azide (N_3^-) is a stronger competitive inhibitor at high rather than at low potential. Since this "hard" ligand is expected to prefer metal ions in higher oxidation states, they proposed that the peak in activity reveals the crucial involvement of Mo^V (but see below).[42] Thus, a consistent relation emerged between mechanism (effective binding of nitrate to Mo^V) and physiology, with nitrate in micromolar levels being reduced only at high potentials.

Regarding *R. sphaeroides* periplasmic **nitrate reductase** (NapAB, 108 kDa, pdb 1OGY),[338] we recently examined the hypothesis that differential substrate binding to Mo in its redox states V and IV is the reason the maximal reductase activity is not obtained under the most reducing condition by using the model in section 2.2.4.2, which allows slow substrate binding to any redox state of the active site.[156,186] NapAB consists of a large catalytic subunit (NapA) containing a [4Fe−4S] cluster and the molybdenum active site cofactor (Moco), and of a small ET subunit (NapB) housing two surface-exposed *c*-type hemes. Using the general predictions of the six-member scheme in section 2.2.4.2 and by examining how the positions of the main features of the wave compare to the reduction potentials of the active site measured in potentiometric titrations and depend on substrate concentration (eqs. 23), we could conclude that nitrate binding is essentially irreversible on the time scale of turnover. A second simplification, based on the fact that the reduction potential of the $Mo^{VI/V}$ couple is very high, is that the steady state concentration of Mo^{VI} is always small in the range of electrode potential where catalysis occurs, so that substrate binding to "O" (Mo^{VI}) can be neglected. This decreases greatly (from ten in eq 22 to five) the number of parameters that need to be adjusted to fit the voltammetric data to the current equation corresponding to scheme 2B. Figures 46A and B show the baseline subtracted voltammograms for nitrate reduction by NapAB, recorded at low substrate concentration ($s < K_m$) and for two different values of the pH. Each pair of nearly-superimposed solid lines corresponds to data recorded by scanning the electrode potential in either direction: the fair overlay demonstrates that steady state was achieved. A unique set of parameters could be determined by fitting each bundle of voltammograms at every pH (dashed lines in panels A and B); the values of the active site reduction potentials are plotted against pH in panel C (the primed E^0 are for substrate-bound species, according to the notations in section 2.2.4.2). This was interpreted to deduce the sequence of events that occur in the reductive catalytic cycle. The emerging picture is that at moderate driving force, substrate binds to Mo^V, and the resulting complex takes up one proton. The second protonation occurs only after a second electron transfer from the proximal $[4Fe4S]^+$ cluster further reduces the substrate-bound active site to Mo^{IV}, yielding the species that is competent to produce nitrite. The protonation may be the main reason the reduction potential of the substrate-bound $Mo^{V/IV}$ couple is significantly raised upon substrate binding (*ca.* 200 mV, Figure 46C). This may have a strong influence on the kinetics of iET since raising the reduction potential of $Mo^{V/IV}$ makes the reduction of the Moco by the proximal [4Fe4S] cluster exergonic. This illustrates a situation where the value of the reduction potential of the *substrate-free* $Mo^{V/IV}$ couple obtained from equilibrium titrations is not relevant to describe the thermodynamics of reduction of the

active site in the catalytic cycle. NapAB also illustrates the situation where the position of the main catalytic wave greatly differs from the reduction potential of the substrate-free active site *even when s tends to zero*; this is quantitatively interpreted as resulting from an interplay between thermodynamics (substrate binding and protonation raising the reduction potential of the $Mo^{V/IV}$ couple) and kinetics (the irreversibility of the chemical steps triggered by substrate binding making this happen even under nitrate concentrations well below saturation).[156]

Butt and co-workers recently studied the periplasmic **nitrate reductase** from *P. pantotrophus*, which is homologous to that from *R. sphaeroides* and exhibits identical voltammetry.[343] The authors suggest that the peak in activity may not simply arise from preferential substrate binding to Mo^{V}, and they favor an explanation in terms of a modulation of activity caused by the change in redox state of a center whose reduction potential lies in the vicinity of E_{sw}. A similar signal was also observed by the same authors in another nitrate reductase, *Synechococcus elongatus* NarB, which is homologous to *D. desulfuricans* NAP[385,397] in that it houses a single redox cofactor (a [4Fe4S] cluster) in addition to the Moco.[160] NarB appears to be optimized to operate only under very reducing conditions: the Mo^{V} could not be reduced in potentiometric titrations, and consistently, the value of E_{cat} is about 350 mV below that of NapAB or NarGH. The operating potential of NarB matches well the low reduction potential of its redox partner NADH, whereas NapAB and NarGH receive electrons from the membrane pool of ubiquinol at higher potential.

We can now summarize and compare the studies of enzymes from the **DMSO reductase family**. Similar voltammetric signatures, showing an extremum in activity at moderate driving force, have now been observed for six homologous enzymes,[39,42,156,159,160,186,343] and it is safe to assume that these signals have a similar origin in terms of catalytic mechanism. Yet two distinct models have been proposed so far. (The same indetermination exists regarding the voltammetry of Complex II[41,146] and of the Fp subcomplex of Complex I,[158] and the arguments and counterarguments are quite similar, but here we shall only focus on nitrate reductases.) (1) The first model is based on the idea that the catalytic pathway in the reductive half-cycle depends on the driving force: under very reducing conditions, the active site is reduced so quickly that certain coupled steps can only occur after reduction to Mo^{IV}, but this route is slower than when these steps proceed *before* complete reduction. The two parallel pathways include rate limiting protonation and/or substrate binding steps, and modeling relies on a scheme such as Scheme 2B with $k_5 > k_4$. (2) The second hypothesis is that the enzyme switches between two different *forms* (rather than two catalytic pathways) depending on the electrode potential, as a result of subtle conformational changes; the low potential form has lower turnover rate, possibly because the Michaelis constant is greater or because intramolecular electron or proton transfer is slower.[343] The transition between the two forms must be fast (since no hysteresis is observed), and it is triggered by the reduction of a center that may be remote from the active site (eq 42). Regarding the identity of this center in nitrate reductase, Butt and co-workers emphasized that the reduction potential of the [4Fe4S] cluster is close to E_{sw} in the case of *P. pantotrophus* NapAB.[343] However, this is so neither in *S. elongatus* NarB[160] nor in *R. sphaeroides* NapAB.[156,186,338]

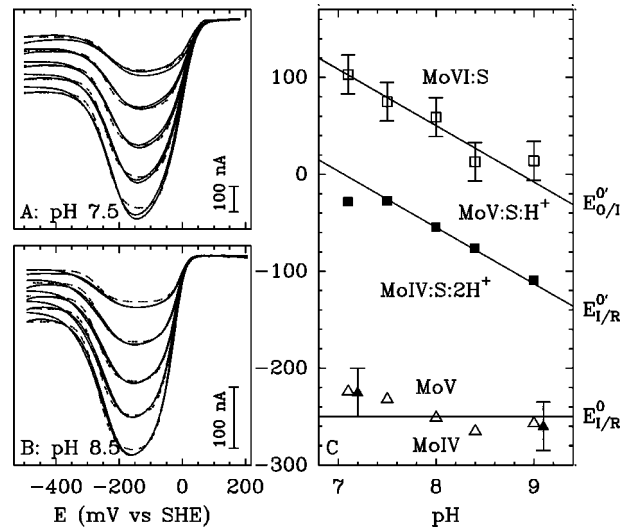

Figure 46. (A and B) Steady state, baseline subtracted voltammograms for nitrate reduction by *R. sphaeroides* NapAB at pH 7.5 and 8.5, for increasing substrate concentrations in the range 1−10 μM. The dashed lines are the fits to a simplified version of eq 22 where substrate binding to Mo^{VI} and substrate release are neglected. This can be used to measure the reduction potentials plotted in the Pourbaix diagram (panel C). The filled triangles are values determined independently from potentiometric titrations followed by EPR. Species O, I, and R correspond to the Mo in its redox states VI, V, and IV, respectively. The primed E^0 are for substrate-bound species. Adapted with permission from ref 156. Copyright 2007 American Chemical Society.

The defense of the second model has mainly been based on the criticism of the first;[343] here we list the pros and cons of this first model, in an attempt to clarify a controversy which is not yet resolved.

• An obvious quality of the first model is that it can be quantitatively assessed by examining the predictions of a rate equation derived from a kinetic scheme. Figure 46 shows that a model which is based on a simplified version of Scheme 2B and which includes very few adjustable parameters describes accurately the wave shape and its dependence on *s* and pH, at least over a limited range of experimental parameters (pH ≥ 7 and $s \ll K_m$).[156] One of the adjustable parameters is the reduction potential of the $Mo^{V/IV}$ couple, whose value and pH-dependence are found to be consistent with the results of potentiometric titrations (compare the empty and filled triangles in Figure 46C). This model also predicts that the value of K_m should depend on *E* and that the ratio K_m^{lim}/K_m^{peak} should be equal to i_{peak}/i_{lim} (see the discussion of eqs 2 in ref 186). This is in agreement with independent observations in refs 186 and 343.

• Against the model is the fact that it accounts for the wave shape only at low substrate concentration: Scheme 2B predicts that the wave should become sigmoidal at high enough *s*.[343] (The same argument has also been used to disregard the use of Scheme 2B in the case of Complex II; Figure 50 and ref 146.) We acknowledged that Scheme 2B is expected to apply only if substrate binding limits the rate of the two parallel pathways, and this should be so only at low *s*.[156,186] Under saturating conditions, certain steps that are ignored in Scheme 2B may become rate-limiting and influence the wave shape, but this does not challenge the relevance of the approach. Moreover, we have demonstrated that the value of *s*, which is "high enough" that the switch disappears, is not simply related to K_m; see the discussion of eq 24 above and of eq 13 in ref 156.

• We have mentioned above that the model is supported by the agreement between Mo reduction potentials measured in titrations and from fitting the wave shapes. Against this argument, Butt and co-workers emphasized that the Mo^V EPR signal has low intensity despite full molybdenum loading.[343] This may reveal the 2-electron reduction of Mo^{VI} to Mo^{IV} ($E^0(Mo^{VI/V}) < E^0(Mo^{V/IV})$, as in arsenite oxidase[165]), whereas the model can fit the data only on the condition that $E^0(Mo^{VI/V}) > E^0(Mo^{V/IV})$. In *R. sphaeroides* NapAB, the titration of the "visible" Mo^V is consistent with there being a large range of potential where the Mo^V species is stable,[338,398] but the signal is substoichiometric (quantitation yields 0.2 spin per enzyme whereas elemental analysis confirms full occupancy) and the substoichiometry is even worse in certain mutants.[398] Hence, at least for 20% of the Mo, the 2-electron reduction of Mo^{VI} to Mo^{IV} can be excluded. It seems that a fraction of the Mo behaves in EPR titrations as expected from the analysis of the electrochemical data with Scheme 2B, whereas the rest is EPR silent in "as prepared" samples. However, recent results of ours suggest that the Mo which is EPR-active arises from a dead-end species (V. Fourmond et al., unpublished data). Whether or not the forms of the Mo that engage in catalysis are those detected in EPR will have to be investigated using spectroscopies that are sensitive to all three redox states of the Mo.

• Last, inhibition studies were also used to assess the relevance of Scheme 2B. In their study of *E. coli* NarGHI, Armstrong and co-workers[42] showed that the competitive inhibitor azide binds more strongly at high potential (on the peak) than at low potential. They concluded that the peak current results from nitrate binding more strongly to Mo^V than to Mo^{IV}, in support of a mechanism like that in Scheme 2B (*vide supra*). In contrast, in their study of *P. pantotrophus* NapAB, Butt and co-workers recently used the effect of azide on the wave shape *against* the hypothesis that the peak in activity simply arises from preferential substrate-binding to Mo^V.[343] However, it is important to note that, in the context of Scheme 2B, the peak in activity does not reveal a greater steady state concentration of Mo^V: the turnover rate is proportional to the concentration of substrate-bound *reduced* state (RS), and the decrease in activity at low potential results from an increased concentration of *substrate-free* Mo^{IV} (R). The related observation in ref 39 that the potential window of activity of DmsABC correlates with the appearance of the Mo^V signal in potentiometric titrations is explained in the context of Scheme 2B by the fact that E_{sw} is close to $E^0(Mo^{V/IV})$ (eq 2a in ref 186), whereas E_{cat} is related to the reduction potential of the substrate-bound species (eq 2b in ref 186) and may be coincidently close to $E^0(Mo^{VI/V})$. We presume that the model in Scheme 2B will have to be extended to include inhibitor binding before it becomes possible to use the effects of inhibitors to learn about the mechanism.

Monoheme cytochrome c peroxidase (33 kDa, pdb 2CYP)[399,400] provides another example of PFV data being interpreted in terms of a rate-determining step occurring between the two ET steps that make the active site competent to transform the substrate. Figure 47A, from ref 37 shows the voltammograms of adsorbed yeast ccp in the presence of H_2O_2 in the range 0−200 μM, as indicated. The small slope at high driving force, which we now think results from a distribution of k_0 values (section 2.2.5.4) was corrected by subtracting a polynomial baseline, and the data were differentiated to make the underlying features of the wave more apparent (panel B). A convincing fit of i_{lim} in panel C and di/dE in panel D was obtained by assuming that the active site cycles between the fully oxidized form "Compound I" and the two-electron reduced "resting state" Fe^{III} which irreversibly binds and reduces H_2O_2. Since the latter chemical step is not rate-determining, the authors proposed that one of the two steps corresponding to the reduction of the active site is gated by a follow-up reaction. The preferred explanation was that compound II undergoes a rate-determining chemical transformation before further reduction to the resting state.

Di-heme cytochrome *c* peroxidases house a high potential electron-transferring heme *c* (E) and a peroxidatic heme *c* (P) (see ref 401 for a review). Their mechanism is thought to differ from that of monoheme peroxidases in that the reaction of the resting (reduced) state $Fe_E^{II}Fe_P^{III}$ with H_2O_2 produces a $Fe_E^{III}Fe_P^{IV}$-oxo state: hence, the second oxidizing equivalent is stored on heme E rather than as a porphyrin or tryptophanyl radical in mono-heme peroxidases. The low potential $Fe_P^{III/II}$ couple is not involved in the catalytic cycle. In a recent electrochemical study of the peroxidase from *Nitrosomonas europaea*,[330,250] Elliott and co-workers emphasized important differences between this enzyme and other di-heme peroxidases. First, the enzyme does not display any evidence of redox-linked activation, as required in other di-heme peroxidases. Second, the catalytic wave in Figure 27 could be modeled as a $n_{cat} = 1$ process, but its dependence on substrate concentration (inset in this figure) and pH (Figure 3 in ref 330) argues against the rate limiting step being electron transfer from Fe_E. From the observation in Figure 27 that $E_{cat} > 515$ mV is well above the reduction potential of heme $Fe_E^{III/II}$ (+450 mV), and all the more so that substrate concentration is low, the authors propose that the resting state of the enzyme is $Fe_E^{III}Fe_P^{III}$, not $Fe_E^{II}Fe_P^{III}$; this places the mechanism rather close to that of the monoheme eukaryotic peroxidases such as horseradish peroxidase and ccp.[403] In a subsequent paper,[250] the dependence of K_m on pH clearly revealed a single ionization, and it was shown that cyanide, just as H_2O_2, shifts E_{cat} in the negative direction. It acts as a competitive inhibitor whereas azide exhibits mixed[46] inhibition.

We have already discussed catalysis by **cytochrome c nitrite reductase** (ccNiR) in the section on intramolecular ET (section 3.3), where we restated the conclusions of the group in Norwich on the reason the nitrite reductase activity of the enzyme shuts down at low potential (Figure 38).[150] We now focus on the low driving force part of the data which informs on active site chemistry.[149,189] The same authors explain that the main (high potential) wave recorded at low concentration of nitrite can be fit to a $n_{cat} = 2$ sigmoid in terms of nitrite reduction being facilitated by the cooperative two-electron reduction of the pair of magnetically-coupled hemes (labeled 1 and 3 in Figure 37). This cooperative reduction is evidenced in potentiometric titrations followed by EPR by the concomitant disappearance of EPR signals at $g = 3.5$ and 10.8. However, this modification of the signal is not accompanied by the apparition of a new spectral contribution arising from uncoupled hemes in the partly reduced enzyme molecules. The authors suggest that this results from the reduction being a cooperative, two-electron process, although the $g = 3.5$ and 10.8 signals titrate at ≈ -107 mV in the manner expected for $n = 1$ centers.[149] Their interpretation of the catalytic wave is explicitly based on the

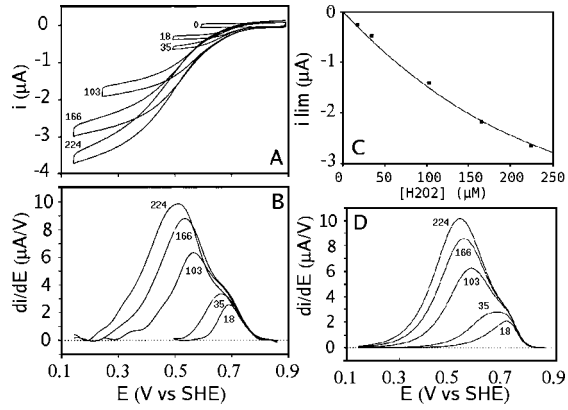

Figure 47. Catalytic voltammograms of adsorbed yeast cytochrome *c* peroxidase at 4 °C, 20 mV/s, H_2O_2 concentration in the range 0−224 μM as indicated (panel A). Panel B shows the same data after baseline subtraction and differentiation. Panel C shows the change in limiting current against *s*, and the modeled data is shown in panel D. Reprinted with permission from ref 37. Copyright 1998 American Chemical Society.

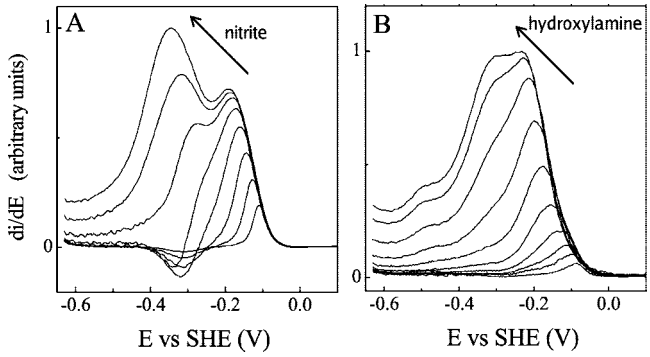

Figure 48. The complexity of the wave shapes for nitrite and hydroxylamine reduction by cytochrome *c* nitrite reductase from *E. coli* is clearly seen in these derivatives of the catalytic voltammograms. The arrows indicate how the signals are modified upon increasing the concentration of substrates. pH 7, 20°C, ω = 3000 rpm. Reprinted and adapted with permission from ref 149. Copyright 2002 American Society for Biochemistry and Molecular Biology.

idea that, under conditions of low substrate concentration, the catalytic potential should reflect the result of titrations carried out in the absence of substrate. The authors have recently revised their interpretation after they carried out spectroelectrochemical and MCD titrations which provided no evidence for an $n = 2$ event in the thermodynamic properties of the enzyme.[402] We have put forward another point of view[189] according to which the voltammetry of ccNiR may be thought of in terms of an active site moiety consisting of a heme initially bound to nitrite and undergoing six one-electron reductions until ammonium is produced and released. Then it may occur that, along the reaction pathways, a relatively slow chemical step immediately follows two successive one-electron reductions whose thermodynamics is such that they appear as a cooperative process. Considering the complexity of the kinetics in this enzyme,[373] which is ranked only by its intricate spectroscopy,[375,404] we could not elaborate further.

Figure 48 shows the derivatives (d*i*/d*E*) of voltammetric data obtained for nitrite (panel A) and hydroxylamine (panel B) reduction by *E. coli* cytochrome *c* nitrite reductase under conditions of high concentration of either substrate;[149] the enzyme from *D. desulfuricans* exhibits similar electrochemical signatures at neutral pH (unpublished data of ours). These enzymes reduce hydroxylamine even more quickly than nitrite, and hydroxylamine is believed to be an intermediate along the physiological reaction pathway.[373] The derivatives of the voltammetric data in Figure 48 show two positive peaks: the main wave at ≈ -100 mV is followed by a boost at higher driving force (≈ -350 mV) rather than the switch observed at low concentration of nitrite (Figure 38). The meaning of the boost is still unclear. It was noted that this must reveal a change in rate-limiting steps as the substrate concentrations are raised and that the similarity between the signatures for nitrite and hydroxylamine may reflect the intervention of similar rate-limiting events.[149,50]

We recently examined the kinetics of CO inhibition of nitrite reduction by the cytochrome *c* nitrite reductase from *D. desulfuricans* in ref 189. At a given concentration of nitrite, inhibition by CO followed bimolecular kinetics whereas the process of CO-release was first-order. Nitrite protects the enzyme in a manner that demonstrates that CO-inhibition is competitive (eq 55; that is, CO and nitrite exclude each other from binding to the same site). Having demonstrated that only the catalytic heme binds CO, we could attribute the deformation of the noncatalytic signal upon exposure to CO to the shift in reduction potential of the catalytic heme. This was used to measure both the value of this reduction potential (−200 mV at pH 7, in moderate agreement with the interpretation of EPR and Mössbauer titrations, −80 mV in ref 371) and how this depends on pH: the reduction of the catalytic heme is coupled to a single protonation at pH < pK_r = 8.2.[189] Thiocyanate, cyanate, nitrate, and azide were all shown to slow down nitrite reduction; in contrast, sulfate, chloride, and the product of nitrite reduction, ammonium, are ineffective.[405] The change in catalytic wave potential as a function of inhibitor concentration was interpreted in terms of tighter binding of thiocyanate, nitrate, and azide to the oxidized than the reduced active site.[406,405] For azide and cyanide, the mechanism of inhibition was investigated in ref 406. Inhibition by azide appears to be reversible and "mixed" (i.e. azide binds both to the Michaelis complex and to the substrate-free enzyme).[46] In contrast, cyanide equilibrates slowly with the enzyme, has higher affinity for reduced *vs* oxidized enzyme, and appears to bind to two distinct sites which have not been identified yet. The monocyano enzyme retains nitrite reduction activity, but the wave shape is very different from that of the cyanide-free enzyme: it shows a $n_{cat} = 1$ rather than $n_{cat} = 2$ main wave, followed by a boost of activity at lower potential rather than an attenuation (Figure 7 in ref 406). The former observation suggested to the authors that the reduction of the heme pair 1,3 is no longer cooperative in the monocyano enzyme. This clearly illustrates the complexity that can be associated with inhibitor binding to redox enzymes.

3.5. Bidirectional Catalysis

Understanding the molecular bases of catalytic directionality in redox enzymes is certainly a great and exciting challenge. It is all the more difficult to address that the very idea that some redox enzymes may work better in one direction than the other is still sometimes mistakenly thought to transgress thermodynamics (see the discussion in section 2.7.3 of ref 46). For a bidirectional enzyme, the catalytic PFV signal recorded in the presence of both the reduced and oxidized substrates is naturally very demonstrative of the difference between thermodynamics and kinetics, because

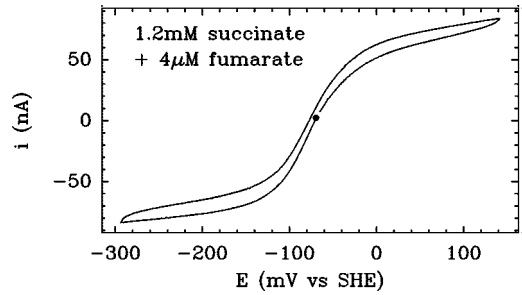

Figure 49. Reversible conversion between succinate and fumarate by *E. coli* fumarate reductase at pH 7, $\omega = 3$ krpm, $\nu = 1$ mV/s. The open circuit potential is indicated by a black circle. Reprinted with permission from ref 36. Copyright 2001 American Chemical Society.

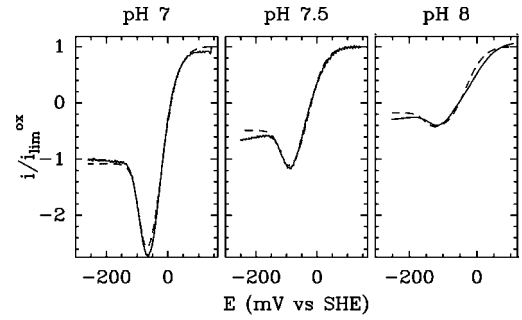

Figure 50. Reversible catalysis by *E. coli* succinate dehydrogenase (SdhAB) for 1:1 solutions of fumarate and succinate at 38 °C, 10 mV/s, 500 rpm. The voltammograms have been normalized by the limiting oxidative current. The model is shown as dashed lines. Redrawn with permission from Figure 4 in ref 146 using the data provided by J. Hirst. Copyright 1996 American Chemical Society.

it is a direct readout of the rate of turnover as a function of the thermodynamic driving force; hence, the catalytic bias may be visualized in a single potential sweep. This is illustrated in Figure 49, which shows the succinate/fumarate conversion by *E. coli* **fumarate reductase** (FrdAB) under conditions where both molecules are simultaneously present in solution. Thermodynamics predicts only the value of the open circuit potential (OCP) where $i = 0$, such that the forward and backward reactions proceed at exactly the same rate. This potential equates the formal reduction potential of the substrate/product couple, which can be calculated for any concentration ratio using the Nernst equation and the published value $E^{0'}_{F/S} \approx +20$ mV at 25 °C, pH 7.[407] Therefore, the OCP does not characterize the enzyme, unlike the rest of the electrochemical signal, which shows comparable oxidative and reductive currents despite the fact that succinate is in large excess over fumarate in this experiment. This demonstrates and somehow quantifies the fact that fumarate reductase is biased to work in the physiological direction. However, it is important to note that the enzyme's bias, should we define it as the ratio of *maximal* rates in either direction, is not simply in proportion to the ratio of substrate concentrations that make the magnitudes of the oxidative and reductive currents similar. For example, in Figure 49, the succinate concentration is in excess over the Michaelis constant for succinate, whereas the fumarate concentration is well below the corresponding value for fumarate; hence, only the oxidative current corresponds to a maximal rate. Another complication is that the signal recorded under saturating conditions of both substrates cannot be directly interpreted because either substrate may inhibit the transformation of the other.[36,157] Hence, the bias is more easily determined in two successive experiments carried out with a single substrate under saturating conditions.

Similar observations regarding the bias, the value of the OCP, and its dependence on pH and/or substrate concentrations were made in discussing the data for NiFe and FeFe **hydrogenases** (H^+/H_2),[55,144,187] **CO dehydrogenase** (CO_2/CO),[188] **succinate dehydrogenases** (succinate/fumarate),[12,146–148] and the so called 1λ subcomplex of **Complex I** ($NAD^+/NADH$).[151] Copper nitrite reductase also oxidizes NO,[408] but this has not yet been investigated in PFV.[167]

The catalytic conversion between fumarate and succinate has been thoroughly investigated in the case of succinate dehydrogenases (the soluble subcomplex SdhAB of **Complex II**).[11,41,146–148] In this system, a spectacular observation is that, under physiological conditions, the enzyme would be biased to operate in the direction of fumarate reduction, in reverse of the normal tricarboxylic acid (TCA) cycle, if a mechanism did not slow down reductive turnover under the most reducing conditions: the wave shape shows a "normal" sigmoidal increase in succinate oxidation activity upon increasing the electrode potential, but the wave for fumarate reduction exhibits a sharp ($n = 2$) "switch" at a potential that is close to that of the substrate-free flavin at all pH values (Figure 50).[146–148] The exact origin of the effect remains unclear,[146] but should this situation also hold for the entire Complex II, this driving-force dependent attenuation of reductive activity would provide an unprecedented way for controlling the TCA cycle as a function of the redox state of the quinone pool.[146] It is striking that an attenuation of reductive activity at low potential was also observed for another mitochondrial enzyme, the "Fp" subcomplex of **Complex I**. This protein houses the flavin where NADH/NAD^+ conversion occurs, one [2Fe2S] cluster and one [4Fe4S] cluster; only the latter belongs to the ET chain that transfers electrons to the quinone pool in the holo enzyme. Hirst and co-workers could reproduce the effect using either of two models, one considering an enhanced catalytic ability of the half-reduced state of the active site (as proposed above for NapAB and DmsABC, for example) and the other one considering a modulation of activity resulting from a change in redox state of the [2Fe2S] cluster.[158]

Regarding H^+/H_2 conversion by **hydrogenases**, all sorts of molecular determinants of directionality have been proposed. Peters suggested that the difference between the two FeFe hydrogenases from *C. pasteurianum* may result from their active sites having different reduction potentials.[409] In the case of NiFe hydrogenase, he emphasized the absence of free cysteines and the large number of histidines in the active site environment and proposed that this may direct proton flow.[409] We have demonstrated that, in NiFe hydrogenases, changing the histidine ligand of the distal cluster (Figure 29A) to a cysteine has no effect on the cluster's reduction potential, decreases 200-fold the hydrogen-oxidation activity of the enzyme, and has only a 2-fold effect on proton reduction: this demonstrates that a structural feature that is remote from the active site can have a major role in modulating the directionality of a multicenter enzyme.[360] Van Haaster[381] proposed that the lower K_m for H_2 of NiFe hydrogenases with respect to their FeFe counterparts is the reason the former are used for H_2-oxidation. PFV has been used to distinguish hydrogenases on the basis of their directionality. At pH 6 and under 1 bar of H_2, *D. desulfuricans* FeFe hydrogenase exhibits currents of similar ampli-

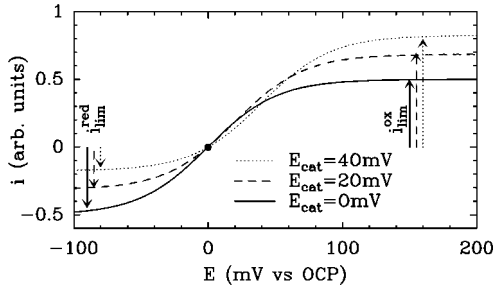

Figure 51. Illustration of the relation between (E_{cat} − OCP) and $i_{lim}^{ox}/i_{lim}^{red}$ in the case of a sigmoidal wave. The values of (E_{cat} − OCP) are as follows: 0 (solid line), 20 mV (dashed line), and 40 mV (dotted line).

tudes in either direction and the proton reduction current is independent of hydrogen pressure.[169] In contrast, under 1 bar of H_2, the prototypical NiFe hydrogenases from *A. vinosum* and *D. gigas* and the membrane bound NiFe hydrogenase (MBH) from *Ralstonia eutropha* show hardly any or no detectable reductive activity; this is at least partly because hydrogen inhibits the proton reduction activity of NiFe hydrogenases.[157,169,187] Defining the bias as the ratio of limiting currents recorded at high and low potentials under 1 bar of H_2 or argon, respectively, we have emphasized that the enzymes from *Allochromatium vinosum* and *Desulfovibrio fructosovorans*, which are both thought to illustrate the typical properties of the NiFe class of hydrogenases, exhibit actually very different bias.[187] The *D. fructosovorans* enzyme is an efficient catalyst for both H_2 oxidation and formation (solid lines in Figure 31A) whereas the catalytic current for H_2 oxidation by the enzyme from *A. vinosum* is at least ten times larger than that corresponding to optimal reductive activity (Figures 28 and 42). We hope that site-directed mutagenesis will make it possible to investigate further the subtle relation between bias and structure in this family of enzymes.

We now discuss the relation between catalytic bias and catalytic wave shapes recorded when both substrates are present. It was noted that which direction the enzyme prefers is either related to or caused by the deviation of the value of E_{cat} from the reduction potential of the substrate/product couple (the OCP).[144,146,151,169] As noted in ref 147, the separation between E_{cat} and the OCP defines the ratio of oxidation and reduction limiting currents if the wave shape is roughly sigmoidal (i.e. if there is no switch or boost). In other words, since E_{cat} is defined graphically, it is equivalent to observe that E_{cat} > OCP or that $i_{lim}^{ox} > i_{lim}^{red}$ or *vice versa* (Figure 51), and thus the former observation cannot be considered as an explanation of the latter. In the case of both *E. coli* **succinate dehydrogenase**[146] and *M. elsdenii* FeFe **hydrogenase**,[144] the value of E_{cat} exhibits a weak dependence on pH, but the reduction potential of the substrate/product couple decreases 60 mV per pH unit (both succinate reduction and hydrogen formation are two-electron two-proton reactions); referring to Figure 51, it is inferred that these enzymes are relatively better catalysts of oxidation at higher pH.

How E_{cat} compares to the OCP is a property of the enzyme which does relate to the bias, but the challenge is to understand how it is defined by the thermodynamics and kinetics of the entire catalytic cycle. Bidirectional catalysis by an adsorbed redox enzyme was never treated in the framework of a kinetic scheme, as presented in section 2 for unidirectional catalysis. In refs 146–148, the reversible conversion between succinate and fumarate was fit to a combination of sigmoidal functions, so that the *n*-values of the voltammograms' features could be measured (dashed lines in Figure 50). This cannot substitute for a complete kinetic description of the system, but we acknowledge that this is a rather difficult task. Clearly, it is not possible to model bidirectional voltammograms by adding algebraically the current equations derived for irreversible catalysis in opposite directions.

We finally note that all the aspects of the reactivity mentioned in section 2 are potentially related to the problem of the catalytic bias in bidirectional enzymes. For example, in our study of periplasmic nitrate reductase (Figure 46),[156] we proposed that the irreversibility of nitrate binding in NapAB may be one of the reasons this enzyme, unlike the homologous nitrite oxidases in *Nitrobacter* species,[410,411] has no detectable oxidative activity even under the most oxidizing conditions: this may be because catalytic nitrite oxidation would necessarily involve a step of nitrate release from the active site that is precluded in NapAB.

3.6. Redox-Dependent, Slow or Irreversible (In)activation Processes

Examples have been given in sections 3.3, 3.4, and 3.5 of *reversible* attenuations of activity which occur under certain conditions of driving force. In these cases, the activity responds instantly to a change in driving force, or at least no deviation from steady state could be observed in experiments carried out at moderate scan rates (typically $\nu < 100$ mV/s). Hereafter, we address the distinct issue of *slow* (in)activation. We do so only briefly because hydrogenases provide the most prominent examples,[43,169–173,176,187] and the use of PFV to study their redox (in)activation has recently been reviewed.[52,174,412] Slow interconversions between active and inactive states of an enzyme as a function of the redox poise may have physiological relevance; some enzymes which occur in anaerobic yet aerotolerant organisms (e.g. *Desulfovibrio* species) exist in a reduced, active form which is irreversibly damaged by O_2, but this form can be reversibly oxidized into an inactive state which resists oxygen. Therefore, reversible oxidative inactivation may afford protection against oxidative damage. This is exemplified by *Desulfovibrio africanus* pyruvate-ferredoxin oxidoreductase[413,414] and *Desulfovibrio vulgaris* Hildenborough FeFe-hydrogenase.[377,378] Other examples of redox-poise controlling catalytic efficiency include diheme peroxydases and galactose oxidase. Pre-steady-state measurements in PFV can easily resolve these potential-dependent processes.

Our first example is Butt and co-workers' recent report on the reductive, irreversible activation of two distinct **nitrate reductases**, the NarGH subcomplex from *Paracoccus pantotrophus* and *Synechococcus elongatus* NarB.[166] In both cases, the reductive activation manifests as a sudden increase in activity which occurs only during the first sweep to negative potentials, at a potential that is lower than the catalytic potential. The conditions under which the effect is observed are not entirely clear. In the case of NarGH, whether or not the reductive activation is detected depends on apparently minor changes in the content of the buffers used in the purification procedure. The effect could be confirmed in stopped flow experiments as a lag of a few seconds before steady state catalysis is achieved; this makes it unlikely that the increase in activity seen in PFV is actually a consequence of a potential-dependent reorientation of the

enzyme on the electrode the first time it is taken to low potential. The comparison of the EPR signatures of the different samples shows that, in enzymes that require activation, the Mo^V exhibits a previously unreported EPR signal, characterized by the absence of the usual hyperfine structure due to an exchangeable proton. The authors propose that the new signal and the species that requires activation arise from the aspartate ligand of the Mo ion providing bidentate (rather than monodentate) coordination, as observed in one of the two available X-ray structures of the enzyme from *E. coli*.[388,394] In NarB,[160] as in *D. desulfuricans* NAP,[397] the Mo ion is coordinated by a cysteine. The reductive activation of this enzyme is clearly demonstrated (Figure 8 in ref 166), but it is not observed with all enzyme samples and no spectroscopic differences could be detected between NarB preparations displaying the distinct PFV responses. Yet, this demonstrates that PFV can approach with great facility reductive activation processes that could otherwise only be accessed through techniques requiring rapid mixing of reactants.[166]

The recent study of **copper nitrite reductase** in ref 167 also established that the reduced type-2 active site can exist in an active conformation and an inactive conformation that interconvert with a rate of $\approx 0.1\ s^{-1}$. This is evidenced in chronoamperometric experiments where the electrode potential is poised at an oxidizing potential (+560 mV) where the enzyme is fully activated and then stepped to a lower potential (+60 mV; E_{cat} is about halfway in between). After the step, the activity decreases towards a steady state value, and the transient relaxation can be fit to an exponential decay (Figure 3 in ref 167). It is proposed that this results from the reduced type-2 copper site equilibrating between a four-coordinate active form and a three-coordinate form incapable of binding substrate, detected in earlier investigations by EXAFS and X-ray crystallography.

Recent results in the same group have demonstrated that direct electrochemistry can be used to study the anaerobic, oxidative inactivation of *Carboxydothermus hydrogenoformans* **CO dehydrogenase**.[188]

The oxidative inactivation of **NiFe hydrogenases**, a process first characterized in the mid-1980s,[415] has recently become a very hot topic because this reaction is the main obstacle to using these enzymes in biofuel cells[416,417] or in photosynthetic hydrogen production processes. Hence, much effort is currently devoted to identifying enzymes that can function in air[416] or to understanding the molecular bases of the oxygen sensitivity[418–420] in order to use genetic engineering techniques to design oxygen-resistant enzymes.[421] The prototypical NiFe hydrogenases from *Allochromatium vinosum* or *Desulfovibrio* species exist in a mixture of oxidized, inactive forms when they are purified under aerobic conditions, and activation requires reduction.[415] There exist two EPR-detectable fully-oxidized and inactive states called NiA and NiB. NiA is formed under aerobic conditions, and its reactivation requires hours of incubation under H_2. In contrast, the formation of NiB can occur under anaerobic oxidizing conditions and its reduction is fast. Hence, NiA and NiB are sometimes termed "unready" and "ready," respectively. The inactivation by oxygen takes only seconds whereas anaerobic oxidation is slow. In crystallographic studies, both oxidized forms are modeled with an oxygen species bridging the Ni and Fe ions of the active site (alternatively a bridging sulfur in the enzyme from *D. vulgaris* Miyazaki F[422,172]). NiA and NiB do not interconvert, and the structural difference that makes their kinetics of formation and reactivation so different is still unresolved.[51] A recent hypothesis refers to the presence of a bridging peroxo in NiA, which may be an oxo in NiB.[423,424] Among the various other proposals, it was suggested that they differ in the presence of a bridging oxo versus terminal hydroxo ligand,[425] or in the orientation of a nearby glutamate side chain.[426] Recently, by allowing a detailed characterization of how the rates of (in)activation depend on temperature, pH, potential, and hydrogen pressure, elaborate PFV experiments have been very useful for disentangling the complex and concurrent (in)activation processes of NiFe hydrogenase. This is summarized below.

The reversible conversion between the active and NiB forms of hydrogenase under *anaerobic* conditions is easily visualized in voltammetry, as illustrated in panels A and B of Figure 19. The decrease in hydrogen-oxidation current at high potential reveals the inactivation (in addition to slight film loss), and the fact that the enzyme reactivates when the potential is taken back to more reducing conditions is obvious from the increase in current on the reverse scan.[43] That this effect is only visible at low scan rate demonstrates that the anaerobic inactivation is slow, and the comparison between panels A and B makes it clear that the inactivation is faster under more alkaline conditions (all things being equal, the high potential decrease in activity is more pronounced at higher pH). Chronoamperometric experiments were designed to probe the potential dependence of the rates of activation and inactivation. It was shown that the rate of anaerobic inactivation is pH-dependent and potential-independent; thus, the process is gated by a preceding chemical step. In contrast, reductive activation of NiB is too fast to be measured. This activation involves a one-electron reduction, judging by the width of the sigmoidal increase in current on the voltammetric sweep toward low potential, and the reduction potential of the reductive activation is simply read as the position of the inflection point; the temperature dependence of this potential returns large positive ΔS and ΔH values, and its pH dependence is consistent with the one-electron reduction of NiB being coupled to a single protonation at pH below $pK_{red} \approx 7.6$ and 45 °C. Overall, this provides compelling evidence that the chemical step limiting the rate of oxidative inactivation is the uptake of OH^-.[43]

There are several obstacles to using traditional techniques to characterize the kinetics of the inactivation of hydrogenases by O_2, with the most obvious being that aerobic inactivation is fast on the time scale of solution assays and that oxygen cannot be included in the assay buffers because it would interfere with the catalytic reduction of the redox partner (cosubstrate). Hence, the kinetics of the reaction with oxygen was for a long time poorly characterized. In PFV, the turnover rate can be easily measured every tenth of a second (hence, fast inactivation can be resolved) and the hydrogen oxidation activity can be measured in the presence of oxygen simply by setting the potential of the electrode at a value that is high enough that no direct reduction occurs.

Figure 52 illustrates the strategy that we used to characterize the rate of aerobic inactivation of *Desulfovibrio fructosovorans*[34] and *Aquifex aeolicus*[427] NiFe hydrogenases (see section 2.4.2). The enzyme is adsorbed on an electrode poised at high potential; the electrochemical cell is continuously flushed by bubbling hydrogen and aliquots of air-saturated solution are repeatedly injected in the cell. From all sorts of control experiments,[187] it is known that the oxygen concen-

tration decays exactly exponentially with time after each injection (as schematized in Figure 52A). The current is proportional to the concentration of active enzyme and decays with time (panel B). Provided inactivation is first-order in active enzyme, the instant rate of inactivation is simply obtained by differentiating the logarithm of the current (eq 57). The facts that (1) this rate of inactivation in panel C decays exponentially with time and that (2) the initial rate of inactivation extrapolated to the time of injection is proportional to the initial concentration of oxygen (panel D) show that inactivation is first-order in oxygen concentration. The overall bimolecular rate constant is about 40 s^{-1}(atm O_2)$^{-1}$ at 40 °C, under one atm of H_2. The rate of inactivation is offset by a small constant ($\approx 10^{-2}$ s^{-1}) that is the rate of anaerobic formation of NiB under these very oxidizing conditions. We observed that this rate is independent of pH in *D. fructosovorans*.[187] This difference between the kinetic behaviors of the enzymes from *A. vinosum* on one side and *Desulfovibrio gigas* and *D. fructosovorans* on the other side was also noted from FTIR investigations.[428] The weak dependence of the overall rate of aerobic inactivation on hydrogen concentration implies that the inhibition by O_2 is not competitive.[187] Initially, our interpretation was that H_2 need not be released from the active site before O_2 reacts with it. An alternative explanation is that the rate of aerobic inactivation which we measure is the sum of the rates of formation of NiA and NiB, and only the formation of NiA is slowed by protecting the enzyme active site with H_2. This explanation is consistent with the following observations: (1) reaction with O_2 produces a mixture of NiA and NiB,[187,170] and (2) the ratio NiA/NiB is smaller if the aerobic inactivation is carried out under an atmosphere of H_2 than under argon (see below).[170]

In their independent study of the aerobic inactivation of *A. vinosum* NiFe hydrogenases,[170] Armstrong and co-workers focus on the nature of the species formed upon exposing the enzyme to O_2 rather than on the rate of inactivation. The enzyme is fully and quickly inactivated by injecting large amounts of O_2 under different conditions of potential and hydrogen pressure, and the precise fraction of NiA over NiB formed in this process is measured *a posteriori* in a very clever manner: after the inactivation, the enzyme is taken back to a potential that is low enough that it reactivates (but high enough that hydrogen oxidation occurs); Figure 53A clearly shows that the recovery of activity is biphasic. The fast phase corresponds to the reduction of NiB while the slow recovery reveals the reactivation of NiA; hence, the ratio NiA over (NiA + NiB) formed in the inactivation process can be deduced by examining the course of the reactivation. Remarkably, the fraction of NiA (slow phase) is found to be greater under conditions of electron depletion (low H_2 concentration and high electrode potential, Figure 53B). The authors propose that since NiA is formed under conditions that do not favor complete reduction of O_2 at the active site, it may be two-electron more oxidized than NiB.

Further studies in the same group aimed at clarifying the nature of NiA, produced upon partial reduction of O_2 at the NiFe active site, by examining how its rate of reactivation is influenced by a number of parameters.[170,171] The adsorbed enzyme was subjected to various and elaborate sequences consisting of potential steps and gas exposures (O_2, CO, H_2, and/or N_2), and the extent and rate of reactivation was examined in relation to the history of events. An intermediate is identified on the reaction pathway from NiA to the active

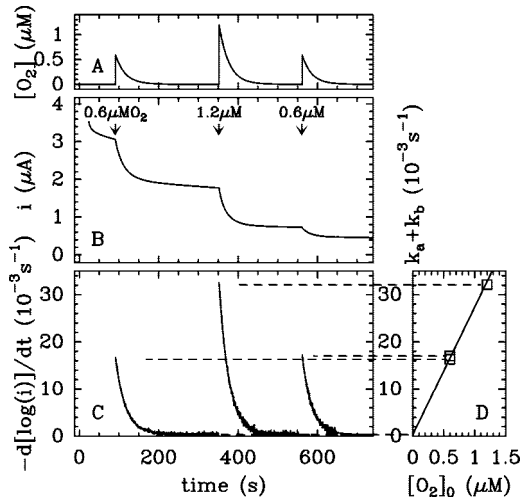

Figure 52. Kinetics of the inhibition of *D. fructosovorans* NiFe hydrogenase by oxygen. The change in oxygen concentration against time is schematized in panel A. Panel B: Activity against time. Panel C: Rate of inactivation against time. Panel D: Initial rate of inactivation against initial oxygen concentration. Adapted with permission from ref 187. Copyright 2004 American Chemical Society.

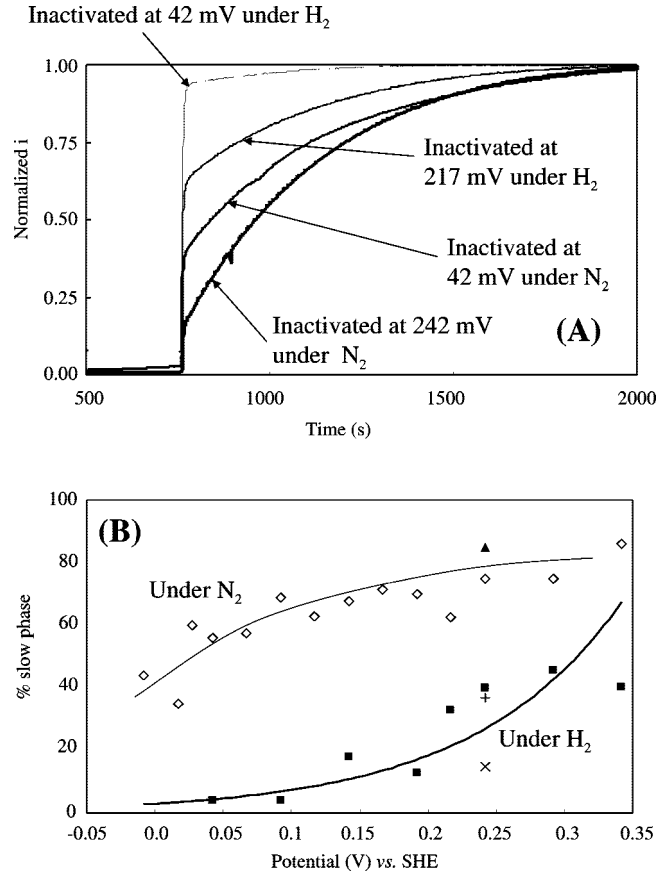

Figure 53. Panel A: Course of reactivation at $E = -160$ mV of the NiFe hydrogenase from *A. vinosum* after it has been fully inactivated by oxygen while the electrode was poised at the potential indicated on each curve. Panel B: Fraction of slow phase in the reactivation process as a function of the electrode potential and the nature of the gas phase (1 bar of H_2 or N_2) during the inactivation. This fraction reveals the ratio of NiA over NiA plus NiB, formed in the inactivation. Reprinted and adapted from ref 170. Copyright 2004 American Chemical Society.

enzyme: by decreasing the electrode potential, NiA can be reversibly reduced to a state that only requires hydrogen to

be irreversibly activated. The competitive inhibitor CO can substitute for H_2 in the latter stage, making it likely that it is a displacement process.

An electrochemical study of the inactivation of the **FeFe hydrogenase** from *Desulfovibrio desulfuricans* is reported in refs 169 and 173. This enzyme is strictly identical to *D. vulgaris* Hildenborough FeFe hydrogenase and houses the so-called "H" cluster which is the active site of iron hydrogenases (it consists of a dinuclear FeFe subsite covalently linked to a [4Fe4S] cluster)[429] and two [4Fe4S] clusters that act as relays (59 kDa, pdb 1HFE).[429] From biochemical studies,[377,378] it was known that the enzyme can be purified under air but that it requires reductive reactivation to become fully active. This is entirely consistent with the result of the electrochemical investigation which evidences the oxidation of the enzyme into an inactive state that is at least partially protected against O_2. The rate of inactivation is limited by a chemical reactions that is coupled to protonation. The reactivation is fast, and the pH dependence of the potential where it occurs reveals coupling with a protonation step at pH above $pK_{ox} \approx 6$. It is also demonstrated that the rate of reactivation of the CO-inhibited enzyme is enhanced upon illumination when H_2 is being oxidized, whereas the enzyme is photoinert under reducing conditions; this suggests the existence of two distinct CO-bound forms; only the form that prevails under oxidizing conditions is photolabile.[173]

In ref 370 we studied and described in detail the oxidative inactivation of *Clostridium acetobutylicum* FeFe hydrogenase (HydA1, strep-tagged and homologously expressed), which is highly homologous to *Clostridium pasteurianum* (CpI) hydrogenase (64kDa, pdb 1FEH).[409] Clostridial FeFe hydrogenases are similar to the enzyme from *D. desulfuricans* except that their ET chain consists of four FeS clusters rather than two. The fact that purifying an active clostridial hydrogenase requires strictly anaerobic conditions had always been interpreted as revealing their extreme oxygen-sensitivity. On the contrary, our detailed analysis of chronoaperometric data shows that this enzyme reacts surprisingly slowly with O_2, in a multistep process which we could untangle. Whereas oxygen irreversibly inactivates the enzyme from *D. desulfuricans* in its active state,[169,173] it binds reversibly (and weakly) to *C. acetobutylicum* hydrogenase ($K_d \approx 0.1$ mM). Although the irreversible oxidation of the oxygen-bound complex is very slow (4×10^{-3} s^{-1}), it is responsible for irreversibly inactivating the enzyme when it is purified under air. A similar behavior was observed in solution experiments where the isotope-exchange activity was monitored in the presence of O_2; hence, the oxygen-tolerance is not a result of the enzyme being adsorbed on the electrode. The observation that the competitive inhibitor CO protects the enzyme against O_2 ruled out the possibility of significant oxidative dammage to electron-transferring FeS clusters. The apparent bimolecular rate constant for reaction with O_2 is much smaller than that for prototypical NiFe hydrogenases, which are usually said to be more resistant to O_2 (4×10^{-2} s^{-1} mM^{-1} *vs* 32 s^{-1} mM^{-1} for the NiFe hydrogenase from *D. fructosovorans* in Figure 52 and ref 187). Last, the rate of anaerobic oxidation is much slower than that for the FeFe enzyme from *D. desulfuricans*, but this inertia is detrimental to *C. pasteurianum* hydrogenase, since the inactive, oxidized state is protected against O_2 and can be reactivated by reduction.[169,173,377,378]

Reference 169 reports a comparative study of several hydrogenases, namely the FeFe hydrogenase from *Desulfovibrio desulfuricans*, the prototypical NiFe hydrogenases from *A. vinosum* and *Desulfovibrio gigas*, and the NiFe membrane-bound hydrogenase (MBH) from *Ralstonia eutropha* H16. The latter does inactivate reversibly when it is oxidized under anaerobic conditions but unlike typical NiFe hydrogenases, and despite high homology with these enzymes,[33] it is *reversibly* inhibited by O_2. This makes this enzyme a good catalyst to be used in aerobic biofuel cells, as demonstrated in refs 174 and 416, despite the fact that it exhibits lower activity than other NiFe hydrogenases (according to Table 4 in ref 33). Later, the MBH NiFe enzyme from *Ralstonia metallidurans* CH34 heterologously overexpressed in *R. eutropha* proved even more resistant to O_2;[417,412] it displays substantial H_2 oxidation activity even below 10 ppm H_2 *in air*.[430]

Beyond the requirement that oxygen sensitivity be quantified in order to sort the different hydrogenases according to their potential use in biofuel cells, the aforesaid studies also have invaluable merit in that they demonstrate how complex and convoluted the processes of aerobic inactivation can be. The enzyme may be inactivated under oxidative anaerobic or aerobic conditions, and provided inactivation is fast, this may actually protect the enzyme against further oxidative damage. Hydrogenases may be inhibited by oxygen, but depending on the enzyme and on its redox state, this inhibition can be fully irreversible (reduced FeFe hydrogenase from *D. desulfuricans*),[173] partly reversible (reduced FeFe hydrogenase from *C. acetobutylicum*),[370] fully reversible (enzymes from *Ralstonia* sp.),[416] or irreversible under oxidizing conditions but reversed upon subsequent reduction in a process whose complex kinetics reveals the heterogeneity of the oxidized inactive state (typical NiFe hydrogenases). Hence, electrochemistry helped *define* the sensitivity of the enzyme by greatly refining earlier conclusions from biochemical studies in addition to providing unique insights into the mechanism of (in)activation. It is still puzzling that very similar proteins may exhibit so different reactivities (compare the MBH NiFe hydrogenases from *Desulfovibrio* sp. and *R. eutropha*, or the FeFe hydrogenases from *D. desulfuricans* and *C. acetobutylicum*), and PFV played a major role in disclosing this variety of behavior. We hope that site-directed mutagenesis studies will make it possible to understand better the relation between structure and reactivity.

3.7. Substrate Channels

Substrate channels are elongated cavities which either connect the active site to the solvent or transport intermediates from one active site to the next in multifunctional enzymes (see refs 431–433 for reviews). As far as redox enzymes are concerned, the best documented example is acetyl-CoA synthase/CO dehydrogenase,[434–437] but channels are also suspected in NiFe hydrogenases (Figure 1),[438–440] FeFe hydrogenases,[439,441] cytochrome *c* oxidase,[442,443] copper-containing amine oxidase,[444] and Photosystem II.[445] However, one may also consider that small diatomic molecules are able to freely diffuse through the protein matrix and, therefore, the requirement for a channel to transport CO, H_2, O_2, and other small substrates is questionable.[444,446] From an experimental point of view, there are few measurements of the rate of intramolecular diffusion in enzymes. We end this review by discussing two results which show that this

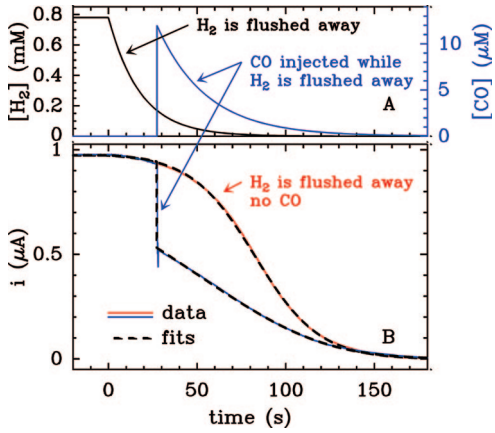

Figure 54. Hydrogen oxidation by WT *D. fructosovorans* NiFe hydrogenase: measurement of the Michaelis constant relative to H_2 and of the inhibition constant relative to CO. Panel A shows the change in hydrogen (black) and CO (blue) concentrations against time. The red line in panel B shows the change in current against time in the experiment where H_2 is flushed away at $t > 0$. The blue line is the result of a similar experiment, but a solution saturated with CO was injected at $t = 30$ s while the concentration of H_2 was decreasing. The fits to eqs 50 and 58 are shown as dashed lines. 1 bar of H_2 at $t > 0$, $E = -160$ mV, pH 7, 40 °C, 3 krpm. (Unpublished data.)

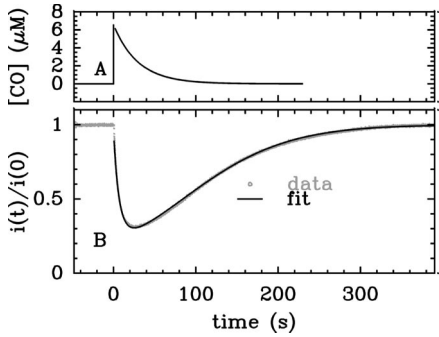

Figure 55. Inhibition by CO of H_2 oxidation by a mutant of *D. fructosovorans* NiFe hydrogenase where a double mutation narrows the gas channel. Panel A: CO concentration against time. Panel B: The change in current against time (gray) is fit to eq 54 (solid line). The aliquot of solution saturated with CO was injected at $t = 0$. 1 bar of H_2, $E = -160$ mV, pH 7, 40 °C, 3 krpm.[447]

particular aspect of the catalytic mechanism may also be approached in PFV with surprising ease.

Figure 54A shows in black the change in concentration of dissolved H_2 against time that is obtained when, after having maintained an atmosphere of 1 bar of H_2 until $t = 0$, a small tube is suddenly plunged into the buffer and used to bubble argon. This flushes hydrogen away from the cell and its concentration decreases exponentially with time, with a time-constant which we denote by τ_{H_2} (*cf.* section 2.4.2). The red curve in panel B shows the sigmoidal change in current for hydrogen oxidation by *D. fructosovorans* NiFe **hydrogenase** in the same experiment. Importantly, the change in H_2 concentration is slow enough with respect to turnover rate that steady state conditions apply at all times. Therefore, steady state rate equations can be used to model the transients:[187] the equation used to fit this data (black dashed line) is simply obtained by inserting into the Michaelis−Menten equation a substrate concentration whose time-dependence is $[H_2](t) = [H_2]_0 \exp(-t/\tau_{H_2})$ (eq 50). A very different strategy in solution assays consists in interpreting the change in turnover rate against time following the complete consumption of the substrate by the enzyme (in which case, kinetic equations must be integrated to account for the time courses of reactions; see e.g. ref 381). Armstrong and coworkers have used the electrochemical method described above in their study of CO dehydrogenase, to measure the K_m values relative to CO and CO_2.[188]

In the experiment shown as a blue curve in Figure 54B, an aliquot of CO-saturated solution is injected at $t \approx 30$ s while the hydrogen concentration is decreasing (blue line in Figure 54A). In this experiment, the concentrations of both CO and H_2 evolve with time, but the equation for the transient current is again simply obtained by using the rate equation that considers competitive inhibition by CO, in which we insert time-dependent concentrations of both H_2 and CO:

$$i(t) = \frac{i_{max}}{1 + \frac{K_m}{[H_2](t)}\left(1 + \frac{[CO](t)}{K_i}\right)} \qquad (58)$$

The fit is shown as a dashed curve; no better agreement was obtained assuming mixed inhibition, and the fit was worse if an uncompetitive mechanism is assumed. Two conclusions can be drawn from this very simple experiment. (1) Since CO-inhibition is competitive, CO binds to the active site, most likely by using the same gas channel (if there is any) as hydrogen. Establishing the competitive character of CO inhibition in traditional assays would require measuring the rates of hydrogen oxidation for discrete values of the substrate and inhibitor concentrations and determining the dependence of the K_m for H_2 on the concentration of CO. This is actually a time-consuming and difficult set of experiments, since it may not be easy to precisely set the concentrations of gaseous substrate and inhibitors to values that remain constant during the solution assays. Here the information is obtained in an experiment that takes a couple of minutes. (2) CO binds and is released *quickly* (reversibly) on the time scale of the activity measurement: inhibition occurs with no apparent delay (in the experiment in Figure 54, the current was sampled every tenth of a second), and the recovery of activity exactly follows CO exhaustion from the cell.

The experiment in Figure 55 was carried out with a mutant of *D. fructosovorans* NiFe hydrogenase in which the gas channel observed in the X-ray structure (Figure 1) has been partly blocked with no effect on the maximal rate of hydrogen oxidation in solution assays. The cell was under 1 bar of H_2, and an aliquot of CO was injected in the buffer at $t = 0$. In contrast with the observation made with the WT enzyme (Figure 4 in ref 187), the decrease in activity following the injection can be resolved, suggesting that the mutation slows down CO access to the active site, and the recovery of activity occurs only well after CO has vanished from the cell; hence, the diffusion of CO out of the enzyme is also slow. This brings the first evidence for the existence of a functional channel (or at least a preferred path) that connects the active site to solvent and is blocked by the mutation. The data could be fit to eq 54, initially derived for studying the CO-inhibition of cytochrome *c* nitrite reductase,[189] to measure the rates of CO diffusion along the gas channel, to and from the buried NiFe active site. This strategy is now used in our group to study in detail how the molecular structure of the gas channel influences the kinetics of intramolecular diffusion.[447]

4. Conclusion

In PFV, the enzyme works under conditions that are certainly not physiological, since it exchanges electrons with an electrode rather than with a soluble redox partner and the accessible range of driving force is extremely large. However, provided one is able to bring evidence that the native properties of the enzyme are retained (section 3.1), this configuration greatly simplifies the kinetic investigation by making the activity measurement virtually instantaneous and by providing the thermodynamic driving force as an invaluable additional control parameter. The whole set of results discussed here clearly demonstrates that this provides fresh perspectives in enzymology.

Anticipation is all the more difficult that every new enzyme which is studied may bring new, fascinating prospects, by offering opportunities to approach certain aspects of the reactivity for the first time. However, several general directions for future work stand out. New strategies for adsorbing the enzymes onto innocent electrodes must be developed, ideally with emphasis on configurations that are suitable for combining spectroscopic techniques and direct, *catalytic* electrochemistry. The modeling of the catalytic data also needs to mature: the reader has surely noticed that, in some cases exposed herein, our understanding of what the signal may mean is rather approximate and our interpretation somewhat ambiguous, whereas electrochemistry is certainly a technique that is ideally suited to probe the kinetic aspects of chemical reactivity in the most quantitative fashion. Direct electrochemistry of enzymes is a relatively new method in the context of enzyme kinetics, and we are confident that the efforts of all the teams that are taking part in this research will prove incredibly fruitful. We can't wait!

5. List of Abbreviations

A	electrode surface
d	distance between the electrode and the surface-exposed relay
d_0	width of the probability density function of d
E	electrode potential
$E^0_{O/I}$, $E^0_{I/R}$	reduction potentials of the active site alone, $E^0_{O/R} = (E^0_{O/I} + E^0_{I/R})/2$
$E^{0'}_{O/I}$, $E^{0'}_{I/R}$	reduction potentials of the active site bound to substrate
$E^{app}_{O/I}$	apparent reduction potentials of the active site
ET	electron transfer
F, R, T, f	Faraday constant, gas constant, temperature, $f = F/RT$
i	current
I	inhibitor concentration
iET	intramolecular electron transfer
i_{lim}	limiting current
i_p	peak current
K_o, K_i, K_r	dissociation constants from the active site. $K_o = k_{-o}/k_o$, etc.
k_o, k_i, k_r	bimolecular rate constants for binding of substrate to O, I, R
k_{-o}, k_{-i}, k_{-r}	first-order rate constants for substrate release
k_a, k_i	activation and inhibition or inactivation rate constants
K_1, K'_1	ratios of rate constants for intramolecular ET
k_1, k'_1, k_{-1}, k'_{-1}	1st-order rate constants for intramolecular ET
k_i	slowest rate constant for forward iET in eq 39
k_2	depending on context, 1st- or 2nd-order rate constant for substrate transformation and product release or turnover rate
k_{cat}	turnover rate
k_0	prefactor in the BV equation
k_∞	prefactor in the Marcus equation
k_{max}	maximal rate predicted by Marcus theory of interfacial ET
K_m	Michaelis constant on the plateau
m_0	$0.62D^{2/3}\omega^{1/2}\nu^{-1/6}$
m'_0	$m_0 s_b/\Gamma k_{cat}$
n_{cat}, E_{cat}	parameters characterizing the wave shape
n_{sw}, E_{sw}	parameters characterizing a "switch"
O, I, R	oxidized, half-reduced, and reduced forms of the active site
OS, IS, RS	the substrate-bound forms of the active site
pdb	protein data bank accession number, http://www.rcsb.org/pdb/
PFV	protein film voltammetry
RDE	rotating disk electrode
s	substrate concentration
s_b, s_0	substrate concentration in the bulk and at the electrode surface
α	depending on context, transfer coefficient or ratio of rate constants, $\alpha_i = k_i/k_r$, $\alpha_o = k_o/k_r$
δ	$= \exp[f(E^0_{I/R} - E^0_{O/I})]$
Γ	electroactive coverage
ΔE	redox interaction in section 2.1.1.2
ΔE^{lim}	shift of E^{app} when iET is fully rate limiting, in section 2.2.6.1
λ	depending on context, reorganization energy (Figure 6) or dimensionless parameter
τ	time constant for the decrease in substrate or inhibitor concentration
ν	depending on context, scan rate (V/s) or kinematic viscosity (eq 43)
ω	electrode rotation rate

6. Acknowledgments

The studies in our group could not have been carried out without the active collaboration of the following biologists and biochemists. For working with us, we particularly thank A. Magalon, M.-T. Giudici-Orticoni, L. Girbal and P. Soucaille, D. Pignol, S. Dementin and M. Rousset, and also the people in their teams.

We are grateful to G. Almeida, F. A. Armstrong, F. Baymann, B. Burlat, J. Butt, C. Cavazza, L. Dutton, A. Cornish Bowden, S. J. Elliott, F. Guerlesquin, B. Guigliarelli, H. A. Heering, J. Hirst, A. Ivancich, L. J. C. Jeuken, A. Jones, B. Limoges, E. Lojou, R. Louro, L. L. Martin, K. Meffrou, W. Nitschke, and L. Pieulle for fruitful discussions and sometimes for providing figures or data. We thank C. Baffert, B. Frangioni, F. Leroux, and V. Fourmond for commenting on the preliminary versions of the manuscript and for taking part in Marseilles in some of the experiments we mentioned.

Our work is funded by the CNRS, the University of Provence, the City of Marseilles, and ANR programs. We gratefully acknowledge support from the *Pôle de compétitivité CAPENERGIES*.

7. Supporting Information Available

The complete list of references, including article titles and clickable DOI numbers. This material is available free of charge via the internet at http://pubs.acs.org.

8. References

(1) Lee, C.-W.; Gray, H. B.; Anson, F. C. *J. Electroanal. Chem.* **1984**, *172*, 289.

(2) Yaropolov, A. I.; Karyakin, A. A.; Varfolomeev, S. D.; Berezin, I. V. *Bioelectrochem. Bioenerg.* **1984**, *12*, 267.
(3) Armstrong, F. A.; Lannon, A. M. *J. Am. Chem. Soc.* **1987**, *109*, 7211.
(4) Guo, L. H.; Hill, H. A. O.; Lawrance, G. A.; Sanghera, G. S.; Hopper, D. J. *J. Electroanal. Chem.* **1989**, *266*, 379.
(5) Paddock, R. M.; Bowden, E. F. *J. Electroanal. Chem.* **1989**, *260*, 487.
(6) Guo, L. H.; Hill, H. A.; Hopper, D. J.; Lawrance, G. A.; Sanghera, G. S. *J. Biol. Chem.* **1990**, *265*, 1958.
(7) Burrows, A. L.; Hill, H. A. O.; Leese, T. A.; McIntire, W. S.; Nakayama, H.; Sanghera, G. S. *Eur. J. Biochem.* **1991**, *199*, 73.
(8) Ikeda, T.; Matsushita, F.; Senda, M. *J. Electroanal. Chem.* **1991**, *6*, 299.
(9) Khan, G. F.; Shinohara, H.; Ikariyama, Y.; Aizawa, M. *J. Electroanal. Chem.* **1991**, *315*, 263.
(10) Bianco, P.; Haladjian, J. *J. Electrochem. Soc.* **1992**, *139*, 2428.
(11) Sucheta, A.; Ackrell, B. A. C.; Cochran, B.; Armstrong, F. A. *Nature* **1992**, *356*, 361.
(12) Sucheta, A.; Cammack, R.; Weiner, J.; Armstrong, F. A. *Biochemistry* **1993**, *32*, 5455.
(13) Kinnear, K. T.; Monbouquette, H. G. *Langmuir* **1993**, *9*, 2255.
(14) Zhang, W.; Li, G. *Anal. Sci.* **2004**, *20*, 603.
(15) Gorton, L.; Lindgren, A.; Larseson, T.; Munteanu, F. D.; Ruzgas, T.; Gazaryan, I. *Anal. Chim. Acta* **1999**, *400*, 91.
(16) Stoica, L.; Ludwig, R.; Haltrich, D.; Gorton, L. *Anal. Chem.* **2006**, *78*, 393.
(17) Armstrong, F. A.; Vincent, K.; Vareiro, M.; Cracknell, J. *Chem. Rev.* **2008**, *108*, 2439.
(18) Calabrese Barton, S.; Gallaway, J.; Atanassov, P. *Chem. Rev.* **2004**, *104*, 4867.
(19) Hambourger, M.; Gervaldo, M.; Svedruzic, D.; King, P. W.; Gust, D.; Ghirardi, M.; Moore, A. L.; Moore, T. A. *J. Am. Chem. Soc.* **2008**, *130*, 2015.
(20) Vincent, K. A.; Li, X.; Blanford, C. F.; Belsey, N. A.; Weiner, J. H.; Armstrong, F. A. *Nat. Chem. Biol.* **2007**, *3*, 761.
(21) Pita, M.; Katz, E. *J. Am. Chem. Soc.* **2008**, *130*, 36.
(22) Zhang, J.; Chi, Q.; Kuznetsov, A. M.; Hansen, A. G.; Wackerbarth, H.; Christensen, H. E. M.; Andersen, J. E. T.; Ulstrup, J. *J. Phys. Chem. B* **2002**, *106*, 1131.
(23) Ulstrup, J.; Zhang, J.; Kuznetsov, A. M.; Medvedev, I. G.; Chi, Q.; Albrecht, T.; Jensen, P. S. *Chem. Rev.* **2008**, *108*, 2737.
(24) Murgida, D. H.; Hildebrandt, P. *Phys. Chem. Chem. Phys.* **2005**, *7*, 3773.
(25) Bonanni, B.; Andolfi, L.; Bizzarri, A. R.; Cannistraro, S. *J. Phys. Chem. B* **2007**, *111*, 5062.
(26) Nicholls, D. G.; Ferguson, S. J. *Bioenergetic 3*; Academic Press: New York, 2002.
(27) Fraústo da Silva, J. J. R.; Williams, R. J. P. *The Biological Chemistry of the Elements: The Inorganic Chemistry of Life*; Oxford University Press: 2006.
(28) Carroll, J.; Fearnley, I. M.; Skehel, J. M.; Shannon, R. J.; Hirst, J.; Walker, J. E. *J. Biol. Chem.* **2006**, *281*, 32724.
(29) Sazanov, L. A.; Hinchliffe, P. *Science* **2006**, *311*, 1430.
(30) Sazanov, L. A. *Biochemistry* **2007**, *46*, 2275.
(31) Cammack, R.; Frey, M.; Robson, R., Eds. *Hydrogen as a fuel, learning from Nature*; Taylor and Francis: London and New York: 2001.
(32) Volbeda, A.; Charon, M. H.; Piras, C.; Hatchikian, E. C.; Frey, M.; Fontecilla-Camps, J. C. *Nature* **1995**, *373*, 580.
(33) Fontecilla-Camps, J. C.; Volbeda, A.; Cavazza, C.; Nicolet, Y. *Chem. Rev.* **2007**, *107*, 4273.
(34) Dementin, S.; Burlat, B.; de Lacey, A. L.; Pardo, A.; Adryanczyk-Perrier, G.; Guigliarelli, B.; Fernandez, V. M.; Rousset, M. *J. Biol. Chem.* **2004**, *279*, 10508.
(35) Savéant, J. M. *Elements of molecular and biomolecular electrochemistry*; John Willey & Sons, Inc.: 2006.
(36) Léger, C.; Heffron, K.; Pershad, H. R.; Maklashina, E.; Luna-Chavez, C.; Cecchini, G.; Ackrell, B. A. C.; Armstrong, F. A. *Biochemistry* **2001**, *40*, 11234.
(37) Heering, H. A.; Hirst, J.; Armstrong, F. A. *J. Phys. Chem. B* **1998**, *102*, 6889.
(38) Hudson, J. M.; Heffron, K.; Kotlyar, V.; Sher, Y.; Maklashina, E.; Cecchini, G.; Armstrong, F. A. *J. Am. Chem. Soc.* **2005**, *127*, 6977.
(39) Heffron, K.; Léger, C.; Rothery, R. A.; Weiner, J. H.; Armstrong, F. A. *Biochemistry* **2001**, *40*, 3117.
(40) Léger, C.; Elliott, S. J.; Hoke, K. R.; Jeuken, L. J. C.; Jones, A. K.; Armstrong, F. A. *Biochemistry* **2003**, *42*, 8653.
(41) Elliott, S. J.; Léger, C.; Pershad, H. R.; Hirst, J.; Heffron, K.; Blasco, F.; Rothery, R.; Weiner, J.; Armstrong, F. A. *Biochim. Biophys. Acta* **2002**, *1555*, 54.
(42) Elliott, S. J.; Hoke, K. R.; Heffron, K.; Palak, M.; Rothery, R. A.; Weiner, J. H.; Armstrong, F. A. *Biochemistry* **2004**, *43*, 799.
(43) Jones, A. K.; Lamle, S. E.; Pershad, H. R.; Vincent, K. A.; Albracht, S. P. J.; Armstrong, F. A. *J. Am. Chem. Soc.* **2003**, *125*, 8505.
(44) Léger, C.; Jones, A. K.; Albracht, S. P. J.; Armstrong, F. A. *J. Phys. Chem. B* **2002**, *106*, 13058.
(45) Jones, A. K. Investigations of electron transfer in redox enzymes. Thesis, University of Oxford, 2002.
(46) Cornish-Bowden, A. *Fundamental of Enzyme kinetics*; Portland Press: 2004.
(47) Heering, H. A.; Wiertz, F. G. M.; Dekker, C.; de Vries, S. *J. Am. Chem. Soc.* **2004**, *126*, 11103.
(48) Armstrong, F. A.; Heering, H. A.; Hirst, J. *Chem. Soc. Rev.* **1997**, *26*, 169.
(49) Armstrong, F. A.; Wilson, G. S. *Electrochim. Acta* **2000**, *45*, 2623.
(50) Butt, J. N. *Recent Res. Dev. Biochem.* **2003**, *4*, 159.
(51) Armstrong, F. A. *Curr. Opin. Chem. Biol.* **2005**, *9*, 110.
(52) Vincent, K. A.; Armstrong, F. A. *Inorg. Chem.* **2005**, *44*, 798.
(53) Hirst, J. *Biochim. Biophys. Acta* **2006**, *1757*, 225.
(54) Bernhardt, P. V. *Aust. J. Chem.* **2006**, *59*, 233.
(55) Pershad, H. R.; Duff, J. L. C.; Heering, H. A.; Duin, E. C.; Albracht, S. P. J.; Armstrong, F. A. *Biochemistry* **1999**, *38*, 8992.
(56) Jones, A. K.; Camba, R.; Reid, G. A.; Chapman, S. K.; Armstrong, F. A. *J. Am. Chem. Soc.* **2000**, *122*, 6494.
(57) Armstrong, F. A.; Camba, R.; Heering, H. A.; Hirst, J.; Jeuken, L. J. C.; Jones, A. K.; Léger, C.; McEvoy, J. P. *Faraday Discuss.* **2001**, *116*, 191.
(58) Bard, A. J.; Faulkner, L. R. *Electrochemical methods. Fundamental and applications*, 3rd ed.; John Wiley & Sons, Inc.: 2004.
(59) Honeychurch, M. J.; Rechnitz, G. A. *Electroanalysis* **1998**, *10*, 285.
(60) Albery, W. J.; Boutelle, M. G.; Colby, P. J.; Hillman, A. R. *J. Electroanal. Chem.* **1982**, *133*, 135.
(61) Rowe, G. K.; Carter, M. T.; Richardson, J. N.; Murray, R. W. *Langmuir* **1995**, *11*, 1797.
(62) Nahir, T. M.; Bowden, E. F. *J. Electroanal. Chem.* **1996**, *410*, 9.
(63) Xie, Y.; Anson, F. C. *J. Electroanal. Chem.* **1995**, *384*, 145.
(64) Chobot, S. E.; Hernandez, H. H.; Drennan, C. L.; Elliott, S. J. *Angew. Chem., Int. Ed.* **2007**, *46*, 4145.
(65) Plichon, V.; Laviron, E. *J. Electroanal. Chem.* **1976**, *71*, 143.
(66) Heering, H. A.; Weiner, J. H.; Armstrong, F. A. *J. Am. Chem. Soc.* **1997**, *119*, 11628.
(67) Laviron, E. *J. Electroanal. Chem.* **1972**, *35*, 333.
(68) Kurnikov, I. V.; Ratner, M. A.; Pacheco, A. A. *Biochemistry* **2005**, *44*, 1856.
(69) Louro, R. O. *J. Biol. Inorg. Chem.* **2007**, *12*, 1.
(70) Louro, R. O.; Catarino, T.; Paquete, C. M.; Turnera, D. L. *FEBS Lett.* **2004**, *576*, 77.
(71) Santos, H.; Moura, J. J. G.; Moura, I.; LeGall, J.; Xavier, A. V. *Eur. J. Biochem.* **1984**, *141*, 283.
(72) Gayda, J. P.; Benosman, H.; Bertrand, P.; More, C.; Asso, M. *Eur. J. Biochem.* **1988**, *177*, 199.
(73) Niki, K.; Kawasaki, Y.; Nishimura, N.; Higuchi, Y.; Yasuoka, N.; Kakudo, M. *J. Electroanal. Chem.* **1984**, *168*, 275.
(74) Niki, K.; Kawasaki, Y.; Matsuda, H. *J. Electroanal. Chem.* **1984**, *178*, 333.
(75) Flanagan, J. B.; Margel, S.; Bard, A. J.; Anson, F. C. *J. Am. Chem. Soc.* **1978**, *100*, 4248.
(76) Pulcu, G. S.; Elmore, B. L.; Arciero, D. M.; Hooper, A. B.; Elliott, S. J. *J. Am. Chem. Soc* **2007**, *129*, 1838.
(77) Johnson, D. L.; Thompson, J. L.; Brinkmann, S. M.; Schuller, K. A.; Martin, L. L. *Biochemistry* **2003**, *42*, 10229.
(78) Jeuken, L. J. C.; Jones, A. K.; Chapman, S. K.; Cecchini, G.; Armstrong, F. A. *J. Am. Chem. Soc.* **2002**, *124*, 5702.
(79) Laviron, E. *J. Electroanal. Chem.* **1979**, *101*, 19.
(80) Laviron, E. *J. Electroanal. Chem.* **1983**, *146*, 1.
(81) Marchal, D.; Boireau, W.; Laval, J. M.; Bourdillon, C.; Moiroux, J. *J. Electroanal. Chem.* **1998**, *451*, 139.
(82) Marcus, R. A. *Angew. Chem., Int. Ed.* **1993**, *32*, 1111.
(83) Marcus, R. A.; Sutin, N. *Biochim. Biophys. Acta* **1985**, *811*, 265.
(84) Hale, J. M. *J. Electroanal. Chem.* **1968**, *19*, 315.
(85) Chidsey, C. E. D. *Science* **1991**, *251*, 919.
(86) Press, W. H.; Teukolsky, S. A.; Vetterling, W. T.; Flannery, B. P. *Numerical Recipes in Fortran 90*, 2nd ed.; Cambridge University Press: 1996.
(87) Nahir, T. M.; Clark, R. A.; Bowden, E. F. *Anal. Chem.* **1994**, *66*, 2595.
(88) Hirst, J.; Armstrong, F. A. *Anal. Chem.* **1998**, *70*, 5062.
(89) Honeychurch, M. J.; Rechnitz, G. A. *Electroanalysis* **1998**, *10*, 453.
(90) Smith, C. P.; White, H. S. *Anal. Chem.* **1992**, *64*, 2398.
(91) Lecomte, S.; Hildebrandt, P.; Soulimane, T. *J. Phys. Chem. B* **1999**, *103*, 10053.
(92) Andreu, R.; Calvente, J. J.; Fawcett, W. R.; Molero, M. *Langmuir* **1997**, *13*, 5189.
(93) Calvente, J. J.; Andreu, R.; Molero, M.; Lopez-Perez, G.; Dominguez, M. *J. Phys. Chem. B* **2001**, *105*, 9557.

(94) Honeychurch, M. J. *Langmuir* **1998**, *14*, 6291.
(95) Gerischer, H.; Scherson, D. A. *J. Electroanal. Chem.* **1985**, *188*, 33.
(96) Pilloud, D. L.; Chen, X. X.; Dutton, P. L.; Moser, C. C. *J. Phys. Chem. B* **2000**, *104*, 2868.
(97) Albery, W. J.; Bartlett, P. N.; Wilde, C. P.; Darwent, J. R. *J. Am. Chem. Soc.* **1985**, *107*, 1854.
(98) Creager, S. E.; Wooster, T. T. *Anal. Chem.* **1998**, *70*, 4257.
(99) Tender, L.; Carter, M. T.; Murray, R. W. *Anal. Chem.* **1994**, *66*, 3173.
(100) Weber, K.; Creager, S. E. *Anal. Chem.* **1994**, *66*, 3164.
(101) Richardson, J. N.; Rowe, G. K.; Carter, M. T.; Tender, L. M.; Curtin, L. S.; Peck, S. R.; Murray, R. W. *Electrochim. Acta* **1995**, *40*, 1331.
(102) Ingram, R. S.; Murray, R. W. *Faraday Trans.* **1996**, *92*, 3941.
(103) Carter, M. T.; Rowe, G. K.; Richardson, J. N.; Tender, L. M.; Terrill, R. H.; Murray, R. W. *J. Am. Chem. Soc.* **1995**, *117*, 2896.
(104) Brevnov, D. A.; Finklea, H. O.; van Ryswyk, H. *J. Electroanal. Chem.* **2001**, *500*, 100.
(105) Finklea, H. O.; Hanshew, D. D. *J. Am. Chem. Soc.* **1992**, *114*, 3173.
(106) Katz, E.; Willner, I. *Langmuir* **1997**, *13*, 3364.
(107) Li, J. H.; Schuler, K.; Creager, S. E. *J. Electroanal. Chem.* **2000**, *147*, 4584.
(108) Heering, H. A.; Mondal, M. S.; Armstrong, F. A. *Anal. Chem.* **1999**, *71*, 174.
(109) Jeuken, L. J. C.; McEvoy, J. P.; Armstrong, F. A. *J. Phys. Chem. B* **2002**, *106*, 2304.
(110) Guo, S.; Zhang, J.; Elton, D. M.; Bond, A. M. *Anal. Chem.* **2004**, *76*, 166.
(111) Zhang, J.; Guo, S.-X.; Bond, A. M.; Honeychurch, M. J.; Oldham, K. B. *J. Phys. Chem. B* **2005**, *109*, 8935.
(112) Fleming, B. D.; Barlow, N. L.; Zhang, J.; Bond, A. M.; Armstrong, F. A. *Anal. Chem.* **2006**, *78*, 2948.
(113) Fleming, B. D.; Zhang, J.; Elton, D.; Bond, A. M. *Anal. Chem.* **2007**, *79*, 6515.
(114) Fleming, B. D.; Bell, S. G.; Wong, L.-L.; Bond, A. M. *J. Electroanal. Chem.* **2007**, *611*, 149.
(115) Baymann, F.; Barlow, N. L.; Aubert, C.; Schoepp-Cothenet, B.; Leroy, G.; Armstrong, F. A. *FEBS Lett.* **2003**, *539*, 91.
(116) Feng, Z. Q.; Imabayashi, S.; Kabiuchi, T.; Niki, K. *Faraday Trans.* **1997**, *93*, 1367.
(117) Avila, A.; Gregory, B. W.; Niki, K.; Cotton, T. M. *J. Phys. Chem. B* **2000**, *104*, 2759.
(118) Chi, Q.; Zhang, J.; Andersen, J. E. T.; Ulstrup, J. *J. Phys. Chem. B* **2001**, *105*, 4669.
(119) Song, S.; Clark, R. A.; Bowden, E. F.; Tarlov, M. J. *J. Phys. Chem.* **1993**, *97*, 6564.
(120) Murgida, D. H.; Hildebrandt, P. *J. Am. Chem. Soc.* **2001**, *123*, 4062.
(121) Murgida, D. H.; Hildebrandt, P. *J. Phys. Chem. B* **2002**, *106*, 12814.
(122) Khoshtariya, D. E.; Wei, J.; Liu, H.; Yue, H.; Waldeck, D. *J. Am. Chem. Soc.* **2003**, *125*, 7704.
(123) Niki, K.; Hardy, W. R.; Hill, M. G.; Li, H.; Sprinkle, J. R.; Margoliash, E.; Fujita, K.; Tanimura, R.; Nakamura, N.; Ohno, H.; Richards, J. H.; Gray, H. B. *J. Phys. Chem. B* **2003**, *107*, 9947.
(124) Fujita, K.; Nakamura, N.; Ohno, H.; Leigh, B. S.; Niki, K.; Gray, H. B.; Richards, J. H. *J. Am. Chem. Soc.* **2004**, *126*, 13954.
(125) Wei, J. J.; Liu, H.; Niki, K.; Margoliash, E.; Waldeck, D. *J. Phys. Chem. B* **2004**, *108*, 16912.
(126) Yue, H.; Khoshtariya, D.; Waldeck, D. H.; Grochol, J.; Hildebrandt, P.; Murgida, D. H. *J. Phys. Chem. B* **2006**, *110*, 19906.
(127) Chi, Q.; Zhang, J.; Jensen, P. S.; Christensen, H. E. M.; Ulstrup, J. *Faraday Discuss.* **2006**, *131*, 181.
(128) Yue, H.; Waldeck, D. H. *Curr. Opin. Solid State Mater. Sci.* **2005**, *9*, 28.
(129) Jeuken, L. J. C. *Biochim. Biophys. Acta* **2003**, *1604*, 67.
(130) Hoffman, B. M.; Ratner, M. A. *J. Am. Chem. Soc.* **1987**, *109*, 6237.
(131) Davidson, V. L. *Acc. Chem. Res.* **2000**, *33*, 87.
(132) Davidson, V. L. *Biochemistry* **2002**, *41*, 14633.
(133) Bernhardt, P. V.; Schenk, G.; Wilson, G. J. *Biochemistry* **2004**, *43*, 10387.
(134) Boon, E. M.; Livingston, A. L.; Chmiel, N. H.; David, S. S.; Barton, J. K. *Proc. Natl. Acad. Sci. U.S.A.* **2003**, *100*, 12543.
(135) Laviron, E. *J. Electroanal. Chem.* **1980**, *109*, 57.
(136) Meunier-Prest, R.; Laviron, E. *J. Electroanal. Chem.* **1992**, *328*, 33.
(137) Hirst, J.; Duff, J. L. C.; Jameson, G. N. L.; Kemper, M. A.; Burgess, B. K.; Armstrong, F. A. *J. Am. Chem. Soc.* **1998**, *120*, 7085.
(138) Chen, K.; Hirst, J.; Camba, R.; Bonagura, C. A.; Stout, C. D.; Burgess, B. K.; Armstrong, F. A. *Nature* **2000**, *405*, 814.
(139) Camba, R.; Jung, Y. S.; Hunsicker-Wang, L. M.; Burgess, B. K.; Stout, C. D.; Hirst, J.; Armstrong, F. A. *Biochemistry* **2003**, *42*, 10589.
(140) Jeuken, L. J. C.; van Vliet, P.; Verbeet, M. P.; Camba, R.; McEvoy, J. P.; Armstrong, F. A.; Canters, G. W. *J. Am. Chem. Soc.* **2000**, *122*, 12186.
(141) Limoges, B.; Savéant, J.-M. *J. Electroanal. Chem.* **2004**, *562*, 43.
(142) Bond, A. M. *Modern polarographic methods in analytical electrochemistry*; Marcel Dekker, Inc.: 1980.
(143) Bernhardt, P. V.; Santini, J. M. *Biochemistry* **2006**, *45*, 2804.
(144) Butt, J. N.; Filipiak, M.; Hagen, W. R. *Eur. J. Biochem.* **1997**, *245*, 116.
(145) Léger, C.; Lederer, F.; Guigliarelli, B.; Bertrand, P. *J. Am. Chem. Soc.* **2006**, *128*, 180.
(146) Hirst, J.; Sucheta, A.; Ackrell, B. A. C.; Armstrong, F. A. *J. Am. Chem. Soc.* **1996**, *118*, 5031.
(147) Hirst, J.; Ackrell, B. A. C.; Armstrong, F. A. *J. Am. Chem. Soc.* **1997**, *119*, 7434.
(148) Pershad, H. R.; Hirst, J.; Cochran, B.; Ackrell, B. A. C.; Armstrong, F. A. *Biochim. Biophys. Acta* **1999**, *1412*, 262.
(149) Angove, H. C.; Cole, J. A.; Richardson, D. J.; Butt, J. N. *J. Biol. Chem.* **2002**, *277*, 23374.
(150) Gwyer, J. D.; Richardson, D. J.; Butt, J. N. *J. Am. Chem. Soc.* **2005**, *127*, 14964.
(151) Zu, Y.; Shannon, R. J.; Hirst, J. *J. Am. Chem. Soc.* **2003**, *125*, 6020.
(152) Page, C. C.; Moser, C. C.; Chen, X.; Dutton, P. L. *Nature* **1999**, *402*, 47.
(153) Moser, C. C.; Keske, J. M.; Warncke, K.; Farid, R. S.; Dutton, P. L. *Nature* **1992**, *355*, 796.
(154) Xie, Y.; Anson, F. C. *J. Electroanal. Chem.* **1996**, *404*, 209.
(155) Andrieux, C. P.; Dumas-Bouchiat, J. M.; Savéant, J. M. *J. Electroanal. Chem.* **1982**, *131*, 1.
(156) Bertrand, P.; Frangioni, B.; Dementin, S.; Sabaty, M.; Arnoux, P.; Guigliarelli, B.; Pignol, D.; Léger, C. *J. Phys. Chem. B* **2007**, *111*, 10300.
(157) Léger, C.; Jones, A. K.; Roseboom, W.; Albracht, S. P. J.; Armstrong, F. A. *Biochemistry* **2002**, *41*, 15736.
(158) Barker, C. D.; Reda, T.; Hirst, J. *Biochemistry* **2007**, *46*, 3454.
(159) Anderson, L. J.; Richardson, D. J.; Butt, J. N. *Biochemistry* **2001**, *40*, 11294.
(160) Jepson, B. J. N.; Anderson, L. J.; Rubio, L. M.; Taylor, C. J.; Butler, C. S.; Flores, E.; Herrero, A.; Butt, J. N.; Richardson, D. J. *J. Biol. Chem.* **2004**, *279*, 32212.
(161) Reda, T.; Hirst, J. *J. Phys. Chem. B* **2006**, *10*, 1394.
(162) Honeychurch, M. J.; Bernhardt, P. V. *J. Phys. Chem. B* **2005**, *109*, 5766.
(163) Andreu, R.; Ferapontova, E. E.; Gorton, L.; Calvente, J. J. *J. Phys. Chem. B* **2007**, *111*, 469.
(164) Jiang, R. Z.; Anson, F. C. *J. Electroanal. Chem.* **1991**, *305*, 171.
(165) Hoke, K. R.; Cobb, N.; Armstrong, F. A.; Hille, R. *Biochemistry* **2004**, *43*, 1667.
(166) Field, S. J.; Thornton, N. P.; Anderson, L. J.; Gates, A. J.; Reilly, A.; Jepson, B. J. N.; Richardson, D. J.; George, S. J.; Cheesmana, M. R.; Butt, J. N. *Dalton Trans.* **2005**, 3580.
(167) Wijma, H. J.; Jeuken, L. J. C.; Verbeet, M. P.; Armstrong, F. A.; Canters, G. W. *J. Am. Chem. Soc.* **2007**, *129*, 8557.
(168) Alric, J.; Lavergne, J.; Rappaport, F.; Vermeglio, A.; Matsuura, K.; Shimada, K.; Nagashima, K. V. P. *J. Am. Chem. Soc.* **2006**, *128*, 4136.
(169) Vincent, K. A.; Parkin, A.; Lenz, O.; Albracht, S. P. J.; Fontecilla-Camps, J. C.; Cammack, R.; Friedrich, B.; Armstrong, F. A. *J. Am. Chem. Soc.* **2005**, *127*, 18179.
(170) Lamle, S. L.; Albracht, S. P. J.; Armstrong, F. A. *J. Am. Chem. Soc.* **2004**, *126*, 14899.
(171) Lamle, S. L.; Albracht, S. P. J.; Armstrong, F. A. *J. Am. Chem. Soc.* **2005**, *127*, 6595.
(172) Vincent, K. A.; Belsey, N. A.; Lubitz, W.; Armstrong, F. A. *J. Am. Chem. Soc.* **2006**, *128*, 7448.
(173) Parkin, A.; Cavazza, C.; Fontecilla-Camps, J.; Armstrong, F. *J. Am. Chem. Soc.* **2006**, *128*, 16808.
(174) Vincent, K. A.; Cracknell, J. A.; Parkin, A.; Armstrong, F. A. *Dalton Trans.* **2005**, 3397.
(175) Mondal, M. S.; Fuller, H. A.; Armstrong, F. A. *J. Am. Chem. Soc.* **1996**, *118*, 263.
(176) Lamle, S. E.; Vincent, K. A.; Halliwell, L. M.; Albracht, S. P. J.; Armstrong, F. A. *Dalton Trans.* **2003**, 4152.
(177) Jones, A. K.; Sillery, E.; Albracht, S. P. J.; Armstrong, F. A. *Chem. Commun.* **2002**, 866.
(178) Armstrong, F. A.; Bond, A. M.; Büchi, F. N.; Hamnett, A.; Hill, H. A. O.; Lannon, A. M.; Lettington, O. C.; Zoski, C. G. *Analyst* **1993**, *118*, 973.
(179) Andrieux, C. P.; Savéant, J. M. *J. Electroanal. Chem.* **1978**, *93*, 163.
(180) Aoki, K.; Tokuda, K.; Matsuda, H. *J. Electroanal. Chem.* **1986**, *199*, 69.
(181) Honeychurch, M. J.; Bernhardt, P. V. *J. Phys. Chem. B* **2004**, *108*, 15900.
(182) Zhang, J.; Welinder, A. C.; Hansen, A. G.; Christensen, H. E. M.; Ulstrup, J. *J. Phys. Chem. B* **2003**, *107*, 12480.
(183) Aguey-Zinsou, K. F.; Bernhardt, P. V.; Leimkühler, S. *J. Am. Chem. Soc.* **2003**, *15*, 15352.

(184) Aguey-Zinsou, K. F.; Bernhardt, P. V.; Kappler, U.; McEwan, A. G. *J. Am. Chem. Soc.* **2003**, *125*, 530.
(185) Wijma, H. J.; Jeuken, L. J. C.; Verbeet, M. P.; Armstrong, F. A.; Canters, G. W. *J. Biol. Chem.* **2006**, *281*, 16340.
(186) Frangioni, B.; Arnoux, P.; Sabaty, M.; Pignol, D.; Bertrand, P.; Guigliarelli, B.; Léger, C. *J. Am. Chem. Soc.* **2004**, *126*, 1328.
(187) Léger, C.; Dementin, S.; Bertrand, P.; Rousset, M.; Guigliarelli, B. *J. Am. Chem. Soc.* **2004**, *126*, 12162.
(188) Parkin, A.; Seravalli, J.; Vincent, K. A.; Ragsdale, S. W.; Armstrong, F. A. *J. Am. Chem. Soc.* **2007**, *129*, 10328.
(189) Almeida, M. G.; Guigliarelli, B.; Bertrand, P.; Moura, J. J. G.; Moura, I.; Léger, C. *FEBS Letts.* **2007**, *581*, 284.
(190) Carugo, O.; Carugo, K. D. *Trends Biochem. Sci.* **2005**, *30*, 213.
(191) Yano, J.; Kern, J.; Irrgang, K.-D.; Latimer, M. J.; Bergmann, U.; Glatzel, P.; Pushkar, Y.; Biesiadka, J.; Loll, B.; Sauer, K.; Messinger, J.; Zouni, A.; Yachandra, V. K. *Proc. Natl. Acad. Sci. U.S.A.* **2005**, *102*, 12047.
(192) Ferapontova, E. E.; Shleev, S.; Ruzgas, T.; Stoica, L.; Christenson, A.; Tkac, J.; Yaropolov, A. I.; Gorton, L. Direct electrochemistry of proteins and enzymes. In *Perspectives in Bioanalysis. Electrochemistry of nucleic acids and proteins*; Elsevier: 2005.
(193) Murphy, L. *Curr. Opin. Chem. Biol.* **2006**, *10*, 1.
(194) Chen, D.; Wang, G.; Li, J. *J. Phys. Chem. C* **2007**, *111*, 2351.
(195) Banks, C. E.; Compton, R. G. *Analyst* **2006**, *131*, 15.
(196) Blanford, C. F.; Armstrong, F. A. *J. Solid State Electrochem.* **2006**, *10*, 826.
(197) Guiral-Brugna, M.; Giudici-Orticoni, M.-T.; Bruschi, M.; Bianco, P. *J. Electroanal. Chem.* **2001**, *510*, 136.
(198) Rudiger, O.; Abad, J. M.; Hatchikian, E. C.; Fernandez, V. M.; de Lacey, A. L. *J. Am. Chem. Soc.* **2005**, *127*, 16008.
(199) Tominaga, M.; Shirakihara, C.; Taniguchi, I. *J. Electroanal. Chem.* **2007**, *610*, 1.
(200) Ji, X.; Banks, C. E.; Crossley, A.; Compton, R. G. *ChemPhysChem* **2006**, *7*, 1337.
(201) Hagen, W. F. *Eur. J. Biochem.* **1989**, *182*, 523.
(202) Fujieda, N.; Mori, M.; Kano, K.; Ikeda, T. *Biochemistry* **2002**, *41*, 13736.
(203) Shleev, S.; Jarosz-Wilkolazk, A.; Khalunin, A.; Morozov, O.; Yaropolov, A.; Ruzgas, T.; Gorton, L. *Bioelectrochemistry* **2005**, *67*, 115.
(204) Karyakin, A. A.; Morozov, S. V.; Karyakina, E. E.; Varfolomeyev, S. D.; Zorin, N. A.; Cosnier, S. *Electrochem. Commun.* **2002**, *4*, 417.
(205) Morozov, S. V.; Vignais, P. M.; Cournac, L.; Zorin, N. A.; Karyakina, E. E.; Karyakin, A. A.; Cosnier, S. *Int. J. Hydrogen Energy* **2002**, *27*, 1501.
(206) Karyakin, A. A.; Morozov, S. V.; Karyakin, E. E.; Zorin, N. A.; Perelygin, V. V.; Cosnier, S. *Biochem. Soc. Trans.* **2005**, *33*, 73.
(207) Male, K. B.; Hrapovic, S.; Santini, J. M.; Luong, J. H. T. *Anal. Chem.* **2007**, *79*, 7831.
(208) Wu, Y.; Hu, S. *Anal. Chim. Acta* **2007**, *602*, 181.
(209) Minteer, S. D.; Liaw, B. Y.; Cooney, M. J. *Curr. Opin. Biotechnol.* **2006**, *18*, 228.
(210) Banks, C. E.; Crossley, A.; Salter, C.; Wilkins, S. J.; Compton, R. G. *Angew. Chem., Int. Ed.* **2006**, *45*, 2533.
(211) Blanford, C. F.; Heath, R. S.; Armstrong, F. A. *Chem. Commun.* **2007**, 1710.
(212) Chi, Q.; Zhang, J.; Nielsen, J. U.; Friis, E. P.; Chorkendorff, I.; Canters, G. W.; Andersen, J. E. T.; Ulstrup, J. *J. Am. Chem. Soc.* **2000**, *122*, 4047.
(213) Davis, J. J.; Bruce, D.; Canters, G. W.; Croziera, J.; Hill, H. A. O. *Chem. Commun.* **2003**, 576.
(214) Andolfi, L.; Bruce, D.; Cannistraro, S.; Canters, G. W.; Davis, J. J.; Hill, H. A. O.; Crozier, J.; Verbeet, M. P.; Wrathmell, C. L.; Astier, Y. *J. Electroanal. Chem.* **2004**, *565*, 21.
(215) Andolfi, L.; Caroppi, P.; Bizzarri, A. R.;; Piro, M. C.; Sinibaldi, F.; Ferri, T.; Polticelli, F.; Cannistraro, S.; Santucci, R. *Protein J.* **2007**, *26*, 271.
(216) Astier, Y.; Canters, G. W.; Davis, J. J.; Hill, H. A. O.; Verbeet, M. P.; Wijma, H. J. *ChemPhysChem* **2005**, *6*, 1114.
(217) Gwyer, J. D.; Zhang, J.; Butt, J. N.; Ulstrup, J. *Biophys. J.* **2006**, *91*, 3897.
(218) Hasan, M. N.; Kwakernaak, C.; Sloof, W. G.; Hagen, W. R.; Heering, H. A. *J. Biol. Inorg. Chem.* **2006**, *11*, 651.
(219) Ferapontova, E. E.; Castillo, J.; Hushpulian, D.; Tishkov, V.; Chubar, T.; Gazaryan, I.; Gorton, L. *Electrochem. Commun.* **2005**, *7*, 1291.
(220) Pita, M.; Shleev, S.; Ruzgas, T.; Fernández, V. M.; Yaropolov, A. I.; Gorton, L. *Electrochem. Commun.* **2006**, *8*, 747.
(221) Astier, Y.; Bond, A. M.; Wijma, H. J.; Canters, G. W.; Hill, H. A. O.; Davis, J. J. *Electroanalysis* **2004**, *16*, 1155.
(222) Bonanni, B.; Bizzarri, A. R.; Cannistraro, S. *J. Phys. Chem. B* **2006**, *110*, 14574.
(223) Davis, J. J.; Burgess, H.; Zauner, G.; Kuznetsova, S.; Salverda, J.; Aartsma, T.; Canters, G. W. *J. Phys. Chem. B* **2006**, *110*, 20649.
(224) Ye, T.; Kaur, R.; Wen, X.; Bren, K. L.; Elliott, S. J. *Inorg. Chem.* **2005**, *44*, 8999.
(225) Michel, L. V.; Ye, T.; Bowman, S. E. J.; Levin, B. D.; Hahn, M. A.; Russell, B. S.; Elliott, S. J.; Bren, K. L. *Biochemistry* **2007**, *46*, 11753.
(226) Fedurco, M. *Coord. Chem. Rev.* **2000**, *209*, 263.
(227) Zhang, J.; Christensen, H. E. M.; Ooi, B. L.; Ulstrup, J. *Langmuir* **2004**, *20*, 10200.
(228) Lopes, H.; Pettigrew, G. W.; Moura, I.; Moura, J. J. G. *J. Biol. Inorg. Chem.* **1998**, *3*, 632.
(229) Ferapontova, E. E.; Ruzgas, T.; Gorton, L. *Anal. Chem.* **2003**, *75*, 4841.
(230) Hoeben, F. J. M.; Heller, I.; Albracht, S. P. J.; Dekker, C.; Lemay, S. G.; Heering, H. A. *Langmuir* **2008**, *24*, 5925.
(231) Murgida, D. H.; Hildebrandt, P. *Acc. Chem. Res.* **2004**, *37*, 854.
(232) Butt, J. N.; Thornton, J.; Richardson, D. J.; Dobbin, P. S. *Biophys. J.* **2000**, *78*, 1001.
(233) Nakano, K.; Yoshitake, T.; Yamashita, Y.; Bowden, E. F. *Langmuir* **2007**, *23*, 6270.
(234) Lindgren, A.; Tanaka, M.; Ruzgas, T.; Gorton, L.; Gazaryan, I.; Ishimori, K.; Morishima, I. *Electrochem. Commun.* **1999**, *1*, 767.
(235) Alonso-Lomillo, M. A.; Rudiger, O.; Maroto-Valiente, A.; Velez, M.; Rodriguez-Ramos, I.; Munoz, F. J.; Fernandez, V. M.; de Lacey, A. L. *Nano Lett.* **2007**, *7*, 1603.
(236) Willner, I.; Heleg-Shabtai, V.; Blonder, R.; Katz, E.; Tao, G.; Buckmann, A.; Heller, A. *J. Am. Chem. Soc.* **1996**, *118*, 10321.
(237) Zayats, M.; Katz, E.; Willner, I. *J. Am. Chem. Soc.* **2002**, *124*, 14724.
(238) Zayats, M.; Katz, E.; Willner, I. *J. Am. Chem. Soc.* **2002**, *124*, 2120.
(239) Wang, J. *Chem. Rev.* **2008**, *108*, 814.
(240) Patolsky, F.; Weizmann, Y.; Willner, I. *Angew. Chem., Int. Ed.* **2004**, *43*, 2113.
(241) Xiao, Y.; Patolsky, F.; Katz, E.; Hainfeld, J.; Willner, I. *Science* **2003**, *299*, 1877.
(242) Madoz-Gurpide, J.; Abad, J.; Fernandez-Recio, J.; Velez, M.; Vazquez, L.; Gomez-Moreno, C.; Fernandez, V. M. *J. Am. Chem. Soc.* **2000**, *122*, 9808.
(243) Ataka, K.; Giess, F.; Knoll, W.; Naumann, R.; Haber-Pohlmeier, S.; Richter, B.; Heberle, J. *J. Am. Chem. Soc.* **2004**, *126*, 16199.
(244) Ataka, K.; Richter, B.; Heberle, J. *J. Phys. Chem. B* **2006**, *110*, 9339.
(245) Hrabakova, J.; K, K. A.; Heberle, J.; Hildebrandt, P.; Murgida, D. H. *Phys. Chem. Chem. Phys.* **2006**, *8*, 759.
(246) Blankespoor, R.; Limoges, B.; Schollhorn, B.; Syssa-Magale, J.-L.; Yazidi, D. *Langmuir* **2005**, *21*, 3362.
(247) Haddour, N.; Cosnier, S.; Gondran, C. *J. Am. Chem. Soc.* **2005**, *127*, 5752.
(248) Johnson, D. L.; Polyak, S. W.; Wallace, J. C.; Martin, L. L. *Int. J. Pept. Res. Ther.* **2003**, *10*, 495.
(249) Johnson, D. L.; Martin, L. L. *J. Am. Chem. Soc.* **2005**, *127*, 2018.
(250) Elliott, S. J.; Amy, L.; Bradley, D. M. A.; Hooper, A. B. *J. Inorg. Biochem.* **2006**, *101*, 95173.
(251) Fleming, B. D.; Tian, Y.; Bell, S. G.; Wong, L.-L.; Urlacher, V.; Hill, H. A. O. *Eur. J. Biochem.* **2003**, *270*, 4082.
(252) Udit, A. K.; Hill, M. G.; Bittner, V. G.; Arnold, F. H.; Gray, H. B. *J. Am. Chem. Soc.* **2004**, *126*, 10218.
(253) Haas, A. S.; Pilloud, D. L.; Reddy, K. S.; Babcock, G. T.; Moser, C. C.; Blasie, J. K.; Dutton, P. L. *J. Phys. Chem. B* **2001**, *105*, 11351.
(254) Heering, H. A.; Williams, K. A.; de Vries, S.; Dekker, C. *ChemPhysChem* **2006**, *7*, 1705.
(255) Lebedev, N.; Trammell, S. A.; Spano, A.; Lukashev, E.; Griva, I.; Schnur, J. *J. Am. Chem. Soc.* **2006**, *128*, 12044.
(256) Dronov, R.; Kurth, D. G.; Mohwald, H.; Spricigo, R.; Leimkuhler, S.; Wollenberger, U.; Rajagopalan, K. V.; Scheller, F. W.; Lisdat, F. *J. Am. Chem. Soc.* **2008**, *130*, 1122.
(257) Fourmond, V.; Lagoutte, B.; Setif, P.; Leibl, W.; Demaille, C. *J. Am. Chem. Soc.* **2007**, *129*, 9201.
(258) Rusling, J. F. *Acc. Chem. Res.* **1998**, *31*, 363.
(259) Marchal, D.; Pantigny, J.; Laval, J. M.; Moiroux, J.; Bourdillon, C. *Biochemistry* **2001**, *40*, 1248.
(260) Jeuken, L. J. C.; Connell, S. D.; Nurnabi, M.; O'Reilly, J.; Henderson, P. J. F.; Evans, S. D.; Bushby, R. J. *Langmuir* **2005**, *21*, 1481.
(261) Jeuken, L. J. C.; Connell, S. D.; Henderson, P. J. F.; Gennis, R. B.; Evans, S. D.; Bushby, R. J. *J. Am. Chem. Soc.* **2006**, *128*, 1711.
(262) Burgess, J. D.; Rhoten, M. C.; Hawkridge, F. M. *J. Am. Chem. Soc.* **1998**, *120*, 4488.
(263) Su, L.; Kelly, J. B.; Hawkridge, F. M.; Rhoten, M. C.; Baskin, S. I. *J. Electroanal. Chem.* **2005**, *581*, 241.
(264) Lei, C.; Wollenberger, U.; Jung, C.; Scheller, F. W. *Biochem. Biophys. Res. Commun.* **2000**, *268*, 740.
(265) Shumyantseva, V. V.; Ivanov, Y. D.; Bistolas, N.; Scheller, F. W.; Archakov, A. I.; Wollenberger, U. *Anal. Chem.* **2004**, *76*, 6046.
(266) Shumyantseva, V. V.; Bulko, T. V.; Rudakov, Y. O.; Kuznetsova, G. P.; Samenkova, N. F.; Lisitsa, A. V.; Karuzina, I. I.; Archakov, A. I. *J. Inorg. Biochem.* **2007**, *101*, 859.
(267) Liu, H.; Tian, Y.; Deng, Z. *Langmuir* **2007**, *23*, 9487.

(268) Scott, D.; Toney, M.; Muzikar, M. *J. Am. Chem. Soc.* **2008**, *130*, 865.
(269) McDonald, T. J.; Svedruzic, D.; Kim, Y. H.; Blackburn, J. L.; Zhang, S. B.; King, P. W.; Heben, M. J. *Nano Lett.* **2007**, *7*, 3528.
(270) Salimi, A.; Hallaj, R.; Soltanian, S. *Biophys. Chem.* **2007**, *130*, 122.
(271) Salimi, A.; Sharifi, E.; Noorbakhsh, A.; Soltanian, S. *Biophys. Chem.* **2007**, *125*, 540.
(272) Hartmann, M. *Chem. Mater.* **2005**, *17*, 4577.
(273) Kim, J.; Jia, H.; Wang, P. *Biotechnol. Adv.* **2006**, *24*, 296.
(274) Pumera, M.; Sánchez, S.; Ichinose, I.; Tang, J. *Sensors Actuators B: Chem.* **2007**, *123*, 1195.
(275) Petrovic, J.; Clark, R. A.; Yue, H.; Waldeck, D. H.; Bowden, E. F. *Langmuir* **2005**, *21*, 6308.
(276) Yue, H.; Waldeck, D. H.; Petrovic, J.; Clark, R. A. *J. Phys. Chem. B* **2006**, *110*, 5062.
(277) El Kasmi, A.; Wallace, J. M.; Bowden, E. F.; Binet, S. M.; Linderman, R. J. *J. Am. Chem. Soc.* **1998**, *120*, 225.
(278) Maklashina, E.; Iverson, T. M.; Sher, Y.; Kotlyar, V.; Andréll, J.; Mirza, O.; Hudson, J. M.; Armstrong, F. A.; Rothery, R. A.; Weiner, J. H.; Cecchini, G. *J. Biol. Chem.* **2006**, *281*, 11357.
(279) Turner, K. L.; Doherty, M. K.; Heering, H. A.; Armstrong, F. A.; Reid, G. A.; Chapman, S. K. *Biochemistry* **1999**, *38*, 3302.
(280) Pankhurst, K. L.; Mowat, C. G.; Rothery, E. L.; Hudson, J. M.; Jones, A. K.; Miles, C. S.; Walkinshaw, M. D.; Armstrong, F. A.; Reid, G. A.; Chapman, S. K. *J. Biol. Chem.* **2006**, *281*, 20589.
(281) Elliott, S. J.; McElhaney, A. E.; Feng, C.; Enemark, J. H.; Armstrong, F. A. *J. Am. Chem. Soc.* **2002**, *124*, 11612.
(282) Moreno, C.; Costa, C.; Moura, I.; Gall, J. L.; Liu, M. Y.; Payne, W. J.; van Dijk, C.; Moura, J. J. *Eur. J. Biochem.* **1993**, *212*, 79.
(283) Cordas, C. M.; Peireira, A. S.; Martins, C. E.; Timóteo, C. G.; Moura, J. J. G.; Tavares, P. *ChemBioChem* **2006**, *7*, 1878.
(284) Tarasev, M.; Pinto, A.; Kim, D.; Elliott, S. J.; Ballou, D. P. *Biochemistry* **2006**, *45*, 10208.
(285) Mondal, M. S.; Goodin, D. B.; Armstrong, F. A. *J. Am. Chem. Soc.* **1998**, *120*, 13284.
(286) Ciobanu, M.; Kincaid, H. E.; Lo, V.; Dukes, A. D.; Jennings, G. K.; Cliffel, D. E. *J. Electroanal. Chem.* **2007**, *599*, 72.
(287) Kong, J.; Lu, Z.; Lvov, Y. M.; Desamero, R. Z. B.; Frank, H. A.; Rusling, J. F. *J. Am. Chem. Soc.* **1998**, *120*, 7371.
(288) Munge, B.; Das, S. K.; Ilagan, R.; Pendon, Z.; Yang, J.; Frank, H. A.; Rusling, J. F. *J. Am. Chem. Soc.* **2003**, *125*, 12457.
(289) Alcantara, K.; Munge, B.; Pendon, Z.; Frank, H. A.; Rusling, J. F. *J. Am. Chem. Soc.* **2006**, *128*, 14930.
(290) Bernhardt, P. V.; Honeychurch, M. J.; McEwan, A. G. *Electrochem. Commun.* **2006**, *8*, 257.
(291) Aguey-Zinsou, K.-F.; Bernhardt, P. V.; McEwan, A. G.; Ridge, J. P. *J. Biol. Inorg. Chem.* **2002**, *7*, 879.
(292) Ridge, J. P.; Aguey-Zinsou, K. F.; Bernhardt, P. V.; Brereton, I. M.; Hanson, G. R.; McEwan, A. G. *Biochemistry* **2002**, *41*, 15762.
(293) Ridge, J. P.; Aguey-Zinsou, K.-F.; Bernhardt, P. V.; Hanson, G. R.; McEwan, A. G. *FEBS Lett.* **2004**, *563*, 197.
(294) Kappler, U.; Bailey, S.; Feng, C.; Honeychurch, M. J.; Hanson, G. R.; Bernhardt, P. V.; Tollin, G.; Enemark, J. H. *Biochemistry* **2006**, *45*, 9696.
(295) Udit, A. K.; Belliston-Bittner, W.; Glazer, E. C.; Nguyen, Y. H. L.; Gillan, J. M.; Hill, M. G.; Marletta, M. A.; Goodin, D. B.; Gray, H. B. *J. Am. Chem. Soc.* **2005**, *127*, 11212.
(296) Bayachou, M.; Boutros, J. A. *J. Am. Chem. Soc.* **2004**, *126*, 12722.
(297) Coreia dos Santos, M. M.; Sousa, P. M. P.; Gonçalves, M. L. S.; Romao, M. J.; Moura, I.; Moura, J. J. G. *Eur. J. Biochem.* **2004**, *271*, 1329.
(298) Fleming, B. D.; Johnson, D. L.; Bond, A. M.; Martin, L. L. *Expert Opin. Drug Metab. Toxicol.* **2006**, *2*, 581.
(299) Lvov, Y. M.; Lu, Z.; Schenkman, J. B.; Zu, X.; Rusling, J. F. *J. Am. Chem. Soc.* **1998**, *120*, 4073.
(300) Estavillo, C.; Lu, Z.; Jansson, I.; Schenkman, J. B.; Rusling, J. F. *Biophys. Chem.* **2003**, *104*, 291.
(301) Fantuzzi, A.; Fairhead, M.; Gilardi, G. *J. Am. Chem. Soc.* **2004**, *126*, 5040.
(302) Joseph, S.; Rusling, J. F.; Lvov, Y. M.; Friedberg, T.; Fuhr, U. *Biochem. Pharmacol.* **2003**, *65*, 363.
(303) Aguey-Zinsou, K. F.; Bernhardt, P. V.; De Voss, J. J.; Slessor, K. E. *Chem. Commun.* **2003**, *7*, 418.
(304) Zhang, Z.; Nassar, A.-E. F.; Lu, Z.; Schenkman, J. B.; Rusling, J. F. *J. Chem. Soc., Faraday Trans.* **1997**, *83*, 1769.
(305) Johnson, D. L.; Conley, A. J.; Martin, L. L. *J. Mol. Endocrinol.* **2006**, *36*, 349.
(306) Udit, A. K.; Hindoyan, N.; Hill, M. G.; Arnold, F.; Gray, H. B. *Inorg. Chem.* **2005**, *44*, 4109.
(307) Udit, A. K.; Hill, M. G.; Gray, H. B. *Langmuir* **2006**, *22*, 10854.
(308) Udit, A. K.; Hagen, K. D.; Goldman, P. J.; Star, A.; Gillan, J. M.; Gray, H. B.; Hill, M. G. *J. Am. Chem. Soc.* **2006**, *128*, 10320.
(309) Udit, A. K.; Hill, M. G.; Gray, H. B. *J. Inorg. Biochem.* **2006**, *100*, 519.
(310) Munge, B.; Estavillo, C.; Schenkman, J. B.; Rusling, J. F. *ChemBioChem* **2003**, *4*, 82.
(311) Iwuoha, E. I.; Kane, S.; Ania, C. O.; Smyth, M. R.; de Montellano, P. R. O.; Fuhr, U. *Electroanalysis* **2000**, *12*, 987.
(312) Taylor, P.; Pealing, S. L.; Reid, G. A.; Chapman, S. K.; Walkinshaw, M. D. *Nat. Struct. Mol. Biol.* **1999**, *6*, 1108.
(313) Lancaster, C. R. D.; Kröger, A.; Auer, M.; Michel, H. *Nature* **1999**, *402*, 377.
(314) Iverson, T. M.; Luna-Chavez, C.; Cecchini, G.; Rees, D. C. *Science* **1999**, *284*, 1961.
(315) Kisker, C.; Schindelin, H.; Pacheco, A.; Wehbi, W. A.; Garrett, R. M.; Rajagopalan, K. V.; Enemark, J. H.; Rees, D. C. *Cell* **1997**, *91*, 973.
(316) Kazlauskaite, J.; Westlake, A. C. G.; Wong, L.-L.; Hill, H. A. O. *Chem. Commun.* **1996**, 1817.
(317) Sligar, S. G.; Gunsalus, I. C. *Proc. Natl. Acad. Sci. U.S.A.* **1976**, *73*, 1078.
(318) Fisher, M. T.; Sligar, S. G. *J. Am. Chem. Soc.* **1985**, *107*, 5018.
(319) Sharp, R. E.; Chapman, S. K. *Biochim. Biophys. Acta* **1999**, *1432*, 143.
(320) Das, A.; Grinkova, Y. V.; Sligar, S. G. *J. Am. Chem. Soc.* **2007**, *129*, 13778.
(321) Todorovic, S.; Jung, C.; Hildebrandt, P.; Murgida, D. H. *J. Biol. Inorg. Chem.* **2006**, *11*, 119.
(322) Rodrigues, C. G.; Wedd, A. G.; Bond, A. M. *J. Electroanal. Chem.* **1991**, *312*, 131.
(323) de Groot, M. T.; Merkx, M.; Koper, M. T. M. *J. Am. Chem. Soc.* **2005**, *127*, 16224.
(324) Guto, P. M.; Rusling, J. F. *Electrochem. Commun.* **2006**, *8*, 455.
(325) de Groot, M. T.; Merkx, M.; Koper, M. T. M. *Electrochem. Commun.* **2006**, *8*, 999.
(326) de Groot, M. T.; Merkx, M.; Koper, M. T. M. *J. Biol. Inorg. Chem.* **2007**, *12*, 761.
(327) Lorkovic, I. M.; Ford, P. C. *Inorg. Chem.* **2000**, *39*, 632.
(328) Wolak, M.; Stochel, G.; Hamza, M.; van Eldik, R. *Inorg. Chem.* **2000**, *39*, 2018.
(329) Wolak, M.; van Eldik, R. *Coord. Chem. Rev.* **2002**, *230*, 263.
(330) Bradley, A. L.; Chobot, S. E.; Arciero, D. M.; Hooper, A. B.; Elliott, S. J. *J. Biol. Chem.* **2004**, *279*, 13297.
(331) Ferapontova, E. E. *Electroanalysis* **2004**, *16*, 13.
(332) Castillo, J.; Ferapontova, E.; Hushpulian, D.; Tasca, F.; Tishkov, V.; Chubar, T.; Gazaryan, I.; Gorton, L. *J. Electroanal. Chem.* **2006**, *588*, 112.
(333) Scott, D. L.; Paddock, R. M.; Bowden, E. F. *J. Electroanal. Chem.* **1992**, *341*, 307.
(334) Bateman, L.; Léger, C.; Goodin, D. B.; Armstrong, F. A. *J. Am. Chem. Soc.* **2001**, *123*, 9260.
(335) Shigehara, K.; Anson, F. C. *J. Phys. Chem.* **1982**, *86*, 2776.
(336) Bertrand, P.; Dole, F.; Asso, M.; Guigliarelli, B. *J. Biol. Inorg. Chem.* **2000**, *5*, 682.
(337) De Lacey, A. L.; Santamaria, E.; Hatchikian, E. C.; Fernandez, V. M. *Biochim. Biophys. Acta* **2000**, *1481*, 371.
(338) Arnoux, P.; Sabaty, M.; Alric, J.; Frangioni, B.; Guigliarelli, B.; Adriano, J. M.; Pignol, D. *Nat. Struct. Mol. Biol.* **2003**, *10*, 928.
(339) Sabaty, M.; Avazeri, C.; Pignol, D.; Vermeglio, A. *Appl. Environ. Microbiol.* **2001**, *67*, 5122.
(340) Yankovskaya, V.; Horsefield, R.; Törnroth, S.; Luna-Chavez; , H. M.; Léger, C.; Byrne, B.; Cecchini, G.; Iwata, S. *Science* **2003**, *299*, 700.
(341) Ackrell, B. A. C.; Armstrong, F. A.; Cochran, B.; Sucheta, A.; Yu, T. *FEBS Lett.* **1993**, *326*, 92.
(342) Butt, J. N.; Anderson, L. J.; Rubio, L. M.; Richardson, D. J.; Flores, E.; Herrero, A. *Bioelectrochemistry* **2002**, *56*, 17.
(343) Gates, A. J.; Richardson, D. J.; Butt, J. N. *Biochem. J.* **2008**, *409*, 159.
(344) Ikeda, T.; Miyaoka, S.; Miki, K. *J. Electroanal. Chem.* **1993**, *352*, 267.
(345) Dobbin, P. S.; Butt, J. N.; Powell, A. K.; Reid, G. A.; Richardson, D. J. *Biochem. J.* **1999**, *342*, 439.
(346) Gwyer, J. D.; Angove, H. C.; Richardson, D. J.; Butt, J. N. *Bioelectrochemistry* **2004**, *63*, 43.
(347) McLendon, G. *Structure Bonding* **1991**, *75*, 159.
(348) Jeng, M.-F.; Englander, S. W.; Pardue, K.; Rogalskyj, J. S.; McLendon, G. *Nat. Struct. Mol. Biol.* **1994**, *1*, 234.
(349) Ren, Y.; Wang, W.-H.; Wang, Y.-H.; Case, M.; Qian, W.; McLendon, G.; Huang, Z.-X. *Biochemistry* **2004**, *43*, 3527.
(350) Crowley, P. B.; Ubbink, M. *Acc. Chem. Res.* **2003**, *36*, 723.
(351) Worrall, J. A. R.; Reinle, W.; Bernhardt, R.; Ubbink, M. *Biochemistry* **2003**, *42*, 7068.
(352) Prudencio, M.; Ubbink, M. *J. Mol. Recognit.* **2004**, *17*, 524.
(353) Simonneaux, G.; Bondon, A. *Chem. Rev.* **2005**, *105*, 2627.
(354) Volkov, A. N.; Worrall, J. A. R.; Holtzmann, E.; Ubbink, M. *Proc. Natl. Acad. Sci. U.S.A.* **2006**, *103*, 18945.

(355) Morelli, X.; Dolla, A.; Czjzek, M.; Palma, P. N.; Blasco, F.; Krippahl, L.; Moura, J. J. G.; Guerlesquin, F. *Biochemistry* **2000**, *39*, 2530.
(356) Bizzarri, A. R.; Brunori, E.; Bonanni, B.; Cannistraro, S. *J. Mol. Recognit.* **2007**, *20*, 122.
(357) Rivas, L.; Soares, C. M.; Baptista, A. M.; Simaan, J.; Paolo, R. E. D.; Murgida, D. H.; Hildebrandt, P. *Biophys. J.* **2005**, *88*, 4188.
(358) Anderson, L. J. Thesis, University of East Anglia, 2002.
(359) Murphy, M. E. P.; Turley, S.; Adman, E. T. *J. Biol. Chem.* **1997**, *272*, 28455.
(360) Dementin, S.; Belle, V.; Bertrand, P.; Guigliarelli, B.; Adryanczyk-Perrier, G.; De Lacey, A.; Fernandez, V. M.; Rousset, M.; Léger, C. *J. Am. Chem. Soc.* **2006**, *128*, 5209.
(361) Kowal, A. T.; Werth, M. T.; Manodori, A.; Cecchini, G.; Schroeder, I.; Gunsalus, R. P.; Johnson, M. K. *Biochemistry* **1995**, *34*, 12284.
(362) Verkhovskaya, M. L.; Belevich, N.; Euro, L.; Wikstrom, M.; Verkhovsky, M. I. *Proc. Natl. Acad. Sci. U.S.A.* **2008**, *105*, 3763.
(363) Page, C. C.; Moser, C. C.; Dutton, P. L. *Curr. Opin. Chem. Biol.* **2003**, *7*, 551.
(364) Rousset, M.; Montet, Y.; Guigliarelli, B.; Forget, N.; Asso, M.; Bertrand, P.; FontecillaCamps, J. C.; Hatchikian, E. C. *Proc. Natl. Acad. Sci. U.S.A.* **1998**, *95*, 11625.
(365) Koppenhofer, A.; Turner, K. L.; Allen, J. W. A.; Chapman, S. K.; Ferguson, S. J. *Biochemistry* **2000**, *39*, 4243.
(366) Farver, O.; Kroneck, P. M. H.; Zumft, W. G.; Pecht, I. *Proc. Natl. Acad. Sci. U.S.A.* **2003**, *100*, 7622.
(367) Blatt, Y.; Pecht, I. *Biochemistry* **1979**, *18*, 2917.
(368) Spence, J. T.; Kipke, C. A.; Enemark, J. H.; Sunde, R. A. *Inorg. Chem.* **1991**, *30*, 3011.
(369) Sullivan, E. P.; Hazzard, J. T.; Tollin, G.; Enemark, J. H. *Biochemistry* **1993**, *32*, 12465.
(370) Baffert, C.; Demuez, M.; Cournac, L.; Burlat, B.; Guigliarelli, B.; Soucaille, P.; Bertrand, P.; Girbal, L.; Léger, C. *Angew. Chem., Int. Ed.* **2008**, *47*, 2052.
(371) Almeida, M. G.; Macieira, S.; Goncalves, L. L.; Huber, R.; Cunha, C. A.; Romao, M. J.; Costa, C.; Lampreia, J.; Moura, J. J. G.; Moura, I. *Eur. J. Biochem.* **2003**, *279*, 3904.
(372) Einsle, O.; Messerschmidt, A.; Stach, P.; Bourenkov, G. P.; Bartunik, H. D.; Huber, R.; Kroneck, P. M. H. *Nature* **1999**, *400*, 476.
(373) Einsle, O.; Messerschmidt, A.; Huber, R.; Kroneck, P.; Neese, F. *J. Am. Chem. Soc.* **2002**, *124*, 11737.
(374) Rodrigues, M. L.; Oliveira, T. F.; Pereira, I. A. C.; Archer, M. *EMBO J.* **2006**, *25*, 5951.
(375) Bamford, V. A.; Angove, H. C.; Seward, H. E.; Thomson, A. J.; Cole, J. A.; Butt, J. N.; Hemmings, A. M.; Richardson, D. J. *Biochemistry* **2002**, *41*, 2921.
(376) Stankovich, M. T. Redox properties of flavins and flavoproteins. In *Chemistry and Biochemistry of Flavoenzymes*; Müller, F., Ed.; CRC Press, Inc.: Boca Raton, Ann Arbor, Boston, London, 1991; Vol. 1.
(377) Pereira, A. S.; Tavares, P.; Moura, I.; Moura, J. J. G.; Huynh, B. H. *J. Am. Chem. Soc.* **2001**, *123*, 2771.
(378) Pierik, A. J.; Hagen, W. R.; Redeker, J. S.; Wolbert, R. B. G.; Boersma, M.; Verhagen, M.; Grande, H. J.; Veeger, C.; Mutsaers, P. H. A.; Sands, R. H.; Dunham, W. R. *Eur. J. Biochem.* **1992**, *209*, 63.
(379) de Lacey, A. L.; Fernandez, V. M.; Rousset, M.; Cammack, R. *Chem. Rev.* **2007**, *107*, 4304.
(380) Bleijlevens, B.; van Broekhuizen, F. A.; de Lacey, A. L.; Roseboom, W.; Fernandez, V. M.; Albrach, S. P. J. *J. Biol. Inorg. Chem.* **2004**, *9*, 743.
(381) van Haaster, D. J.; Hagedoorn, P. L.; Jongejan, J. A.; Hagen, W. R. *Biochem. Soc. Trans.* **2005**, *33*, 12.
(382) Ellis, P. J.; Conrads, T.; Hille, R.; Kuhn, P. *Structure* **2001**, *9*, 125.
(383) Hille, R. *Chem. Rev.* **1996**, *96*, 2757.
(384) Hille, R. *Trends Biochem. Sci.* **2002**, *27*, 360.
(385) Moura, J. J.; Brondino, C. D.; Trincao, J.; Romao, M. J. *J. Biol. Inorg. Chem.* **2004**, *9*, 791.
(386) González, P. J.; Correia, C.; Moura, I.; Brondino, C. D.; Moura, J. *J. Inorg. Biochem.* **2006**, *100*, 1015.
(387) Jormakka, M.; Tornroth, S.; Byrne, B.; Iwata, S. *Science* **2002**, *295*, 1863.
(388) Bertero, M. G.; Rothery, R. A.; Palak, M.; Hou, C.; Lim, D.; Blasco, F.; Weiner, J. H.; Strynadka, N. C. J. *Nat. Struct. Mol. Biol.* **2003**, *10*, 681.
(389) Bertero, M. G.; Rothery, R. A.; Boroumand, N.; Palak, M.; Blasco, F.; Ginet, N.; Weiner, J. H.; Strynadka, N. C. J. *J. Biol. Chem.* **2005**, *280*, 14836.
(390) Grimaldi, S.; Lanciano, P.; Bertrand, P.; Blasco, F.; Guigliarelli, B. *Biochemistry* **2005**, *44*, 1300.
(391) Lanciano, P.; Magalon, A.; Bertrand, P.; Guigliarelli, B.; Grimaldi, S. *Biochemistry* **2007**, *46*, 5323.
(392) Anderson, G. L.; Williams, J.; Hille, R. *J. Biol. Chem.* **1992**, *267*, 23674.
(393) Rothery, R. A.; Workun, G. J.; Weiner, J. H. *Biochim. Biophys. Acta* **2007**, http://dx.doi.org/10.1016/j.bbamem.2007.09.002.
(394) Jormakka, M.; Richardson, D.; Burne, B.; Iwata, S. *Structure* **2004**, *12*, 95.
(395) Rothery, R. A.; Bertero, M. G.; Cammack, R.; Palak, M.; Blasco, F.; Strynadka, N. C. J.; Weiner, J. H. *Biochemistry* **2004**, *43*, 5324.
(396) Lanciano, P.; Savoyant, A.; Grimaldi, S.; Magalon, A.; Guigliarelli, B.; Bertrand, P. *J. Phys. Chem. B* **2007**, *111*, 13632.
(397) Dias, J. M.; Than, M. E.; Humm, A.; Huber, R.; Bourenkov, G. P.; Bartunik, H. D.; Bursakov, S.; Calvete, J.; Caldeira, J.; Carneiro, C.; Moura, J. J. G.; Moura, I.; Romão, M. J. *Structure* **1999**, *7*, 65.
(398) Dementin, S.; Arnoux, P.; Frangioni, B.; Grosse, S.; Léger, C.; Burlat, B.; Guigliarelli, B.; Sabaty, M.; Pignol, D. *Biochemistry* **2007**, *46*, 9713.
(399) Finzel, B. C.; Poulos, T. L.; Kraut, J. *J. Biol. Chem.* **1984**, *259*, 13027.
(400) Bonagura, C. A.; Bhaskar, B.; Shimizu, H.; Li, H.; Sundaramoorthy, M.; McRee, D. E.; Goodin, D. B.; Poulos, T. L. *Biochemistry* **2003**, *42*, 5600.
(401) Pettigrew, G. W.; Echalier, A.; Pauleta, S. R. *J. Inorg. Biochem.* **2006**, *100*, 551.
(402) Marritt, S. J.; Kemp, G. L.; Xiaoe, L.; Durrant, J. R.; Cheesman, M. R.; Butt, J. N. *J. Am. Chem. Soc.*, published online June 13, 2008, http://dx.doi.org/10.1021/ja802641a.
(403) Dunford, B. H. *Heme Peroxidases*; John Wiley & Sons: New York, 1999.
(404) Burlat, B.; Gwyer, J. D.; Poock, S.; Clarke, T.; Cole, J. A.; Hemmings, A. M.; Cheesman, M. R.; Butt, J. N.; Richardson, D. J. *Biochem. Soc. Trans.* **2005**, *33*, 137.
(405) Gwyer, J. D.; Richardson, D. J.; Butt, J. N. *Biochem. Soc. Trans.* **2006**, *34*, 133.
(406) Gwyer, J. D.; Richardson, D. J.; Butt, J. N. *Biochemistry* **2004**, *43*, 15086.
(407) Clark, W. M. *Oxidation-reduction potentials of organic systems*; Baillière, Tindal & Cos Ltd.: London, 1960.
(408) Wijma, H. J.; Canters, G. W.; de Vries, S.; Verbeet, M. P. *Biochemistry* **2004**, *43*, 10467.
(409) Peters, J. W.; Lanzilotta, W. N.; Lemon, B. J.; Seefeldt, L. C. *Science* **1998**, *282*, 1853.
(410) Meincke, M.; Bock, E.; Kastrau, D.; Kroneck, P. M. H. *Arch. Microbiol.* **1992**, *158*, 127.
(411) Starkenburg, S. R.; Chain, P. S. G.; Sayavedra-Soto, L. A.; Hauser, L.; Land, M. L.; Larimer, F. W.; Malfatti, S. A.; Klotz, M. G.; Bottomley, P. J.; Arp, D. J.; Hickey, W. J. *Appl. Environ. Microbiol.* **2006**, *72*, 2050.
(412) Vincent, K. A.; Parkin, A.; Armstrong, F. A. *Chem. Rev.* **2007**, *107*, 4366.
(413) Pieulle, L.; Guigliarelli, B.; Asso, M.; Dole, F.; Bernadac, A.; Hatchikian, E. C. *Biochim. Biophys. Acta* **1995**, *1250*, 49.
(414) Chabrière, E.; Charon, M.-H.; Volbeda, A.; Pieulle, L.; Hatchikian, E. C.; FontecillaCamps, J.-C. *Nat. Struct. Mol. Biol.* **1999**, *6*, 182.
(415) Fernandez, V. M.; Hatchikian, E. C.; Cammack, R. *Biochim. Biophys. Acta* **1985**, *832*, 69.
(416) Vincent, K. A.; Cracknell, J. A.; Lenz, O.; Zebger, I.; Friedrich, B.; Armstrong, F. A. *Proc. Natl. Acad. Sci. U.S.A.* **2005**, *102*, 16951.
(417) Vincent, K. A.; Cracknell, J. A.; Clark, J. R.; Ludwig, M.; Lenz, O.; Friedrich, B.; Armstrong, F. A. *Chem. Commun.* **2006**, *48*, 5033.
(418) Buhrke, T.; Lenz, O.; Krauss, N.; Friedrich, B. *J. Biol. Chem.* **2005**, *280*, 23791.
(419) Bleijlevens, B.; Buhrke, T.; van der Linden, E.; Friedrich, B.; Albracht, S. P. J. *J. Biol. Chem.* **2004**, *279*, 46686.
(420) Duché, O.; Elsen, S.; Cournac, L.; Colbeau, A. *FEBS J.* **2005**, *272*, 3899.
(421) Ghirardi, M. L.; Zhang, L.; Lee, J. W.; Flynn, T.; Seibert, M.; Greenbaum, E.; Melis, A. *Trends Biotechnol.* **2000**, *18*, 506.
(422) Higuchi, Y.; Yagi, T.; Yasuoka, N. *Structure* **1997**, *5*, 1671.
(423) Ogata, H.; Hirota, S.; Nakahara, A.; Komori, H.; Shibata, N.; Kato, T.; Kano, K.; Higuchi, Y. *Structure* **2005**, *13*, 1635.
(424) Volbeda, A.; Martin, L.; Cavazza, C.; Matho, M.; Faber, B. W.; Roseboom, W.; Albracht, S. P. J.; Garcin, E.; Rousset, M.; Fontecilla-Camps, J. C. *J. Biol. Inorg. Chem.* **2005**, *10*, 239; erratum **2005**, *10*, 591.
(425) Fan, H.-J.; Hall, M. B. *J. Biol. Inorg. Chem.* **2001**, *6*, 467.
(426) Stadler, C.; de Lacey, A. L.; Montet, Y.; Volbeda, A.; Fontecilla-Camps, J. C.; Conesa, J. C.; Fernandez, V. M. *Inorg. Chem.* **2002**, *41*, 4424.
(427) Guiral, M.; Tron, P.; Belle, V.; Aubert, C.; Léger, C.; Guigliarelli, B.; Orticoni, M.-R. G. *Int. J. Hydrogen Energy* **2006**, *31*, 1424.
(428) de Lacey, A. L.; Pardo, A.; Fernandez, V. M.; Dementin, S.; Adryanczyk-Perrier, G.; Hatichikian, E. C.; Rousset, M. *J. Biol. Inorg. Chem.* **2004**, *9*, 636.
(429) Nicolet, Y.; Piras, C.; Legrand, P.; Hatchikian, C. E.; Fonticella-Camps, J. C. *Structure* **1999**, *7*, 13.

(430) Cracknell, J. A.; Vincent, K. A.; Ludwig, M.; Lenz, O.; Friedrich, B.; Armstrong, F. A. *J. Am. Chem. Soc.* **2008**, *130*, 424.
(431) Miles, E. W.; Rhee, S.; Davies, D. R. *J. Biol. Chem.* **1999**, *274*, 12193.
(432) Raushel, F. M.; Thoden, J. B.; Holden, H. M. *Acc. Chem. Res.* **2003**, *36*, 539.
(433) Weeks, A.; Lund, L.; Raushel, F. M. *Curr. Opin. Chem. Biol.* **2006**, *10*, 465.
(434) Lindahl, P. A. *Biochemistry* **2002**, *41*, 2097.
(435) Darnault, C.; Volbeda, A.; Kim, E. J.; Legrand, P.; Vernède, X.; Lindahl, P. A.; Fontecilla-Camps, J. C. *Nat. Struct. Mol. Biol.* **2003**, *10*, 271.
(436) Tan, X.; Loke, H.-K.; Fitch, S.; Lindahl, P. A. *J. Am. Chem. Soc.* **2005**, *127*, 5833.
(437) Tan, X.; Volbeda, A.; Fontecilla-Camps, J. C.; Lindahl, P. A. *J. Biol. Inorg. Chem.* **2006**, *11*, 371.
(438) Montet, Y.; Amara, P.; Volbeda, A.; Vernede, X.; Hatchikian, E. C.; Field, M. J.; Frey, M.; Fontecilla-Camps, J. C. *Nat. Struct. Mol. Biol.* **1997**, *4*, 523.
(439) Nicolet, Y.; Cavazza, C.; Fontecilla-Camps, J. C. *J. Inorg. Biochem.* **2002**, *91*, 1.
(440) Teixeira, V. H.; Baptista, A. M.; Soares, C. M. *Biophys. J.* **2006**, *91*, 2035.
(441) Cohen, J.; Kim, K.; King, P.; Seibert, M.; Schulten, K. *Structure* **2005**, *13*, 1321.
(442) Schmidt, B.; McCracken, J.; Ferguson-Miller, S. *Proc. Natl. Acad. Sci., U.S.A.* **2003**, *100*, 15539.
(443) Salomonsson, L.; Lee, A.; Gennis, R. B.; Brzezinski, P. *Proc. Natl. Acad. Sci., U.S.A.* **2004**, *101*, 11617.
(444) Johnson, B. J.; Cohen, J.; Welford, R. W.; Pearson, A. R.; Schulten, K.; Klinman, J. P.; Wilmot, C. M. *J. Biol. Chem.* **2007**, *282*, 17767.
(445) Murray, J. W.; Barber, J. *J. Struct. Biol.* **2007**, *159*, 228.
(446) Cohen, J.; Arkhipov, A.; Braun, R.; Schulten, K. *Biophys. J.* **2006**, *91*, 1630.
(447) Leroux, F.; Dementin, S.; Burlat, B.; Cournac, L.; Volbeda, A.; Champ, S.; Martin, L.; Guigliarelli, B.; Bertrand, P.; Fontecilla-Camps, J.; Rousset, M.; Léger, C. *Proc. Natl. Acad. Sci. U.S.A.*, in press.

CR0680742